

APPENDIX H

ENSR CORPORATION, 1999. "EXTENT OF VISUAL IMPAIRMENT IN CALIFORNIA."
REPORT PREPARED FOR SOUTHERN CALIFORNIA EDISON COMPANY, JUNE

**Southern California Edison
Company
Rosemead, California**

**Extent of Visual Impairment in
California
Final Report**

**ENSR Corporation
1220 Avenida Acaso
Camarillo, California 93012
June 1999
Document Number 6200-023-300**

EXECUTIVE SUMMARY

The purpose of this study is to describe the extent of visual impairment in California and to identify historical trends in visibility, visibility-impairing aerosols and emissions. Visual impairment in the atmosphere is caused by scattering and absorption of light by gases and particles. The total effect of scattering and absorption is called light extinction. Light extinction is usually measured in terms of the light extinction coefficient, which is the fractional reduction in light intensity that occurs over a specified distance in the atmosphere. Similarly, light scattering and absorption by particles and gases are expressed in terms of their respective light scattering and absorption coefficients. Light scattering by particles between about 0.1 and 1.0 micrometers (μm) in diameter is usually the major contributor to the light extinction coefficient, but light absorption by particles and gases can also be important. In very clean air, light scattering by air molecules (called Rayleigh scattering) can be comparable to light scattering by particles and absorption by particles and gases.

The principal focus of this study is in defining and describing California-specific visibility issues and concerns. The important issues relate to the nature and extent of visual impairment, its causes, and identification of analytical tools that may be applied in mitigating such impairment. Special attention in this regard was also placed on examining the role of emissions from the energy sector in California on visual impairment.

Several sets of data that include optical measurements of various components of the extinction coefficient were analyzed as well as available measurements of particulate matter smaller than 2.5 μm , called $\text{PM}_{2.5}$ and some of its constituents. Most of the mass of particles smaller than 2.5 μm is in particles between 0.1 and 1.0 μm , so $\text{PM}_{2.5}$ is a good representation of the particles primarily responsible for light scattering. These data were available from the IMPROVE (Interagency Monitoring of Protected Visual Environments) network maintained by the National Park Service and from monitoring sites operated by California local air pollution control agencies.

The data used in the analyses and the time periods covered are indicated by monitoring site in Table ES-1, and site locations are shown in Figure ES-1. As seen in the table, local-agency light scattering coefficient data generally cover the time period from 1985 through 1996, and the IMPROVE data and local-agency particulate matter data generally cover the time period from 1988 through 1996. Although data were available from additional IMPROVE and local-agency sites, those data covered more limited time periods, so they were not used in the analyses. Additionally, some sites reported data for earlier and later periods than shown in the table, but these data were not included in the analyses in order to maintain a consistent period-of-record for comparisons between sites.

The IMPROVE sites, with the exception of South Lake Tahoe, are located in Federal Class I areas (National Parks, Monuments and Wilderness Areas). The local-agency optical data are predominantly from the Sacramento Valley Air Basin, while the particulate matter data are primarily from the San

**Table ES-1
Summary of Data Availability**

Air Basin	Location	Elevation (meters)	Operator	Period Covered	
				Optical Data	Particulate Matter
North Coast	Redwood National Park ^a	232	IMPROVE		1988-1996
Northeast Plateau	Lassen Volcanic National Park ^a	1,798	IMPROVE		1988-1996
Lake County	Lakeport	408	Local	1985-1996	
Lake Tahoe	South Lake Tahoe	1,900	IMPROVE		1989-1996
Sacramento Valley	Arbuckle	43	Local	1985-1996	
	Chico	62	Local	1985-1996	
	Colusa	17	Local	1985-1996	
	Gridley	0	Local	1985-1996	
	Pleasant Grove	50	Local	1985-1996	
	Yuba City	20	Local	1985-1996	
San Francisco Bay	Point Reyes National Seashore ^a	38	IMPROVE		1988-1996
	San Jose	24	Local		1990-1996
San Joaquin Valley	Bakersfield	137	Local		1988-1996
	Fresno	91	Local		1988-1996
	Madera	60	Local		1989-1996
	Modesto	27	Local		1989-1996
	Stockton	19	Local	1985-1996	1989-1996
	Visalia	97	Local		1988-1996
Mountain Counties	Yosemite National Park ^a	1,615	IMPROVE	1989-1996	1988-1996
North Central Coast	Pinnacles National Monument ^a	317	IMPROVE	1988-1993	1988-1996
South Coast	Azusa	183	Local		1988-1996
	Long Beach	6	Local		1989-1996
	Riverside	250	Local		1988-1996
	San Geronio Wilderness Area ^a	1,712	IMPROVE	1989-1996	1988-1996
Salton Sea	El Centro	0	Local		1988-1996
^a Federal Class I Area					

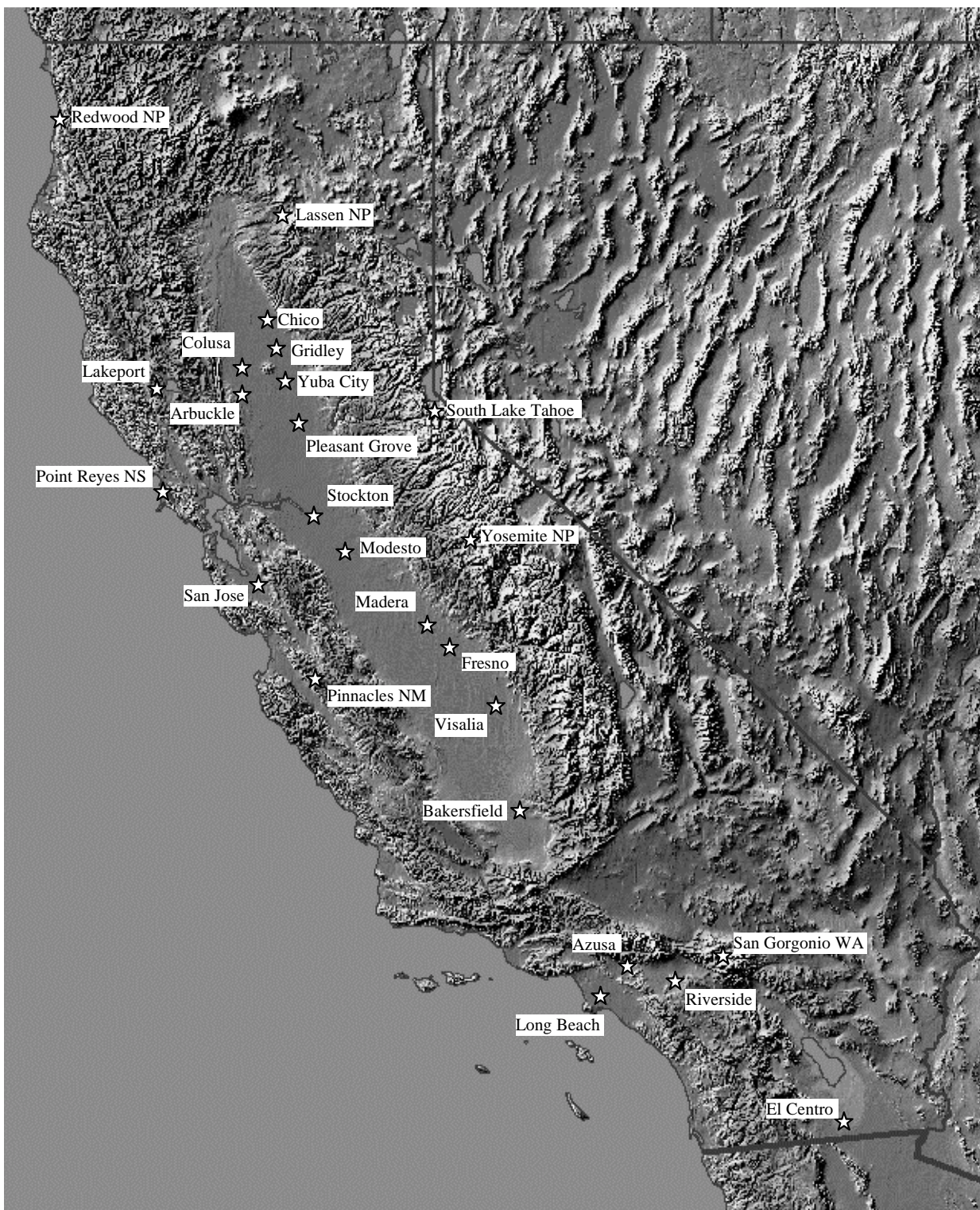


Figure ES-1 Monitoring Site Locations

Joaquin Valley and South Coast Air Basins, with single sites in the Lake County, San Francisco Bay and Salton Sea Air Basins.

Estimates of emissions of particulate matter and precursor gases that can form particulate matter through reactions in the atmosphere were also analyzed. The California Air Resources Board estimated annual average daily emissions of PM₁₀, nitrogen oxides (NO_x), sulfur oxides (SO_x), carbon monoxide (CO) and reactive organic gases (ROG) at five-year intervals from 1985 through 2010, categorized by standard industrial classification (SIC) code and source category code (SCC) within each county and air basin.

The analyses of these data led to the following conclusions:

1. The highest fine particle concentrations in California are present in locations with surrounding topography that limits dispersion. These areas include the Central Valley, the South Coast Air Basin, the San Francisco Bay area and the Lake Tahoe Air Basin.
2. The highest concentrations at these locations generally occur during the fall or winter, when periods of low inversions and low wind speeds accompanied by high humidities lead to the accumulation of emitted particulate matter and formation of secondary particulate matter constituents through atmospheric chemical reactions.
3. Carbon-containing materials and ammonium nitrate are the major constituents of PM_{2.5} at the locations with the highest PM_{2.5} mass concentrations. Wood burning may be a major source of the carbon-containing materials, particularly at locations with cooler fall and winter temperatures, while the ammonium nitrate is formed from atmospheric reactions that involve nitrogen oxides and ammonia.
4. Concentrations at coastal locations, such as Redwood National Park and Point Reyes National Seashore, do not vary as much with season as concentrations at inland locations, although there is a tendency for higher concentrations to occur during fall and winter than during spring and summer.
5. Concentrations at Yosemite and Lassen Volcanic National Parks are highest during the summer, in contrast with the other locations, and sulfate is a larger contributor than ammonium nitrate. This behavior may be caused by summertime park visitors or by transport from the Central Valley.
6. Concentrations at San Geronio Wilderness Area are highest during spring and summer, when conditions are conducive to transport of material from the South Coast Air Basin.
7. Statistically significant decreases in concentrations occurred between 1989 and 1996 in several air basins. Most notable were decreases in the San Joaquin Valley during winter and at San

Gorgonio Wilderness Area during spring, which are the times of year when concentrations are highest at these locations.

8. Estimated emissions of $PM_{2.5}$, nitrogen oxides and sulfur oxides decreased throughout the state between 1990 and 1995. These decreases are consistent with the observed decreases in concentrations. However, decreases in concentrations did not accompany decreases in emissions everywhere. For example, most trends at Azusa, Long Beach and Riverside, in the South Coast Air Basin, and at San Jose, in the San Francisco Bay Air Basin, were not statistically significant.
9. Emissions from energy production are small percentages of $PM_{2.5}$, nitrogen oxide and sulfur oxide emissions in California, so energy production likely does not contribute substantially to decreased visibility or increased $PM_{2.5}$ concentrations.
10. Emissions from non-mobile source energy use (fuel combustion except by mobile sources and electricity generating plants) are a larger percentage of total emissions than emissions from energy production. In particular, wood burning is a substantial contributor to $PM_{2.5}$ emissions in cooler locations, such as the Lake Tahoe and Mountain Counties Air Basins. Therefore, emissions from non-mobile source energy use may be important contributors to reduced visibility and increased $PM_{2.5}$ concentrations in some parts of the state.
11. $PM_{2.5}$ emissions are projected to increase in the future in almost every air basin, largely because of increases in emissions from paved and unpaved road travel and from residential wood combustion. NO_x emissions are expected to continue to decrease, largely because of additional reductions from mobile sources. SO_x emissions are expected to remain fairly constant in the future.
12. The decreases in NO_x emissions may lead to decreases in $PM_{2.5}$ concentrations and improvements in visibility in locations where ammonium nitrate is the major $PM_{2.5}$ constituent and ammonia emissions are high, such as the San Joaquin Valley. The increases in $PM_{2.5}$ emissions from paved and unpaved road travel may not affect visibility much, because the particles in these emissions are not very efficient in scattering light. Increases in emissions from wood combustion, on the other hand, may degrade visibility.
13. Several atmospheric models exist that can be used to better understand relationships between emissions, atmospheric particulate matter, and visibility. However, their application generally requires extensive quantities of data and experience.
14. More extensive spatial coverage is needed to better understand the nature and causes of visibility and particulate matter concentrations in California. Implementation of the $PM_{2.5}$ monitoring network in conjunction with expansion of the IMPROVE network will help provide this information in the future.

15. Recent and ongoing developments in measurement techniques for atmospheric optical parameters and particulate matter mass and constituents will also provide new information to better characterize visibility and particulate matter.

CONTENTS

1.0 INTRODUCTION.....	1-1
2.0 DATABASE COMPILATION	2-1
2.1 Data Overview	2-1
2.2 Data Processing.....	2-3
3.0 CHARACTERISTICS OF OPTICAL AND PARTICULATE MATTER DATA	3-1
3.1 Geographic Patterns	3-1
3.1.1 Geographic Patterns of Particle Light Scattering Coefficients.....	3-1
3.1.2 Geographic Patterns of Particulate Matter Concentrations	3-6
3.2 Characteristics by Air Basin.....	3-20
3.2.1 North Coast Air Basin.....	3-20
3.2.2 Lake County Air Basin.....	3-24
3.2.3 San Francisco Bay Air Basin	3-24
3.2.4 North Central Coast.....	3-27
3.2.5 Sacramento Valley Air Basin	3-30
3.2.6 San Joaquin Valley Air Basin.....	3-34
3.2.7 Northeast Plateau Air Basin.....	3-34
3.2.8 Lake Tahoe Air Basin.....	3-40
3.2.9 Mountain Counties Air Basin.....	3-45
3.2.10 South Coast Air Basin	3-45
3.2.11 Salton Sea (Southeast Desert) Air Basin	3-53
3.3 Summary	3-55
4.0 HISTORICAL TRENDS AND THE ROLE OF EMISSIONS FROM THE ENERGY SECTOR.....	4-1
4.1 Trends in Optical and Particulate Matter Data.....	4-1
4.2 Trends in Emissions and the Role of the Energy Sector.....	4-9
5.0 MODELS FOR SOURCE-RECEPTOR RELATIONSHIPS.....	5-1

5.1	Background	5-1
5.2	Receptor Models for Particulate Matter.....	5-2
5.3	Source Models for Particulate Matter	5-6
5.3.1	Regulatory Plume Models	5-6
5.3.2	Advanced Plume Models	5-8
5.3.3	Advanced Regional Models	5-9
5.4	Calculating Visibility from the Particulate Matter Concentrations.....	5-15
5.5	Assessment of Models.....	5-16
6.0	MEASUREMENT METHOD IMPROVEMENTS	6-1
6.1	Visibility Measurements	6-1
6.2	Aerosol Measurements.....	6-2
7.0	CONCLUSIONS.....	7-1
8.0	REFERENCES.....	8-1

LIST OF TABLES

Table 2-1 Summary of Data Availability by Site 2-4

Table 2-2 Coefficients of Seasonal Relative Humidity Function 2-7

Table 2-3 Seasonal Average Relative Humidities Used for Calculating Light Scattering at IMPROVE Sites..... 2-7

Table 4-1 Number of Tests and Number of Statistically Significant Spearman Rank Order Correlations by Quantity 4-2

Table 4-2 Statistically Significant Trends at the 10% Level from 1989 through 1996 based on the Spearman Rank Order Correlation Coefficient..... 4-4

Table 4-3 Annual Average PM_{2.5} Emissions and Contributions from Energy Production and Non-Mobile Source Energy Use by Air Basin during 1985, 1990 and 1995 4-10

Table 4-4 Annual Average NO_x Emissions and Contributions from Energy Production and Non-Mobile Source Energy Use by Air Basin during 1985, 1990 and 1995 4-11

Table 4-5 Annual Average SO_x Emissions and Contributions from Energy Production and Non-Mobile Source Energy Use by Air Basin during 1985, 1990 and 1995 4-12

Table 5-1 Summary of Receptor Modeling Methods that Apportion Secondary Aerosol 5-3

Table 5-2 Summary of Urban and Regional Particulate Matter Models 5-10

LIST OF FIGURES

Figure 2-1 California Air Basins 2-2

Figure 2-2 Monitoring Site Locations..... 2-5

Figure 2-3 Comparison of Calculated and Measured Seasonal Average Light Extinction Coefficients Averaged Over All Years at Pinnacles National Monument 2-8

Figure 2-4 Comparison of Calculated and Measured Seasonal Average Light Extinction Coefficients Averaged Over All Years at San Geronio Wilderness Area 2-9

Figure 2-5 Comparison of Calculated and Measured Seasonal Average Light Extinction Coefficients Averaged Over All Years at Yosemite National Park 2-9

Figure 3-1 Geographic Distribution of b_{sp} during Spring..... 3-2

Figure 3-2 Geographic Distribution of b_{sp} during Summer 3-3

Figure 3-3 Geographic Distribution of b_{sp} during Fall 3-4

Figure 3-4 Geographic Distribution of b_{sp} during Winter..... 3-5

Figure 3-5 Geographic Distribution of $PM_{2.5}$ Mass during Spring 3-7

Figure 3-6 Geographic Distribution of $PM_{2.5}$ Mass during Summer..... 3-8

Figure 3-7 Geographic Distribution of $PM_{2.5}$ Mass during Fall 3-9

Figure 3-8 Geographic Distribution of $PM_{2.5}$ Mass during Winter 3-10

Figure 3-9 Geographic Distribution of Nitrate Mass during Spring 3-12

Figure 3-10 Geographic Distribution of Nitrate Mass during Summer..... 3-13

Figure 3-11 Geographic Distribution of Nitrate Mass during Fall 3-14

Figure 3-12 Geographic Distribution of Nitrate Mass during Winter 3-15

Figure 3-13 Geographic Distribution of Sulfate Mass during Spring..... 3-16

Figure 3-14 Geographic Distribution of Sulfate Mass during Summer 3-17

Figure 3-15 Geographic Distribution of Sulfate Mass during Fall 3-18

Figure 3-16 Geographic Distribution of Sulfate Mass during Winter..... 3-19

Figure 3-17 Seasonal Median and 20th and 80th Percentiles of the Particle Light Absorption Coefficient at Redwood National Park 3-22

Figure 3-18 Seasonal Median and 20th and 80th Percentiles of $PM_{2.5}$ Mass Concentration at Redwood National Park..... 3-22

Figure 3-19 Seasonal Average $PM_{2.5}$ Mass and Estimated Chemical Constituent Concentrations at Redwood National Park..... 3-23

Figure 3-20 Contributions to Calculated Seasonal Average Light Extinction Coefficient at Redwood National Park..... 3-23

Figure 3-21 Seasonal Median and 20th and 80th Percentiles of the Particle Light Scattering Coefficient Measured at Lakeport..... 3-25

Figure 3-22 Seasonal Median and 20th and 80th Percentiles of the Coefficient of Haze Measured at Lakeport 3-25

Figure 3-23 Seasonal Median and 20th and 80th Percentiles of PM_{2.5} Mass Concentration at San Jose 3-26

Figure 3-24 Seasonal Median PM_{2.5} Mass and PM₁₀ Ammonium Nitrate and Ammonium Sulfate Concentrations at San Jose 3-26

Figure 3-25 Seasonal Median and 20th and 80th Percentiles of the Particle Light Absorption Coefficient at Point Reyes National Seashore 3-28

Figure 3-26 Seasonal Median and 20th and 80th Percentiles of PM_{2.5} Mass Concentration at Point Reyes National Seashore..... 3-28

Figure 3-27 Seasonal Average PM_{2.5} Mass and Estimated Chemical Constituent Concentrations at Point Reyes National Seashore 3-29

Figure 3-28 Contributions to Calculated Seasonal Average Light Extinction Coefficient at Point Reyes National Seashore 3-29

Figure 3-29 Seasonal Median and 20th and 80th Percentiles of the Light Extinction Coefficient at Pinnacles National Monument 3-31

Figure 3-30 Seasonal Median and 20th and 80th Percentiles of the Particle Light Absorption Coefficient at Pinnacles National Monument..... 3-31

Figure 3-31 Seasonal Median and 20th and 80th Percentiles of PM_{2.5} Mass Concentration at Pinnacles National Monument..... 3-32

Figure 3-32 Seasonal Average PM_{2.5} Mass and Estimated Chemical Constituent Concentrations at Pinnacles National Monument 3-32

Figure 3-33 Contributions to Calculated Seasonal Average Light Extinction Coefficient at Pinnacles National Monument..... 3-33

Figure 3-34 Seasonal Median and 20th and 80th Percentiles of the Particle Light Scattering Coefficient Measured at Sacramento Valley Air Basin Sites..... 3-33

Figure 3-35 Seasonal Median and 20th and 80th of the Coefficient of Haze Measured at Sacramento Valley Air Basin Sites..... 3-35

Figure 3-36 Seasonal Median and 20th and 80th Percentiles of the Particle Light Scattering Coefficient Measured at Stockton..... 3-35

Figure 3-37 Seasonal Median and 20 th and 80 th Percentiles of the Coefficient of Haze Measured at Stockton	3-36
Figure 3-38 Seasonal Median and 20 th and 80 th Percentiles of PM _{2.5} Mass Concentration at San Joaquin Valley Air Basin Sites.....	3-36
Figure 3-39 Seasonal Median PM _{2.5} Mass and PM ₁₀ Ammonium Nitrate and Ammonium Sulfate Concentrations at Stockton	3-37
Figure 3-40 Seasonal Median PM _{2.5} Mass and PM ₁₀ Ammonium Nitrate and Ammonium Sulfate Concentrations at Modesto	3-37
Figure 3-41 Seasonal Median PM _{2.5} Mass and PM ₁₀ Ammonium Nitrate and Ammonium Sulfate Concentrations at Madera	3-38
Figure 3-42 Seasonal Median PM _{2.5} Mass and PM ₁₀ Ammonium Nitrate and Ammonium Sulfate Concentrations at Fresno	3-38
Figure 3-43 Seasonal Median PM _{2.5} Mass and PM ₁₀ Ammonium Nitrate and Ammonium Sulfate Concentrations at Visalia.....	3-39
Figure 3-44 Seasonal Median PM _{2.5} Mass and PM ₁₀ Ammonium Nitrate and Ammonium Sulfate Concentrations at Bakersfield	3-39
Figure 3-45 Seasonal Median and 20 th and 80 th Percentiles of the Particle Light Absorption Coefficient at Lassen Volcanic National Park.....	3-41
Figure 3-46 Seasonal Median and 20 th and 80 th Percentiles of PM _{2.5} Mass Concentration at Lassen Volcanic National Park	3-41
Figure 3-47 Seasonal Average PM _{2.5} Mass and Estimated Chemical Constituent Concentrations at Lassen Volcanic National Park	3-42
Figure 3-48 Contributions to Calculated Seasonal Average Light Extinction Coefficient at Lassen Volcanic National Park	3-42
Figure 3-49 Seasonal Median and 20 th and 80 th Percentiles of the Particle Light Absorption Coefficient at South Lake Tahoe.....	3-43
Figure 3-50 Seasonal Median and 20 th and 80 th Percentiles of PM _{2.5} Mass Concentration at South Lake Tahoe	3-43
Figure 3-51 Seasonal Average PM _{2.5} Mass and Estimated Chemical Constituent Concentrations at South Lake Tahoe	3-44
Figure 3-52 Contributions to Calculated Seasonal Average Light Extinction Coefficient at South Lake Tahoe	3-44
Figure 3-53 Seasonal Median and 20 th and 80 th Percentiles of the Light Extinction Coefficient at Yosemite National Park.....	3-46

Figure 3-54 Seasonal Median and 20th and 80th Percentiles of the Particle Light Absorption Coefficient at Yosemite National Park	3-46
Figure 3-55 Seasonal Median and 20th and 80th Percentiles of PM _{2.5} Mass Concentration at Yosemite National Park.....	3-47
Figure 3-56 Seasonal Average PM _{2.5} Mass and Estimated Chemical Constituent Concentrations at Yosemite National Park.....	3-47
Figure 3-57 Contributions to Calculated Seasonal Average Light Extinction Coefficient at Yosemite National Park.....	3-48
Figure 3-58 Seasonal Median and 20 th and 80 th Percentiles of PM _{2.5} Mass Concentration at South Coast Air Basin Sites	3-48
Figure 3-59 Seasonal Median PM _{2.5} Mass and PM ₁₀ Ammonium Nitrate and Ammonium Sulfate Concentrations at Long Beach.....	3-49
Figure 3-60 Seasonal Median PM _{2.5} Mass and PM ₁₀ Ammonium Nitrate and Ammonium Sulfate Concentrations at Azusa	3-49
Figure 3-61 Seasonal Median PM _{2.5} Mass and PM ₁₀ Ammonium Nitrate and Ammonium Sulfate Concentrations at Riverside	3-50
Figure 3-62 Seasonal Median and 20th and 80th Percentiles of the Light Extinction Coefficient at San Gorgonio Wilderness Area	3-51
Figure 3-63 Seasonal Median and 20th and 80th Percentiles of the Particle Light Absorption Coefficient at San Gorgonio Wilderness Area.....	3-51
Figure 3-64 Seasonal Median and 20th and 80th Percentiles of PM _{2.5} Mass Concentration at San Gorgonio Wilderness Area	3-52
Figure 3-65 Seasonal Average PM _{2.5} Mass and Estimated Chemical Constituent Concentrations at San Gorgonio Wilderness Area.....	3-52
Figure 3-66 Contributions to Calculated Seasonal Average Light Extinction Coefficient at San Gorgonio Wilderness Area.....	3-54
Figure 3-67 Seasonal Median and 20 th and 80 th Percentiles of PM _{2.5} Mass Concentration at El Centro	3-54
Figure 3-68 Seasonal Median PM _{2.5} Mass and PM ₁₀ Ammonium Nitrate and Ammonium Sulfate Concentrations at El Centro	3-55
Figure 4-1 Median PM _{2.5} Mass and PM ₁₀ Nitrate and Sulfate Concentrations Measured at Modesto during Winter from 1990 through 1996.....	4-8
Figure 4-2 Average Measured b_{ext} , b_{abs} and PM _{2.5} Mass Concentration and Calculated b_{ext} and b_{sp} during Spring at San Gorgonio Wilderness Area from 1988 through 1996	4-8

Figure 4-3 Average Measured PM_{2.5} Mass, Nitrate and Sulfate Concentrations during Spring at San Geronio Wilderness Area from 1988 through 1996 4-9

Figure 4-4 Estimated Annual Average Emissions in the North Coast Air Basin from 1985 through 2010 4-13

Figure 4-5 Contribution of Energy Production, Stationary Source Fuel Use and Other Sources to Annual Average Emissions in the North Coast Air Basin from 1985 through 2010..... 4-14

Figure 4-6 Estimated Annual Average Emissions in the Lake County Air Basin from 1985 through 2010 4-14

Figure 4-7 Contribution of Energy Production, Stationary Source Fuel Use and Other Sources to Annual Average Emissions in the Lake County Air Basin from 1985 through 2010..... 4-15

Figure 4-8 Estimated Annual Average Emissions in the San Francisco Bay Air Basin from 1985 through 2010 4-15

Figure 4-9 Contribution of Energy Production, Stationary Source Fuel Use and Other Sources to Annual Average Emissions in the San Francisco Bay Air Basin from 1985 through 2010 4-16

Figure 4-10 Estimated Annual Average Emissions in the North Central Coast Air Basin from 1985 through 2010 4-16

Figure 4-11 Contribution of Energy Production, Stationary Source Fuel Use and Other Sources to Annual Average Emissions in the North Central Coast Air Basin from 1985 through 2010..... 4-17

Figure 4-12 Estimated Annual Average Emissions in the Sacramento Valley Air Basin from 1985 through 2010 4-17

Figure 4-13 Contribution of Energy Production, Stationary Source Fuel Use and Other Sources to Annual Average Emissions in the Sacramento Valley Air Basin from 1985 through 2010 4-18

Figure 4-14 Estimated Annual Average Emissions in the San Joaquin Valley Air Basin from 1985 through 2010 4-18

Figure 4-15 Contribution of Energy Production, Stationary Source Fuel Use and Other Sources to Annual Average Emissions in the San Joaquin Valley Air Basin from 1985 through 2010..... 4-19

Figure 4-16 Estimated Annual Average Emissions in the Northeast Plateau Air Basin from 1985 through 2010 4-19

Figure 4-17 Contribution of Energy Production, Stationary Source Fuel Use and Other Sources to Annual Average Emissions in the Northeast Plateau Air Basin from 1985 through 2010..... 4-20

Figure 4-18 Estimated Annual Average Emissions in the Lake Tahoe Air Basin from 1985 through 2010..... 4-20

Figure 4-19 Contribution of Energy Production, Stationary Source Fuel Use and Other Sources to Annual Average Emissions in the Lake Tahoe Air Basin from 1985 through 2010..... 4-21

Figure 4-20 Estimated Annual Average Emissions in the Mountain Counties Air Basin from 1985 through 2010	4-21
Figure 4-21 Contribution of Energy Production, Stationary Source Fuel Use and Other Sources to Annual Average Emissions in the Mountain Counties Air Basin from 1985 through 2010	4-22
Figure 4-22 Estimated Annual Average Emissions in the South Coast Air Basin from 1985 through 2010.....	4-22
Figure 4-23 Contribution of Energy Production, Stationary Source Fuel Use and Other Sources to Annual Average Emissions in the South Coast Air Basin from 1985 through 2010.....	4-23
Figure 4-24 Estimated Annual Average Emissions in the Southeast Desert Air Basin from 1985 through 2010	4-23
Figure 4-25 Contribution of Energy Production, Stationary Source Fuel Use and Other Sources to Annual Average Emissions in the Southeast Desert Air Basin from 1985 through 2010.....	4-24

1.0 INTRODUCTION

The purpose of this report is to describe the extent of visual impairment in California and to identify historical trends in visibility, visibility-impairing aerosols and emissions. Visual impairment in the atmosphere is caused by scattering and absorption of light by gases and particles. The total effect of scattering and absorption is called light extinction. Light extinction is usually measured in terms of the light extinction coefficient, which is the fractional reduction in light intensity that occurs over a specified distance in the atmosphere. Similarly, light scattering and absorption by particles and gases are expressed in terms of their respective light scattering and absorption coefficients. Light scattering by particles between about 0.1 and 1.0 micrometers (μm) in diameter is usually the major contributor to the light extinction coefficient, but light absorption by particles and gases can also be important. In very clean air, light scattering by air molecules (called Rayleigh scattering) can be comparable to light scattering by particles and absorption by particles and gases.

The principal focus of this report is in defining and describing California-specific visibility issues and concerns. The important issues relate to the nature and extent of visual impairment, its causes, and identification of analytical tools that may be applied in mitigating such impairment. Special attention in this regard was also placed on examining the role of emissions from the energy sector in California on visual impairment.

Several sets of data that include optical measurements of various components of the extinction coefficient were acquired and analyzed as well as available measurements of particulate matter smaller than 2.5 μm , called $\text{PM}_{2.5}$ and some of its constituents. Most of the mass of particles smaller than 2.5 μm is in particles between 0.1 and 1.0 μm , so $\text{PM}_{2.5}$ is a good representation of the particles primarily responsible for light scattering. The data sets that were acquired and how they were processed are described in Section 2 of this report.

Section 3 presents and discusses seasonal and geographic variations in the data. Historical trends in the optical and particulate matter data as well as trends in estimated emissions are examined in Section 4. Section 4 also address the potential role of emissions from the energy sector. Section 5 describes simulation models that are available or being developed to relate visibility to emissions, and Section 6 discusses the current state of the science for measuring visibility and particulate matter. Conclusions are presented in Section 7.

2.0 DATABASE COMPILATION

Emissions, optical and particulate matter data were acquired and compiled into databases for subsequent analysis. This section describes the data that were available and how they were processed prior to conducting the data analyses.

2.1 Data Overview

The California Air Resources Board (ARB, 1998) estimated annual average daily emissions of PM₁₀, nitrogen oxides (NO_x), sulfur oxides (SO_x), carbon monoxide (CO) and reactive organic gases (ROG) at five-year intervals from 1985 through 2010, categorized by standard industrial classification (SIC) code and source category code (SCC) within each county and air basin. The air basins are shown in Figure 2-1.

Optical and particulate matter data were available from the IMPROVE (Interagency Monitoring of Protected Visual Environments) network maintained by the National Park Service and from monitoring sites operated by California local air pollution control agencies. Optical data included the light extinction (b_{ext}) and absorption (b_{abs}) coefficients measured at IMPROVE sites and the particle light scattering coefficient (b_{sp}) and coefficient of haze (COH) measured at local-agency sites. Particulate matter data included PM_{2.5} mass and chemical composition and PM₁₀ mass from IMPROVE sites as well as PM_{2.5} mass and PM₁₀ mass and chemical composition measured at local-agency sites. The available optical data were supplemented with light scattering and extinction coefficients calculated from particulate matter data at the IMPROVE sites. The IMPROVE data were acquired from the National Park Service Air Resources Division Internet File Transfer Protocol (FTP) server (ftp://alta_vista.cira.colostate.edu/), and the local agency data were acquired from ARB (1997).

The light extinction coefficient is measured continuously at IMPROVE sites with transmissometers and reported as hourly averages. Particulate matter samples are collected over 24-hour periods twice weekly on filters with IMPROVE samplers and analyzed by the laser integrating plate method (LIPM) for the particle light absorption coefficient and by various techniques for mass, chemical elements, elemental and organic carbon and water-extractable ions. Sisler et al. (1996) provide details of IMPROVE procedures. The IMPROVE measurements may underestimate concentrations of semi-volatile organic compounds because of loss of material from the filter samples.

The light scattering coefficient is measured continuously with integrating nephelometers at local-agency sites and reported as hourly averages. The nephelometers used at these sites generally raise the temperature of the sampled air somewhat above ambient, which can cause a reduction in relative humidity, leading to a loss of water from the particles and an underestimate of the particle light

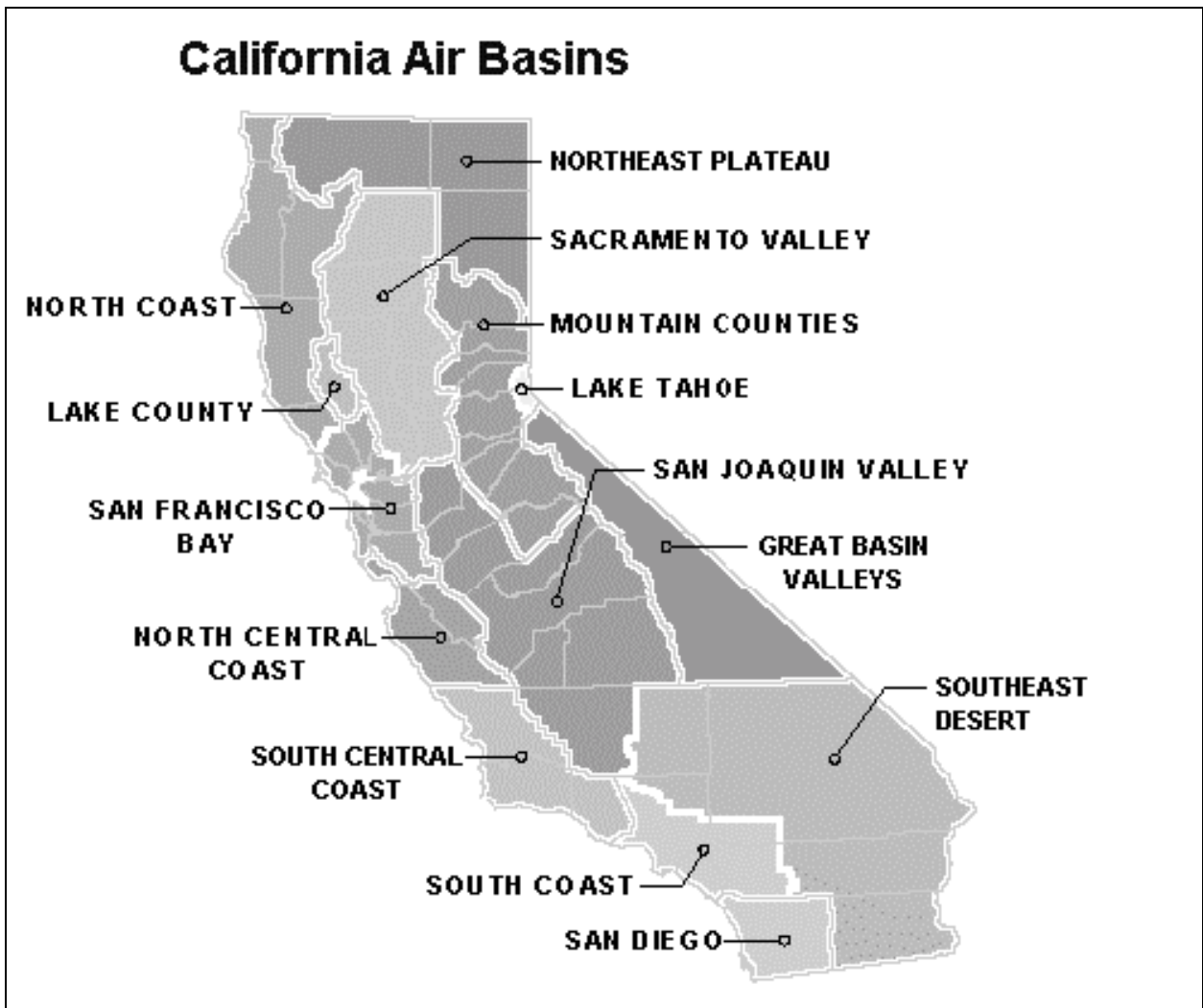


Figure 2-1 California Air Basins

scattering coefficient. The coefficient of haze is measured over two-hour periods by light transmission through samples collected on glass fiber filter tape by moving filter tape samplers. Although the coefficient of haze is not a direct measure of the particle light absorption coefficient, changes in the coefficient of haze at a site should be indicative of relative changes in particle light absorption.

PM_{2.5} filter samples are collected over 24-hour periods with dichotomous samplers at local agency-sites and analyzed gravimetrically for mass. PM₁₀ samples are collected over 24-hour periods with high-volume samplers and analyzed gravimetrically for mass and by various methods for a limited number of chemical constituents, including water-soluble sulfate and nitrate. The collection method can lead to loss of particulate nitrate from the sample by volatilization, so the nitrate values from these sites may be lower bounds on the actual concentrations.

The data used in the analyses and the time periods covered are indicated by monitoring site in Table 2-1, and site locations are shown in Figure 2-2. As seen in the table, the local-agency light scattering coefficient data generally cover the time period from 1985 through 1996, and the IMPROVE data and local-agency particulate matter data generally cover the time period from 1988 through 1996. Although data were available from additional IMPROVE and local-agency sites, those data covered more limited time periods, so they were not used in the analyses. Additionally, some sites reported data for earlier and later periods than shown in the table, but these data were not included in the analyses in order to maintain a consistent period-of-record for comparisons between sites.

The IMPROVE sites, with the exception of South Lake Tahoe, are located in Federal Class I areas (National Parks, Monuments and Wilderness Areas). The local-agency light scattering coefficient data are predominantly from the Sacramento Valley Air Basin, while the particulate matter data are primarily from the San Joaquin Valley and South Coast Air Basins, with single sites in the Lake County, San Francisco Bay and Salton Sea (part of the Southeast Desert) Air Basins.

2.2 Data Processing

The data were processed in various ways prior to analysis. The data processing activities included the following:

- PM_{2.5} emissions were estimated by applying PM_{2.5}-to-PM₁₀ emission ratios to the PM₁₀ emission estimates. The PM_{2.5}-to-PM₁₀ ratios were developed and assigned to source classification codes by ARB (1999).
- IMPROVE transmissometer measurements that were made when the hourly-average relative humidity exceeded 90% were deleted to avoid periods of fog or precipitation.

**Table 2-1
Summary of Data Availability by Site**

Air Basin	Location	Elevation (meters)	Operator	Period Covered		
				b _{ext}	b _{sp} and COH	Particulate Matter ^b
North Coast	Redwood National Park ^a	232	IMPROVE			1988-1996
Northeast Plateau	Lassen Volcanic National Park ^a	1,798	IMPROVE			1988-1996
Lake County	Lakeport	408	Local		1985-1996	
Lake Tahoe	South Lake Tahoe	1,900	IMPROVE			1989-1996
Sacramento Valley	Arbuckle	43	Local		1985-1996	
	Chico	62	Local		1985-1996	
	Colusa	17	Local		1985-1996	
	Gridley	0	Local		1985-1996	
	Pleasant Grove	50	Local		1985-1996	
	Yuba City	20	Local		1985-1996	
San Francisco Bay	Point Reyes National Seashore ^a	38	IMPROVE			1988-1996
	San Jose	24	Local			1990-1996
San Joaquin Valley	Bakersfield	137	Local			1988-1996
	Fresno	91	Local			1988-1996
	Madera	60	Local			1989-1996
	Modesto	27	Local			1989-1996
	Stockton	19	Local		1985-1996	1989-1996
	Visalia	97	Local			1988-1996
Mountain Counties	Yosemite National Park ^a	1,615	IMPROVE	1989-1996		1988-1996
North Central Coast	Pinnacles National Monument ^a	317	IMPROVE	1988-1993		1988-1996
South Coast	Azusa	183	Local			1988-1996
	Long Beach	6	Local			1989-1996
	Riverside	250	Local			1988-1996
	San Geronio Wilderness Area ^a	1,712	IMPROVE	1989-1996		1988-1996
Southeast Desert	El Centro	0	Local			1988-1996
^a Federal Class I Area						
^b IMPROVE sites also measure b _{abs}						

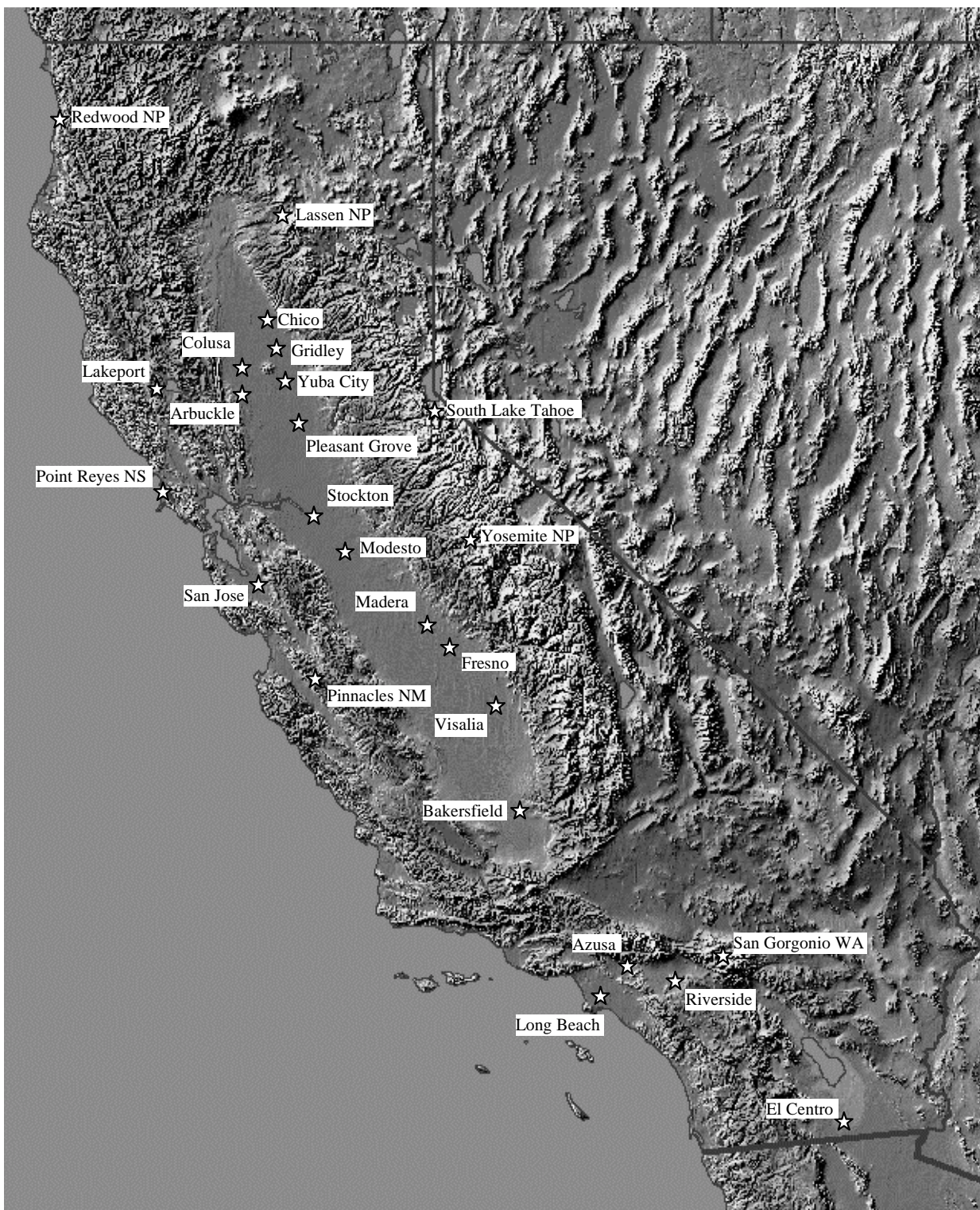


Figure 2-2 Monitoring Site Locations

- 24-hour averages (midnight-to-midnight) of the light scattering coefficient and coefficient of haze measured at local-agency sites and of the light extinction coefficient measured at IMPROVE sites were calculated.
- Medians and 20th and 80th percentiles of all of the 24-hour average data were calculated by season with all years combined, and medians were calculated by season during each year. Winter was defined as December, January and February, spring as March-May, summer as June-August and fall as September-November. December of a year was considered to be part of winter of the following year. Medians by season within each year were not calculated when fewer than half the possible values were available in order to reduce biases caused by non-uniform measurements.

Additionally, as mentioned previously, seasonal average light scattering and extinction coefficients were calculated from IMPROVE particle light absorption coefficient and particulate matter data following the approach described by Sisler et al. (1996). The seasonal average light scattering coefficient is given by:

$$b_{sp} = 3 f(RH) [(NH_4)_2SO_4] + 3 f(RH) [NH_4NO_3] + 4 [OMC] + [FINE SOIL] + 0.6 [CM] \quad (1)$$

where:

b_{sp}	= seasonal average particle scattering coefficient (Mm^{-1})
RH	= seasonal average relative humidity (%)
f(RH)	= function to account for effect of RH on dry scattering efficiency = $T_0 + T_2[100/(100-RH)]^2 + T_3[100/(100-RH)]^3 + T_4[100/(100-RH)]^4$
T_0, T_2, T_3, T_4	= seasonal coefficients in Table 2-2
$[(NH_4)_2SO_4]$	= estimated seasonal average $PM_{2.5}$ ammonium sulfate ($\mu g/m^3$) = $4.125[S]$
[S]	= seasonal average $PM_{2.5}$ sulfur concentration ($\mu g/m^3$)
$[NH_4NO_3]$	= estimated seasonal average $PM_{2.5}$ ammonium nitrate ($\mu g/m^3$) = $1.29[NO_3]$
$[NO_3]$	= seasonal average $PM_{2.5}$ nitrate ion concentration ($\mu g/m^3$)
[OMC]	= estimated seasonal average $PM_{2.5}$ organic mass from carbon ($\mu g/m^3$) = $1.4[OC]$
[OC]	= seasonal average $PM_{2.5}$ organic carbon concentration ($\mu g/m^3$)
[FINE SOIL]	= estimated seasonal average fine soil mass ($\mu g/m^3$) = $2.2[Al] + 2.19[Si] + 1.63[Ca] + 2.42[Fe] + 1.94[Ti]$
[Al]	= seasonal average $PM_{2.5}$ aluminum concentration ($\mu g/m^3$)
[Si]	= seasonal average $PM_{2.5}$ silicon concentration ($\mu g/m^3$)
[Ca]	= seasonal average $PM_{2.5}$ calcium concentration ($\mu g/m^3$)
[Fe]	= seasonal average $PM_{2.5}$ iron concentration ($\mu g/m^3$)

[Ti] = seasonal average PM_{2.5} titanium concentration (µg/m³)
 [CM] = seasonal average coarse mass concentration (µg/m³)

Table 2-2
Coefficients of Seasonal Relative Humidity Function

(from Sisler et al., 1996)

Season	T ₀	T ₂	T ₃	T ₄
Spring	0.755444191	0.309123730	-0.004452367	-0.004452367
Summer	0.510759769	0.465726914	-0.081099333	0.004250618
Fall	-0.026943445	0.828440163	-0.195533654	0.014109026
Winter	1.188625964	0.286931211	-0.033208114	0.001144830

Seasonal average relative humidity values, listed in Table 2-3, were taken from Sisler et al (1996). A single value was used for all years at each site, so the resulting calculations do not reflect year-to-year changes in average relative humidity. This reduces the correspondence to the values of the light scattering and extinction coefficients that actually occurred each year.

Table 2-3
Seasonal Average Relative Humidities Used for Calculating Light Scattering at IMPROVE Sites

Site	Seasonal Average Relative Humidity (percent)			
	Spring	Summer	Fall	Winter
Lassen Volcanic National Park	67	71	55	66
Pinnacles National Monument	73	72	71	75
Point Reyes National Seashore	73	72	71	75
Redwood National Park	73	72	71	75
San Geronio Wilderness Area	55	45	41	51
South Lake Tahoe	53	42	48	57
Yosemite National Park	63	44	45	56

Calculated and measured seasonal average extinction coefficients are compared in Figure 2-3 through Figure 2-5 for the three sites where transmissometer measurements were made (Pinnacles National Monument, San Geronio Wilderness Area and Yosemite National Park). The values in the figures are averages during each season over all years for which data were available.

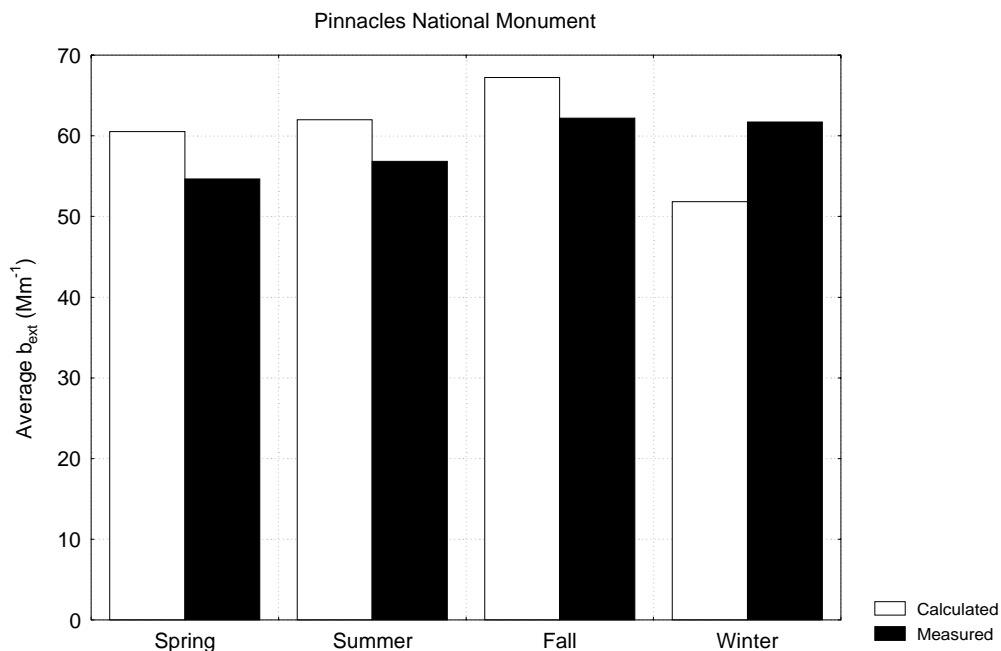


Figure 2-3 Comparison of Calculated and Measured Seasonal Average Light Extinction Coefficients Averaged Over All Years at Pinnacles National Monument

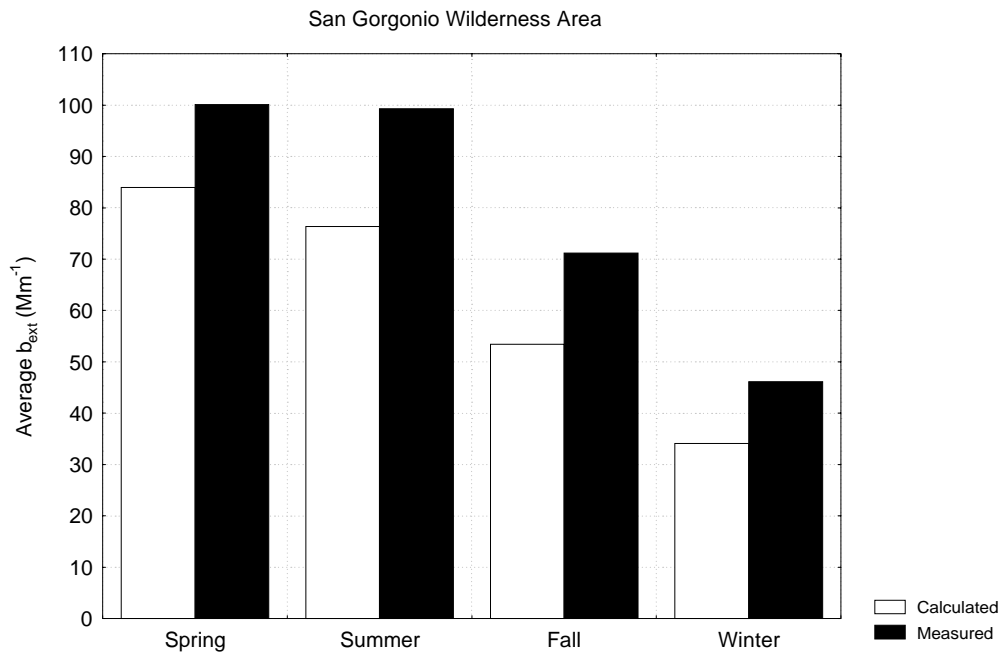


Figure 2-4 Comparison of Calculated and Measured Seasonal Average Light Extinction Coefficients Averaged Over All Years at San Gorgonio Wilderness Area

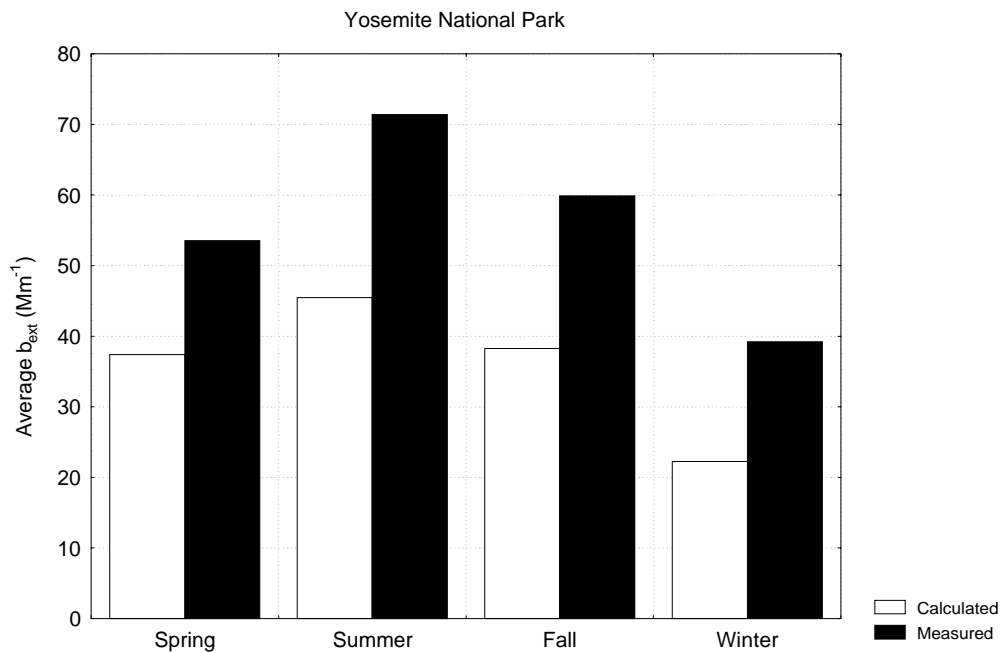


Figure 2-5 Comparison of Calculated and Measured Seasonal Average Light Extinction Coefficients Averaged Over All Years at Yosemite National Park

The agreement between calculated and measured values is best for Pinnacles National Monument and worst for Yosemite National Park. Calculated values are generally higher than the measured values for Pinnacles National Monument and lower than the measured values for San Geronio Wilderness Area and Yosemite National Park.

Several factors may contribute to the differences between the calculated and measured values, including: (1) inaccuracies in the model used to calculate the light scattering coefficient (Equation 1); (2) the use of twice-per-week particulate matter samples to estimate seasonal average chemical composition and particle light absorption; (3) uncertainties in the particulate matter measurements; (4) uncertainties in the transmissometer measurements; and (5) differences between actual relative humidity values and the "typical" values used in the calculations. Thus, relatively small differences in the calculated light scattering or extinction coefficients between sites or time periods may not be indicative of actual differences in the coefficients that would be measured.

3.0 CHARACTERISTICS OF OPTICAL AND PARTICULATE MATTER DATA

This section presents and discusses characteristics of the optical and particulate matter data. It begins with a description of geographic variations in California. This description is followed by presentations and discussions of characteristics within each air basin for which data were available. The data from all years were combined to produce “characteristic” geographic and seasonal distributions. Although a single year could have been selected for these analyses, the patterns that occurred during that year might not be representative of other years.

3.1 Geographic Patterns

The geographic distributions of the particle light scattering coefficient, $PM_{2.5}$ mass, $PM_{2.5}$ nitrate and sulfate at IMPROVE sites and PM_{10} nitrate and sulfate at local-agency sites are presented in a series of maps. Each map shows the median value during a season at each local-agency site and the average value at each IMPROVE site. Average values are presented at the IMPROVE sites, because the light extinction coefficient and contributions from various constituents were calculated using averages, rather than medians, as described in Section 2.2. Spring is defined as March-May, summer as June-August, fall as September-November and winter as December-February.

3.1.1 Geographic Patterns of Particle Light Scattering Coefficients

The geographic distributions of the particle light scattering coefficient (b_{sp}) during the four seasons are shown in Figure 3-1 through Figure 3-4. The values for the IMPROVE sites are seasonal average values calculated as described in Section 2.2, while the values at the other sites are seasonal medians of measured values.

During spring (Figure 3-1), the highest values occur at the Sacramento Valley and San Joaquin Valley sites and at San Geronio Wilderness Area (see Figure 2-2 for site locations). This relatively high value at San Geronio Wilderness Area, compared with the other IMPROVE sites, is probably caused by transport of particulate matter from the South Coast Air Basin. Values tend to be fairly uniform at the California Central Valley sites, although the values at the Yuba City site are substantially higher than the values at the other sites in the Sacramento Valley Air Basin. The lowest value is at Lassen Volcanic National Park. The values tend to increase from north to south at the western sites (Redwood National Park, Lakeport, Point Reyes National Seashore and Pinnacles National Monument). Values at South Lake Tahoe and Yosemite National Park are similar to the values at the northern western sites.

The geographic pattern during summer (Figure 3-2) is similar to the pattern during spring.

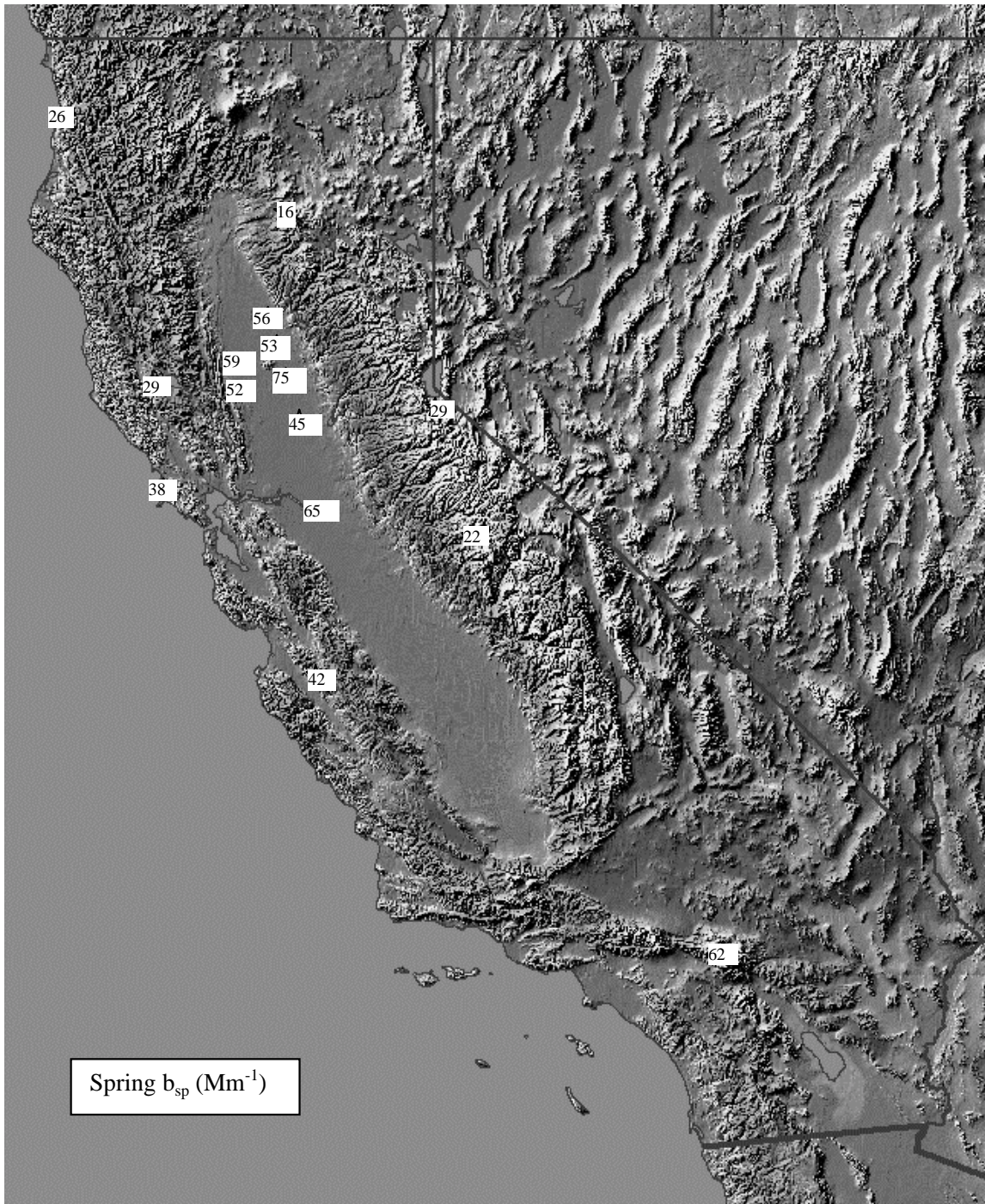


Figure 3-1 Geographic Distribution of b_{sp} during Spring

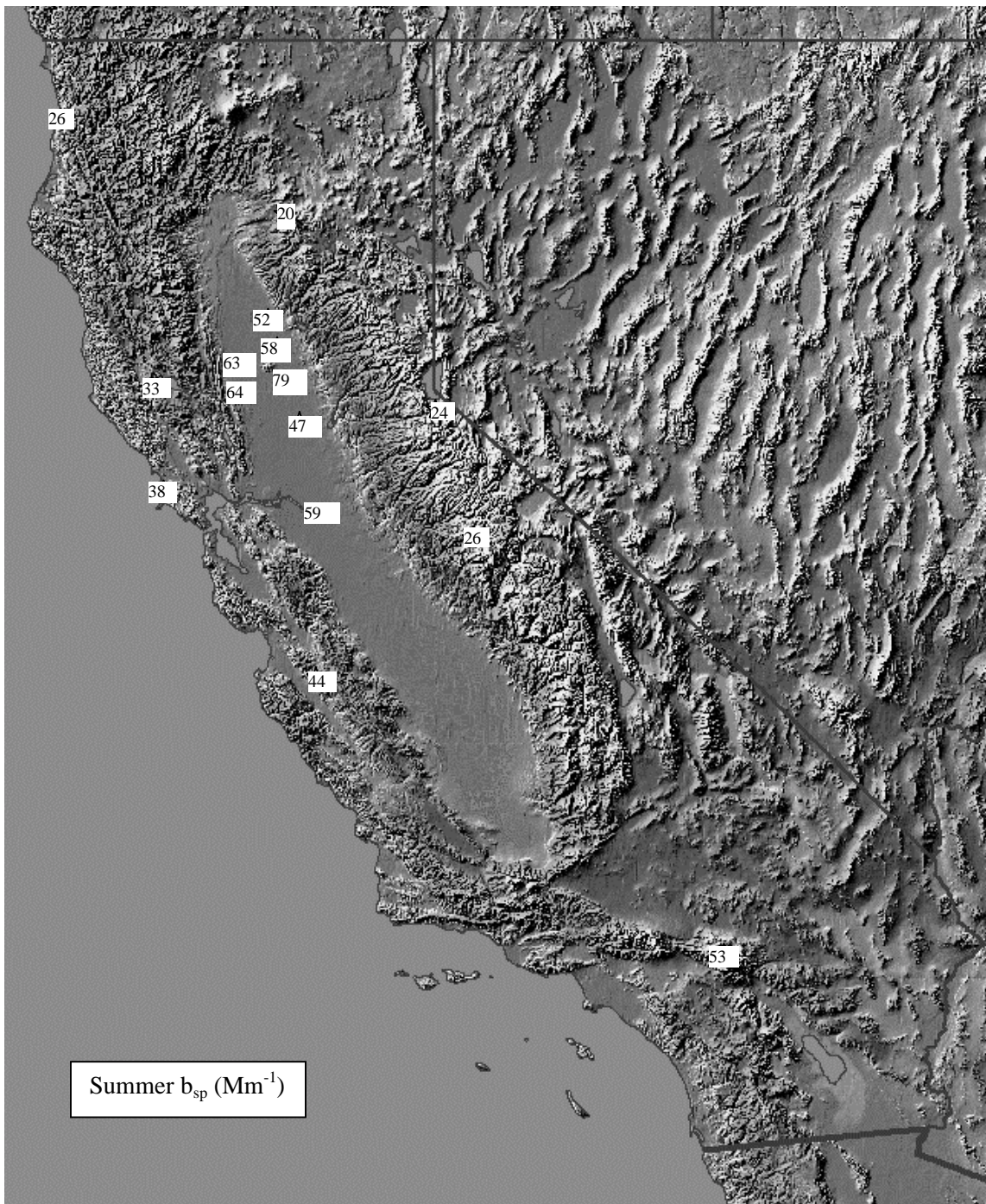


Figure 3-2 Geographic Distribution of b_{sp} during Summer

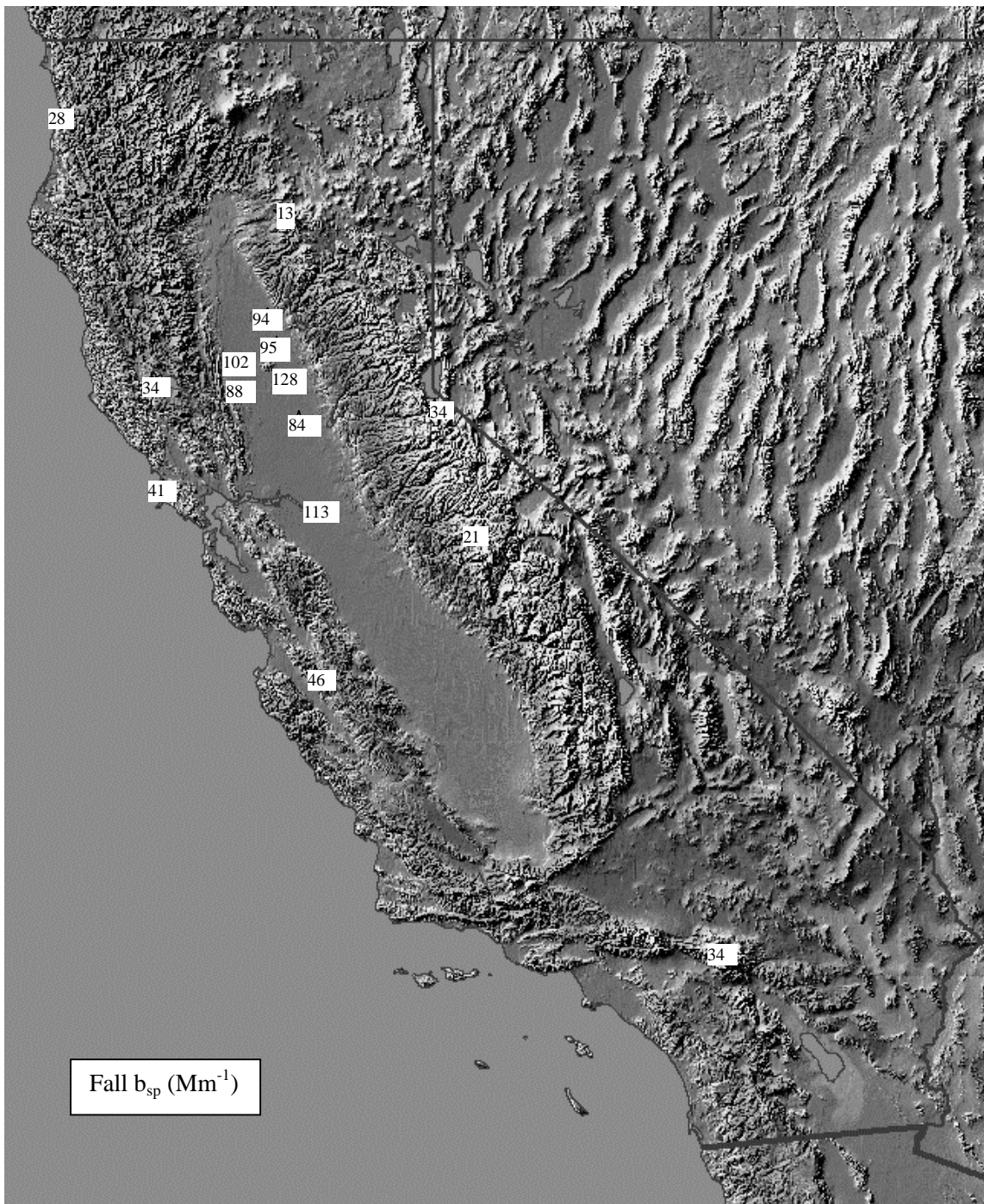


Figure 3-3 Geographic Distribution of b_{sp} during Fall

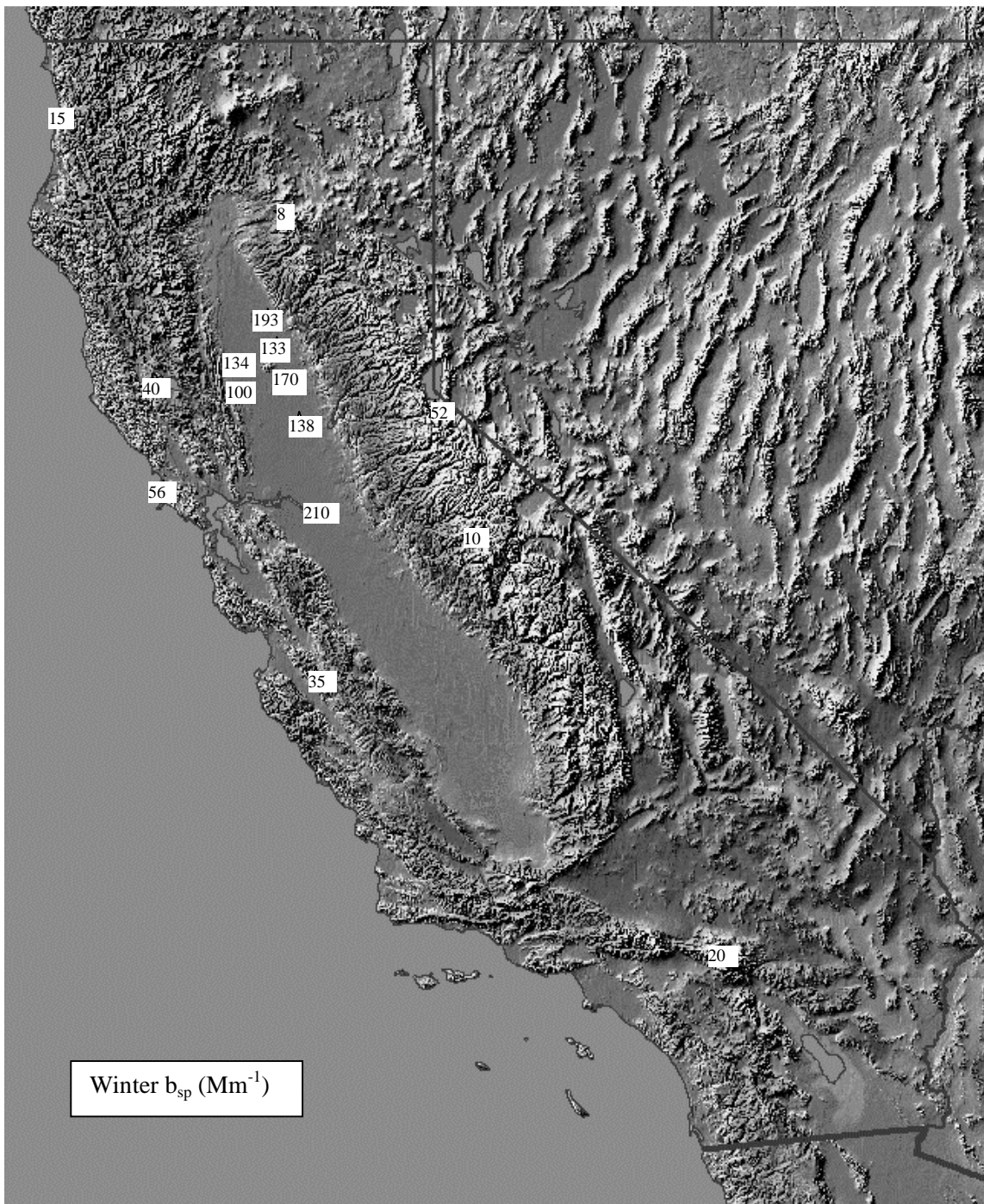


Figure 3-4 Geographic Distribution of b_{sp} during Winter

During fall (Figure 3-3), the values at the Central Valley sites are substantially higher than at any of the other sites. These high values are consistent with lower inversion heights and wind speed during the fall than during spring and summer, which lead to higher concentrations of emitted particulate matter. Lower temperatures than during spring and summer also promote the formation of particulate ammonium nitrate, and higher relative humidity causes hygroscopic particulate matter constituents to acquire liquid water, which increases light scattering. The value at San Geronio Wilderness Area during fall is comparable to the values at the northern western sites, such as Lakeport. This lower value at San Geronio Wilderness Area is probably caused by lower inversion heights in the South Coast Air Basin that are below the site's elevation of more than 1,700 m.

Values are much higher at the Sacramento Valley and San Joaquin Valley Air Basin sites than at the other sites during winter (Figure 3-4) as a result of low inversion heights and high relative humidity. The value at South Lake Tahoe is higher than values at the northern western sites. This higher value is caused by low inversion heights at that location during the winter.

3.1.2 Geographic Patterns of Particulate Matter Concentrations

Geographic distributions of seasonal PM_{2.5} mass concentrations are shown in Figure 3-5 through Figure 3-8.

During spring (Figure 3-5), concentrations tend to increase from north to south in the San Joaquin Valley Air Basin as well as from west to east in the South Coast Air Basin. Values at sites in the coastal air basins are similar to each other, although values at San Jose and Point Reyes National Seashore are somewhat higher than values at Redwood National Park and Pinnacles National Monument. The value at San Geronio Wilderness Area is about the same as at El Centro. The value at South Lake Tahoe is similar to the values in the coastal air basins, and the values at Lassen Volcanic and Yosemite National Parks are the lowest.

The geographic distribution during summer (Figure 3-6) is similar to the distribution during spring, although concentrations are generally higher than during spring, particularly at Yosemite National Park. This increase from spring to summer at Yosemite National Park may be caused by increased local emissions associated with park visitors and, possibly, with transport from the San Joaquin Valley promoted by the higher mixing heights associated with warm summer temperatures.

Differences among sites are greater during fall (Figure 3-7) than during spring and summer. Increases in concentrations from north to south in the San Joaquin Valley Air Basin and from west to east in the South Coast Air Basin are greater. Additionally, the value at San Jose is substantially higher than the value at the other coastal air basin sites, and the difference between San Geronio Wilderness Area and the South Coast Air Basin sites is greater. The higher value at San Jose is probably caused by lower mixing heights during fall than during spring and summer, and the lower

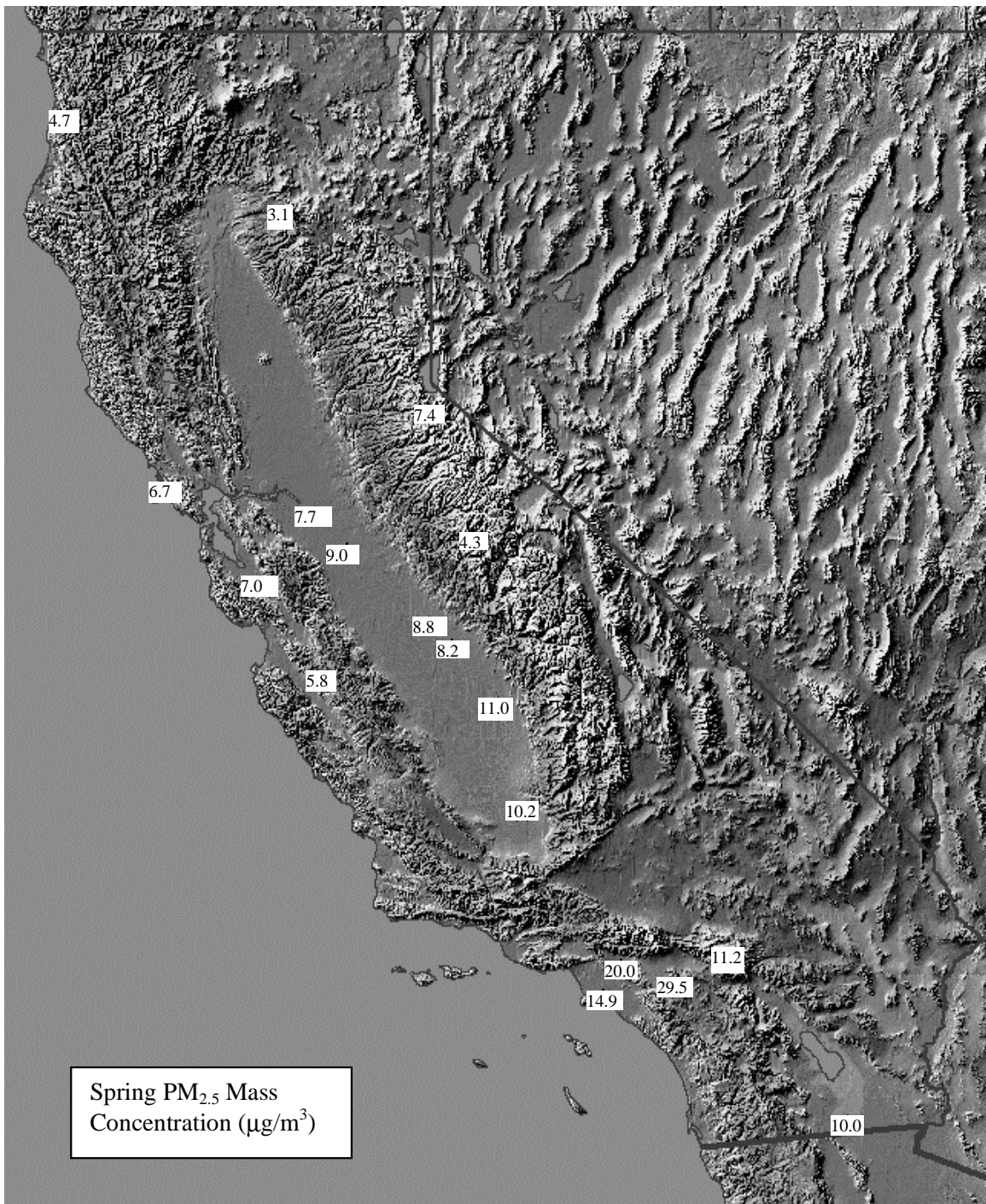


Figure 3-5 Geographic Distribution of PM_{2.5} Mass during Spring

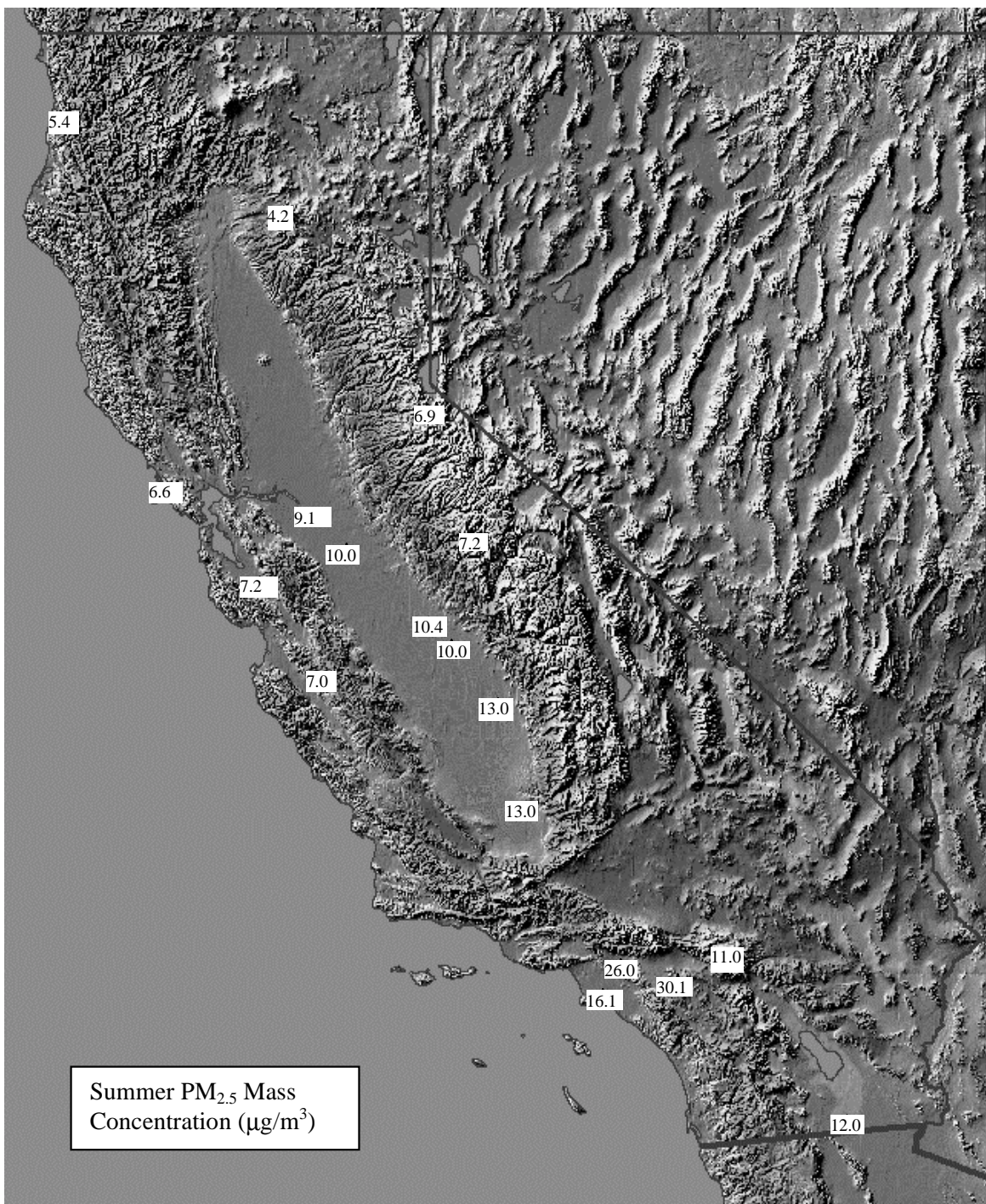


Figure 3-6 Geographic Distribution of PM_{2.5} Mass during Summer

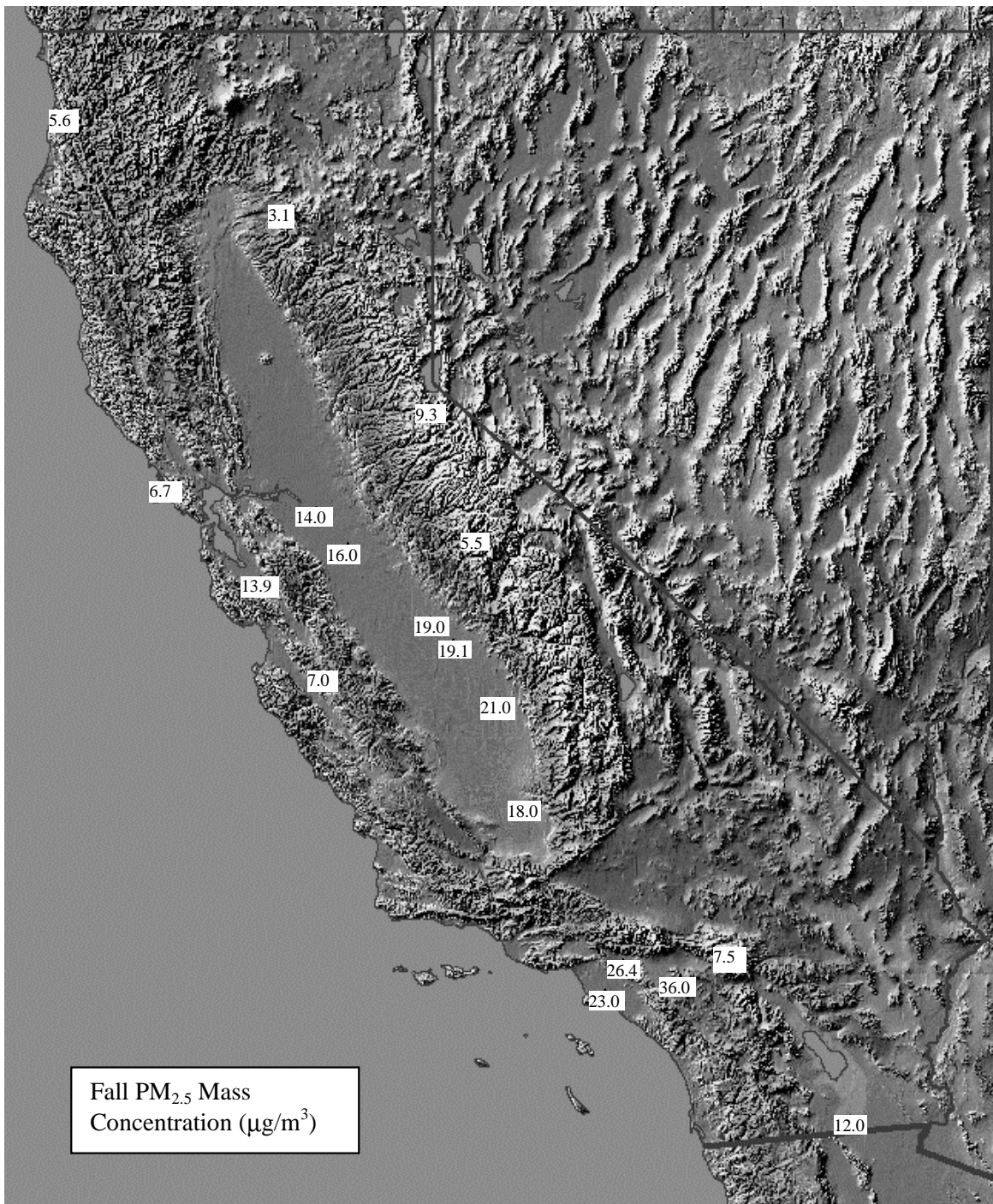


Figure 3-7 Geographic Distribution of PM_{2.5} Mass during Fall

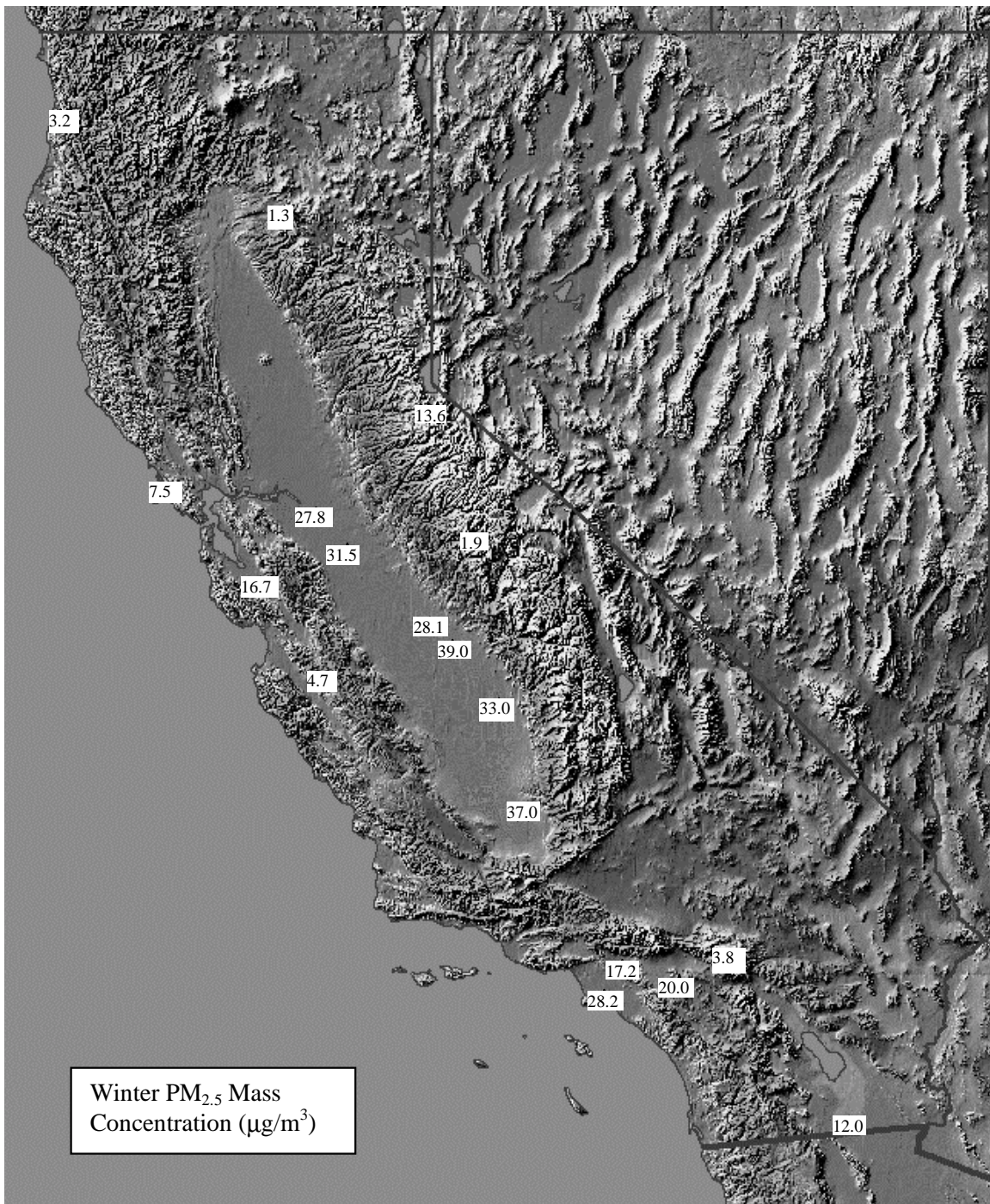


Figure 3-8 Geographic Distribution of PM_{2.5} Mass during Winter

value at San Geronio Wilderness area is indicative of decreased transport from the South Coast Air Basin.

During winter (Figure 3-8), $PM_{2.5}$ concentrations in the San Joaquin Valley Air Basin are higher than anywhere else and the highest anywhere during the entire year. The value at Long Beach is higher than at the other South Coast Air Basin sites, in contrast with the other seasons, when it was the lowest, and the value at San Geronio Wilderness Area is much lower than at the South Coast Air Basin sites. San Jose is substantially higher than other coastal air basin sites. Values at San Geronio Wilderness Area, Lassen Volcanic National Park, Yosemite National Park and Redwood National are substantially lower than at the other sites.

Geographic distributions of nitrate concentrations are shown in Figure 3-9 through Figure 3-12. The values at the IMPROVE sites are average measured $PM_{2.5}$ concentrations, while the values at other sites are medians of measured PM_{10} concentrations. Note that the IMPROVE $PM_{2.5}$ nitrate concentration measurements may not be equivalent to the PM_{10} nitrate concentration measurements, as noted in Section 2.1.

During spring and summer (Figure 3-9 and Figure 3-10), nitrate concentrations are generally low, except at Riverside, in the South Coast Air Basin, and values are extremely low at most of the IMPROVE sites. The high value at Riverside is caused by the predominant east-to-west transport combined with high ammonia emissions from cattle feed lots between it and the other two sites in the South Coast Air Basin. These ammonia emissions promote the formation of particulate ammonium nitrate.

During fall (Figure 3-11), nitrate concentrations in the San Joaquin Valley Air Basin generally increase from north to south and are higher than the coastal air basin sites, except San Jose, and the northern and mountain sites. Additionally, Riverside is substantially higher than the other South Coast Air Basin sites.

During winter (Figure 3-12) nitrate concentrations are much higher in the San Joaquin Valley Air Basin than anywhere else with an increase from north to south, while concentrations in the South Coast Air Basin are fairly uniform. The large concentrations in the San Joaquin Valley Air Basin are caused by stagnant conditions, low temperatures, high relative humidity and ammonia emissions, all of which promote formation of particulate ammonium nitrate.

Geographic distributions of sulfate concentrations are shown in Figure 3-13 through Figure 3-16. Values at the IMPROVE sites were calculated by multiplying average measured $PM_{2.5}$ sulfur concentrations by three to account for the oxygen associated with sulfate, while the values at the other sites are medians of measured PM_{10} sulfate concentrations.

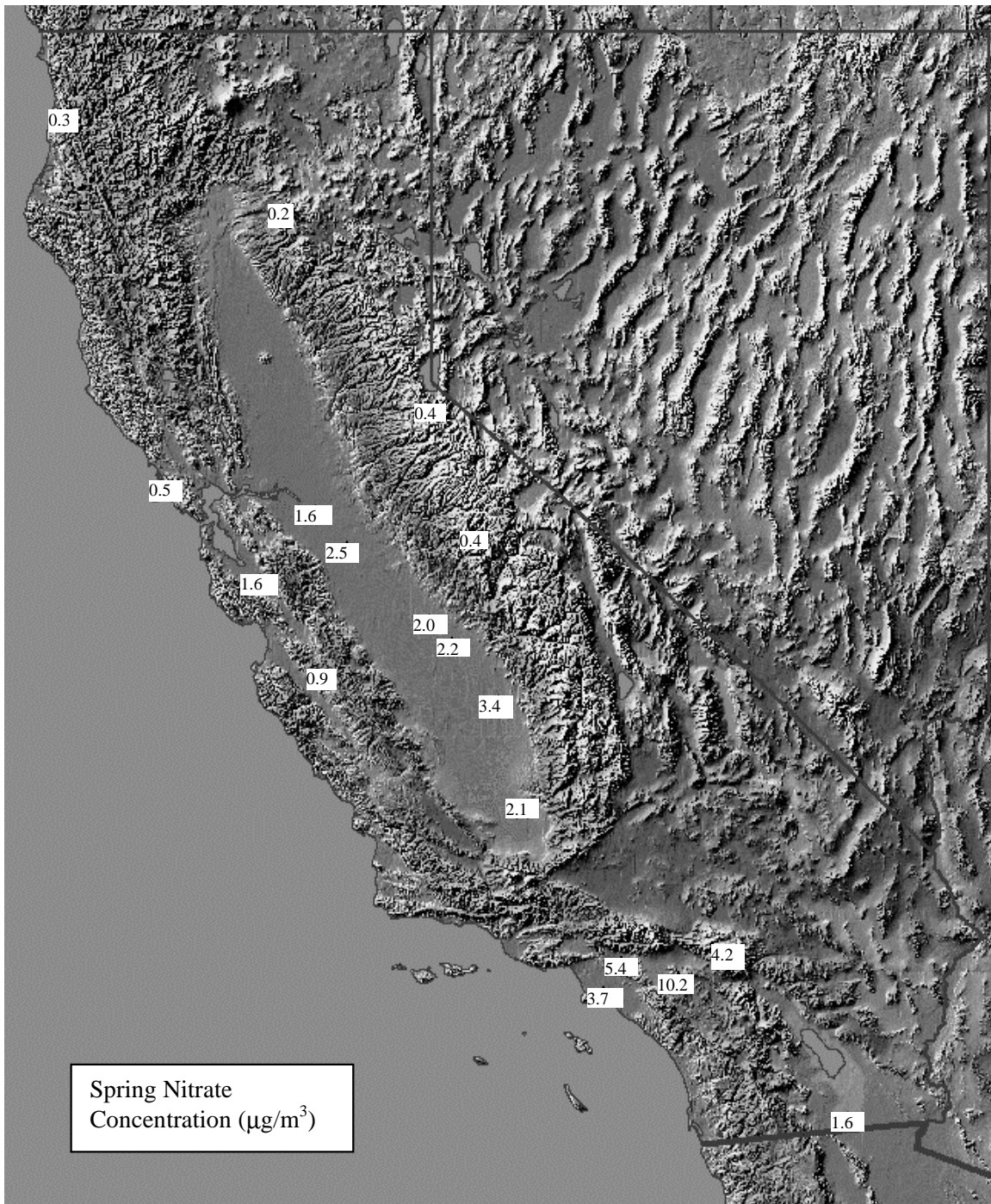


Figure 3-9 Geographic Distribution of Nitrate Mass during Spring

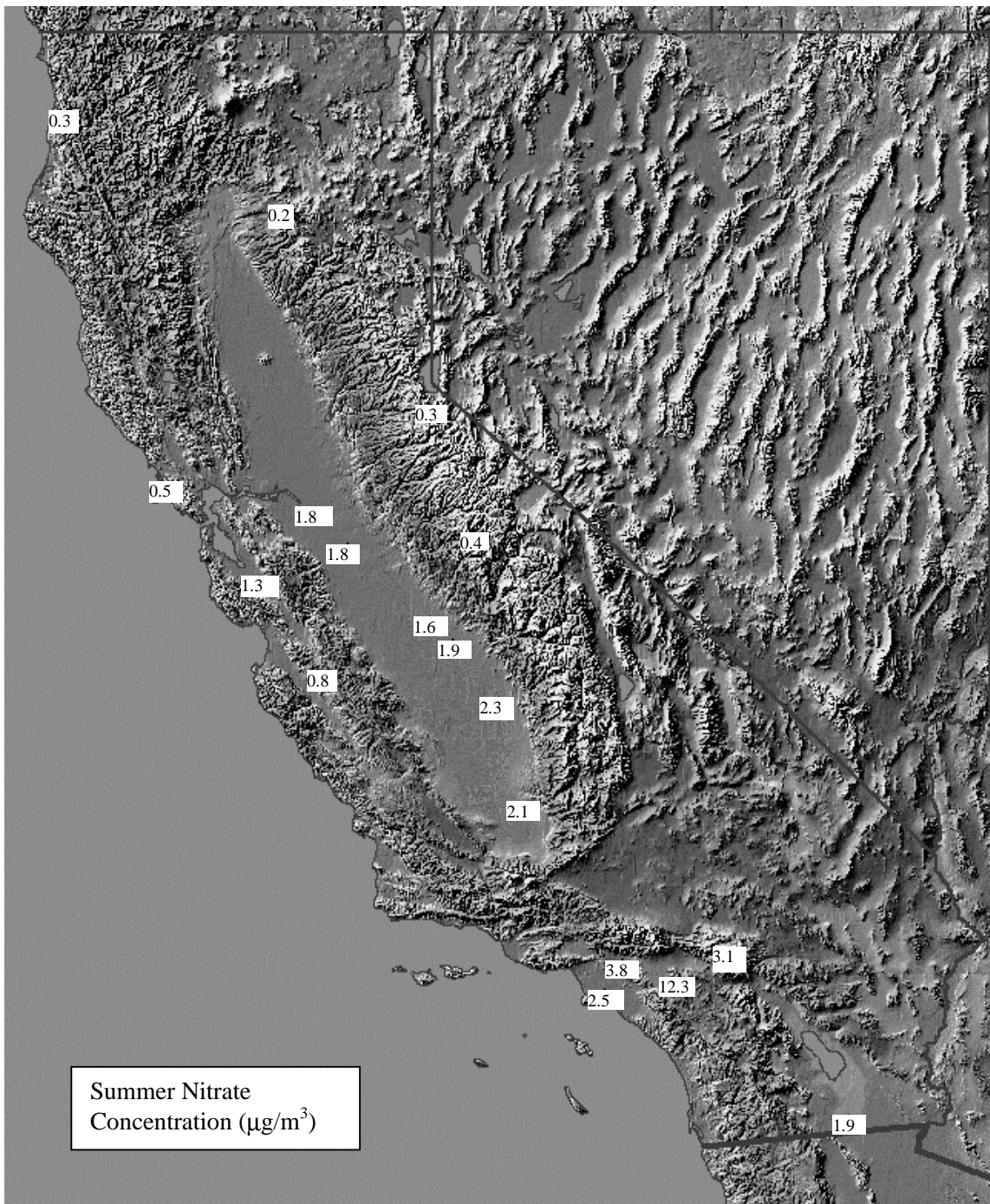


Figure 3-10 Geographic Distribution of Nitrate Mass during Summer

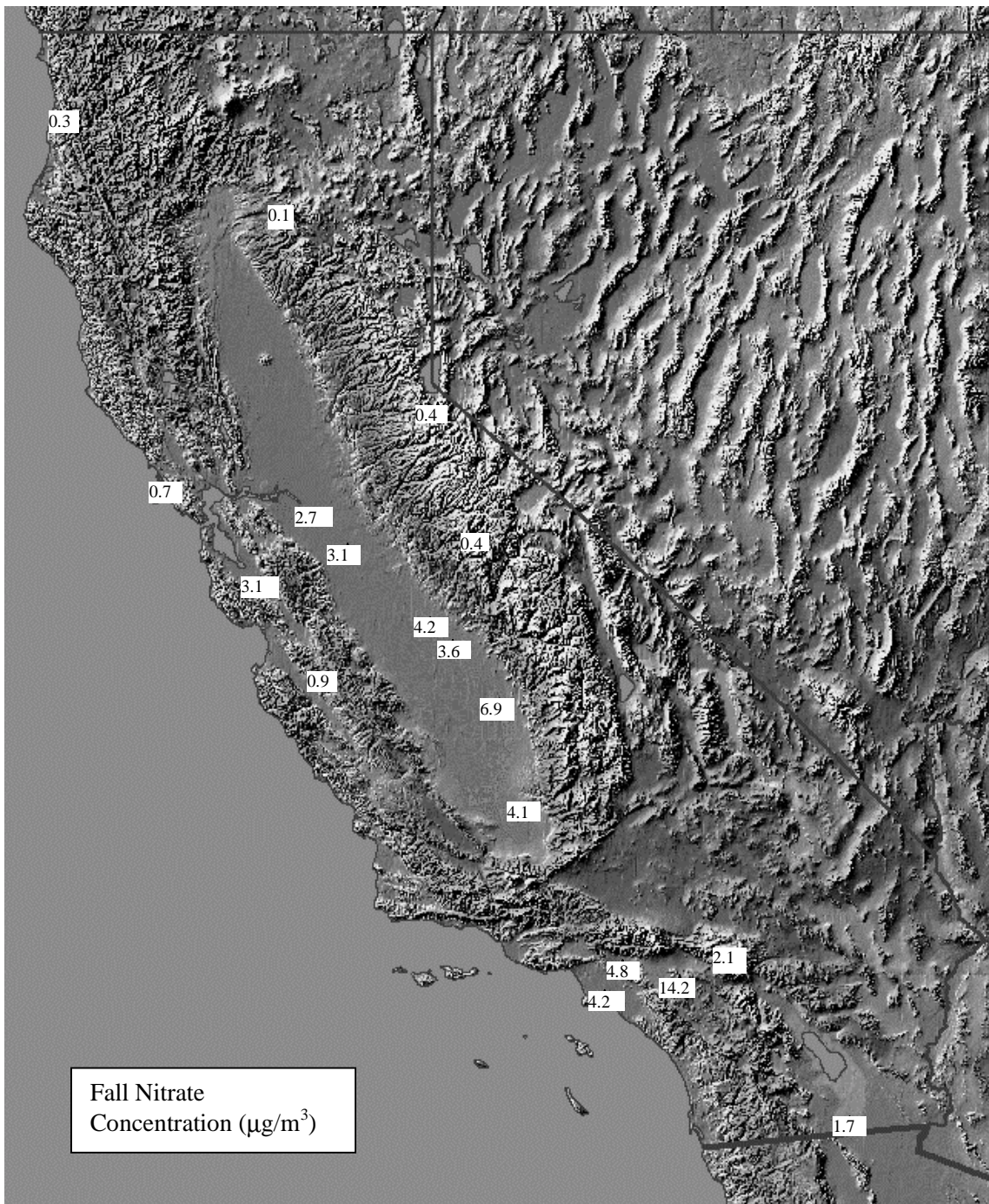


Figure 3-11 Geographic Distribution of Nitrate Mass during Fall

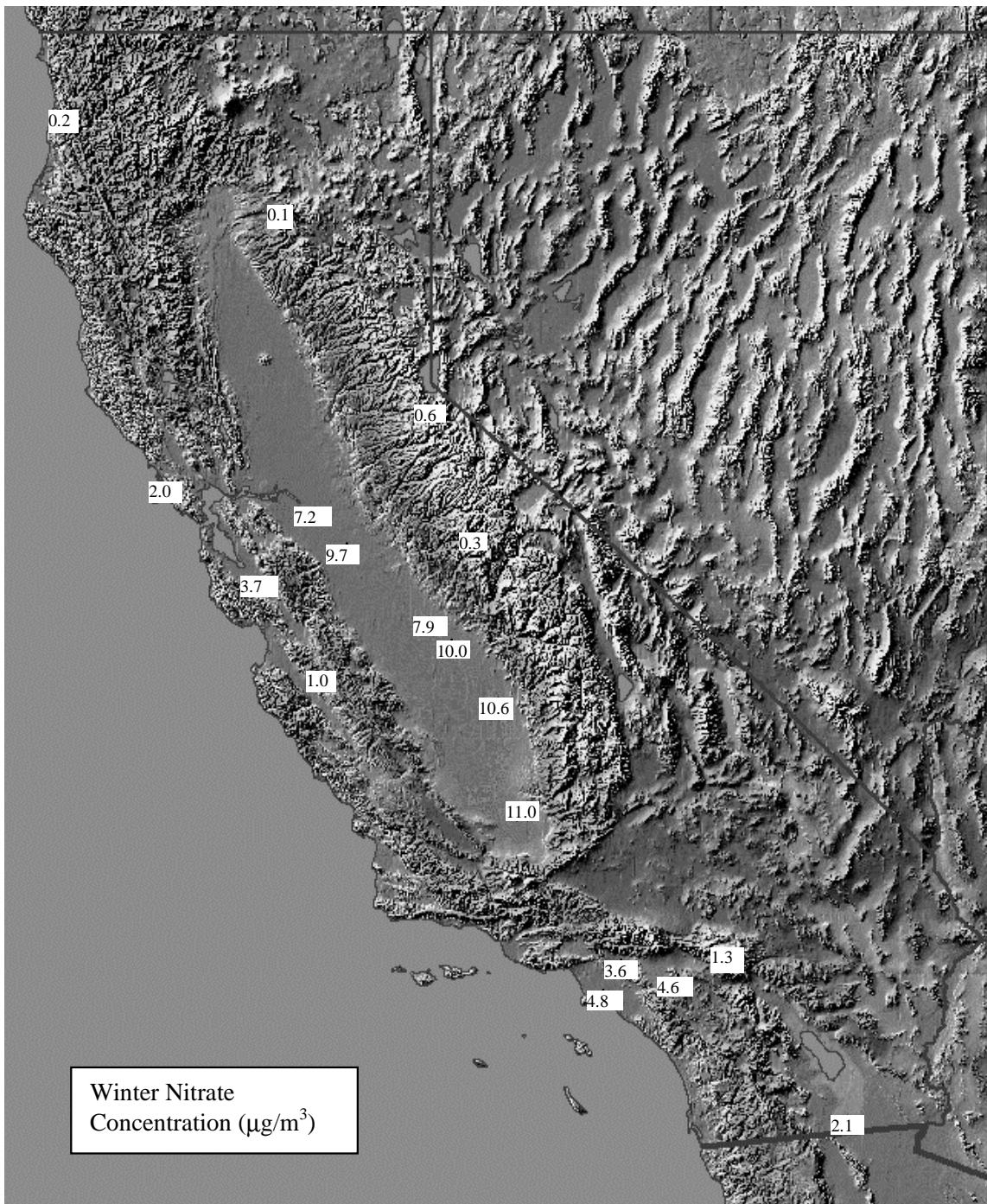


Figure 3-12 Geographic Distribution of Nitrate Mass during Winter

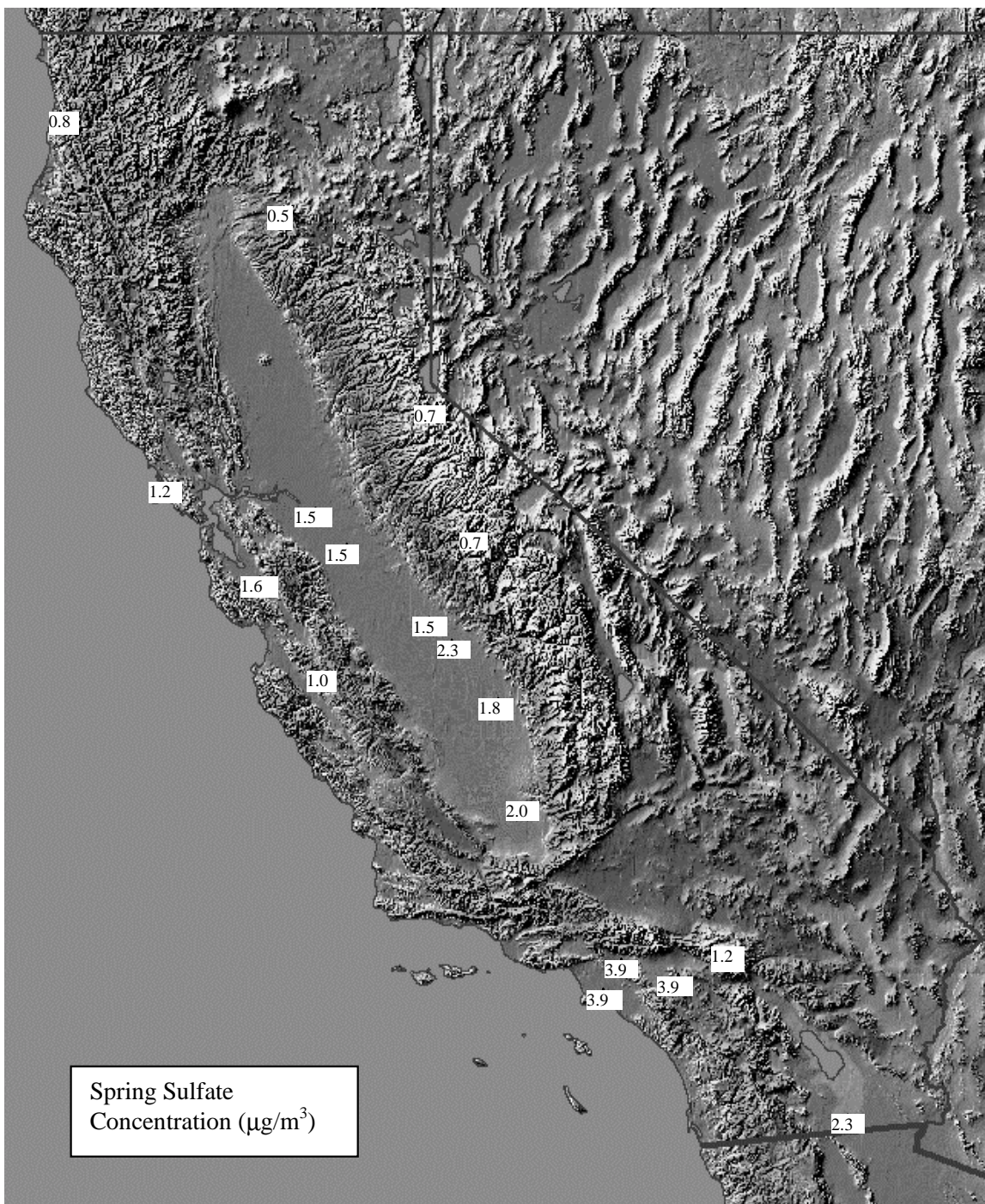


Figure 3-13 Geographic Distribution of Sulfate Mass during Spring

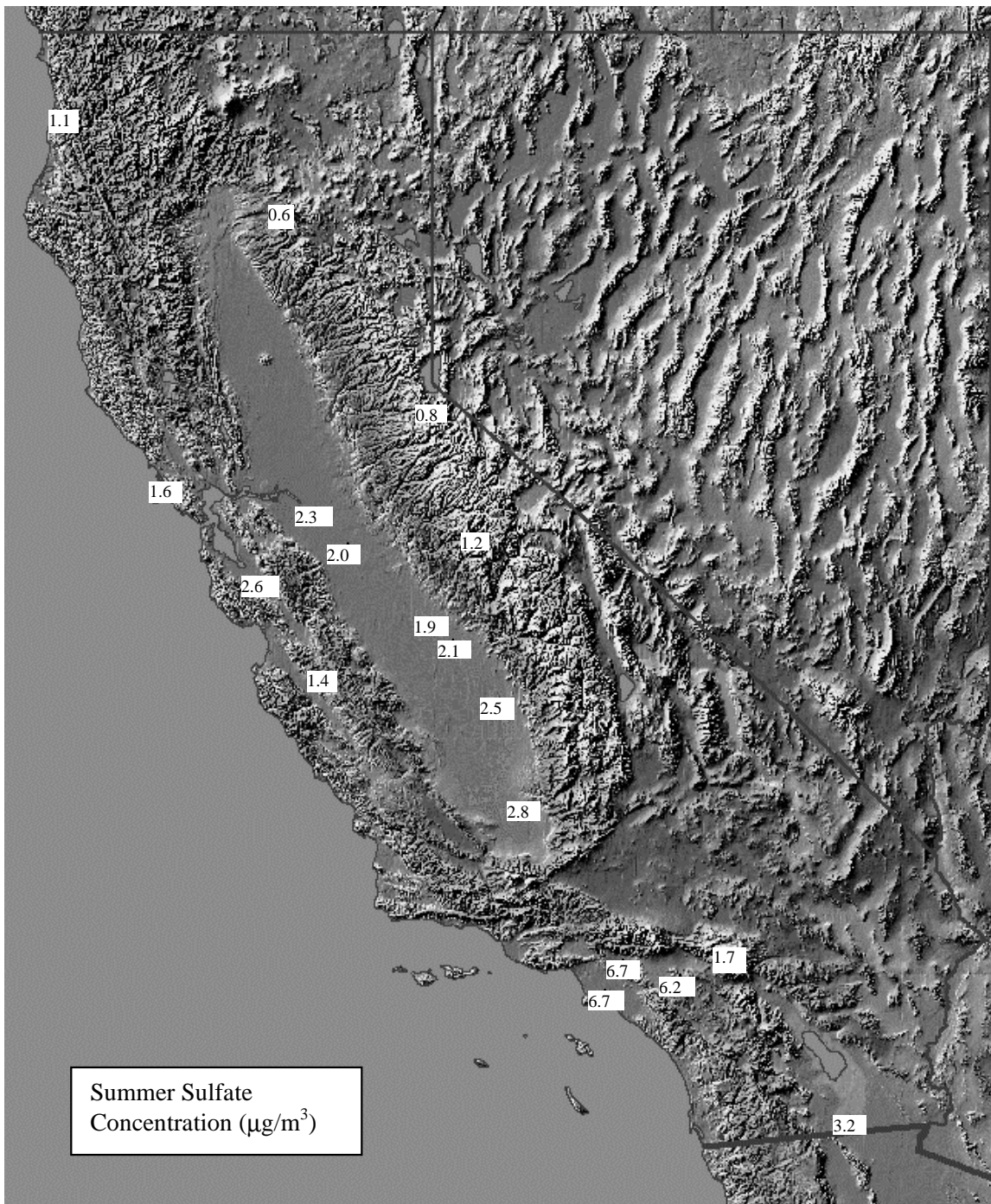


Figure 3-14 Geographic Distribution of Sulfate Mass during Summer

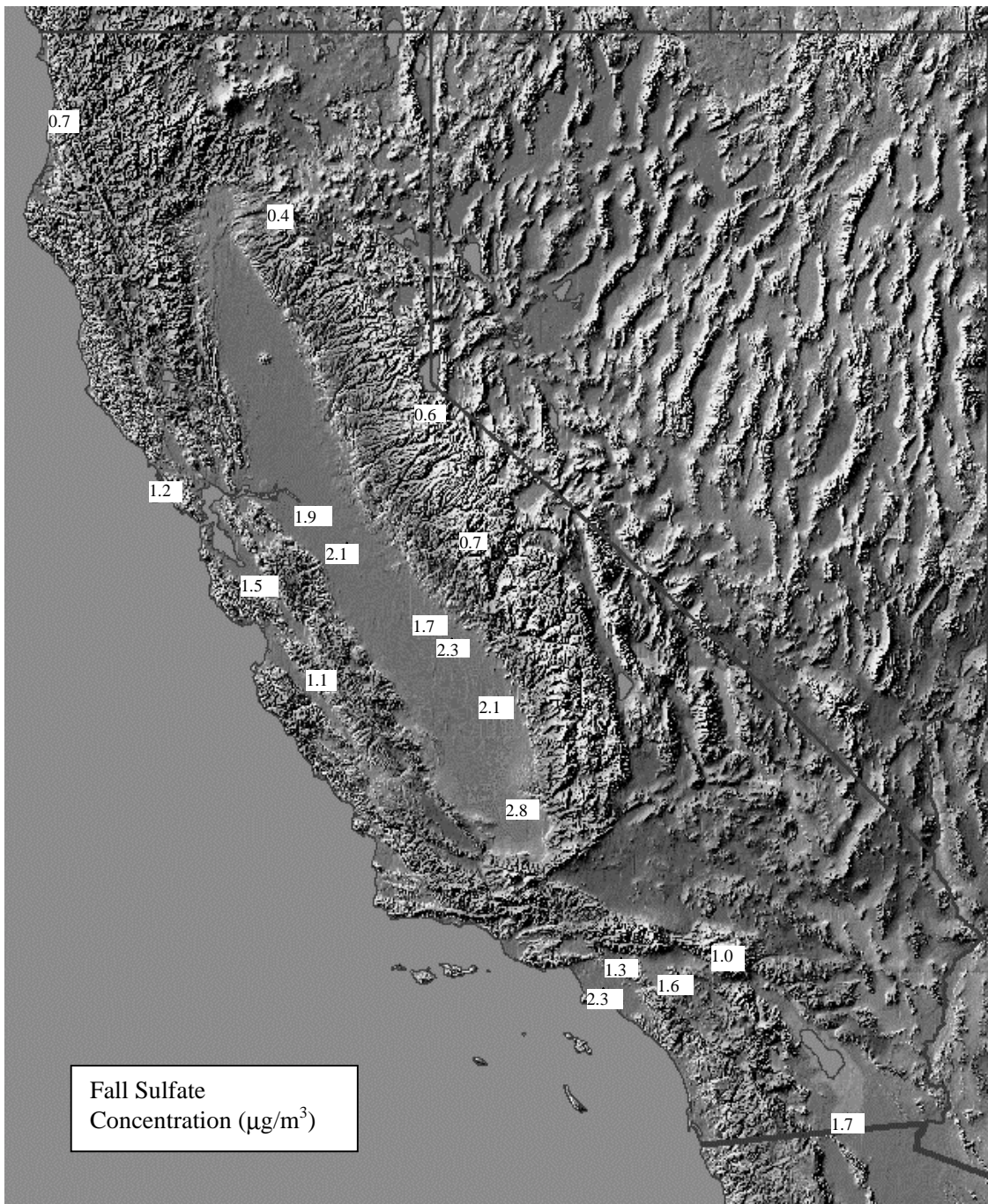


Figure 3-15 Geographic Distribution of Sulfate Mass during Fall

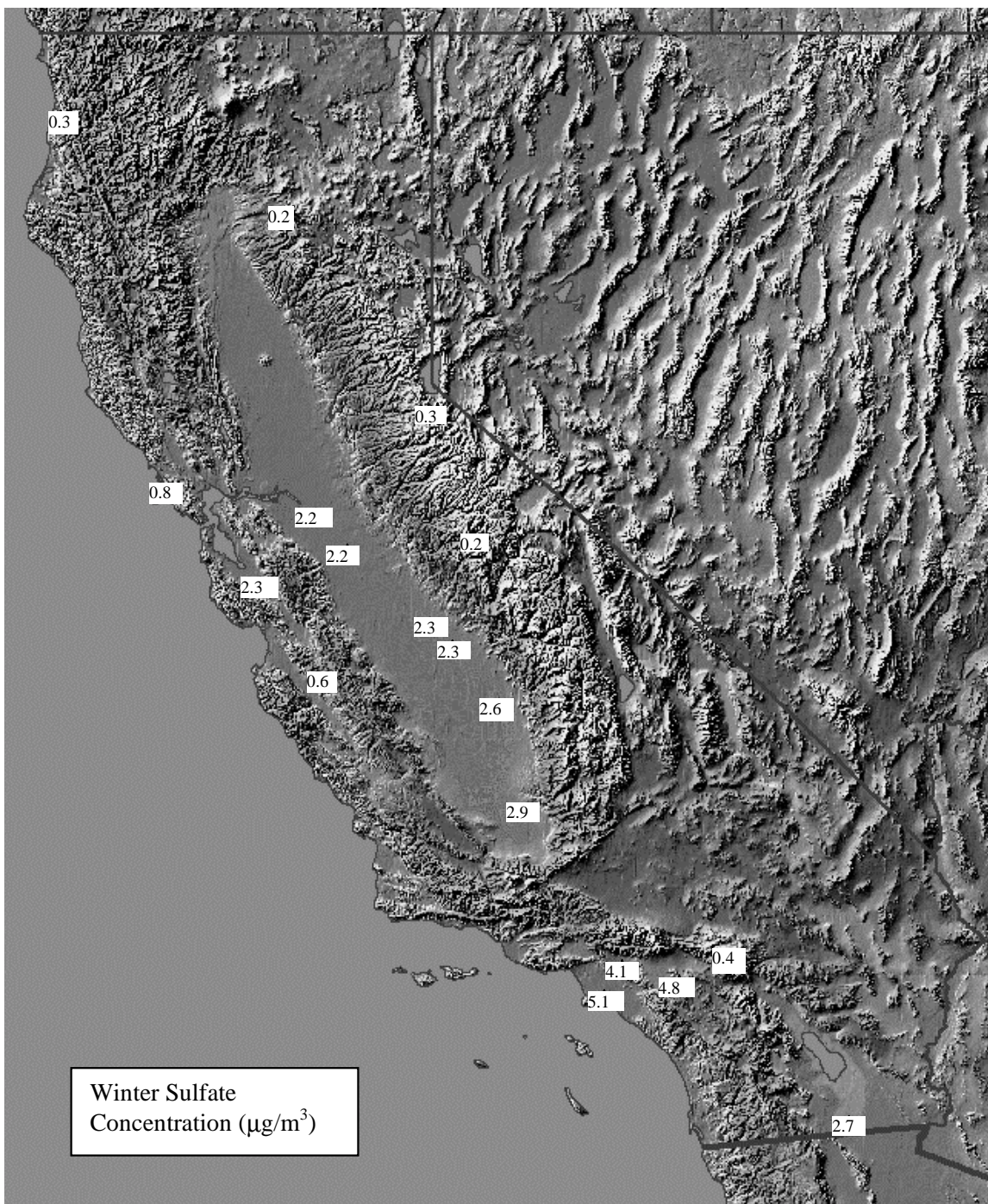


Figure 3-16 Geographic Distribution of Sulfate Mass during Winter

The geographic distributions are similar during all four seasons, with concentrations in the South Coast Air Basin fairly uniform and higher than at other sites, and with concentrations in the San Joaquin Valley Air Basin fairly uniform and somewhat lower than in the South Coast Air Basin. The exception is during fall (Figure 3-15), when concentrations in the San Joaquin Valley Air Basin are similar to concentrations in the South Coast Air Basin. Concentrations at San Jose tend to be close to the concentrations in the San Joaquin Valley Air Basin.

3.2 Characteristics by Air Basin

Several types of graphs were prepared to display characteristics of the optical and particulate matter data at each site:

- “Whisker” plots showing the median and 20th and 80th percentiles of measured optical properties and PM_{2.5} mass concentration
- Bar charts showing median seasonal concentrations (seasonal averages at IMPROVE sites) of PM_{2.5} mass and its constituents
- Bar charts showing the seasonal average calculated light extinction coefficient and its constituents at IMPROVE sites

Nitrate concentrations are expressed as ammonium nitrate (calculated by multiplying measured nitrate by 1.29 to account for ammonium), and sulfate concentrations are expressed as ammonium sulfate (calculated by multiplying sulfur measured at IMPROVE sites by 4.125 and sulfate measured at local-agency sites by 1.375 to account for ammonium). Although it has not been established that all sulfur and sulfate are present exclusively as ammonium sulfate, the relatively high ammonia emission rates in many parts of California, such as the Sacramento and San Joaquin Valleys and the South Coast Air Basin, should provide adequate atmospheric ammonia to react with all of the sulfate. It is possible that some of the sulfate at other locations may not be present as ammonium sulfate.

Additionally, as mentioned in Section 2.1, the nitrate measurements at local-agency sites are probably lower bounds, because some of the nitrate may have been lost from the filter samples by volatilization.

3.2.1 North Coast Air Basin

Redwood National Park is located on the Pacific coast in the North Coast Air Basin.

Seasonal median and 20th and 80th percentile values of the particle light absorption coefficient (b_{abs}) are shown in Figure 3-17. These values do not vary much with season, with the exception of fall, when the median and 80th percentile are substantially higher than during the other three seasons and during winter, when the 20th percentile is somewhat lower than during other seasons. Low values occur

during all seasons, as indicated by the 20th percentile values. This is because periods of substantial atmospheric dispersion occur throughout the year, leading to larger differences between the 80th and 20th percentiles during seasons when high values also occur. The higher values during the fall may be associated with residential wood burning, while the lower values during the winter are probably associated with storms.

Seasonal median and 20th and 80th percentiles of PM_{2.5} mass concentration are shown in Figure 3-18. In contrast with the particle light absorption coefficient, the highest 80th percentile value occurs during summer, although the values during fall are similar to the values during summer. The lowest values occur during winter.

Estimated seasonal average concentrations of PM_{2.5} constituents are shown in Figure 3-19. Concentrations of ammonium sulfate, ammonium nitrate and organic mass from carbon (OMC) were calculated as described in Section 2.2, while elemental carbon (EC) was measured directly. The bar labeled "Difference" is the difference between the measured PM_{2.5} mass concentration and the sum of the constituents that are shown. This difference is substantial during all seasons. However, it can largely be accounted for by sodium chloride from sea salt. Although sodium chloride is not shown in the figure, the average concentration during each season was estimated by multiplying the average measured chloride concentration by 1.65 to account for the associated sodium. The resulting estimated sodium chloride concentrations during spring, summer, fall and winter are 1.1 µg/m³, 1.2 µg/m³, 0.6 µg/m³, and 0.7 µg/m³, respectively. These amounts account for substantial fractions of the "Difference" values in the figure.

Ammonium sulfate, EC+OMC and sodium chloride are the major constituents during spring and summer, while EC+OMC is the largest constituent during fall and winter. This increase in EC+OMC during the cooler seasons is consistent with a possible contribution from residential wood combustion. The large increase in EC+OMC during fall parallels the increase in b_{abs} .

Calculated seasonal average values of the light extinction coefficient (b_{ext}) and its constituents are shown in Figure 3-20. The bars labeled "Amm. Nitrate," "Amm. Sulfate," "Organic Cmpds." and "Soil" represent estimated light scattering by ammonium nitrate, ammonium sulfate, OMC and the sum of fine soil and coarse mass, respectively. Light scattering by sodium chloride was not estimated, so the total light extinction coefficient is likely underestimated. Light scattering by ammonium sulfate is estimated to be the largest contributor during all seasons except winter, when light scattering by air molecules (Rayleigh scattering) is larger. Light scattering by organic compounds is estimated to be a major contributor during the fall. Although the average estimated EC+ OMC concentration is much larger than the estimated ammonium sulfate concentration during the fall, the high relative humidity increases the light scattering estimated for ammonium sulfate relative to the estimate for OMC.

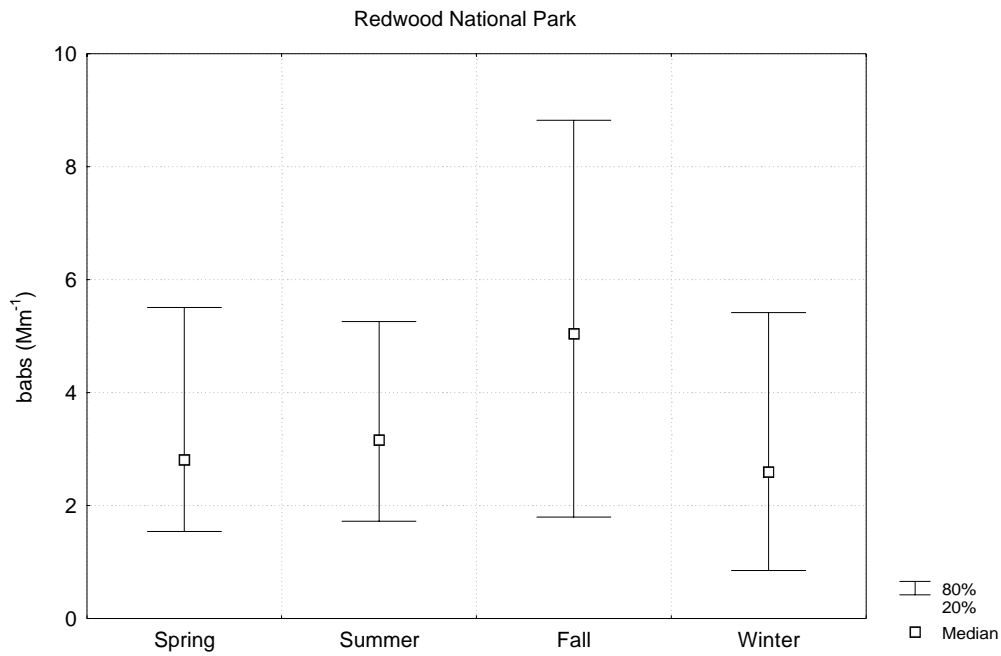


Figure 3-17 Seasonal Median and 20th and 80th Percentiles of the Particle Light Absorption Coefficient at Redwood National Park

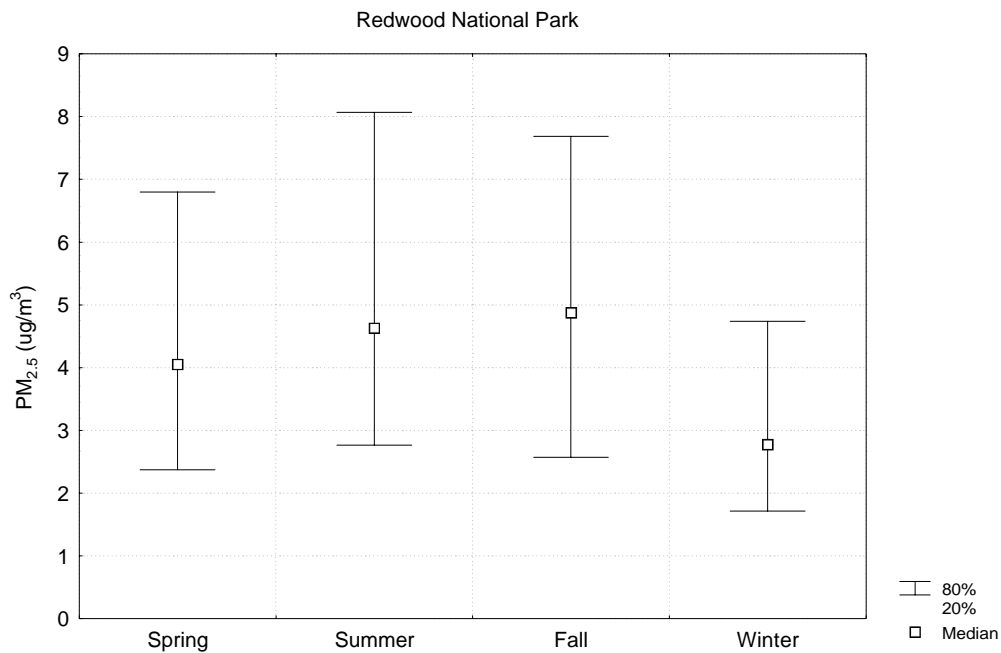


Figure 3-18 Seasonal Median and 20th and 80th Percentiles of PM_{2.5} Mass Concentration at Redwood National Park

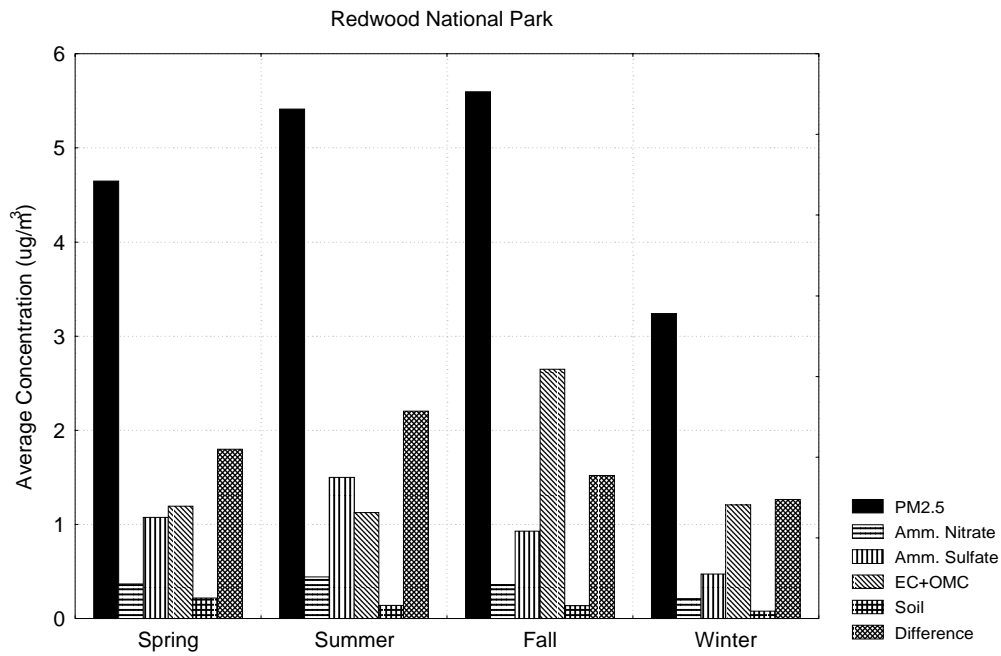


Figure 3-19 Seasonal Average PM_{2.5} Mass and Estimated Chemical Constituent Concentrations at Redwood National Park

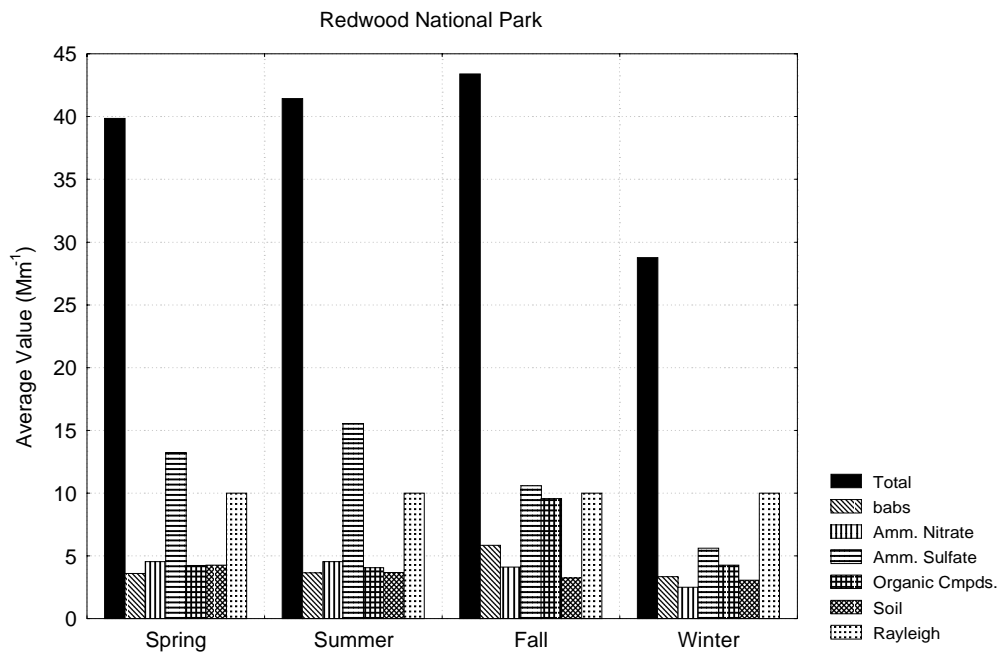


Figure 3-20 Contributions to Calculated Seasonal Average Light Extinction Coefficient at Redwood National Park

3.2.2 Lake County Air Basin

Lakeport is located on the northwestern side of Clear Lake in the Lake County Air Basin.

Seasonal median and 20th and 80th percentile values of the light particle scattering coefficient (b_{sp}) measured at Lakeport are shown in Figure 3-21. The median and 80th percentile values are highest during winter and lowest during spring. Values during summer and fall are similar. The higher values during winter are consistent with periods of stagnation and low mixing heights leading to accumulation of emitted particulate matter. The lower values during spring may be caused by generally higher wind speeds.

Seasonal median and 20th and 80th percentiles of the coefficient of haze (COH) measured at Lakeport are in Figure 3-22. Values are substantially higher in fall and winter than in summer and spring, with the highest values in winter. This pattern is consistent with poorer dispersion during the cooler seasons.

3.2.3 San Francisco Bay Air Basin

San Jose and Point Reyes National Seashore are at opposite ends of the San Francisco Bay area. San Jose is inland from the Pacific coast, while Point Reyes National Seashore is on the ocean.

Seasonal median, 20th and 80th percentiles of $PM_{2.5}$ mass concentration measured at San Jose are shown in Figure 3-23. The values vary strongly with season, with fall and winter values of the median and 80th percentile much higher than the spring and summer values. The winter 80th percentile is much higher than the 80th percentile during the other seasons, which is consistent with periods of stagnation and low mixing heights, leading to accumulation of emitted particulate matter as well as increased formation of ammonium nitrate. The 20th percentile values do not vary much among the seasons, suggesting that periods of strong atmospheric dispersion occur throughout the year.

Seasonal median $PM_{2.5}$ mass and PM_{10} ammonium sulfate and ammonium nitrate concentrations at San Jose are shown in Figure 3-24. The ammonium nitrate and ammonium sulfate values were calculated by multiplying the measured nitrate and sulfate concentrations by 1.29 and 1.375, respectively, to account for the associated ammonium, under the assumption that the sulfate is completely neutralized. The bar labeled "Other" is the difference between the average measured $PM_{2.5}$ mass concentration and the sum of the estimated ammonium nitrate and ammonium sulfate concentrations. It is probably composed primarily of organic compounds, elemental carbon and soil-derived materials.

The "Other" category is the largest category during all seasons, particularly fall and winter, which suggests that organic compounds and elemental carbon may be major constituents of the $PM_{2.5}$ in San Jose. Ammonium sulfate exceeds ammonium nitrate during the spring and summer, while ammonium

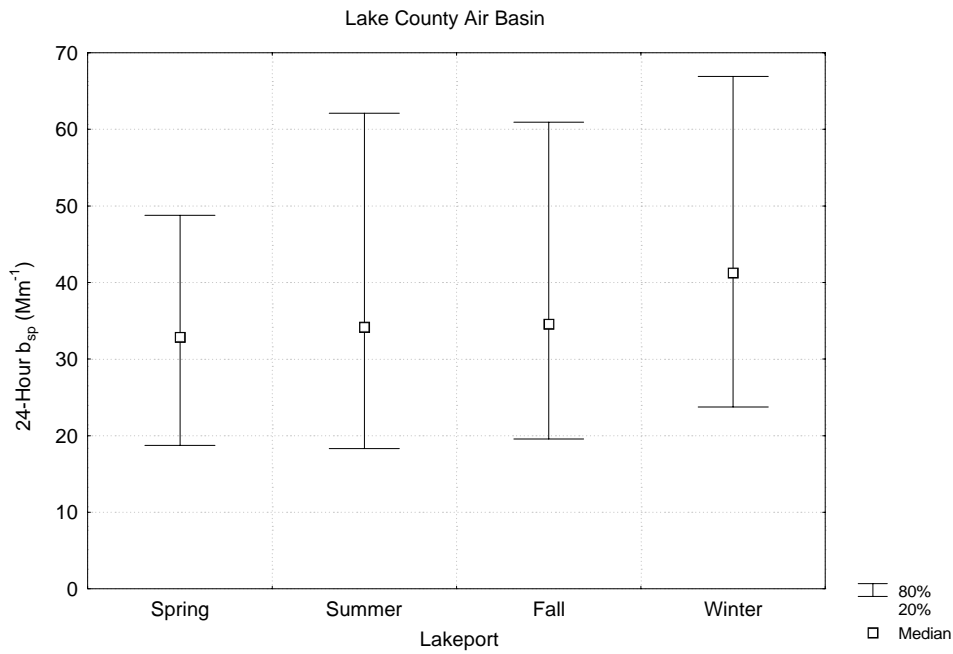


Figure 3-21 Seasonal Median and 20th and 80th Percentiles of the Particle Light Scattering Coefficient Measured at Lakeport

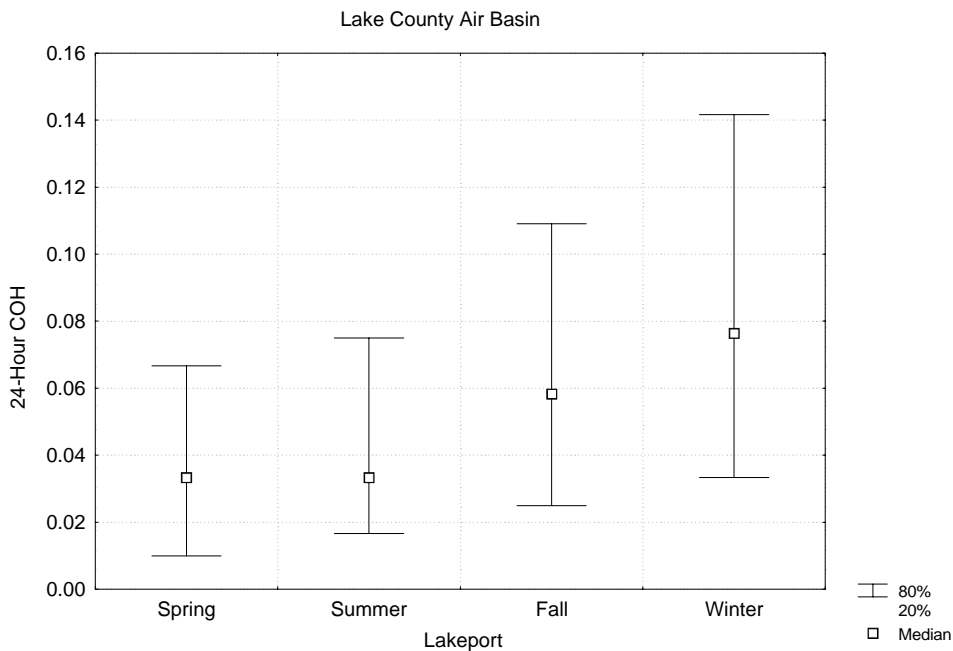


Figure 3-22 Seasonal Median and 20th and 80th Percentiles of the Coefficient of Haze Measured at Lakeport

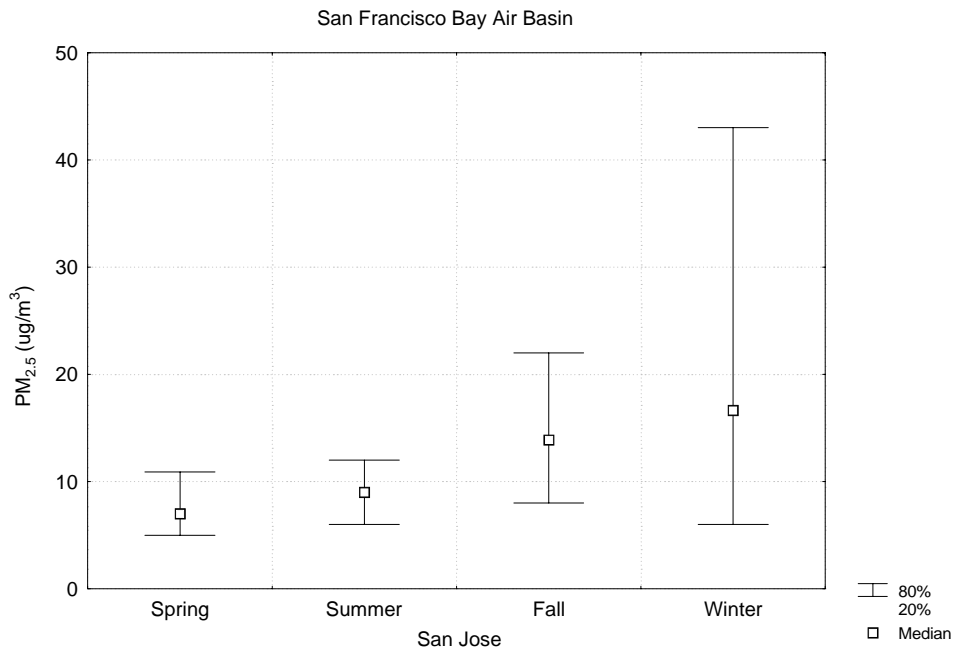


Figure 3-23 Seasonal Median and 20th and 80th Percentiles of PM_{2.5} Mass Concentration at San Jose

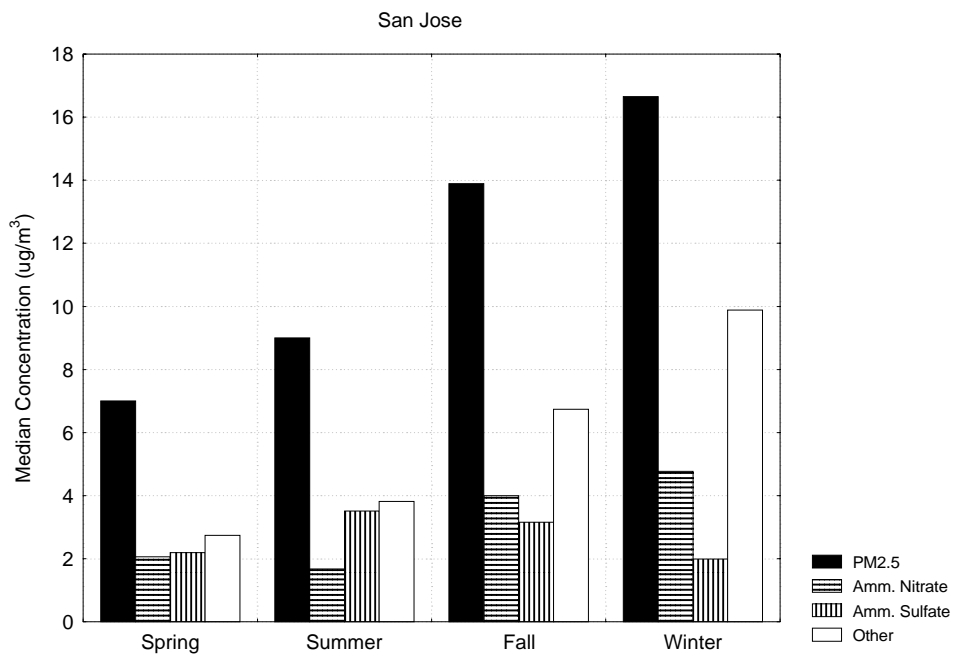


Figure 3-24 Seasonal Median PM_{2.5} Mass and PM₁₀ Ammonium Nitrate and Ammonium Sulfate Concentrations at San Jose

nitrate exceeds ammonium sulfate during the fall and winter. This pattern is consistent with increased formation of ammonium nitrate during the cooler seasons.

Seasonal median, 20th and 80th percentile values of the particle light absorption coefficient measured at Point Reyes National Seashore are shown in Figure 3-25. The highest values occur during the fall and winter, with the winter 80th percentile much higher than the values during the other seasons. Additionally, the spring 80th percentile is higher than the summer value, suggesting that local wood burning may be a major contributor during cooler periods.

Seasonal median, 20th and 80th percentile values of the PM_{2.5} mass concentration measured at Point Reyes National Seashore are shown in Figure 3-26. The seasonal variations are much weaker than the variations in the particle light absorption coefficient. Although the highest value of the 80th percentile occurs during winter, the lowest value of the median also occurs during winter.

Estimated seasonal average concentrations of PM_{2.5} constituents at Point Reyes National Seashore are shown in Figure 3-27. In contrast with the median values in Figure 3-26, the winter average PM_{2.5} mass concentration is higher than averages during the other seasons, suggesting that the highest winter values are much higher than most of the values measured during winter, which make the average value higher than the median. Sodium chloride from sea salt is a major contributor at this location, as it is at Redwood National Park. Estimated sodium chloride concentrations during spring, summer, fall and winter are 2.2 µg/m³, 2.2 µg/m³, 1.1 µg/m³ and 1.0 µg/m³, respectively. These values account for half or more of the "Difference" bars in the figure. Sodium chloride is estimated to be the largest contributor to average PM_{2.5} mass during spring and summer, with ammonium sulfate being the second largest during those seasons. EC+OMC is estimated to be the largest contributor during fall, and ammonium nitrate is the largest estimated contributor during winter with a substantial contribution from EC+OMC. The relative contributions from ammonium nitrate and ammonium sulfate during the winter are similar to the relative contributions at San Jose, suggesting that Point Reyes National Seashore and San Jose may be somewhat influenced by the same sources during this season. Additionally, the relatively high concentration of EC+OMC during the winter and the relatively high values of the particle light absorption coefficient suggest that periods of stagnation may lead to the accumulation of emissions from wood combustion.

Estimated seasonal average values of the light extinction coefficient and its constituents are shown in Figure 3-28. Light scattering by ammonium sulfate is estimated to be the largest contributor during all seasons except winter, when light scattering by ammonium nitrate is estimated to be the largest contributor.

3.2.4 North Central Coast

Pinnacles National Monument is located to the east of the Salinas Valley in the North Central Coast Air Basin.

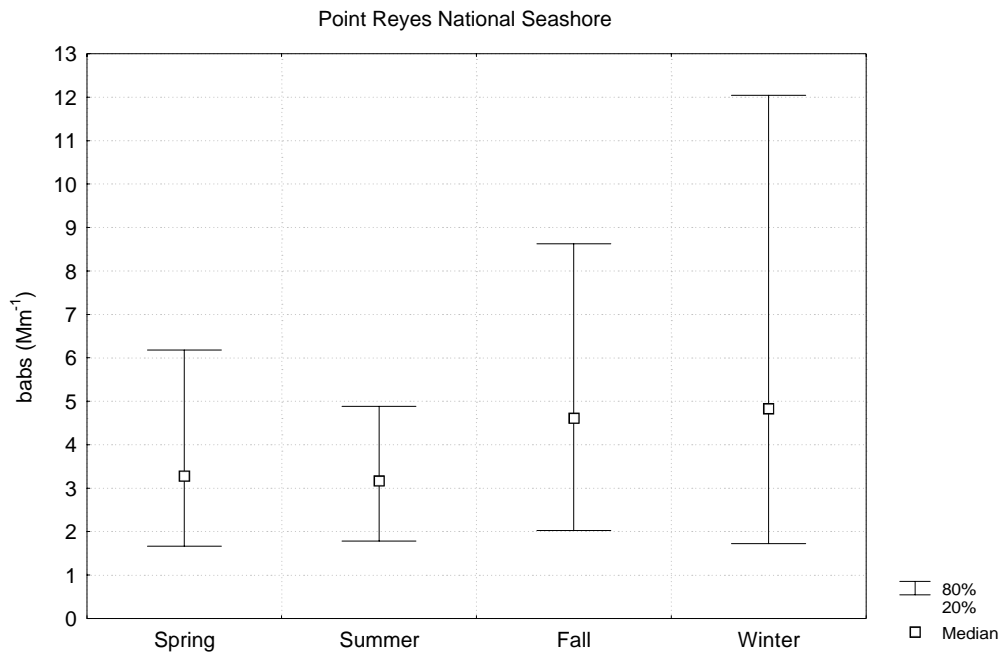


Figure 3-25 Seasonal Median and 20th and 80th Percentiles of the Particle Light Absorption Coefficient at Point Reyes National Seashore

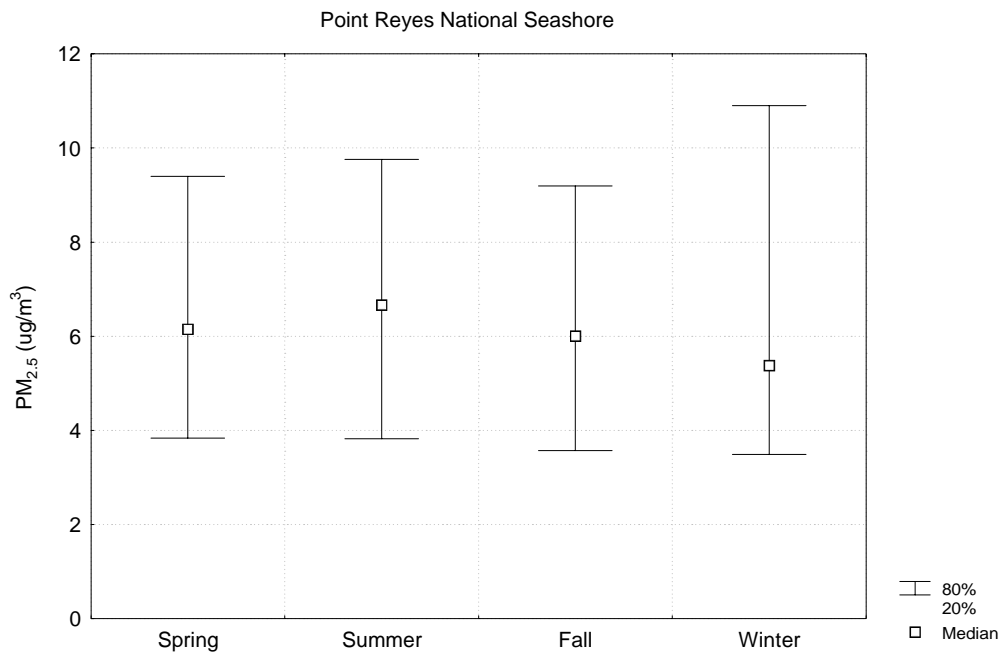


Figure 3-26 Seasonal Median and 20th and 80th Percentiles of PM_{2.5} Mass Concentration at Point Reyes National Seashore

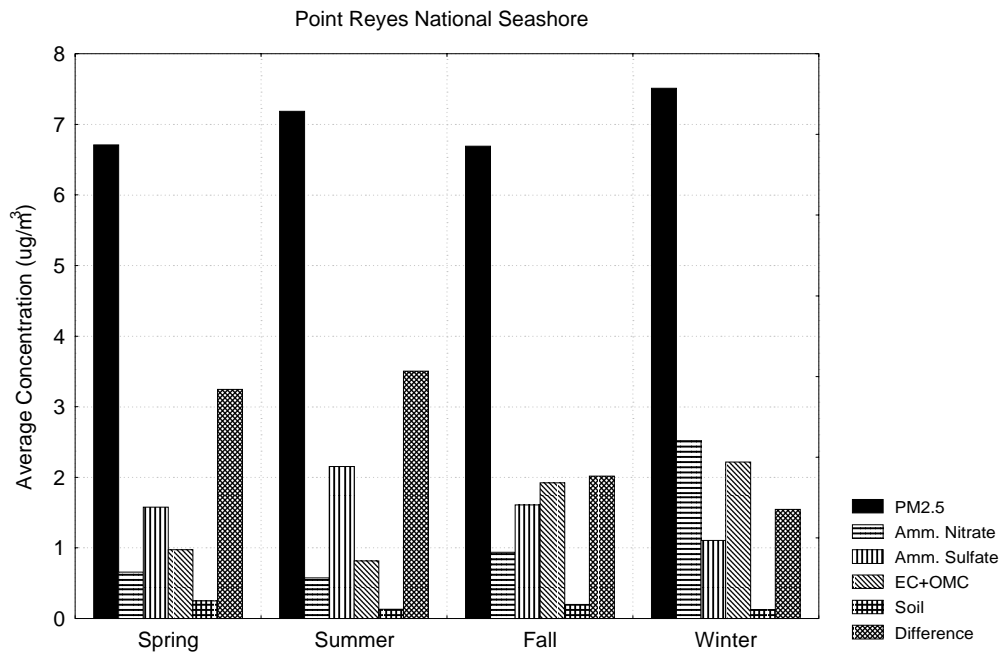


Figure 3-27 Seasonal Average PM_{2.5} Mass and Estimated Chemical Constituent Concentrations at Point Reyes National Seashore

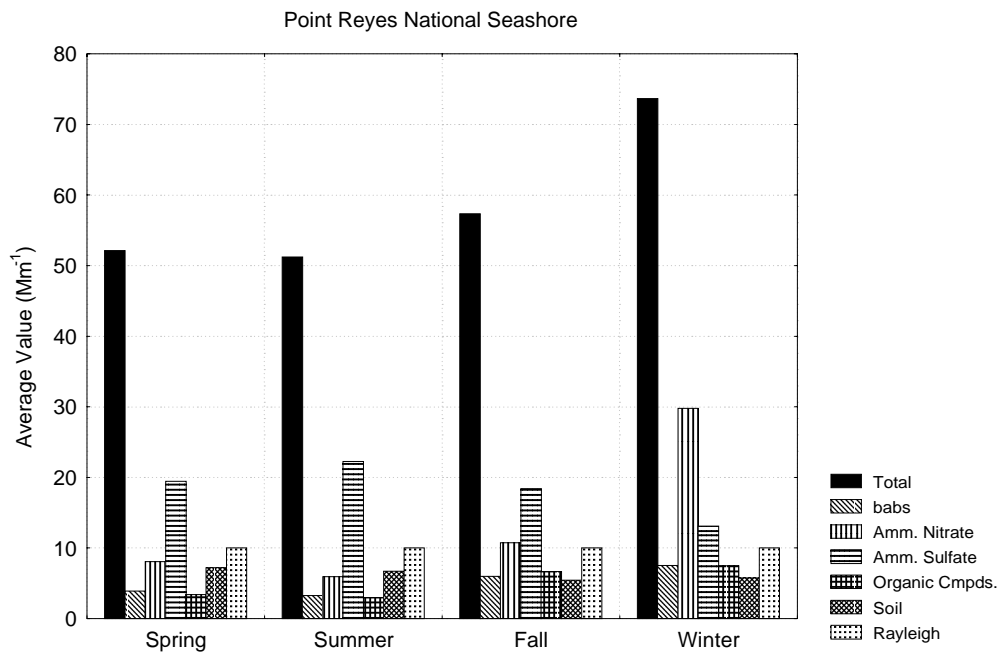


Figure 3-28 Contributions to Calculated Seasonal Average Light Extinction Coefficient at Point Reyes National Seashore

Seasonal median and 20th and 80th percentiles of the light extinction coefficient measured at Pinnacles National Monument are shown in Figure 3-29. The highest 80th percentile values occur during fall and winter, with the fall median value slightly higher than the winter median. The lowest 20th percentile value occurs in the winter, suggesting that winter storms contribute to low values while periods of stagnation during fall and winter contribute to high values.

Seasonal median and 20th and 80th percentiles of the particle light absorption coefficient measured at Pinnacles National Monument are shown in Figure 3-30. The seasonal pattern differs from the pattern for the extinction coefficient, with winter values generally lower than values during the other seasons. The highest values occur during the fall, but the 80th percentile during the spring is higher than the summer and winter 80th percentiles.

Seasonal median and 20th and 80th percentiles of PM_{2.5} mass concentrations measured at Pinnacles National Monument are shown in Figure 3-31. The seasonal pattern is similar to the pattern for the particle light absorption coefficient, with the highest values occurring during the fall and the lowest values during the winter. However, values during the summer tend to be higher than values during the spring.

Estimated seasonal average concentrations of PM_{2.5} constituents are shown in Figure 3-32. The “difference” term is much smaller here than at the more-coastal Redwood National Park and Point Reyes National Seashore sites because sodium chloride is not a major contributor. EC+OMC is the largest contributor during every season except summer, when the estimated contribution from ammonium sulfate is slightly higher. The contribution from ammonium sulfate is higher than the contribution from ammonium nitrate during all seasons except winter. The seasonal patterns suggest that dispersion is poorest during the fall, leading to an accumulation of locally emitted particulate matter or of material transported down the Salinas Valley.

Estimated seasonal average values of the light extinction coefficient and its constituents are shown in Figure 3-33. Light scattering by ammonium sulfate is estimated to be the largest contributor during all seasons except winter, when light scattering by ammonium nitrate is estimated to be the largest contributor. The average value of the calculated light extinction coefficient is highest during fall, with similar estimated contributions from light absorption and light scattering by ammonium nitrate, ammonium sulfate, organic compounds and air molecules.

3.2.5 Sacramento Valley Air Basin

Seasonal median and 20th and 80th percentiles of the particle light scattering coefficient measured at sites in the Sacramento Valley Air Basin are shown in Figure 3-34. The 80th percentile is highest at all sites during winter and second highest during fall. This pattern is consistent with the high incidence of stagnant, cool conditions during the fall and winter, which lead to the accumulation of emitted

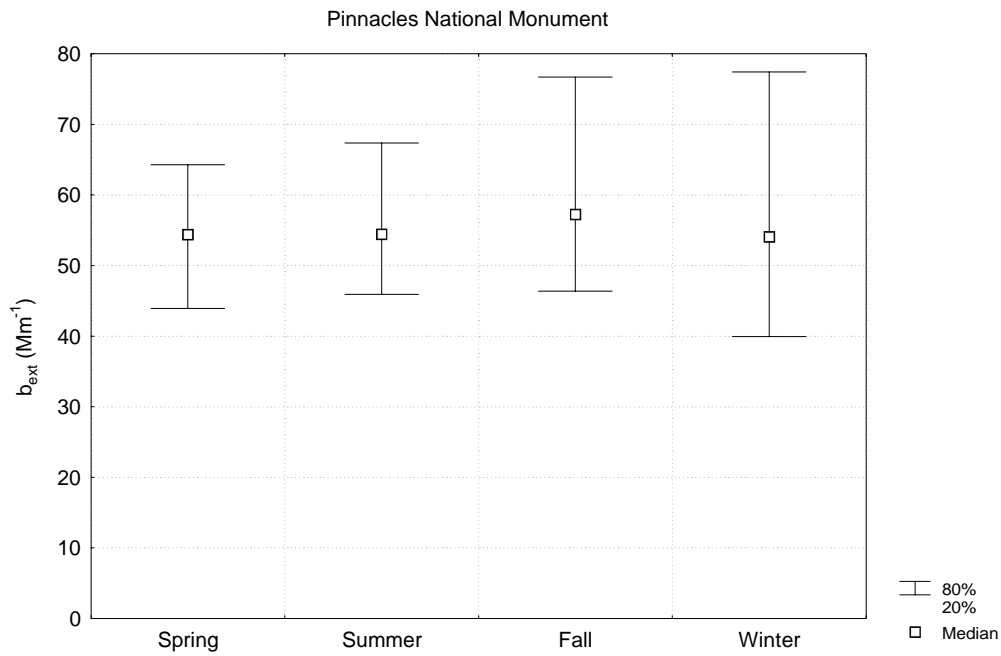


Figure 3-29 Seasonal Median and 20th and 80th Percentiles of the Light Extinction Coefficient at Pinnacles National Monument

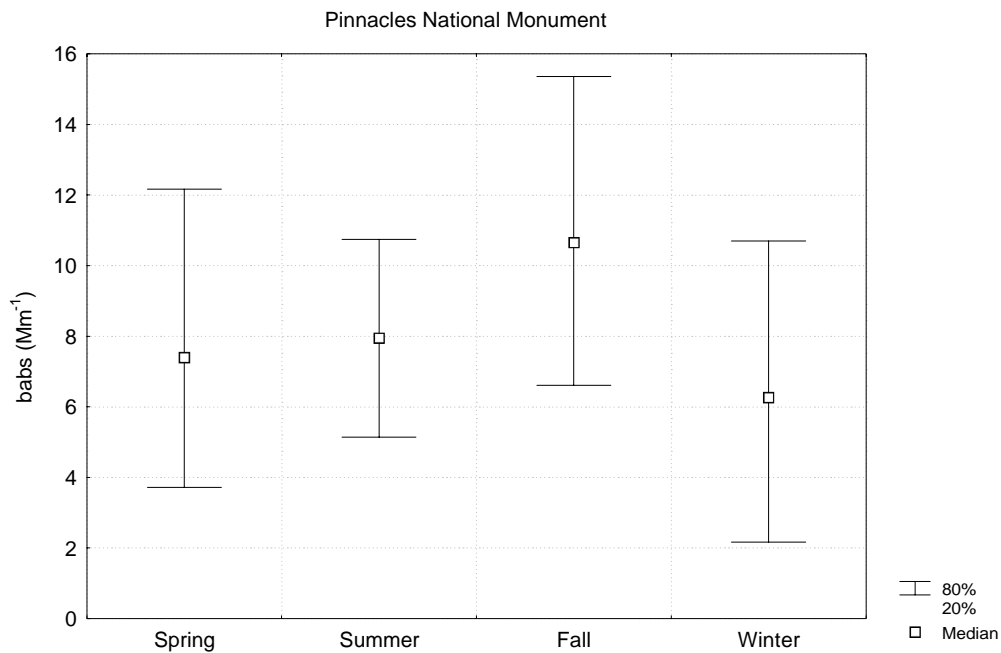


Figure 3-30 Seasonal Median and 20th and 80th Percentiles of the Particle Light Absorption Coefficient at Pinnacles National Monument

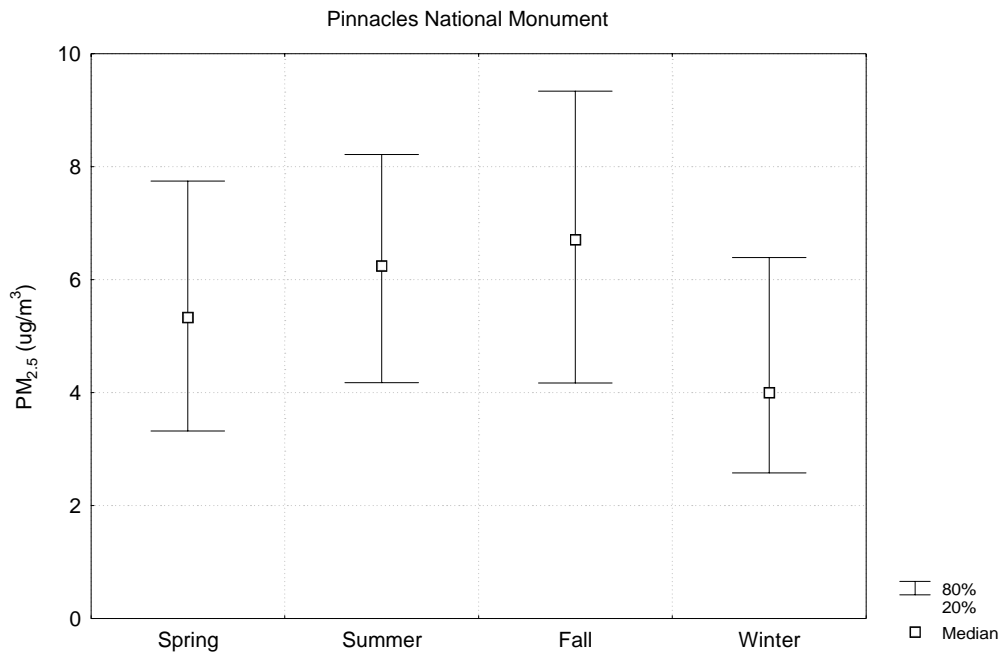


Figure 3-31 Seasonal Median and 20th and 80th Percentiles of PM_{2.5} Mass Concentration at Pinnacles National Monument

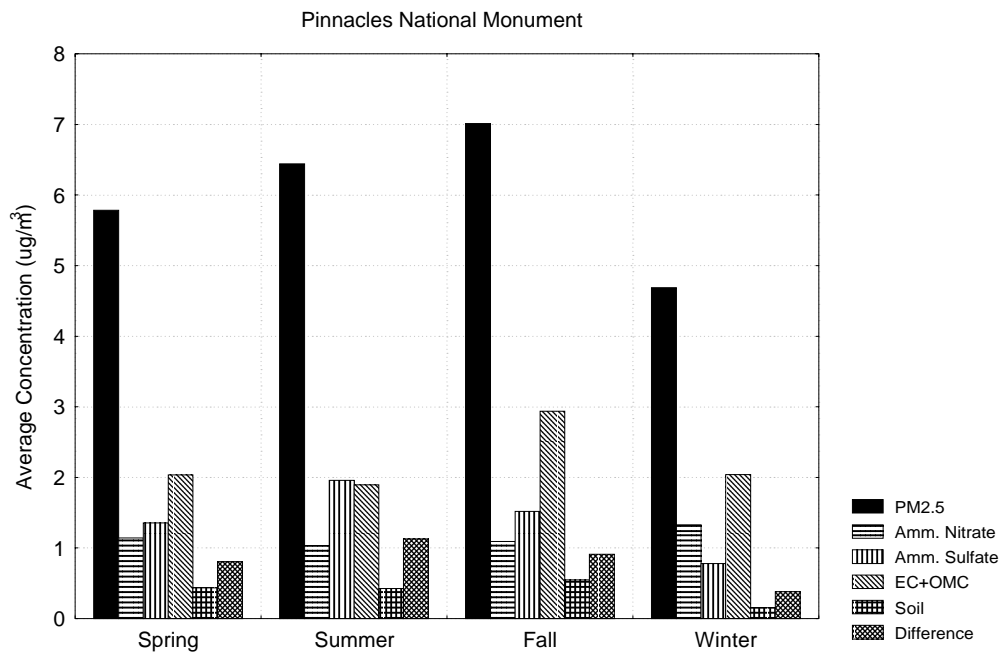


Figure 3-32 Seasonal Average PM_{2.5} Mass and Estimated Chemical Constituent Concentrations at Pinnacles National Monument

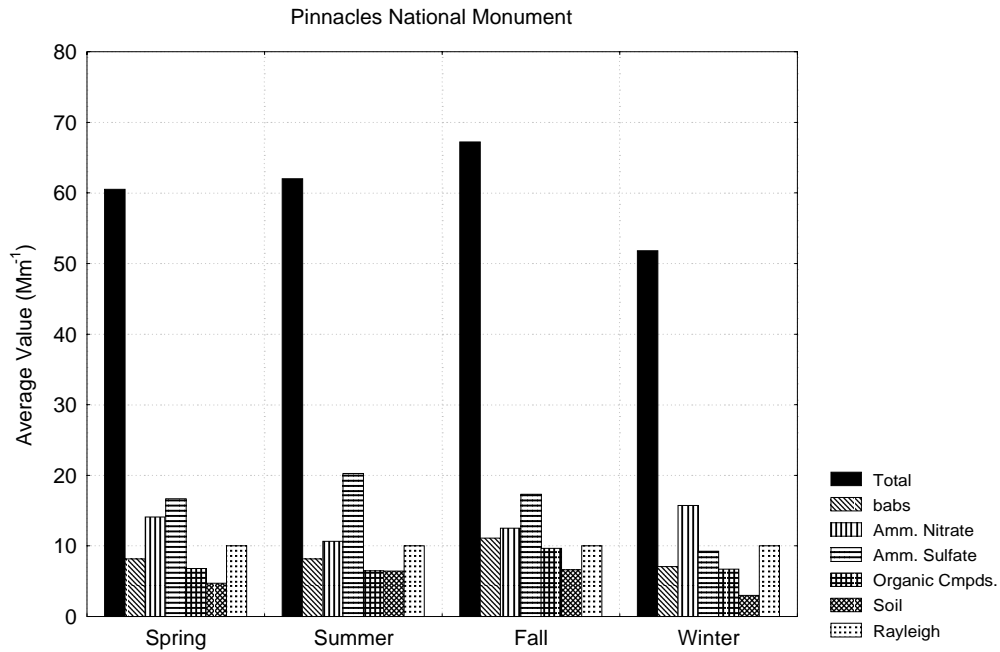


Figure 3-33 Contributions to Calculated Seasonal Average Light Extinction Coefficient at Pinnacles National Monument

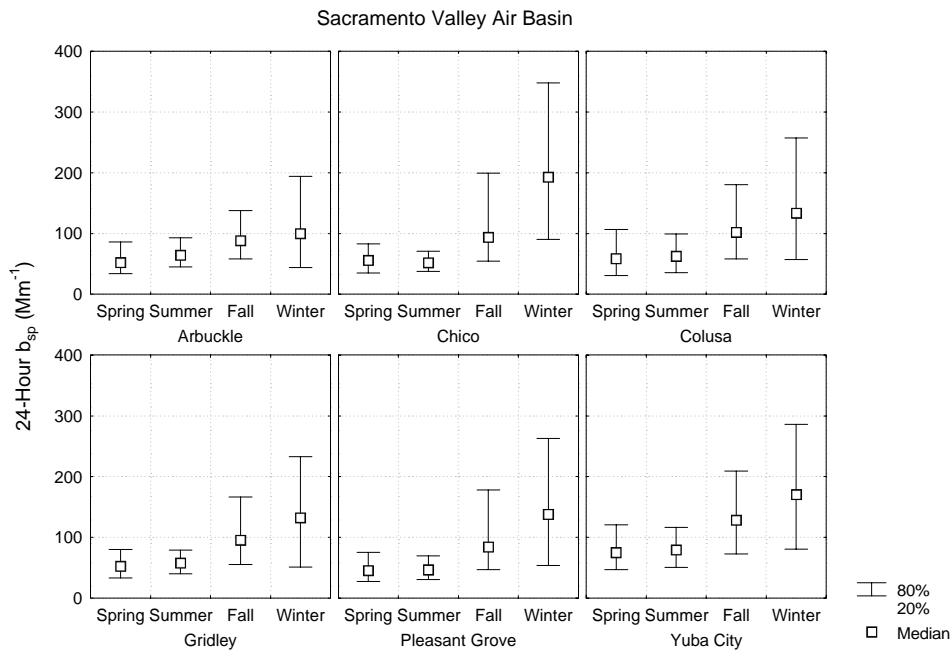


Figure 3-34 Seasonal Median and 20th and 80th Percentiles of the Particle Light Scattering Coefficient Measured at Sacramento Valley Air Basin Sites

particulate matter. The highest values occur at Chico, the northernmost site, and the lowest values occur at Arbuckle, the westernmost site. The pattern among sites suggests that the general flow of air into the Sacramento Valley from the San Francisco Bay and then up to the north may lead to higher concentrations on the eastern side of the valley.

Seasonal median and 20th and 80th percentiles of the coefficient of haze (COH) are shown in Figure 3-35. The patterns are similar to the patterns for the particle light scattering coefficient, although the differences between fall and winter values are not as great. This pattern again suggests that stagnant conditions during fall and winter lead to the accumulation of emitted particulate matter, particularly on the eastern side of the valley.

3.2.6 San Joaquin Valley Air Basin

Seasonal median and 20th and 80th percentiles of the particle light scattering coefficient and the coefficient of haze measured at Stockton are shown in Figure 3-36 and Figure 3-37, respectively. The patterns are similar to the patterns at the Sacramento Valley Air Basin sites and the values of the percentiles are close to the values at Chico.

Seasonal median and 20th and 80th percentiles of the PM_{2.5} mass concentration measured at the San Joaquin Valley sites are shown in Figure 3-38. The highest values occur during fall and winter, with winter values higher than fall values. Additionally, the 20th and 80th percentile values are more symmetric around the median values during winter than during fall, suggesting that periods of high concentrations are more common during winter than during fall.

Seasonal median PM_{2.5} mass concentrations and estimated PM₁₀ ammonium nitrate and ammonium sulfate concentrations are shown in Figure 3-39 through Figure 3-44. The seasonal variations in relative contributions are essentially identical among the sites, with ammonium nitrate about the same as ammonium sulfate during spring, ammonium sulfate higher than ammonium nitrate during summer, ammonium nitrate similar to or higher than ammonium sulfate during fall, and ammonium nitrate substantially higher than ammonium sulfate during winter. These seasonal variations are caused by changes in the estimated ammonium nitrate concentrations, since the estimated average ammonium sulfate concentrations do not vary much among seasons. As mentioned previously, periods of cool, stagnant conditions during winter lead to the accumulation of emitted particulate matter and the formation of ammonium nitrate.

3.2.7 Northeast Plateau Air Basin

Lassen Volcanic National Park is located in the southern Cascade Mountains, east of the northern end of the Sacramento Valley in the Northeast Plateau Air Basin.

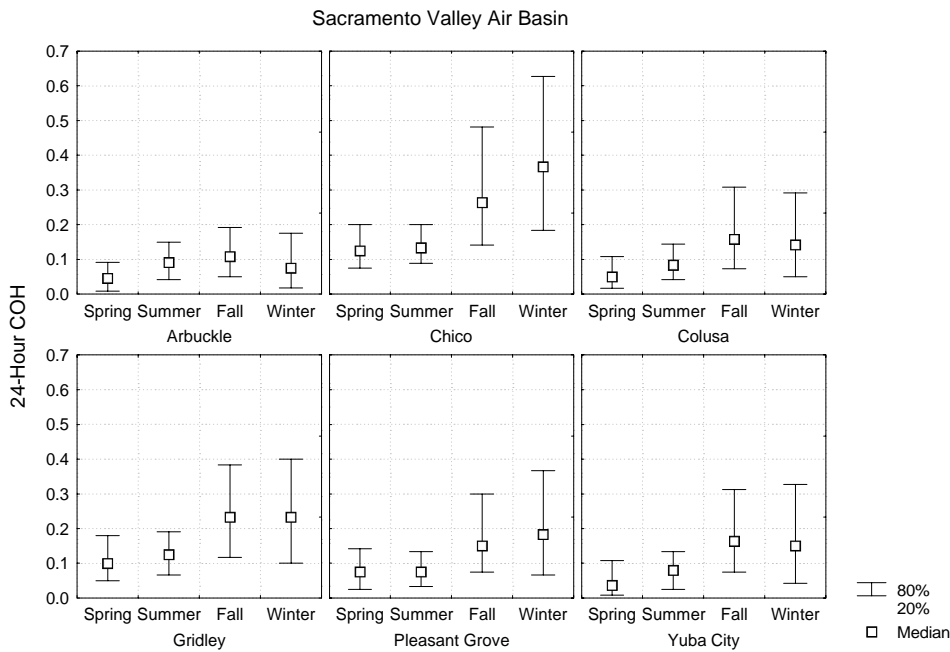


Figure 3-35 Seasonal Median and 20th and 80th of the Coefficient of Haze Measured at Sacramento Valley Air Basin Sites

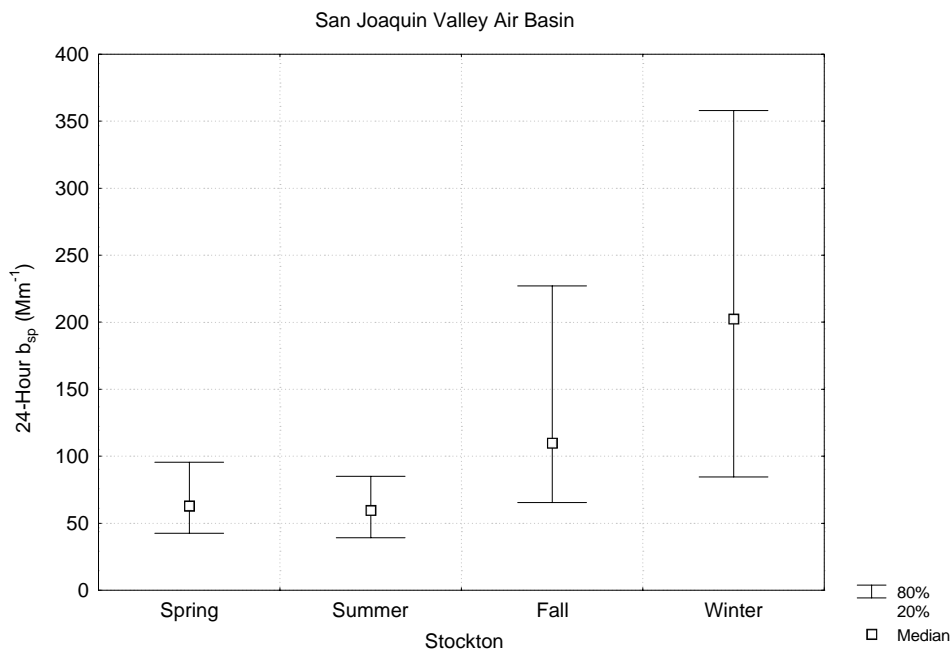


Figure 3-36 Seasonal Median and 20th and 80th Percentiles of the Particle Light Scattering Coefficient Measured at Stockton

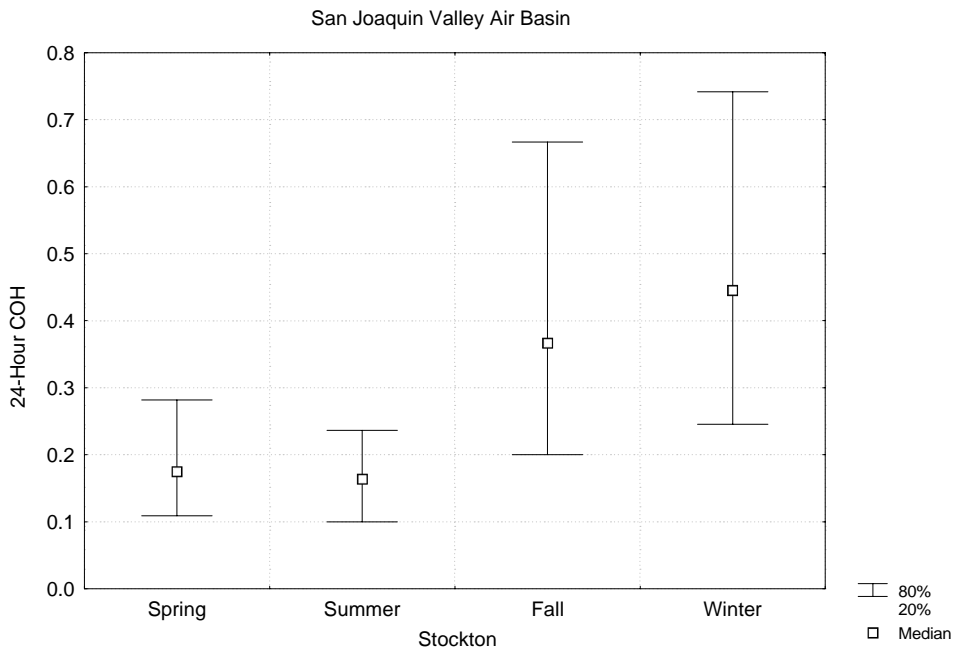


Figure 3-37 Seasonal Median and 20th and 80th Percentiles of the Coefficient of Haze Measured at Stockton

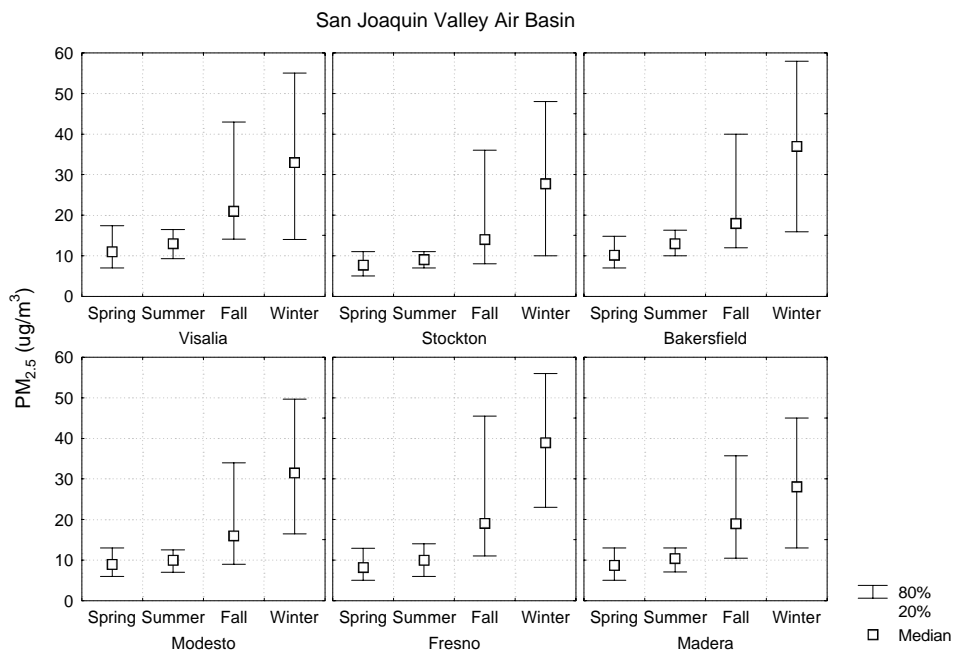


Figure 3-38 Seasonal Median and 20th and 80th Percentiles of PM_{2.5} Mass Concentration at San Joaquin Valley Air Basin Sites

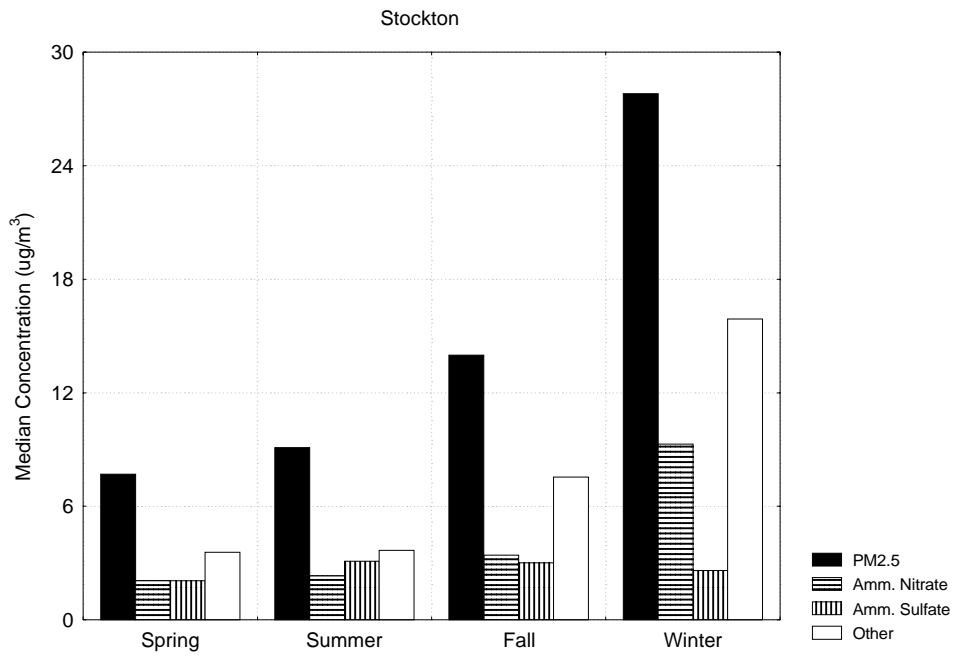


Figure 3-39 Seasonal Median PM_{2.5} Mass and PM₁₀ Ammonium Nitrate and Ammonium Sulfate Concentrations at Stockton

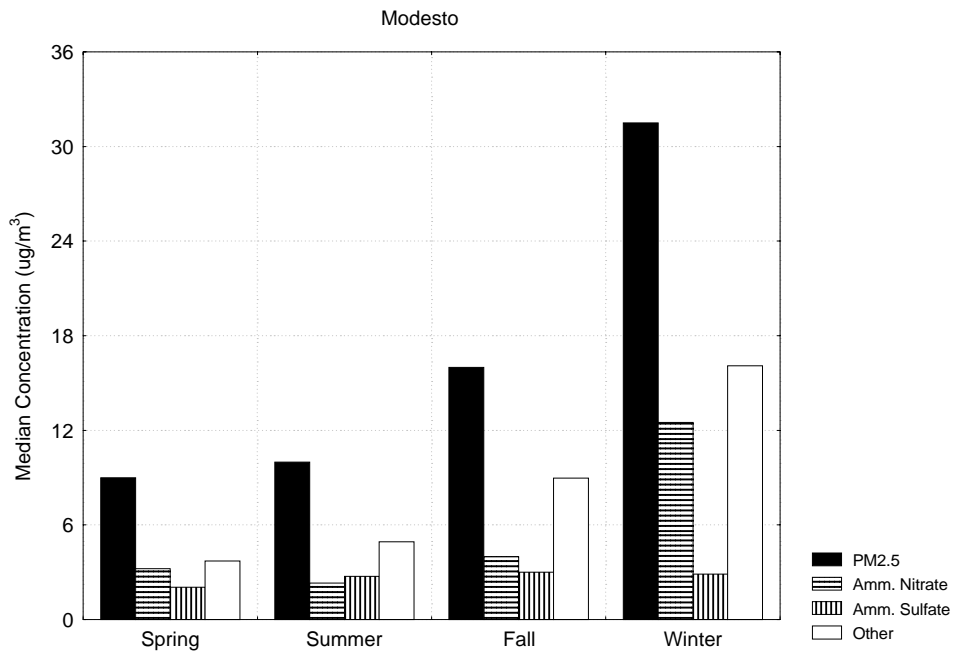


Figure 3-40 Seasonal Median PM_{2.5} Mass and PM₁₀ Ammonium Nitrate and Ammonium Sulfate Concentrations at Modesto

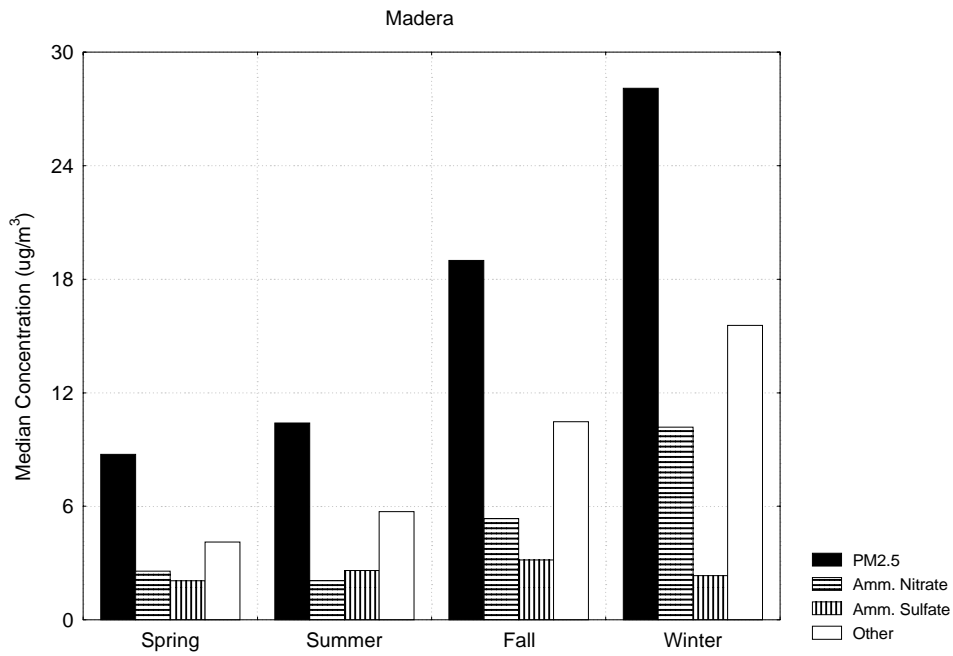


Figure 3-41 Seasonal Median PM_{2.5} Mass and PM₁₀ Ammonium Nitrate and Ammonium Sulfate Concentrations at Madera

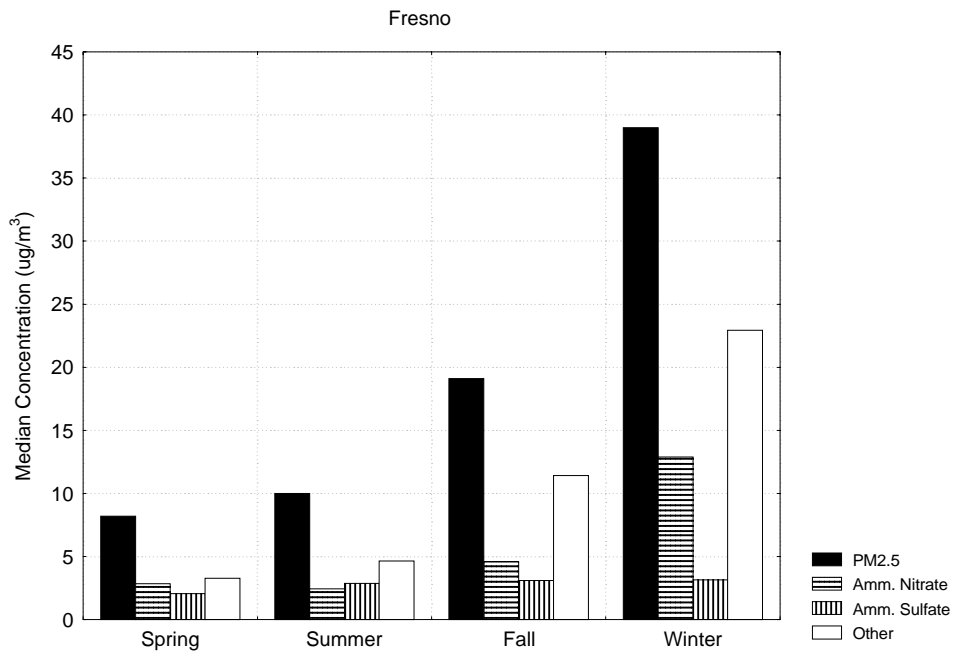


Figure 3-42 Seasonal Median PM_{2.5} Mass and PM₁₀ Ammonium Nitrate and Ammonium Sulfate Concentrations at Fresno

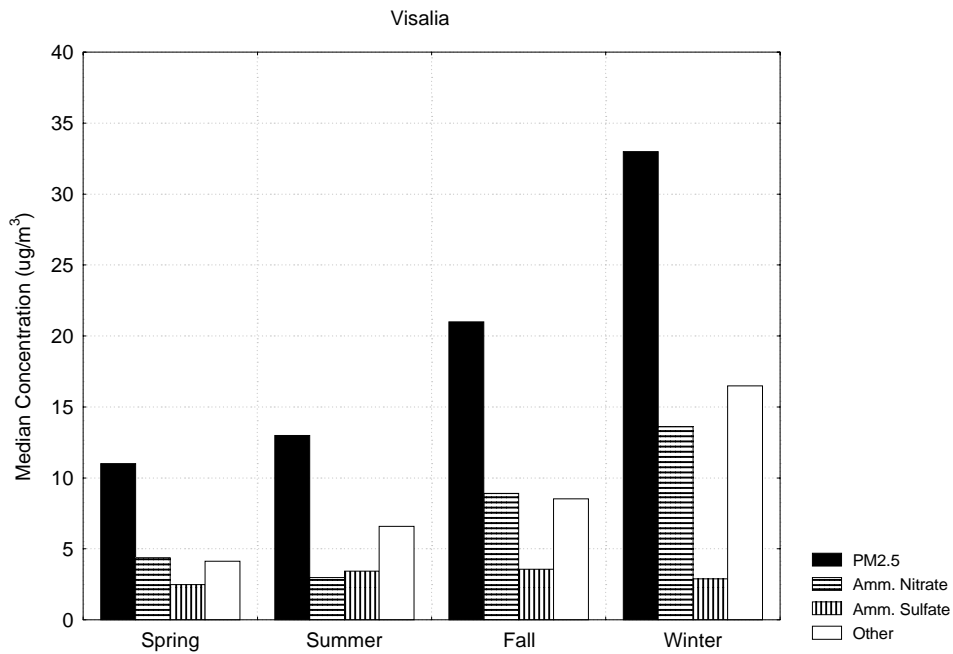


Figure 3-43 Seasonal Median PM_{2.5} Mass and PM₁₀ Ammonium Nitrate and Ammonium Sulfate Concentrations at Visalia

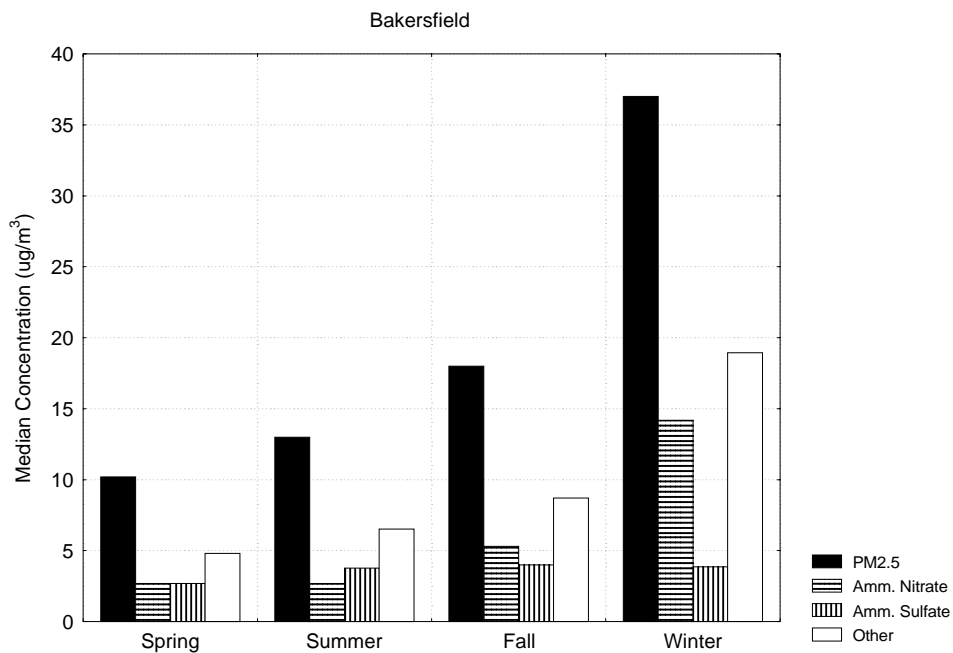


Figure 3-44 Seasonal Median PM_{2.5} Mass and PM₁₀ Ammonium Nitrate and Ammonium Sulfate Concentrations at Bakersfield

Seasonal medians and 20th and 80th percentiles of the measured particle light absorption coefficient and PM_{2.5} mass concentration are shown in Figure 3-45 and Figure 3-46, respectively. The patterns are almost identical, with the highest values occurring during summer and the lowest values during winter. Spring and fall values are about the same. The higher values during summer may be caused by local emissions associated with park visitors as well as by transport from the Sacramento Valley promoted by high temperatures in the Valley, which lead to extensive vertical mixing.

Estimated seasonal average concentrations of PM_{2.5} constituents are shown in Figure 3-47. EC+OMC is the largest estimated contributor during all seasons, with the highest average concentration occurring during summer, although the concentration during fall is only slightly lower than the summer value. Estimated contributions from ammonium sulfate and fine soil are also substantial during spring and summer.

Estimated seasonal average values of the light extinction coefficient and its constituents are shown in Figure 3-48. Light scattering by air molecules is estimated to be the largest contributor during all seasons. Light scattering by ammonium sulfate is the second largest contributor during spring and summer, followed by light scattering by organic compounds and light absorption.

3.2.8 Lake Tahoe Air Basin

South Lake Tahoe is located at the southern end of Lake Tahoe in the northern Sierra Nevada Mountains.

Seasonal medians and 20th and 80th percentiles of the measured particle light absorption coefficient and PM_{2.5} mass concentration are shown in Figure 3-49 and Figure 3-50, respectively. The patterns are similar, with much higher median and 80th percentile values during winter than during the other seasons, and higher values during fall than during spring and summer. These high fall and winter values are indicative of periods poor dispersion caused by surface inversions.

Estimated seasonal average concentrations of PM_{2.5} constituents are shown in Figure 3-51. EC+OMC is the largest estimated contributor during all four seasons, accounting for more than 70 percent of the PM_{2.5} mass during fall and more than 80 percent during winter. This pattern suggests substantial contributions from wood burning, particularly during the cooler seasons, leading to the high PM_{2.5} mass concentrations during these seasons.

Estimated seasonal average values of the light extinction coefficient and its constituents are shown in Figure 3-52. Light absorption is estimated to be the largest contributor to the average extinction coefficient during all seasons, followed by light scattering by organic compounds

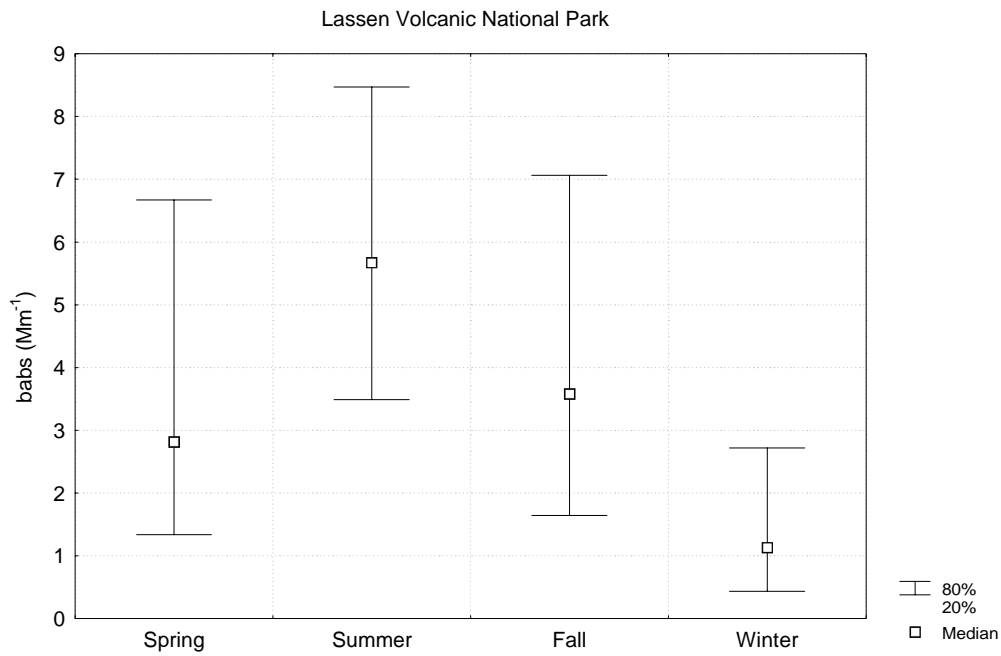


Figure 3-45 Seasonal Median and 20th and 80th Percentiles of the Particle Light Absorption Coefficient at Lassen Volcanic National Park

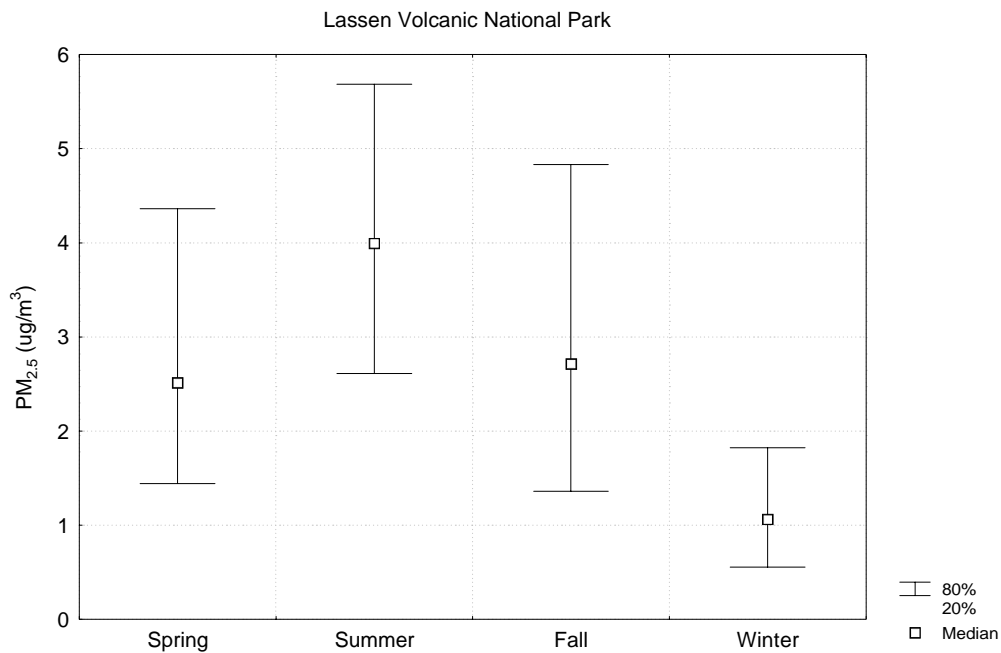


Figure 3-46 Seasonal Median and 20th and 80th Percentiles of PM_{2.5} Mass Concentration at Lassen Volcanic National Park

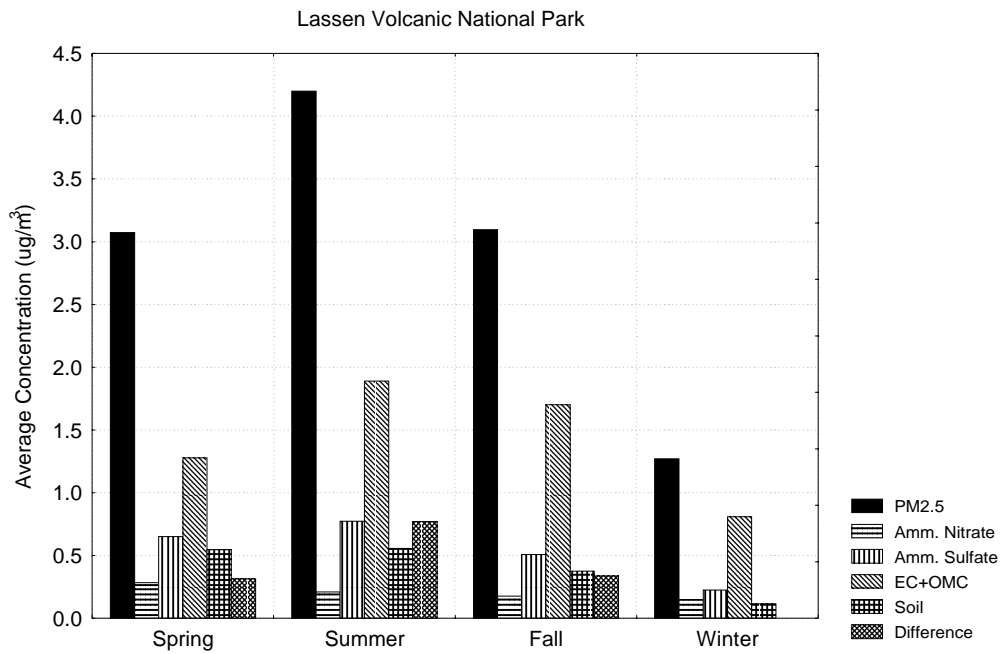


Figure 3-47 Seasonal Average PM_{2.5} Mass and Estimated Chemical Constituent Concentrations at Lassen Volcanic National Park

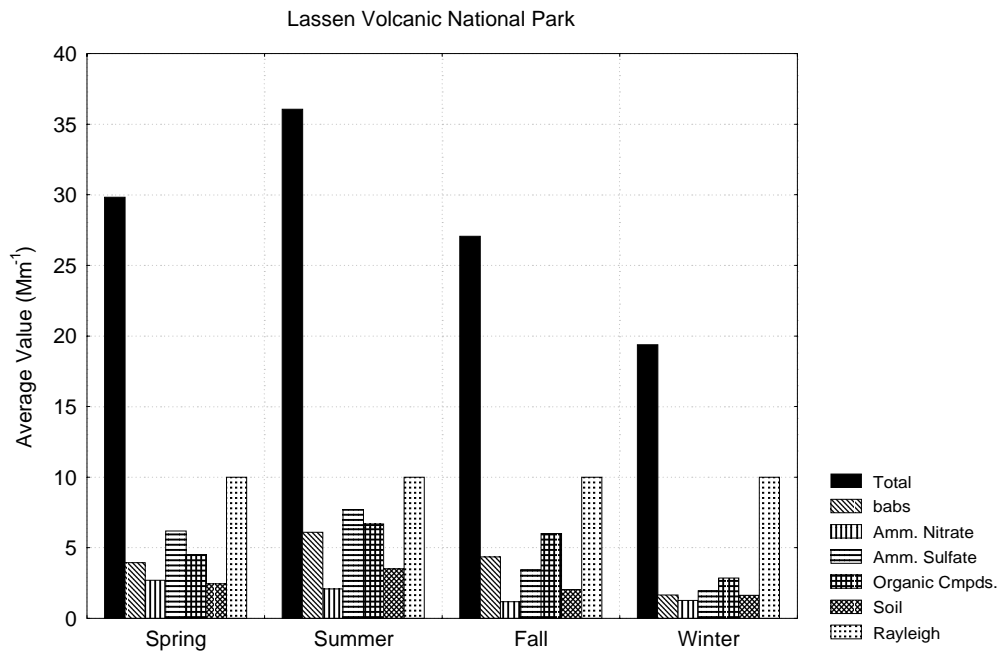


Figure 3-48 Contributions to Calculated Seasonal Average Light Extinction Coefficient at Lassen Volcanic National Park

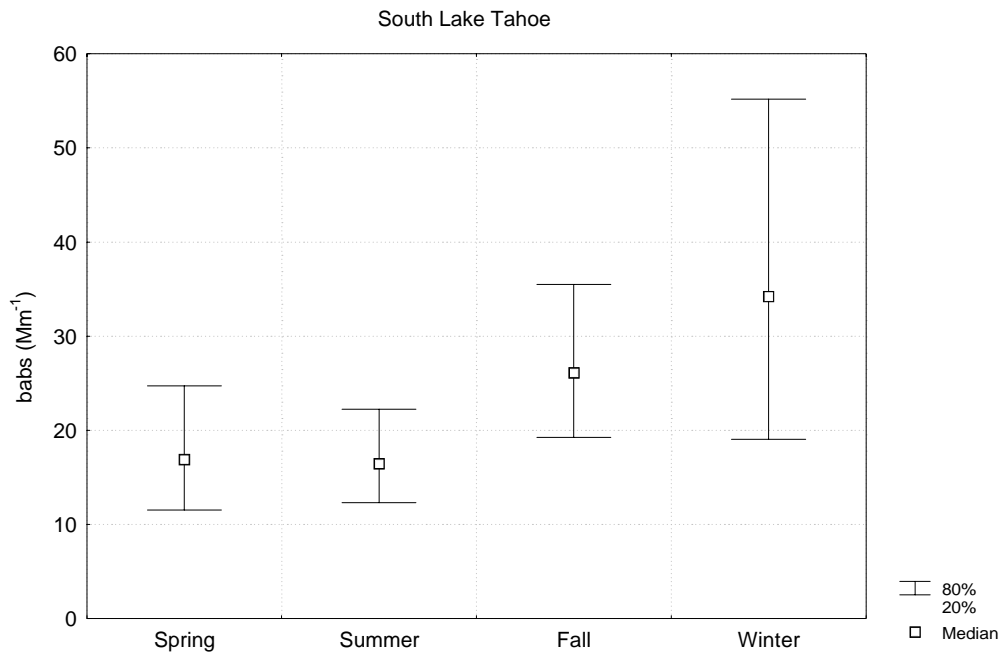


Figure 3-49 Seasonal Median and 20th and 80th Percentiles of the Particle Light Absorption Coefficient at South Lake Tahoe

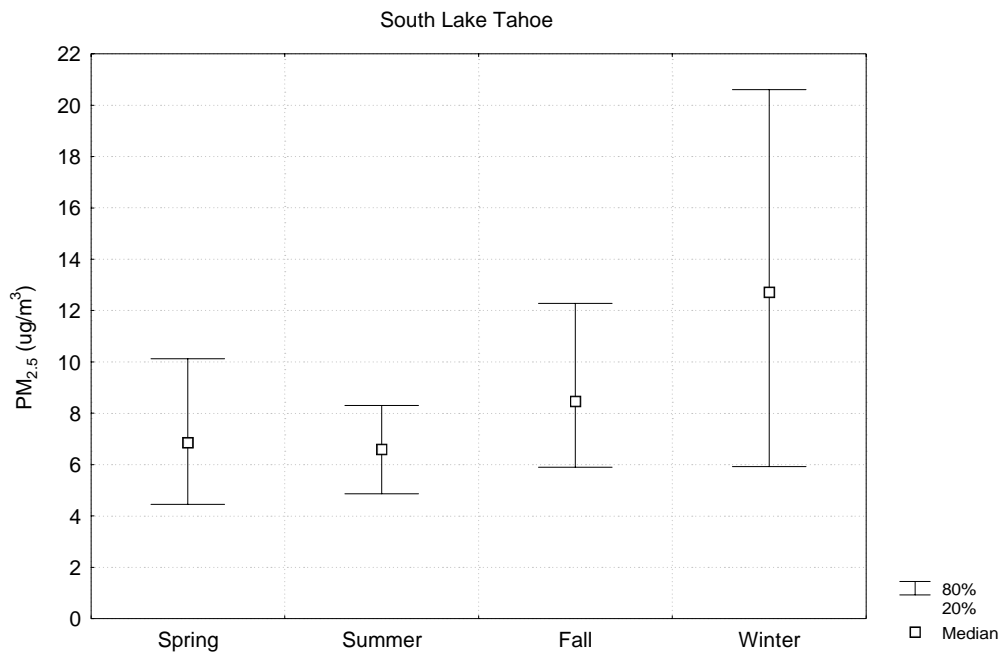


Figure 3-50 Seasonal Median and 20th and 80th Percentiles of PM_{2.5} Mass Concentration at South Lake Tahoe

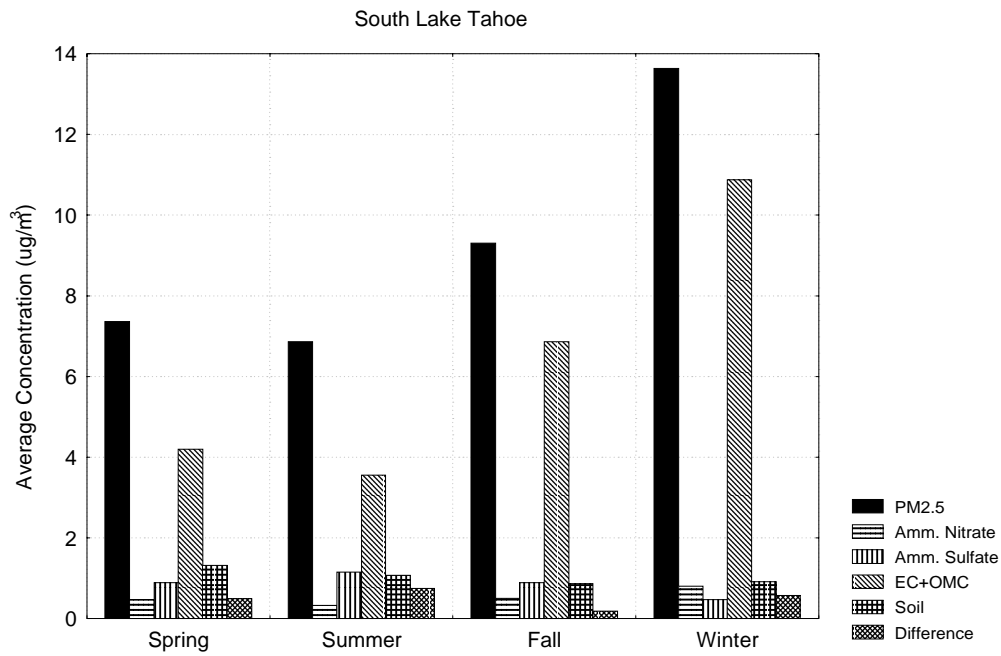


Figure 3-51 Seasonal Average PM_{2.5} Mass and Estimated Chemical Constituent Concentrations at South Lake Tahoe

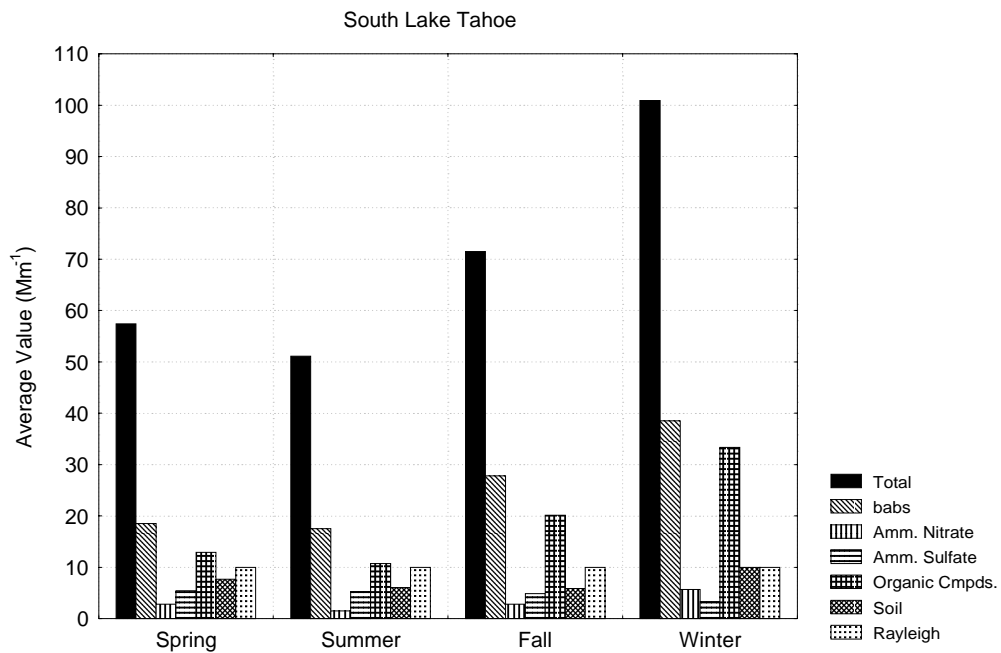


Figure 3-52 Contributions to Calculated Seasonal Average Light Extinction Coefficient at South Lake Tahoe

3.2.9 Mountain Counties Air Basin

Yosemite National Park is located in the Sierra Nevada Mountains, east of the San Joaquin Valley in the Mountain Counties Air Basin. Seasonal median and 20th and 80th percentiles of the measured light extinction and particle light absorption coefficients and measured PM_{2.5} mass concentration are shown in Figure 3-53 through Figure 3-55. The seasonal variations are similar for all three quantities, with the highest values occurring during summer and the second highest during fall. As was the case for Lassen Volcanic National Park, the higher values during the summer may be associated with visitors to the Park and with transport from the Central Valley caused by higher mixing depths and up-slope wind flows.

Seasonal average PM_{2.5} constituent concentrations are shown in Figure 3-56. EC+OMC is the largest estimated constituent during all seasons with substantial estimated contributions from ammonium sulfate during all seasons except winter. The large contributions from EC+OMC during summer and fall is consistent with wood burning by visitors during those seasons.

Estimated seasonal average values of the light extinction coefficient and its constituents are shown in Figure 3-57. Light scattering by organic compounds is estimated to be the largest contributor during summer and fall and a substantial contributor during spring and winter. Light scattering by air molecules is the largest estimated contributor during spring and winter. Light absorption is also a major contributor during all seasons except winter.

3.2.10 South Coast Air Basin

Seasonal median and 20th and 80th percentiles of PM_{2.5} mass concentrations measured at Long Beach, Azusa and Riverside are shown in Figure 3-58. The highest 80th percentile values occur during winter at Long Beach and fall at Azusa and Riverside. The second highest values occur during fall at Long Beach, winter at Azusa and Spring at Riverside. Median values are highest during fall and winter at Long Beach and during summer and fall at Azusa and Riverside.

Seasonal median PM_{2.5} mass and PM₁₀ ammonium nitrate and ammonium sulfate concentrations at Long Beach, Azusa and Riverside are shown in Figure 3-59 through Figure 3-61. The "Other" category, which may be comprised of elemental carbon and organic compounds, is the largest contributor at Long Beach during fall and winter, followed by ammonium sulfate during fall and ammonium nitrate during winter (Figure 3-59). Ammonium sulfate is the largest contributor at Long Beach during spring and summer. At Azusa, the "Other" category is the largest contributor during every season, with ammonium nitrate second largest during all seasons except summer (Figure 3-60). Ammonium nitrate is the largest contributor at Riverside during every season except winter, when the "Other" category is the largest (Figure 3-61).

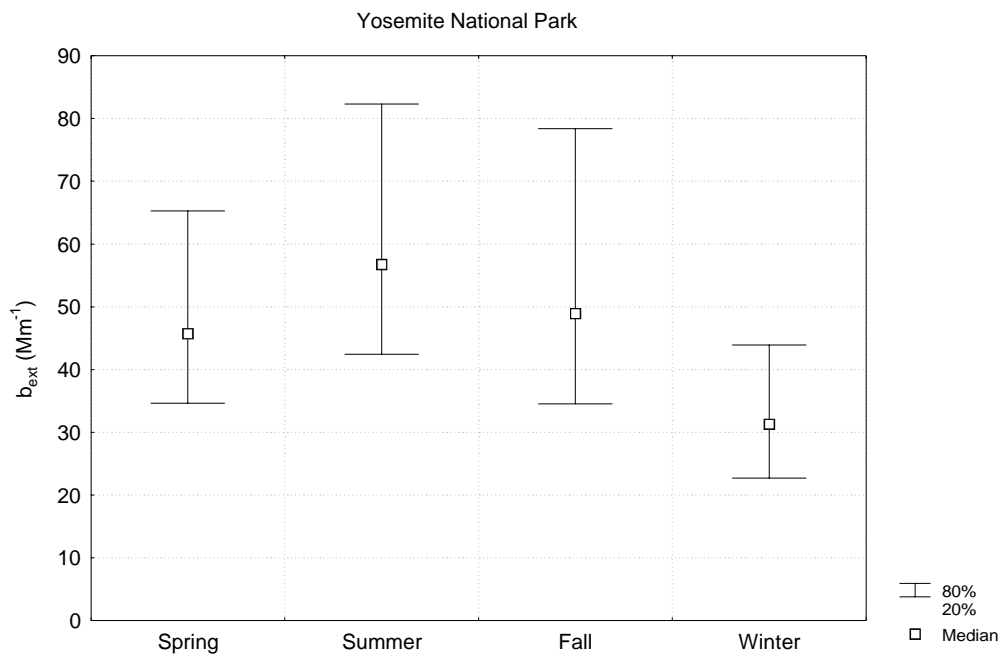


Figure 3-53 Seasonal Median and 20th and 80th Percentiles of the Light Extinction Coefficient at Yosemite National Park

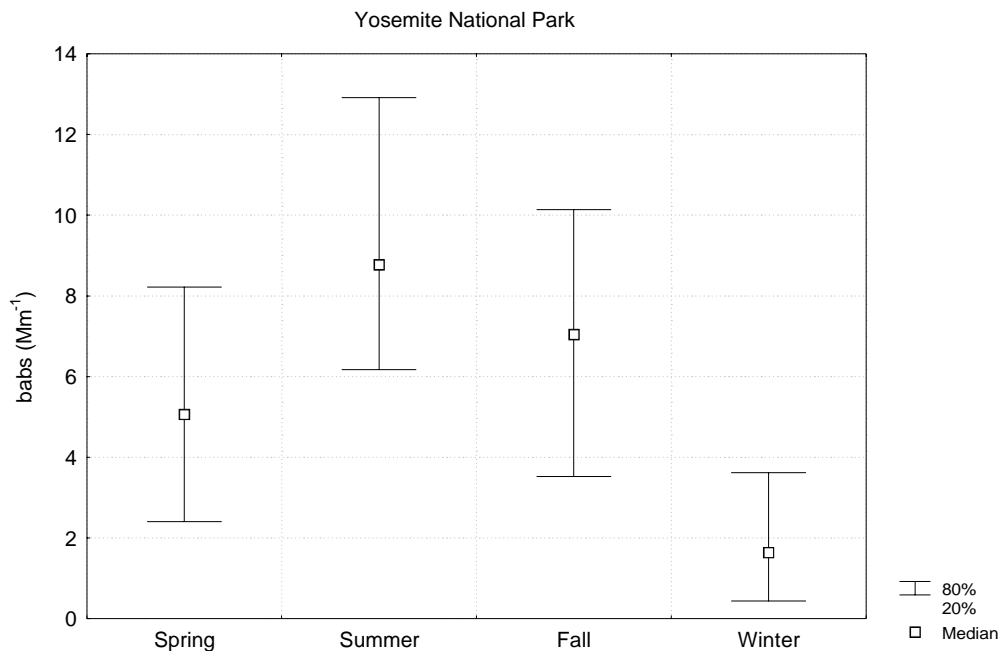


Figure 3-54 Seasonal Median and 20th and 80th Percentiles of the Particle Light Absorption Coefficient at Yosemite National Park

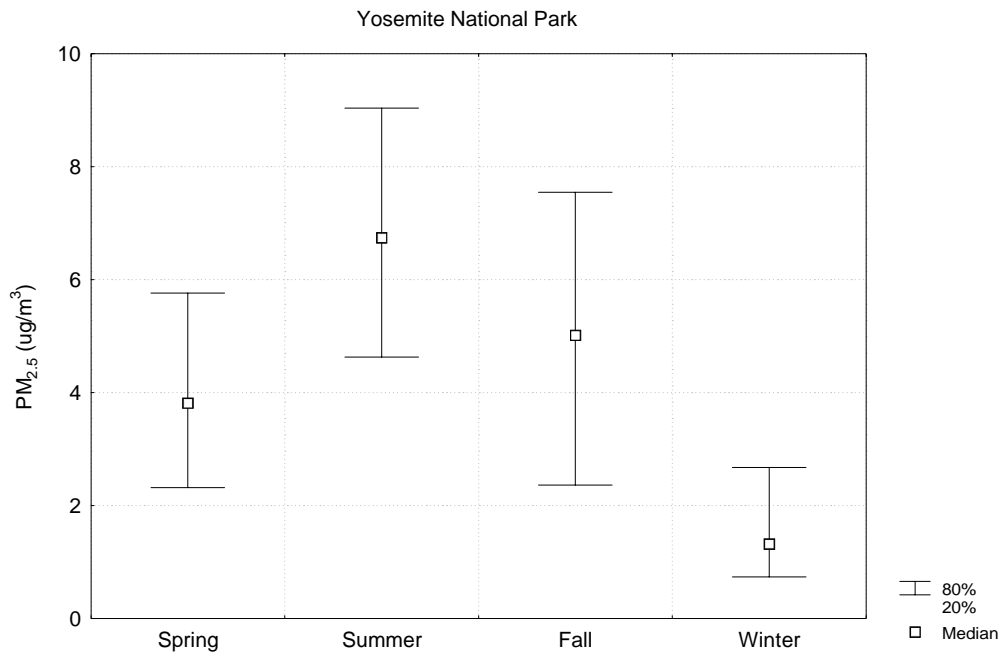


Figure 3-55 Seasonal Median and 20th and 80th Percentiles of PM_{2.5} Mass Concentration at Yosemite National Park

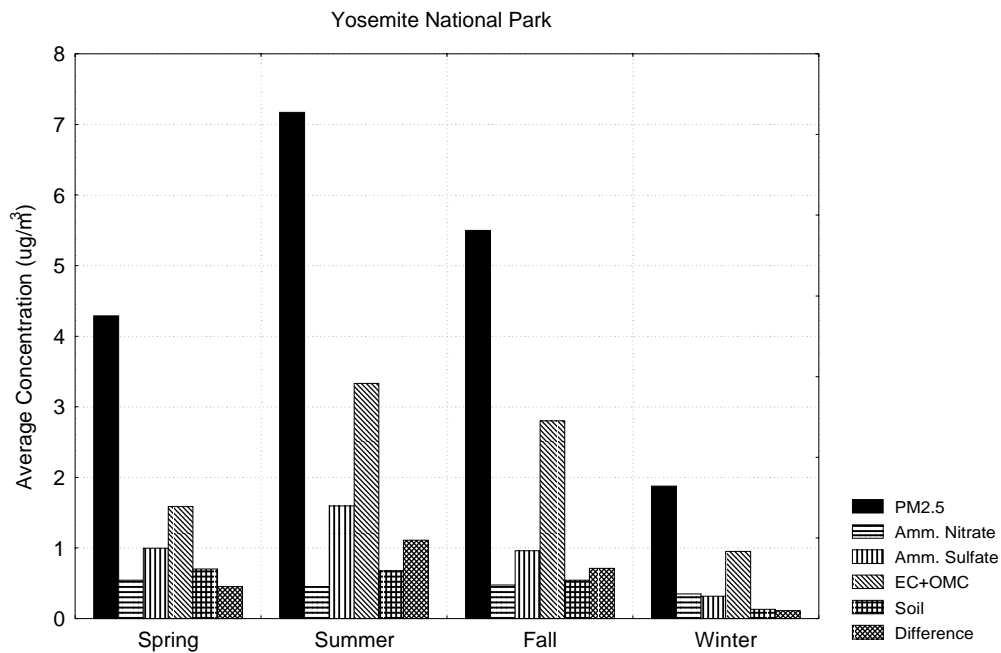


Figure 3-56 Seasonal Average PM_{2.5} Mass and Estimated Chemical Constituent Concentrations at Yosemite National Park

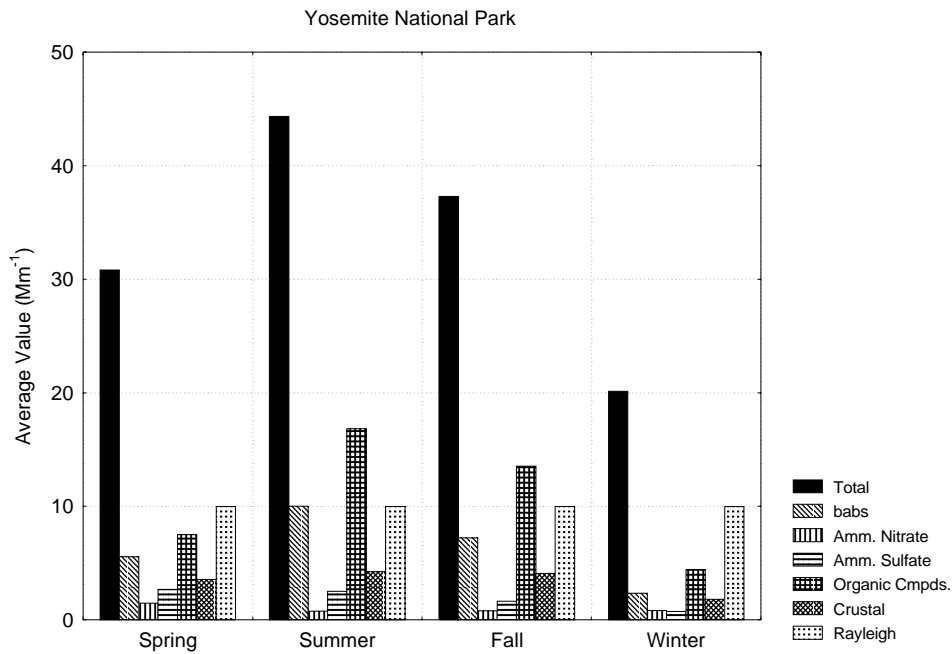


Figure 3-57 Contributions to Calculated Seasonal Average Light Extinction Coefficient at Yosemite National Park

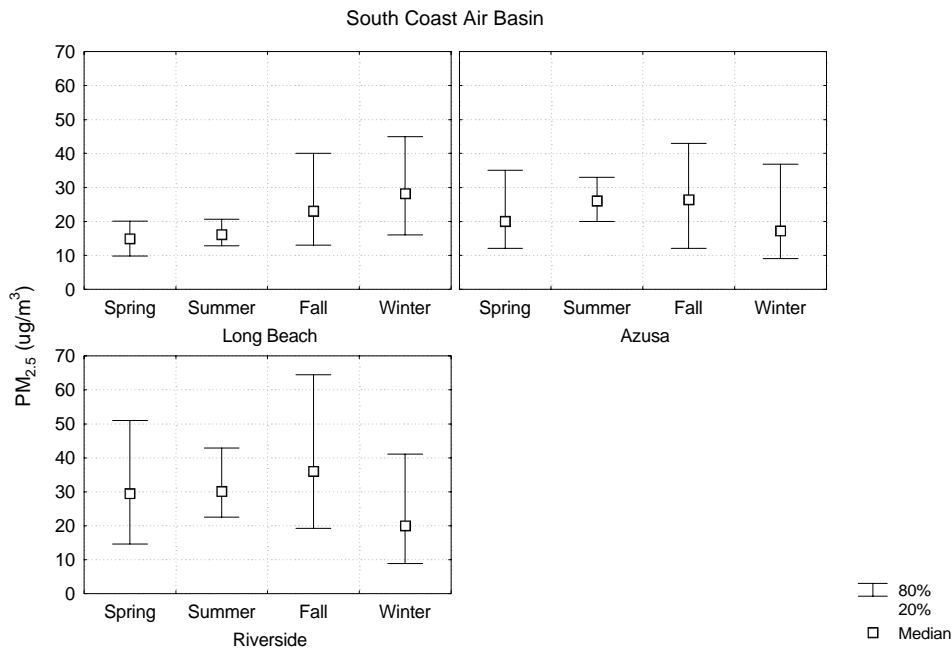


Figure 3-58 Seasonal Median and 20th and 80th Percentiles of PM_{2.5} Mass Concentration at South Coast Air Basin Sites

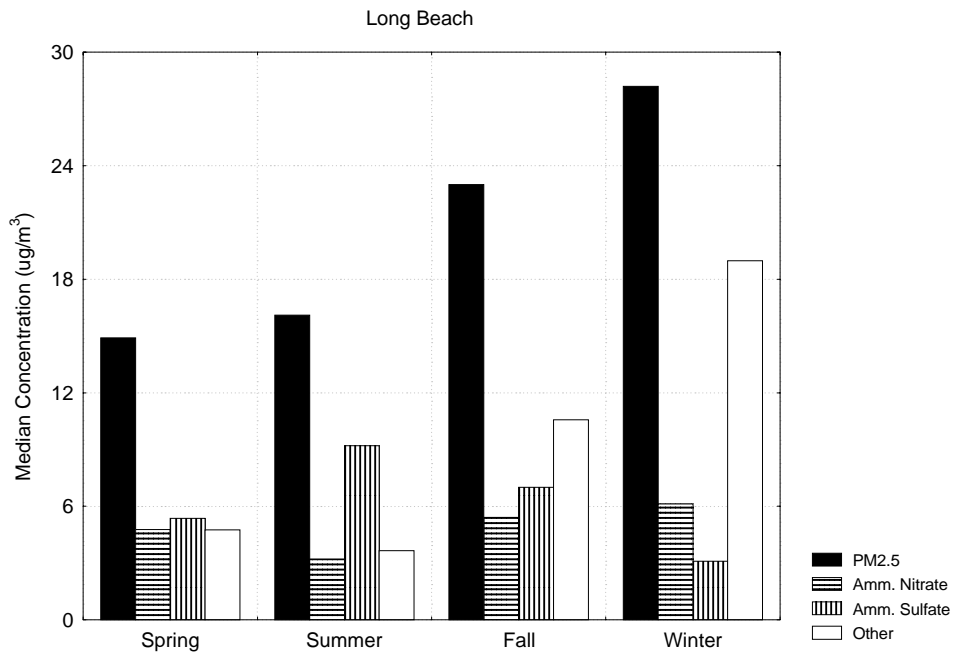


Figure 3-59 Seasonal Median PM_{2.5} Mass and PM₁₀ Ammonium Nitrate and Ammonium Sulfate Concentrations at Long Beach

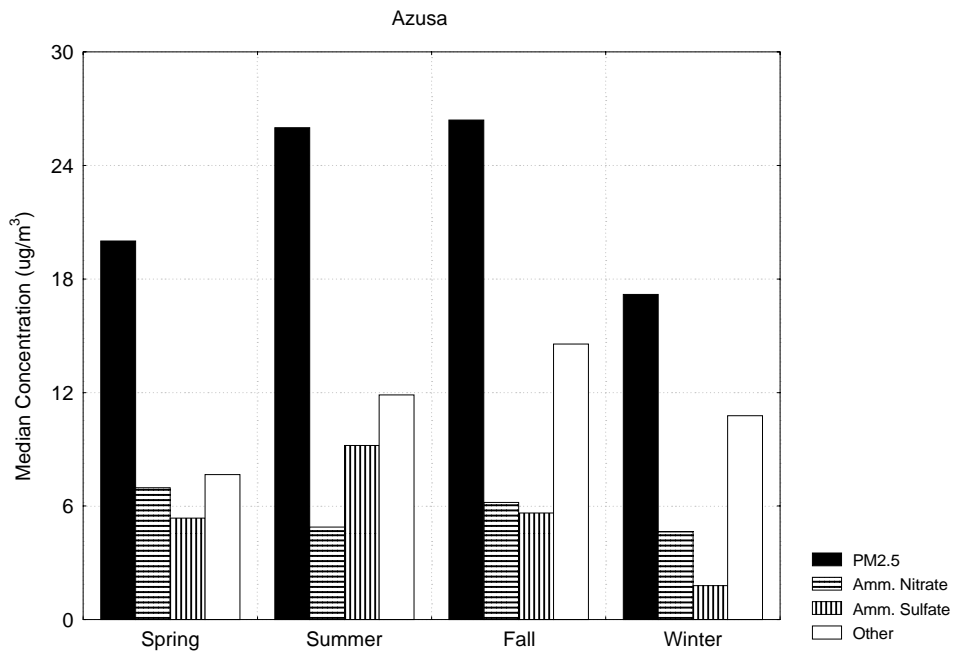


Figure 3-60 Seasonal Median PM_{2.5} Mass and PM₁₀ Ammonium Nitrate and Ammonium Sulfate Concentrations at Azusa

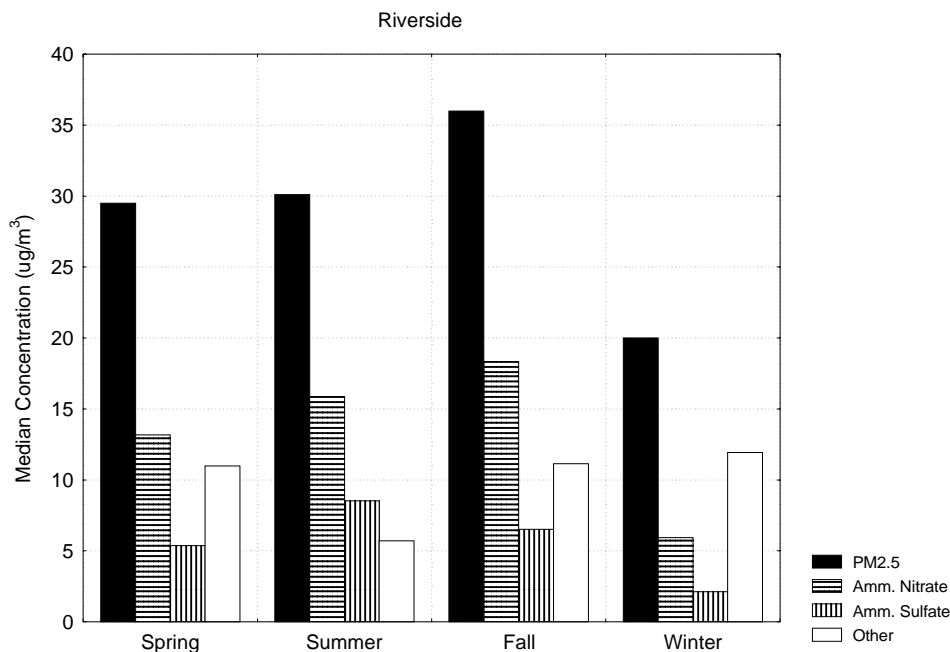


Figure 3-61 Seasonal Median PM_{2.5} Mass and PM₁₀ Ammonium Nitrate and Ammonium Sulfate Concentrations at Riverside

Median ammonium sulfate concentrations are about the same at all three sites during each season, while median ammonium nitrate concentrations tend to increase from west to east (Long Beach to Azusa to Riverside) during all seasons except winter, when the median ammonium nitrate concentration is higher at Long Beach than at the other sites. These seasonal patterns suggest that:

- Morning stratus clouds during early summer may facilitate formation of sulfate
- Cooler temperatures during fall and winter promote formation of ammonium nitrate
- Ammonia emissions upwind of Riverside promote formation of ammonium nitrate at Riverside, even during summer when higher temperatures would otherwise favor the presence of gaseous nitric acid

Seasonal median and 20th and 80th percentiles of the measured light scattering and absorption coefficients and measured PM_{2.5} mass concentration at San Geronio Wilderness Area are shown in Figure 3-62 through Figure 3-65. The highest values of the median and 80th percentiles of all three quantities occur during the spring and summer. As mentioned previously, this is consistent with transport from the South Coast Air Basin during warmer periods with increased mixing depths.

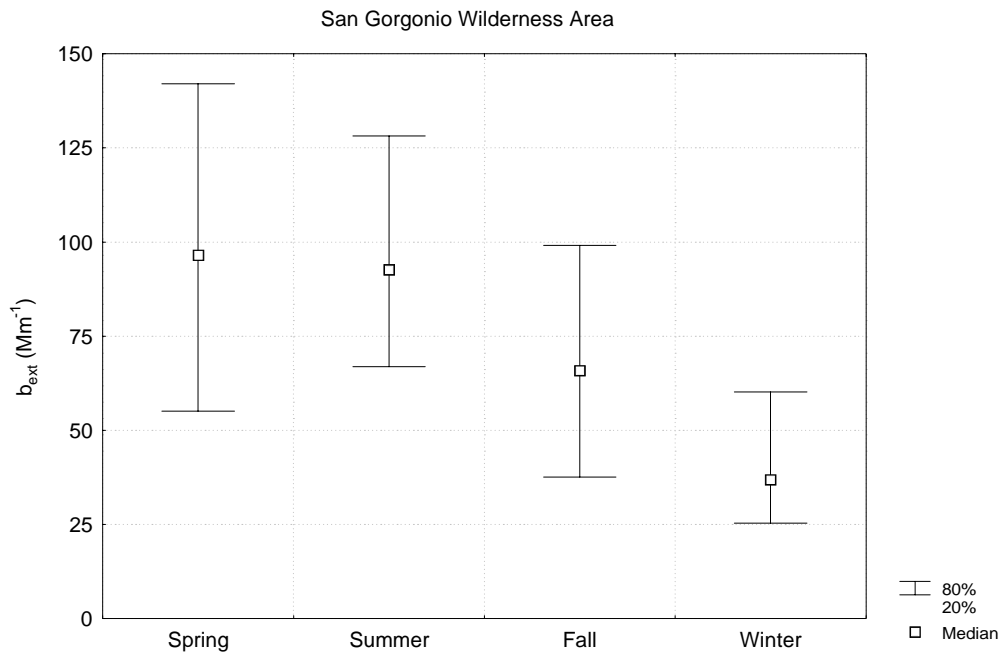


Figure 3-62 Seasonal Median and 20th and 80th Percentiles of the Light Extinction Coefficient at San Gorgonio Wilderness Area

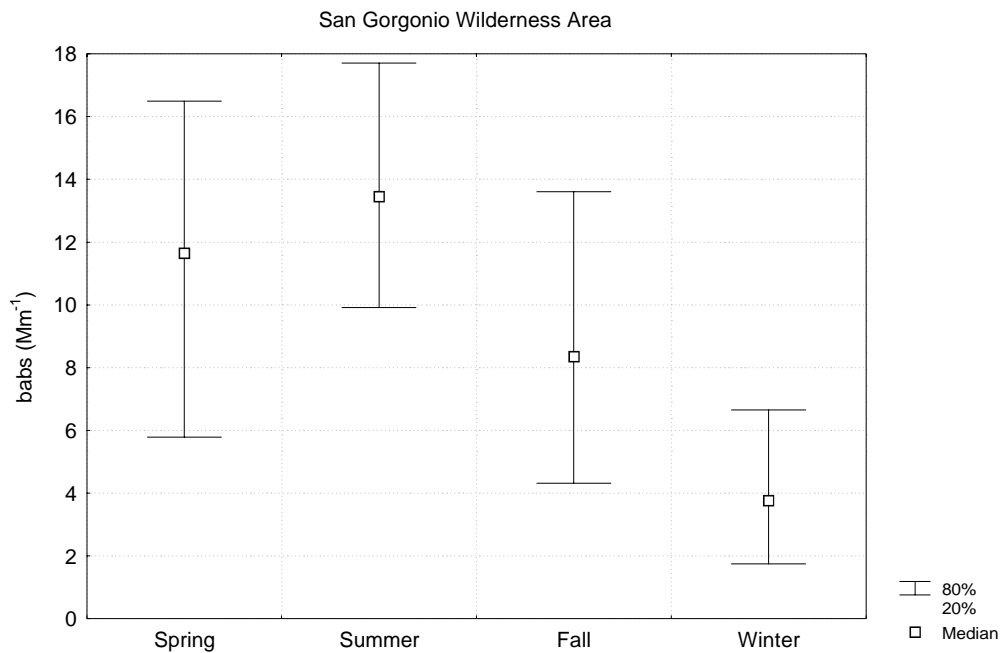


Figure 3-63 Seasonal Median and 20th and 80th Percentiles of the Particle Light Absorption Coefficient at San Gorgonio Wilderness Area

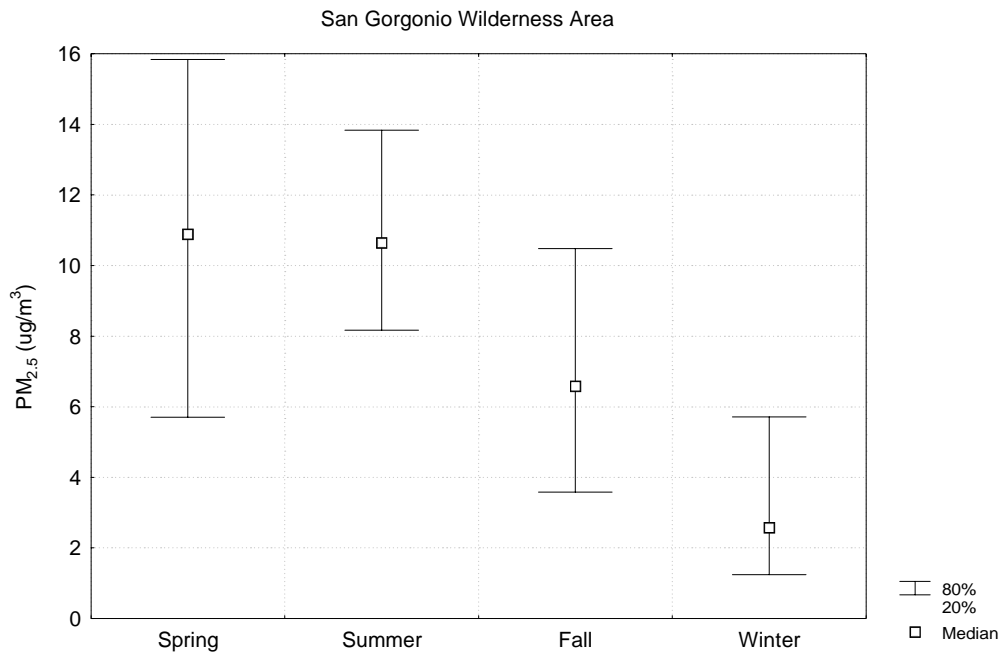


Figure 3-64 Seasonal Median and 20th and 80th Percentiles of PM_{2.5} Mass Concentration at San Geronio Wilderness Area

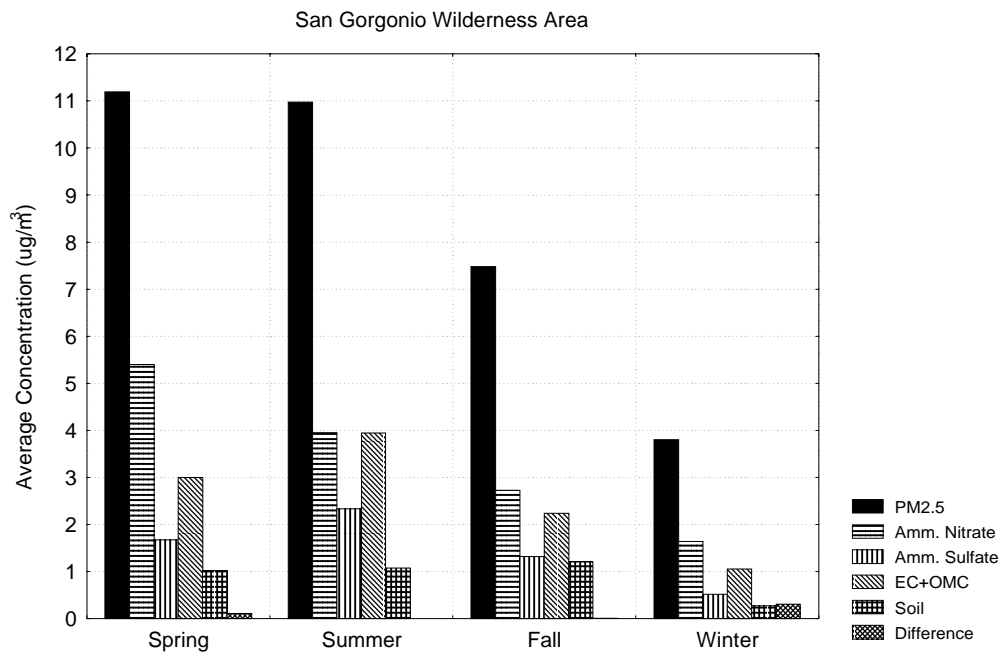


Figure 3-65 Seasonal Average PM_{2.5} Mass and Estimated Chemical Constituent Concentrations at San Geronio Wilderness Area

Seasonal average PM_{2.5} constituent concentrations at San Geronio Wilderness Area are shown in Figure 3-65. Ammonium nitrate is estimated to be the largest constituent during every season, followed by EC+OMC and ammonium sulfate. The similarity in the relative contributions of the constituents at San Geronio Wilderness Area to the relative contributions at Riverside (Figure 3-61), the easternmost site in the South Coast Air Basin, is consistent with much of the particulate matter at San Geronio coming from transport from the South Coast Air Basin.

Estimated seasonal average values of the light extinction coefficient and its constituents are shown in Figure 3-66. Light scattering by ammonium nitrate is estimated to be the largest contributor during every season, particularly spring. The contributions from light absorption and light scattering by the other constituents (ammonium sulfate, organic compounds, soil-derived materials and light molecules) all contribute similar amounts.

3.2.11 Salton Sea (Southeast Desert) Air Basin

El Centro is at the southern end of the Salton Sea Air Basin (located within the Southeast Desert Air Basin), just north of the Mexican border.

Seasonal medians and 20th and 80th percentiles of the measured PM_{2.5} mass concentration are shown in Figure 3-67. Values are lower in the spring than in the other three seasons. The summer, fall and winter median values are all about the same, while the 80th percentile value is highest during winter.

Seasonal median PM_{2.5} mass and PM₁₀ ammonium nitrate and ammonium sulfate concentrations are shown in Figure 3-68. The "Other" category is the largest contributor during every season, followed by ammonium sulfate during all seasons except winter, when the median ammonium nitrate concentration slightly exceeds ammonium sulfate. Ammonium sulfate is highest during the summer, while median ammonium nitrate concentrations vary little with season, except for a slight increase during winter.

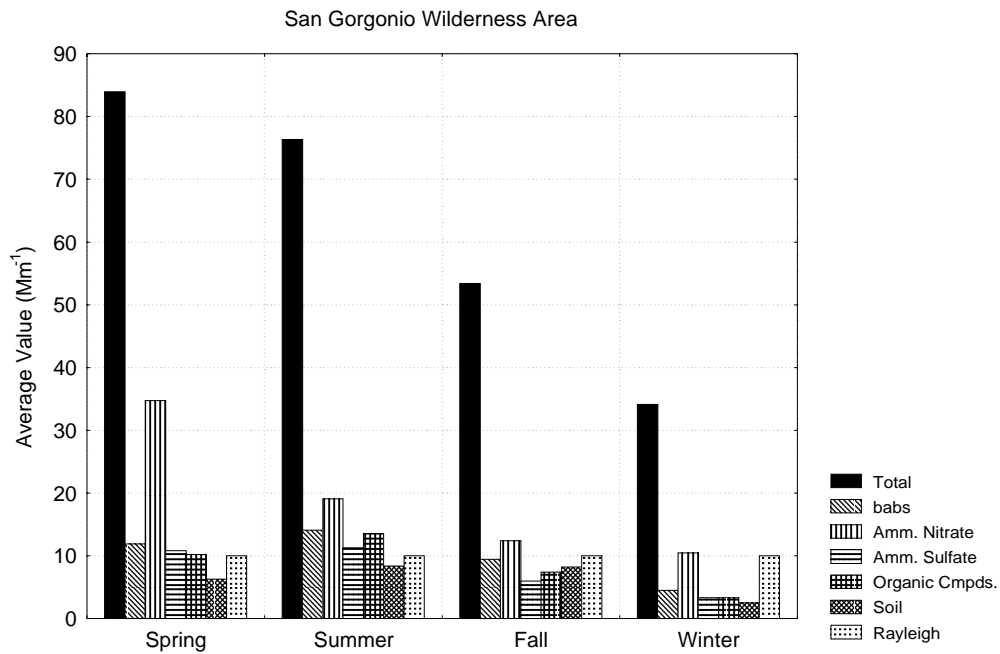


Figure 3-66 Contributions to Calculated Seasonal Average Light Extinction Coefficient at San Gorgonio Wilderness Area

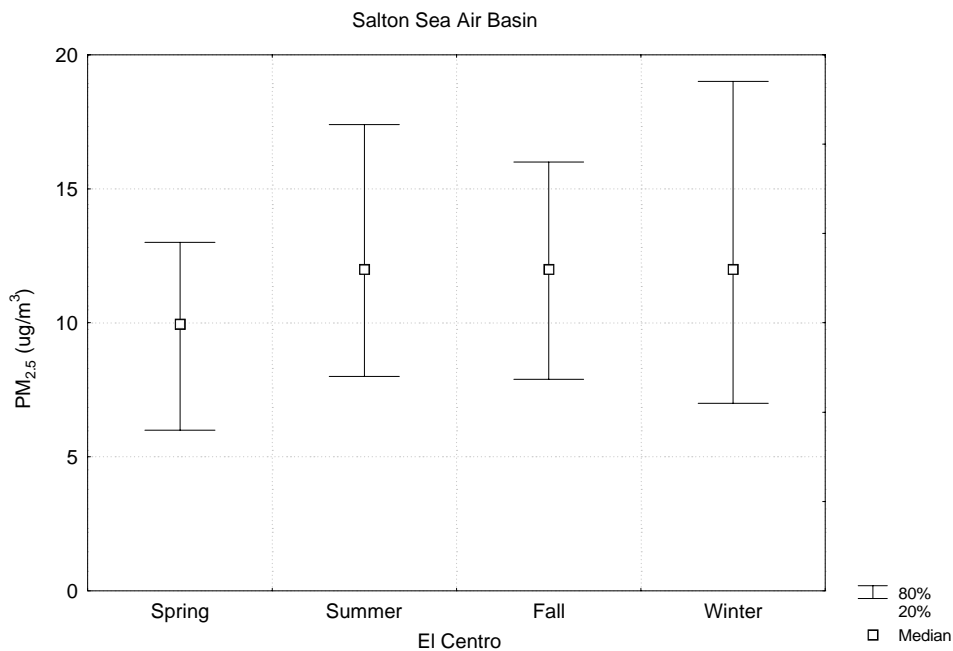


Figure 3-67 Seasonal Median and 20th and 80th Percentiles of PM_{2.5} Mass Concentration at El Centro

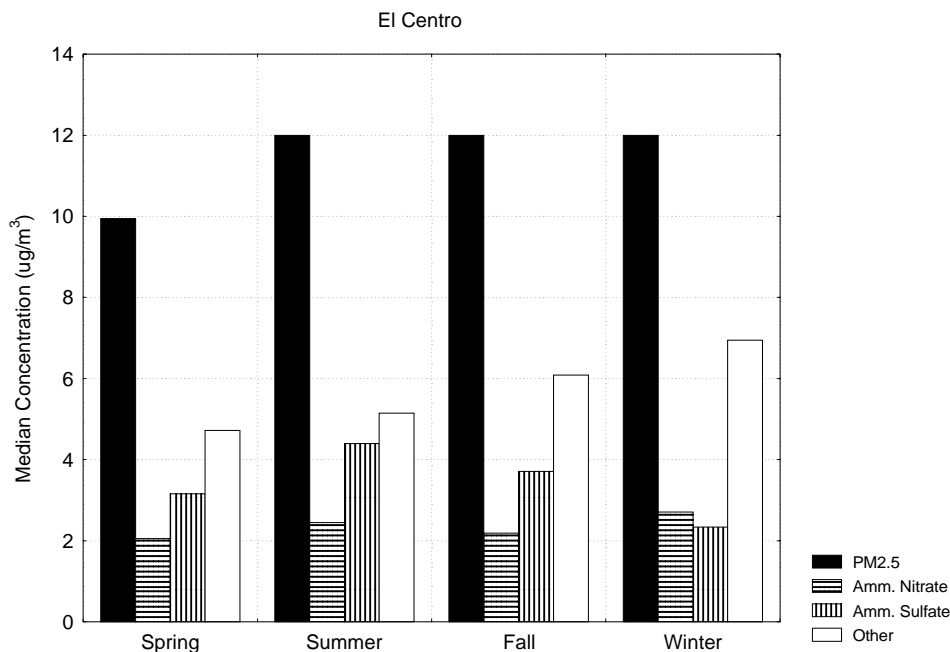


Figure 3-68 Seasonal Median PM_{2.5} Mass and PM₁₀ Ammonium Nitrate and Ammonium Sulfate Concentrations at El Centro

3.3 Summary

The presentations in this section have revealed the following general characteristics of the optical and particulate matter data:

- Carbon-containing materials and ammonium nitrate are the major constituents of PM_{2.5} and the major contributors to light extinction at the locations with the highest PM_{2.5} mass concentrations and the largest estimated light extinction coefficients. Wood burning may be a major source of the carbon-containing materials, particularly at locations with cooler fall and winter temperatures, while the ammonium nitrate is formed from atmospheric reactions that involve nitrogen oxides and ammonia.
- The highest PM_{2.5} concentrations in California are present in locations with surrounding topography that limits dispersion. These areas include the Central Valley, the South Coast Air Basin, the San Francisco Bay area and the Lake Tahoe Air Basin. The highest concentrations at these locations generally occur during the fall or winter, when periods of low inversions and low wind speeds lead to the accumulation of emitted particulate matter.

- Concentrations at coastal locations, such as Redwood National Park and Point Reyes National Seashore, do not vary as much with season as concentrations at inland locations, although there is a tendency for higher concentrations to occur during fall and winter than during spring and summer. Additionally, sodium chloride from sea spray is an important constituent of $PM_{2.5}$ at these locations.
- $PM_{2.5}$ concentrations and estimated light extinction at Yosemite and Lassen Volcanic National Parks are highest during the summer, in contrast with the other locations, and sulfate is a larger contributor than ammonium nitrate. Carbon-containing materials are also major contributors at these locations. This seasonal behavior may be caused by summertime park visitors or by transport from the Central Valley.
- $PM_{2.5}$ concentrations and estimated light extinction at San Geronio Wilderness Area are highest during spring and summer, when conditions are conducive to transport of material from the South Coast Air Basin.

4.0 HISTORICAL TRENDS AND THE ROLE OF EMISSIONS FROM THE ENERGY SECTOR

Historical changes in the available optical and particulate matter data were examined to identify any trends. Trends in estimated emissions were also examined for consistency with those trends. Additionally, the contributions to emissions of energy sector activities (production and use) were evaluated to assess the possible importance of the energy sector to visibility and particulate matter.

4.1 Trends in Optical and Particulate Matter Data

Serial time plots by year of median values of the data at local-agency sites and average values of the data at IMPROVE sites during each season were prepared and reviewed. These plots are contained in Appendix A. Visual examination of the plots suggested that there was a general decrease in some of the values at some of the sites during the period of record.

The statistical significance of the suggested downward trends was evaluated by calculating Spearman rank order correlation coefficients (Kendall, 1970) between the years and the optical and particulate matter data separately for each site and season. White (1996) applied and discussed the usefulness of this non-parametric statistic for examining trends in ambient atmospheric concentrations. It is the more familiar product-moment (Pearson) correlation applied to value rank rather than to the value itself. It is calculated by first numbering the years sequentially, beginning with one. The values for the quantity for all the years are then ranked from lowest to highest, and the resulting ranks are assigned to each year. For example, if the data set consists of eight years, the years would be numbered from one to eight, beginning with the first year, and the values would also be ranked from one to eight, with the lowest value being ranked one and the highest being ranked eight. If the second highest value (rank 7) occurred during the first year, year one would have value rank 7. The correlation coefficient between the year numbers and the associated ranks of the values is then calculated.

In order to allow comparison of the results among sites, the same time period was used for all of the calculations. Although data were available as early as 1985 from some sites, many sites did not begin measurements until 1989. Therefore, correlation coefficients were calculated using data from 1989 through 1996.

As mentioned in Section 2.2, seasonal median and average values were calculated only when at least half the possible measurements were reported. This criterion led to some sites without values available for all quantities during all years for the correlation coefficient calculations. Ideally, in order to avoid biases caused by years without data, the calculations would be made only when data were available for all eight of the years from 1989 through 1996. However, data were unavailable for only one of the eight years during several seasons at several sites. Therefore, correlation coefficients were calculated when either seven or eight years of data were available.

The number of correlation coefficients that were calculated for each quantity, the number of the values of the coefficient that were statistically significant at the five and ten percent levels, and the percent of the values that were significant at these levels are listed in Table 4-1. The significance level is the probability that an absolute value of the correlation coefficient as high as the observed value would occur by chance alone. The table summarizes the results for tests with all eight years of data as well as tests with either seven or eight years. The percentages of the correlation coefficients that were significant at each level are about the same with seven or eight years of data as with only eight years of data.

**Table 4-1
Number of Tests and Number of Statistically Significant Spearman Rank Order Correlations by Quantity**

Quantity	Tests with 7 or 8 Years of Data					Tests with 8 Years of Data				
	Number of Tests	Number Significant		Percent Significant		Number of Tests	Number Significant		Percent Significant	
		5% Level	10% Level	5% Level	10% Level		5% Level	10% Level	5% Level	10% Level
b_{abs}	24	10	16	42	67	18	10	13	56	72
b_{ext}	3	0	0	0	0	1	0	0	0	0
b_{sp}	36	8	10	22	28	26	6	8	23	31
Calc. b_{ext}	24	6	8	25	33	18	5	6	28	33
Calc. b_{sp}	24	4	6	17	25	18	3	4	17	22
COH	36	8	10	22	28	26	7	7	27	27
EC+OMC	24	5	8	21	33	18	4	5	22	28
Nitrate	61	8	14	13	23	42	6	9	14	21
PM _{2.5}	67	16	20	24	30	43	10	12	23	28
Sulfate	61	13	18	21	30	43	8	12	19	28

If there were no relationship between year and the observed values of the quantities, about five percent of the correlation coefficients would be expected to be significant at the five percent level and about ten percent of the values would be expected to be significant at the ten percent level. As seen in the table, these percentages are exceeded for many of the quantities. Forty-two percent of the correlation coefficients for the particle light absorption coefficient (b_{abs}) and more than 20 percent of the correlation coefficients for the measured particle light scattering coefficient (b_{sp}), the calculated light extinction coefficient (b_{ext}), the coefficient of haze (COH), the sum of elemental carbon and estimated organic compounds (EC+OMC), PM_{2.5} mass, and sulfate are significant at the five percent level when sites and seasons with either seven or eight years of data are included. All but six of the correlation coefficients that were statistically significant at the 10 percent level were negative, which means that

there was a statistically significant reduction in PM_{2.5} concentrations and the resulting optical effects between 1989 and 1996 during many seasons at several locations in California.

The correlation coefficients for the sites, seasons and quantities for which the significance level was ten percent or less are listed in Table 4-2 along with the probabilities that the observed values of the correlation coefficient occurred by chance. Statistically significant decreases were consistently observed at:

- South Lake Tahoe during summer and fall
- Pinnacles National Monument during summer, fall and winter
- Redwood National Park during all four seasons
- Several sites in the Sacramento Valley Air Basin during all four seasons
- Several sites in the San Joaquin Valley Air Basin during all four seasons, particularly during winter
- San Geronio Wilderness Area during spring and fall

As an example of the trends, median concentrations of PM_{2.5} mass and PM₁₀ nitrate and sulfate during winter at Modesto are shown in Figure 4-1. Another example is shown in Figure 4-2 and Figure 4-3, which shows average values during spring at San Geronio Wilderness Area. Although the decreases are not as consistent at San Geronio Wilderness Area as at Modesto, the trends are significant at the five percent level or less.

**Table 4-2
Statistically Significant Trends at the 10% Level from 1989 through 1996 based on the Spearman Rank Order Correlation Coefficient**

Air Basin	Season	Site	Quantity	Number Valid ^a	Spearman R ^b	p-Level ^c
Lake County	Winter	Lakeport	COH	8	-0.826	0.011
Lake Tahoe	Summer	South Lake Tahoe	b _{abs}	7	-0.750	0.052
			Calc. b _{ext}	7	-0.893	0.007
			Calc. b _{sp}	7	-0.929	0.003
			PM _{2.5}	7	-0.857	0.014
			EC+OMC	7	-0.929	0.003
	Fall	South Lake Tahoe	b _{abs}	7	-0.679	0.094
			EC+OMC	7	-0.750	0.052
Mountain Counties	Spring	Yosemite NP	b _{abs}	8	-0.714	0.047
	Summer	Yosemite NP	b _{abs}	8	-0.714	0.047
	Winter	Yosemite NP	b _{abs}	8	-0.690	0.058
North Central Coast	Summer	Pinnacles NM	b _{abs}	8	-0.714	0.047
			Calc. b _{ext}	8	-0.833	0.010
	Fall	Pinnacles NM	b _{abs}	8	-0.690	0.058
			PM _{2.5}	8	-0.857	0.007
	Winter	Pinnacles NM	b _{abs}	8	-0.667	0.071
			Calc. b _{ext}	8	-0.857	0.007
			Calc. b _{sp}	8	-0.786	0.021
			PM _{2.5}	8	-0.833	0.010
			Nitrate	8	-0.810	0.015
			Sulfate	8	-0.747	0.033
		EC+OMC	8	-0.714	0.047	
North Coast	Spring	Redwood NP	Calc. b _{ext}	8	-0.643	0.086
			Calc. b _{sp}	8	-0.643	0.086
			Nitrate	8	-0.623	0.099
	Summer	Redwood NP	b _{abs}	8	-0.786	0.021
			EC+OMC	8	-0.857	0.007
	Fall	Redwood NP	b _{abs}	8	-0.738	0.037
			Calc. b _{ext}	8	-0.714	0.047
	Winter	Redwood NP	b _{abs}	8	-0.762	0.028
			EC+OMC	8	-0.762	0.028

**Table 4-2
Statistically Significant Trends at the 10% Level from 1989 through 1996 based on the Spearman
Rank Order Correlation Coefficient**

Air Basin	Season	Site	Quantity	Number Valid^a	Spearman R^b	p-Level^c
Northeast Plateau	Fall	Lassen Volcanic NP	EC+OMC	7	-0.685	0.090
Sacramento Valley	Spring	Colusa	b _{sp}	8	0.786	0.021
		Gridley	COH	7	0.842	0.017
		Yuba City	b _{sp}	8	0.810	0.015
	Summer	Colusa	b _{sp}	8	0.881	0.004
			COH	8	-0.952	0.000
		Pleasant Grove	COH	8	0.762	0.028
	Fall	Colusa	b _{sp}	7	0.929	0.003
			COH	7	-0.750	0.052
		Gridley	b _{sp}	8	-0.743	0.035
		Pleasant Grove	COH	8	0.714	0.047
	Winter	Chico	b _{sp}	8	-0.762	0.028
		Colusa	COH	8	-0.738	0.037
		Gridley	b _{sp}	7	-0.714	0.071
Pleasant Grove		b _{sp}	8	-0.738	0.037	
Salton Sea	Summer	El Centro	Sulfate	7	-0.714	0.071
	Fall	El Centro	Sulfate	7	-0.891	0.007
San Francisco Bay	Spring	Point Reyes NS	b _{abs}	8	-0.786	0.021
		San Jose	PM _{2.5}	7	-0.883	0.008
	Summer	Point Reyes NS	b _{abs}	8	-0.762	0.028
	Fall	Point Reyes NS	b _{abs}	8	-0.810	0.015
			Calc. b _{ext}	8	-0.810	0.015
			Calc. b _{sp}	8	-0.762	0.028
			PM _{2.5}	8	-0.690	0.058
			Nitrate	8	-0.850	0.007
EC+OMC	8	-0.707	0.050			
San Joaquin Valley	Spring	Bakersfield	PM _{2.5}	8	-0.964	0.000
			Nitrate	8	-0.738	0.037
			Sulfate	8	-0.762	0.028
		Fresno	PM _{2.5}	8	-0.743	0.035
			Sulfate	8	-0.699	0.054
		Madera	PM _{2.5}	8	-0.667	0.071
			Sulfate	7	-0.775	0.041

**Table 4-2
Statistically Significant Trends at the 10% Level from 1989 through 1996 based on the Spearman Rank Order Correlation Coefficient**

Air Basin	Season	Site	Quantity	Number Valid ^a	Spearman R ^b	p-Level ^c
		Stockton	COH	8	-0.714	0.047
			PM _{2.5}	8	-0.719	0.045
		Visalia	PM _{2.5}	8	-0.898	0.002
			Sulfate	8	-0.914	0.001
	Summer	Bakersfield	Nitrate	8	-0.881	0.004
			Sulfate	8	-0.743	0.035
		Fresno	Sulfate	8	0.778	0.023
		Modesto	Sulfate	8	-0.659	0.076
	Fall	Bakersfield	Sulfate	8	-0.929	0.001
			Fresno	Sulfate	8	-0.647
		Stockton	COH	8	-0.786	0.021
			Nitrate	7	-0.714	0.071
			Sulfate	7	-0.786	0.036
		Visalia	Sulfate	8	-0.659	0.076
	Winter	Bakersfield	PM _{2.5}	7	-0.679	0.094
			Nitrate	7	-0.750	0.052
			Sulfate	7	-0.757	0.049
		Fresno	Nitrate	7	-0.714	0.071
			Sulfate	8	-0.786	0.021
		Madera	PM _{2.5}	7	-0.786	0.036
		Modesto	PM _{2.5}	7	-0.821	0.023
			Nitrate	7	-0.893	0.007
			Sulfate	7	-0.937	0.002
		Stockton	COH	7	-0.679	0.094
			PM _{2.5}	7	-0.857	0.014
			Sulfate	8	-0.826	0.011
		Visalia	PM _{2.5}	8	-0.762	0.028
			Nitrate	8	-0.690	0.058
South Coast	Spring	Long Beach	PM _{2.5}	8	-0.952	0.000
		San Geronio WA	b _{abs}	8	-0.833	0.010
			Calc. b _{ext}	8	-0.786	0.021
			Calc. b _{sp}	8	-0.714	0.047
			PM _{2.5}	8	-0.762	0.028

**Table 4-2
Statistically Significant Trends at the 10% Level from 1989 through 1996 based on the Spearman
Rank Order Correlation Coefficient**

Air Basin	Season	Site	Quantity	Number Valid ^a	Spearman R ^b	p-Level ^c
			Nitrate	8	-0.762	0.028
			EC+OMC	8	-0.714	0.047
	Summer	Azusa	PM _{2.5}	7	-0.821	0.023
			Riverside	Nitrate	8	-0.690
	Fall	San Gorgonio WA	b _{abs}	7	-0.750	0.052
			Calc. b _{ext}	7	-0.750	0.052
			Calc. b _{sp}	7	-0.750	0.052
			PM _{2.5}	7	-0.750	0.052
			Nitrate	7	-0.775	0.041
	Winter	Long Beach	PM _{2.5}	8	-0.929	0.001
			Nitrate	8	-0.881	0.004
	^a Number of years with at least half of the possible values during the season ^b Value of the Spearman rank order correlation coefficient ^c Probability that the value of the correlation coefficient occurred by chance					

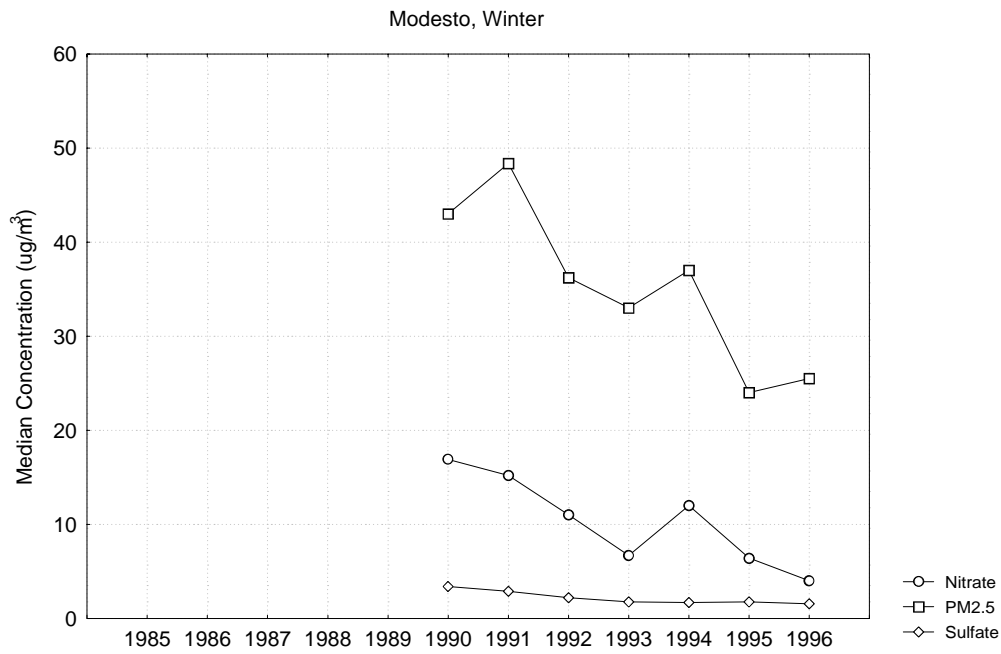


Figure 4-1 Median PM_{2.5} Mass and PM₁₀ Nitrate and Sulfate Concentrations Measured at Modesto during Winter from 1990 through 1996

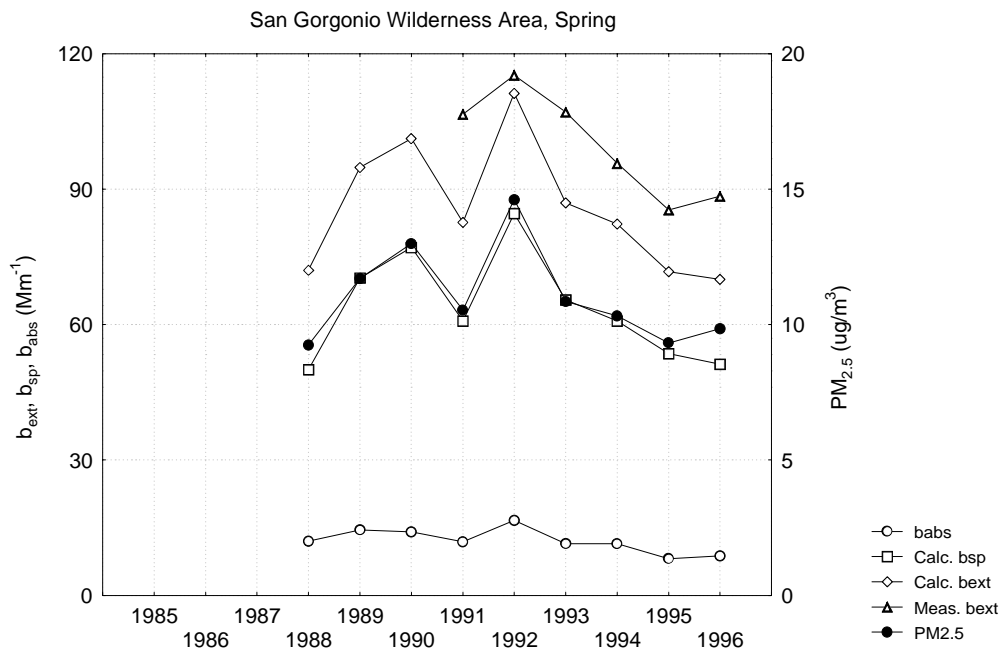


Figure 4-2 Average Measured b_{ext}, b_{abs} and PM_{2.5} Mass Concentration and Calculated b_{ext} and b_{sp} during Spring at San Gorgonio Wilderness Area from 1988 through 1996

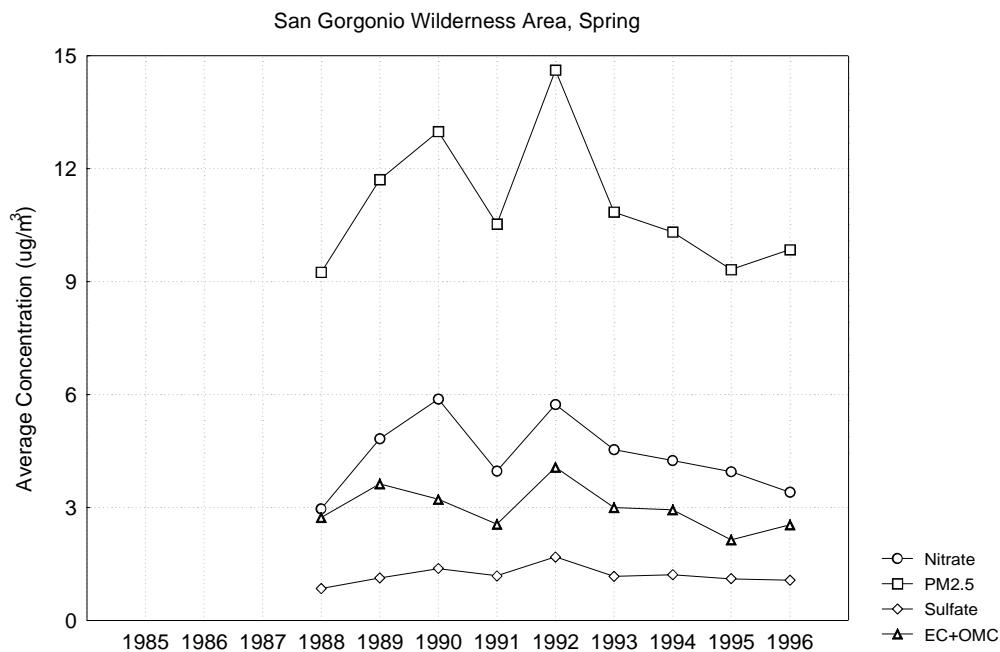


Figure 4-3 Average Measured PM_{2.5} Mass, Nitrate and Sulfate Concentrations during Spring at San Gorgonio Wilderness Area from 1988 through 1996

4.2 Trends in Emissions and the Role of the Energy Sector

Estimated annual average emissions and the percentages contributed by energy production and non-mobile source energy use during 1985, 1990 and 1995 are listed by air basin in Table 4-3 through Table 4-5. Non-mobile source energy use is fuel combustion by all sources except mobile sources and electric generating plants. Mobile sources include both on-road and non-road vehicles and mobile equipment. Increases from one time period to the next are in bold. Note that the Salton Sea Air Basin is within the Southeast Desert Air Basin.

Estimated primary PM_{2.5} emissions (Table 4-3) increased in every air basin between 1985 and 1990 and then decreased between 1990 and 1995 except in the San Francisco Bay and Southeast Desert Air Basins. These decreases between 1990 and 1995 are consistent with the observed decreases in PM_{2.5} mass and EC+OMC that occurred at many of the monitoring sites. The estimated contribution from energy production was two percent or less of the total PM_{2.5} emissions, except during 1990 in the North Coast Air Basin, where it was four percent. These extremely low percentages suggest that emissions from energy production were not major contributors to primary PM_{2.5}. The percentages contributed by non-mobile source energy use varied among air basins. The highest percentage contributions from non-mobile source energy use (about 60 percent) were in the Lake Tahoe Air Basin

because of the substantial emissions from residential wood combustion. Contributions from non-mobile source energy use were about 30 percent in the North Coast and San Francisco Air Basins, primarily from residential fuel use.

Other source categories, excluding energy production and non-mobile source fuel use, that are major contributors to estimated primary PM_{2.5} emissions vary between air basins. However, wind blown dust and fugitive dust from vehicle travel on paved and unpaved roads are major contributors in every air basin. Managed burning and wild fires are also major contributors in all of the air basins listed except the Lake Tahoe, San Francisco, San Joaquin Valley, South Coast and Southeast Desert Air Basins.

**Table 4-3
Annual Average PM_{2.5} Emissions and Contributions from Energy Production and Non-Mobile Source Energy Use by Air Basin during 1985, 1990 and 1995**

Air Basin	Emissions (tons/day)			Percent from Energy Production			Percent from Non-Mobile Source Energy Use		
	1985	1990	1995	1985	1990	1995	1985	1990	1995
Lake County	5.2	5.4	5.6	0	1	1	20	22	22
Lake Tahoe	2.3	2.5	2.4	0	0	0	60	60	62
Mountain Counties	40.6	45.4	48.2	0	1	0	35	34	35
North Central Coast	21.9	24.4	22.2	0	1	0	22	17	16
North Coast	32.8	35.9	33.0	0	4	2	33	24	24
Northeast Plateau	27.5	35.4	35.2	0	0	0	24	19	19
Sacramento Valley	95.5	105.3	97.3	0	0	0	15	16	19
San Francisco	68.5	69.7	70.5	0	1	0	27	29	30
San Joaquin Valley	95.5	105.3	97.3	0	0	0	15	16	19
South Coast	169.9	183.6	161.1	1	1	0	16	16	18
Southeast Desert	81.1	104.6	155.8	0	0	0	3	3	2

Estimated NO_x emissions (Table 4-4) increased between 1985 and 1990 in most air basins and then declined from 1990 to 1995 in all basins. This decline is consistent with observed decreases in nitrate concentrations, particularly during winter at many of the San Joaquin Valley sites. The contribution to estimated NO_x emissions from energy production was five percent or less, except in the North Central Coast Air Basin, where it was about 15 percent. The percentage contribution either remained constant from 1990 to 1995 or declined slightly in all air basins except the North Coast. The relatively low percentages suggest that emissions from energy production were not major contributors to observed nitrate concentrations. Estimated NO_x emissions from non-mobile source energy use varied among

air basins, with the highest percentages occurring in the Southeast Desert, San Francisco and North Central Coast Air Basins. The estimated contributions from non-mobile source energy use increased in about half the air basins in the table between 1990 and 1995. These increases in percentages were caused primarily by decreases in the emissions from mobile sources, which are the largest contributors to NO_x emissions in every air basin, rather than by increases in emissions from energy use.

**Table 4-4
Annual Average NO_x Emissions and Contributions from Energy Production and Non-Mobile Source Energy Use by Air Basin during 1985, 1990 and 1995**

Air Basin	Emissions (tons/day)			Percent from Energy Production			Percent from Non-Mobile Source Energy Use		
	1985	1990	1995	1985	1990	1995	1985	1990	1995
Lake County	5.9	6.4	6.1	0	0	2	4	7	4
Lake Tahoe	4.0	3.9	3.5	0	0	0	6	7	8
Mountain Counties	54.9	69.0	59.9	0	2	1	9	9	12
North Central Coast	102.1	105.1	80.5	14	15	14	18	15	15
North Coast	56.5	63.2	53.8	1	1	3	11	10	9
Northeast Plateau	38.8	40.7	36.9	0	0	0	4	3	5
Sacramento Valley	268.2	301.1	266.7	1	2	2	6	8	10
San Francisco	679.8	669.1	576.3	5	4	2	16	16	18
San Joaquin Valley	268.2	301.1	266.7	1	2	2	6	8	10
South Coast	1380.3	1431.5	1175.4	3	2	2	16	11	9
Southeast Desert	278.1	363.3	316.8	1	2	2	36	21	23

Estimated SO_x emissions (Table 4-5) increased between 1985 and 1990 in about half the air basins and then declined substantially from 1990 to 1995 in all of the air basins. These decreases were generally not accompanied by observed declines in sulfate concentrations, except at the San Joaquin Valley and El Centro sites. The estimated contributions from energy production were less than two percent in all air basins during 1995 except the North Coast (21 percent), Mountain Counties (13 percent) North Central Coast (nine percent) and Southeast Desert (seven percent). The estimated percentage contribution from non-mobile source energy use, such as wood and fuel oil combustion, increased between 1990 and 1995 in most air basins, reaching 41 percent in the Mountain Counties Air Basin, 30 percent in the Northeast Plateau Air Basin, 24 percent in the Lake Tahoe Air Basin, and 20 percent in the Lake County Air Basin. These high percentages and the relatively large fractions of

PM_{2.5} mass measured at Lassen Volcanic and Yosemite National Parks in the Northeast Plateau and Mountain Counties Air Basins, respectively, during the summer suggest that SO_x emissions from non-mobile source energy use may be important contributors to PM_{2.5} mass at those locations.

Other source categories, excluding energy production and non-mobile source fuel use, that are major contributors to estimated SO_x emissions include mobile sources in every air basin and petroleum refineries in the San Francisco and South Coast Air Basins.

**Table 4-5
Annual Average SO_x Emissions and Contributions from Energy Production and Non-Mobile Source Energy Use by Air Basin during 1985, 1990 and 1995**

Air Basin	Emissions (tons/day)			Percent from Energy Production			Percent from Non-Mobile Source Energy Use		
	1985	1990	1995	1985	1990	1995	1985	1990	1995
Lake County	1.0	1.1	0.5	0	0	0	10	10	20
Lake Tahoe	0.6	0.6	0.2	0	0	0	10	11	24
Mountain Counties	9.4	13.4	4.8	0	6	13	10	20	41
North Central Coast	17.6	19.1	4.5	4	18	9	31	14	17
North Coast	12.8	14.2	4.5	0	5	21	24	13	17
Northeast Plateau	7.5	8.1	2.0	0	0	0	9	9	30
Sacramento Valley	40.6	42.9	11.5	0	0	0	4	3	10
San Francisco	119.4	118.0	82.0	2	2	0	14	11	13
San Joaquin Valley	40.6	42.9	11.5	0	0	0	4	3	10
South Coast	123.0	91.7	75.7	6	5	1	10	10	10
Southeast Desert	27.2	19.1	19.0	1	1	7	32	19	15

Estimated emissions and percentage contributions from energy production and non-mobile source fuel use are shown graphically at five-year intervals from 1985 through 2010 in Figure 4-4 through Figure 4-25. As seen in the figures, PM_{2.5} emissions are projected to increase in the future in almost every air basin, largely because of increases in emissions from paved and unpaved road travel and from residential wood combustion. NO_x emissions are expected to continue to decrease, largely because of additional reductions from mobile sources. SO_x emissions are expected to remain fairly constant in the future.

As primary PM_{2.5} emissions increase, the percentage contributed by energy production is generally expected to decline, because substantial increases in primary PM_{2.5} emissions from energy production

are not anticipated. The percentages contributed by energy production to NO_x and SO_x emissions may increase in many air basins because of the large decrease from mobile sources. Similarly, the percentages contributed by non-mobile source energy use are also projected to increase somewhat in the future.

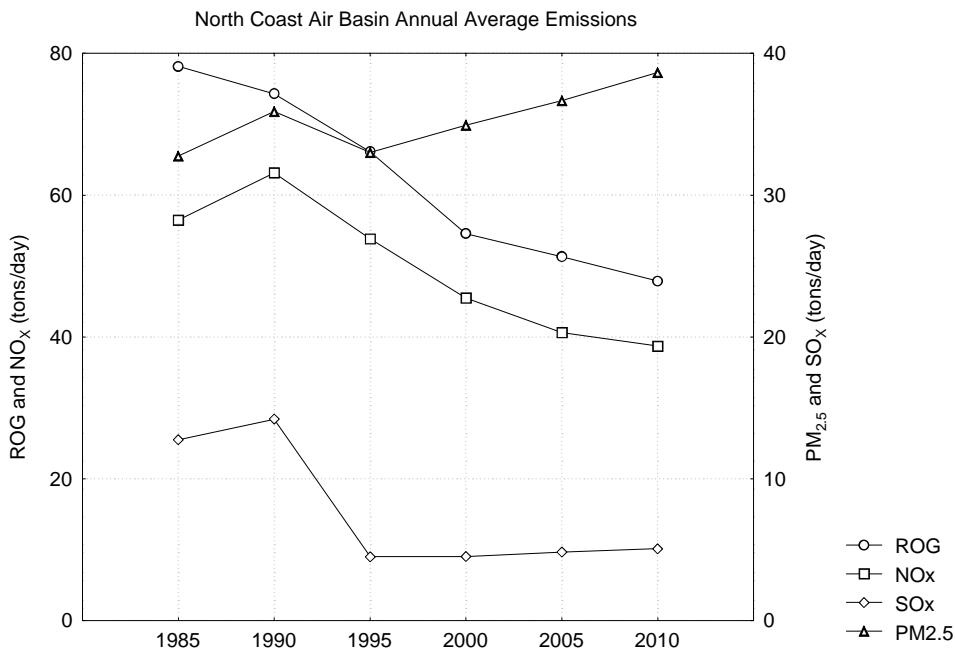


Figure 4-4 Estimated Annual Average Emissions in the North Coast Air Basin from 1985 through 2010

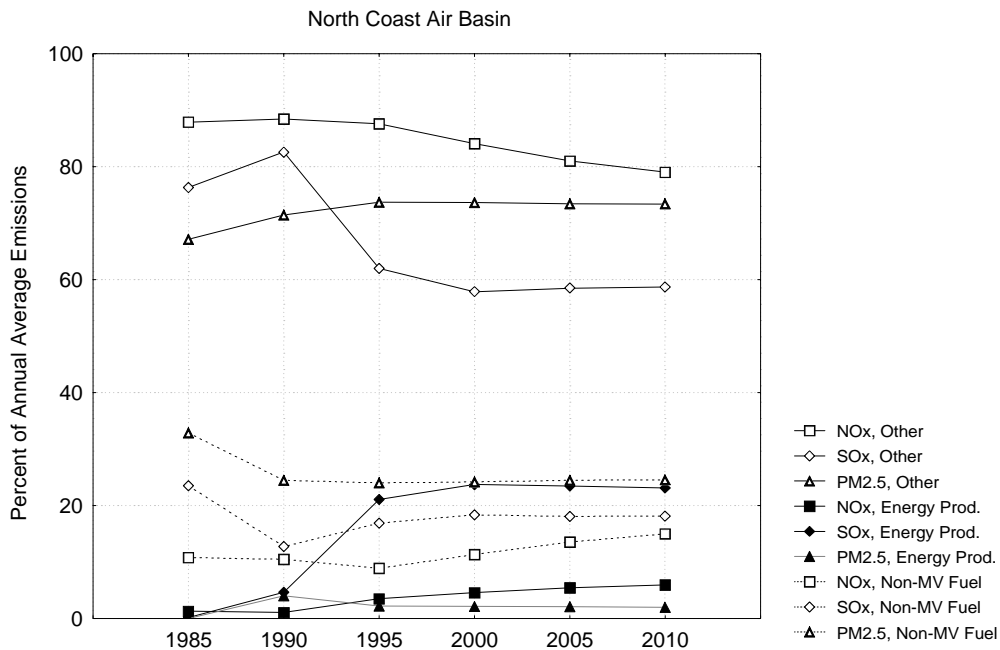


Figure 4-5 Contribution of Energy Production, Stationary Source Fuel Use and Other Sources to Annual Average Emissions in the North Coast Air Basin from 1985 through 2010

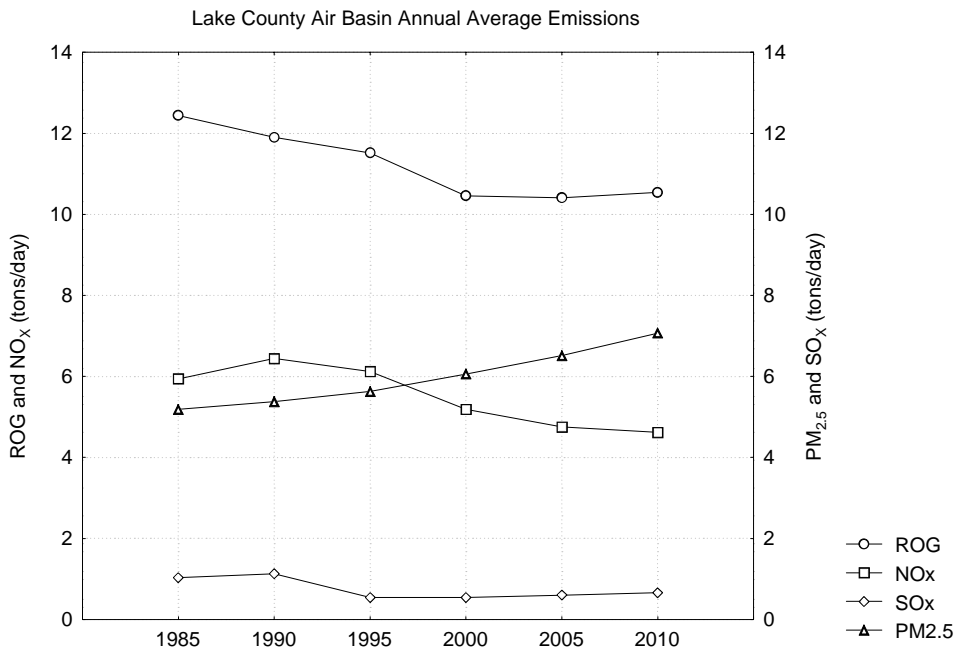


Figure 4-6 Estimated Annual Average Emissions in the Lake County Air Basin from 1985 through 2010

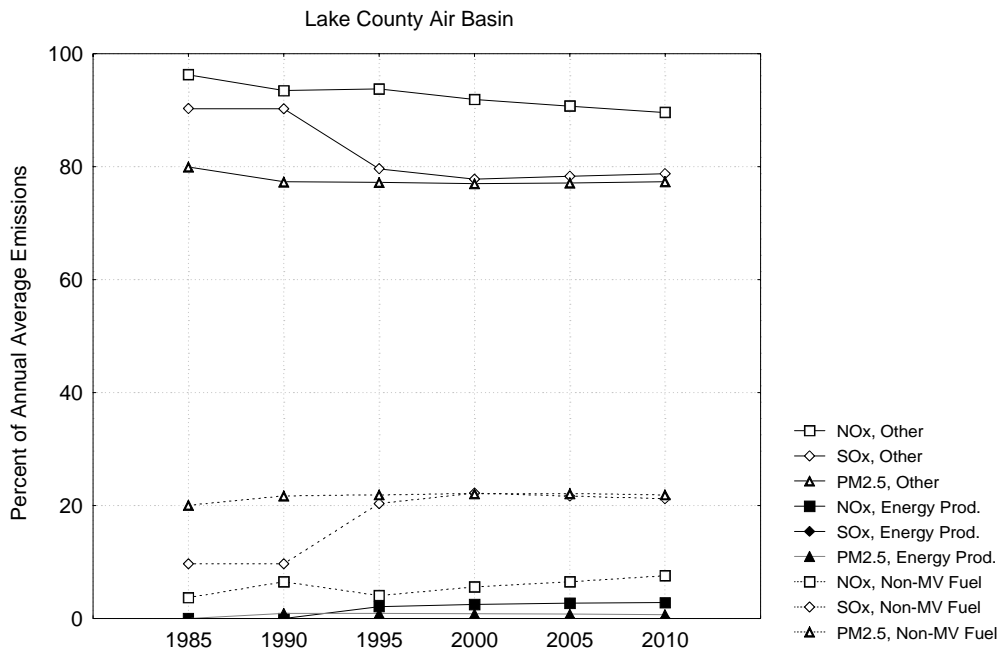


Figure 4-7 Contribution of Energy Production, Stationary Source Fuel Use and Other Sources to Annual Average Emissions in the Lake County Air Basin from 1985 through 2010

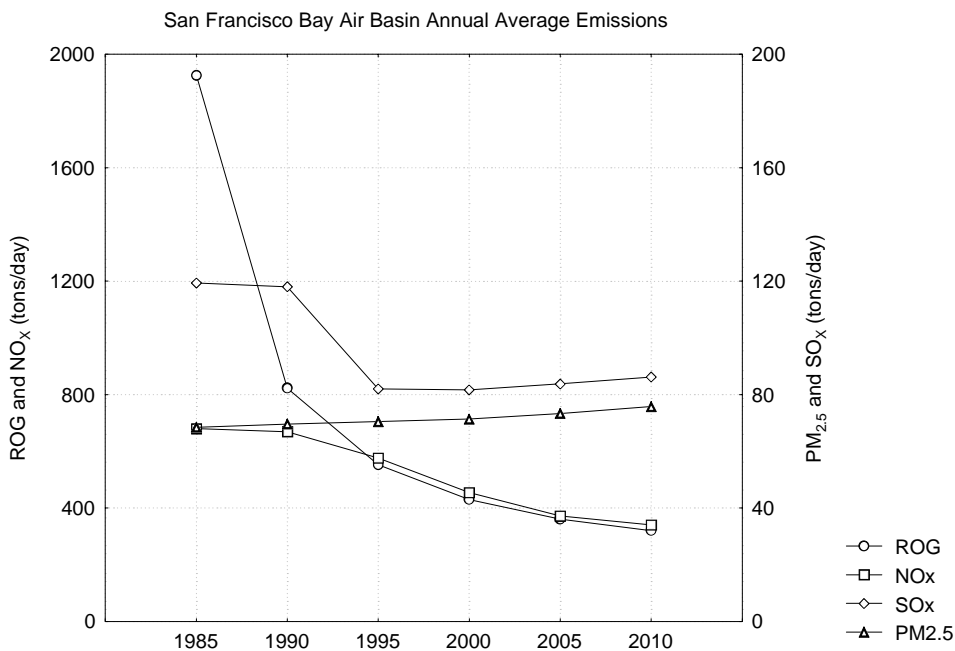


Figure 4-8 Estimated Annual Average Emissions in the San Francisco Bay Air Basin from 1985 through 2010

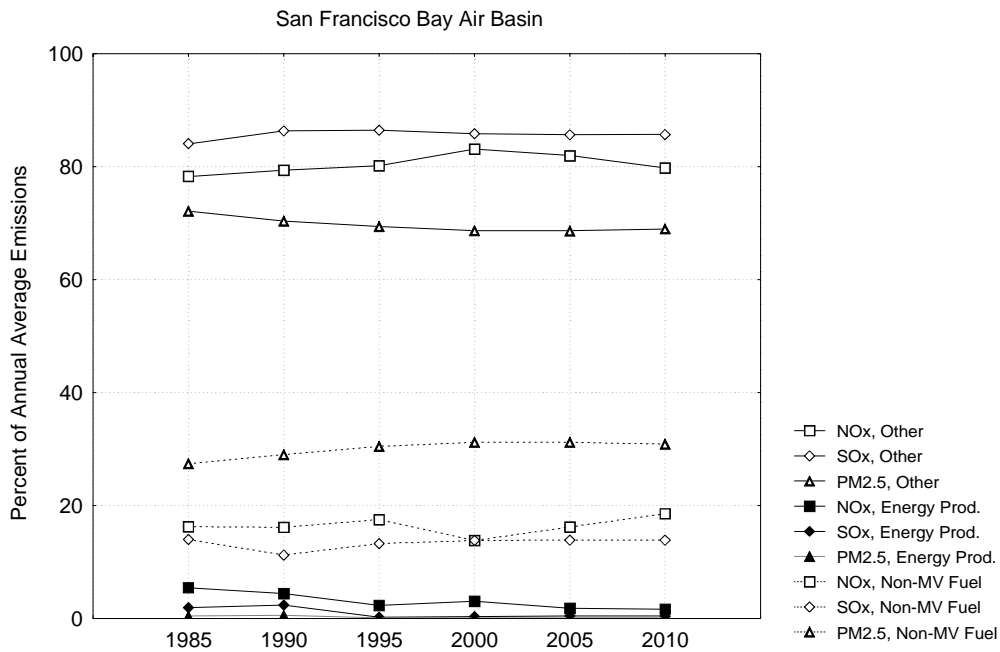


Figure 4-9 Contribution of Energy Production, Stationary Source Fuel Use and Other Sources to Annual Average Emissions in the San Francisco Bay Air Basin from 1985 through 2010

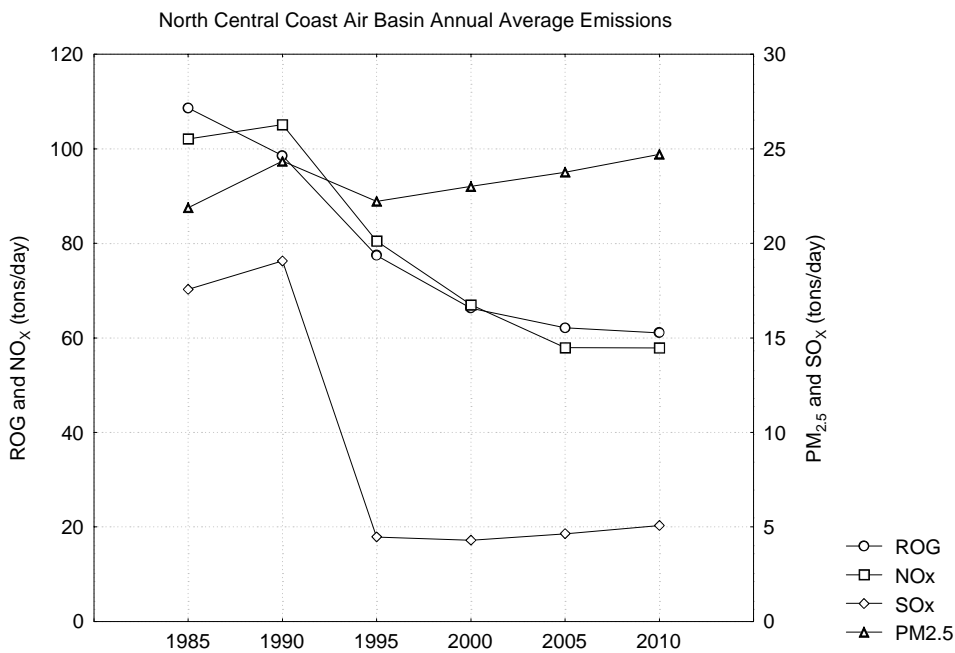


Figure 4-10 Estimated Annual Average Emissions in the North Central Coast Air Basin from 1985 through 2010

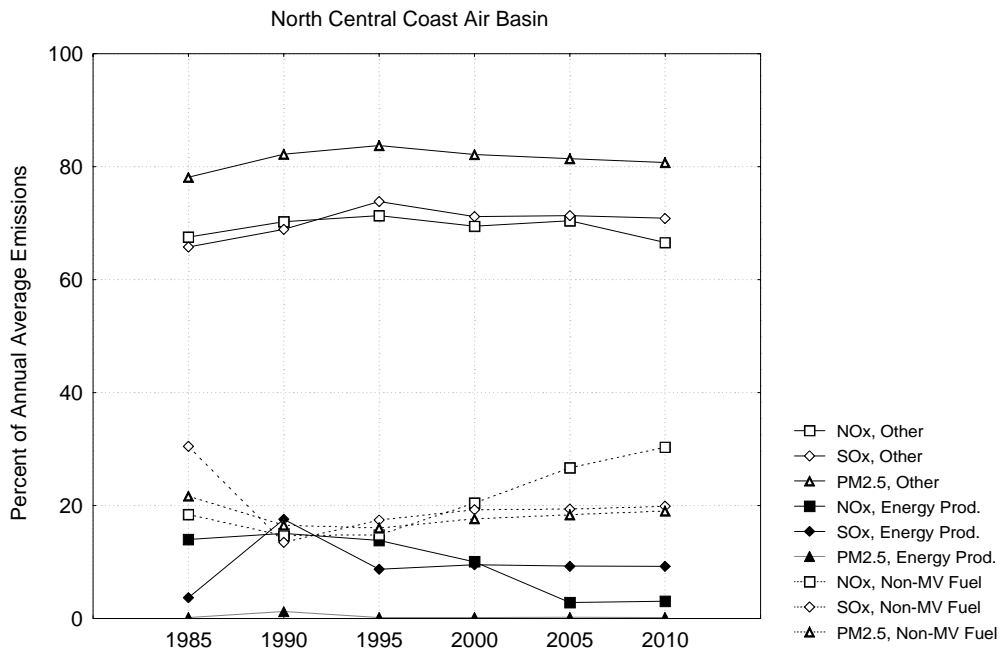


Figure 4-11 Contribution of Energy Production, Stationary Source Fuel Use and Other Sources to Annual Average Emissions in the North Central Coast Air Basin from 1985 through 2010

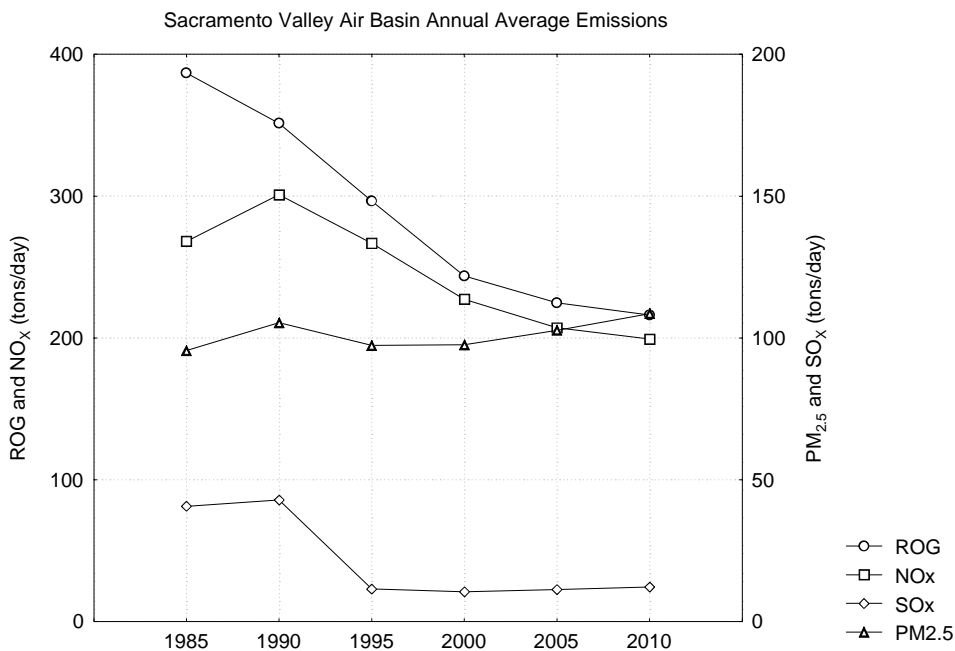


Figure 4-12 Estimated Annual Average Emissions in the Sacramento Valley Air Basin from 1985 through 2010

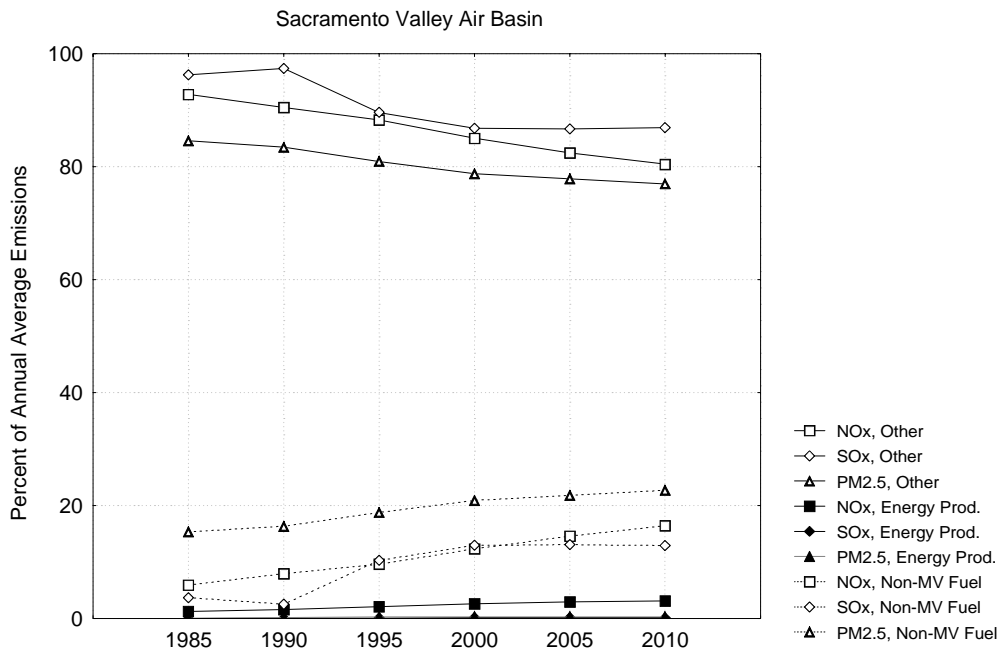


Figure 4-13 Contribution of Energy Production, Stationary Source Fuel Use and Other Sources to Annual Average Emissions in the Sacramento Valley Air Basin from 1985 through 2010

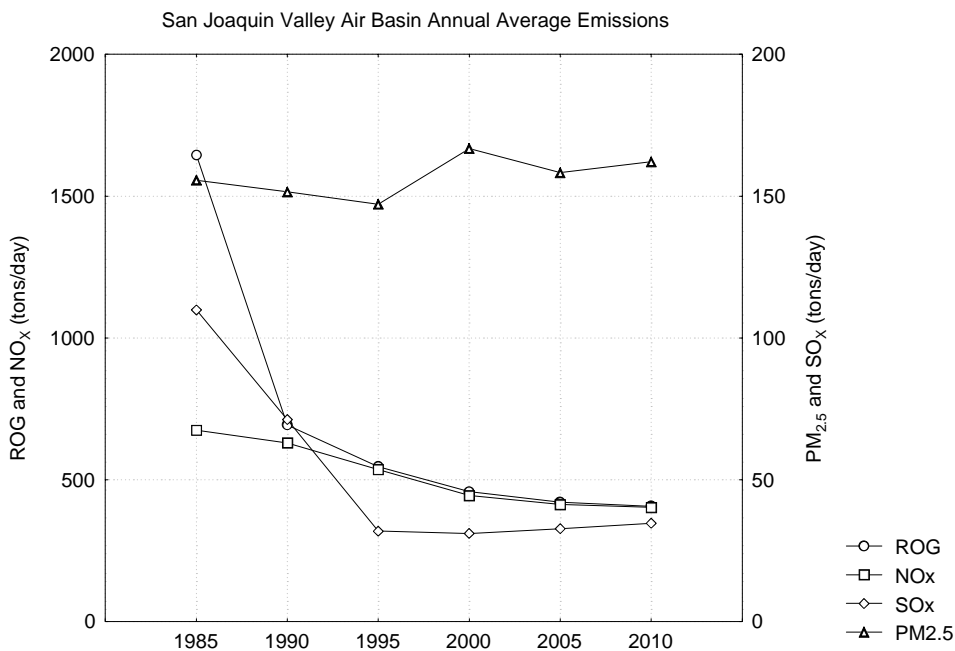


Figure 4-14 Estimated Annual Average Emissions in the San Joaquin Valley Air Basin from 1985 through 2010

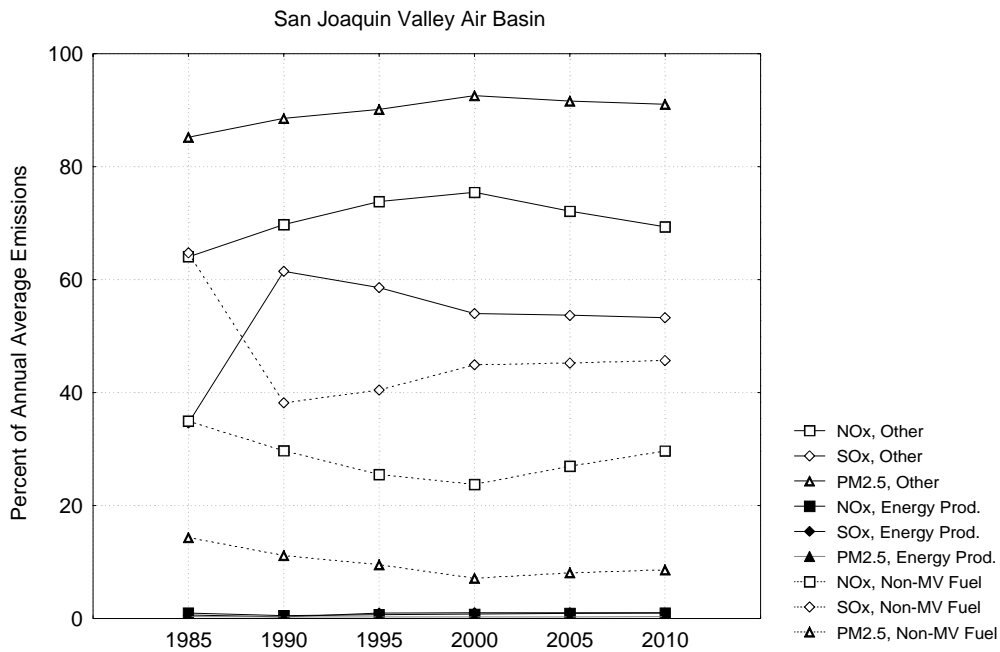


Figure 4-15 Contribution of Energy Production, Stationary Source Fuel Use and Other Sources to Annual Average Emissions in the San Joaquin Valley Air Basin from 1985 through 2010

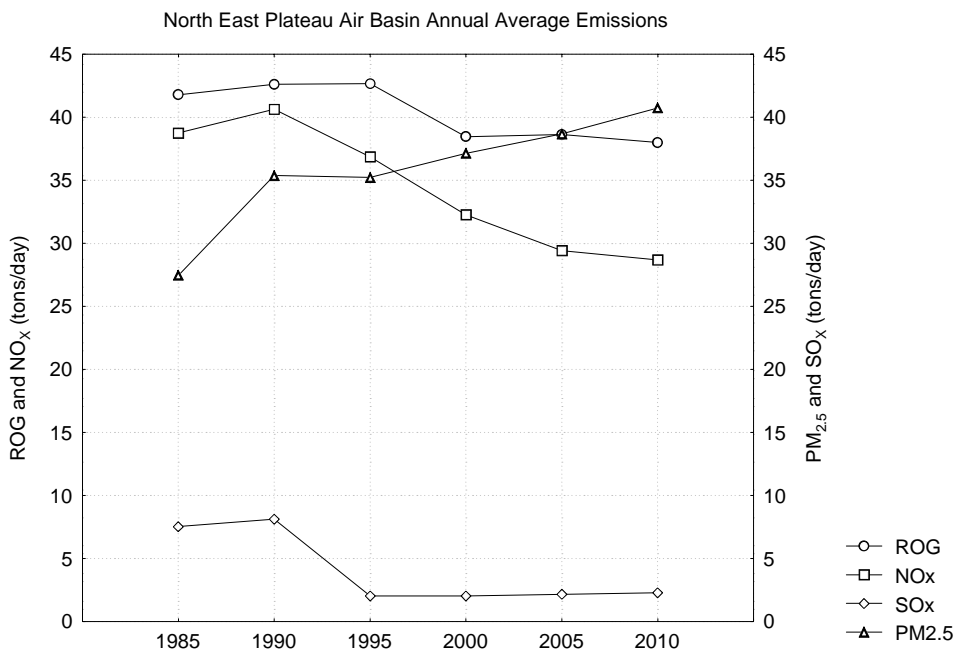


Figure 4-16 Estimated Annual Average Emissions in the Northeast Plateau Air Basin from 1985 through 2010

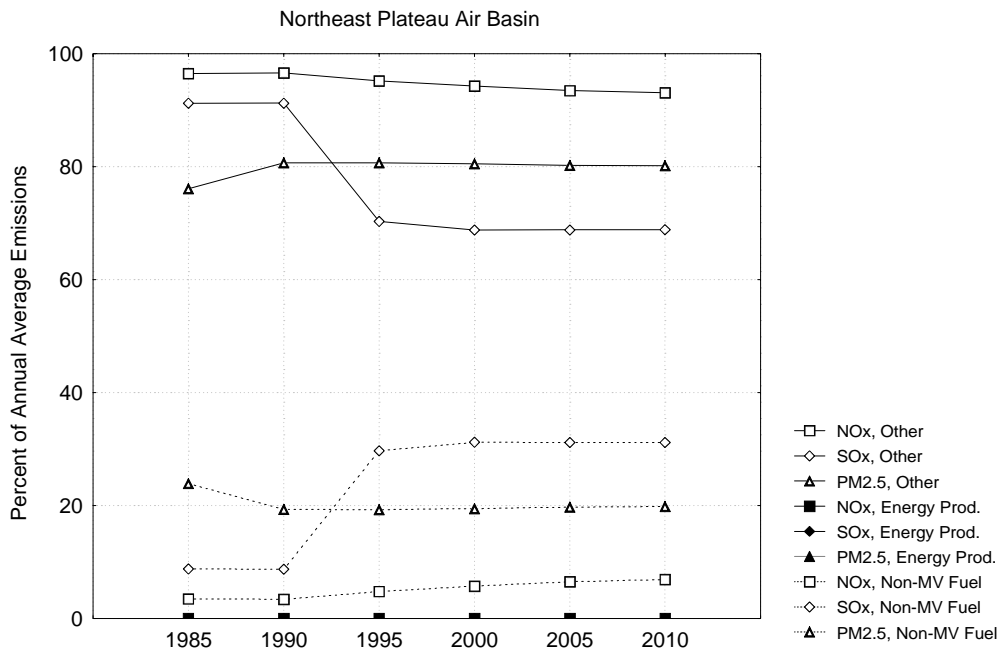


Figure 4-17 Contribution of Energy Production, Stationary Source Fuel Use and Other Sources to Annual Average Emissions in the Northeast Plateau Air Basin from 1985 through 2010

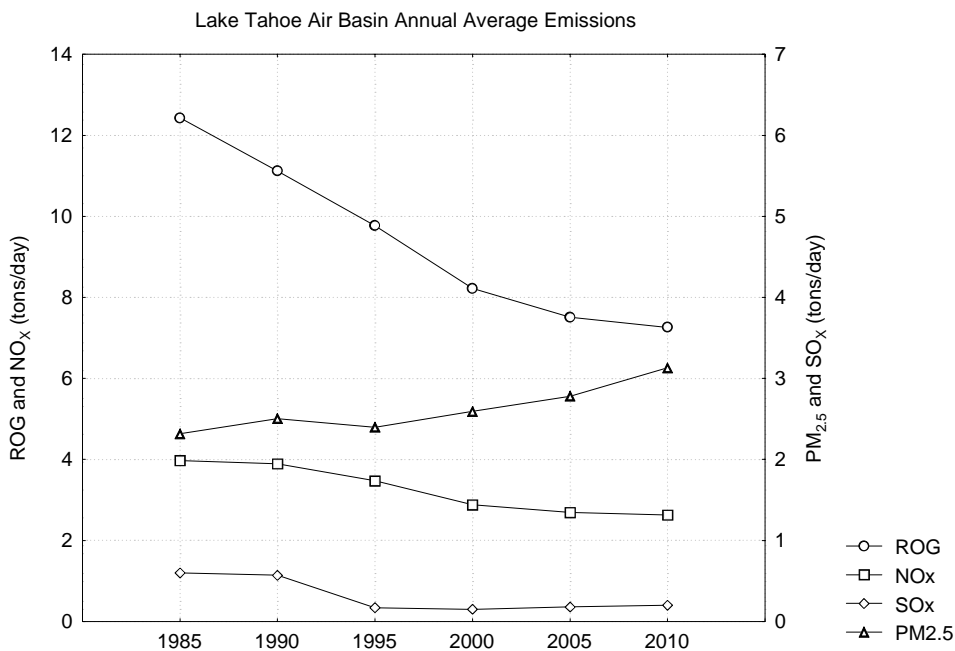


Figure 4-18 Estimated Annual Average Emissions in the Lake Tahoe Air Basin from 1985 through 2010

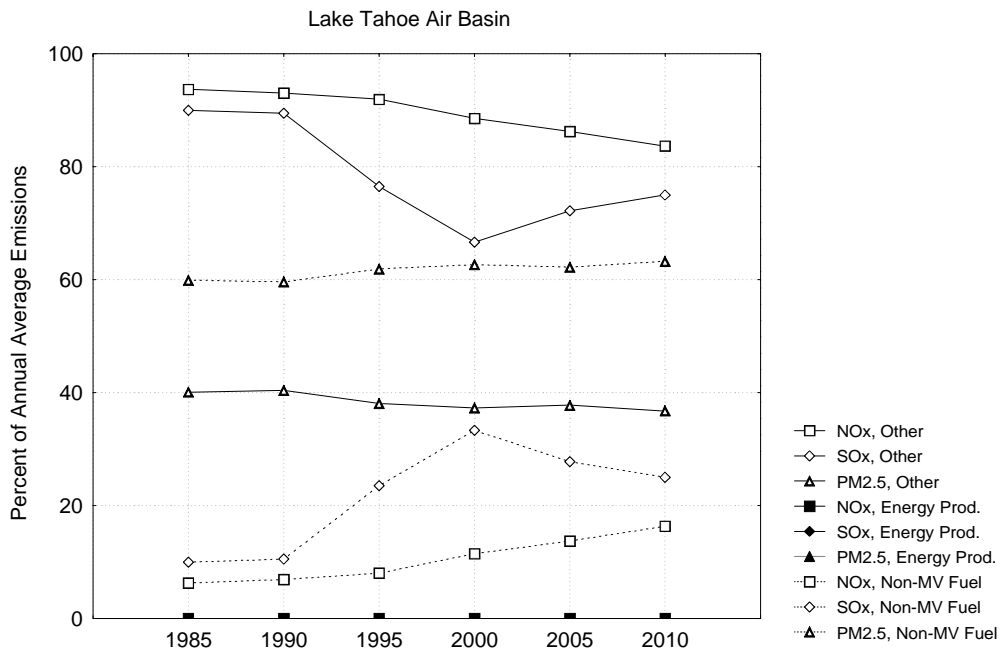


Figure 4-19 Contribution of Energy Production, Stationary Source Fuel Use and Other Sources to Annual Average Emissions in the Lake Tahoe Air Basin from 1985 through 2010

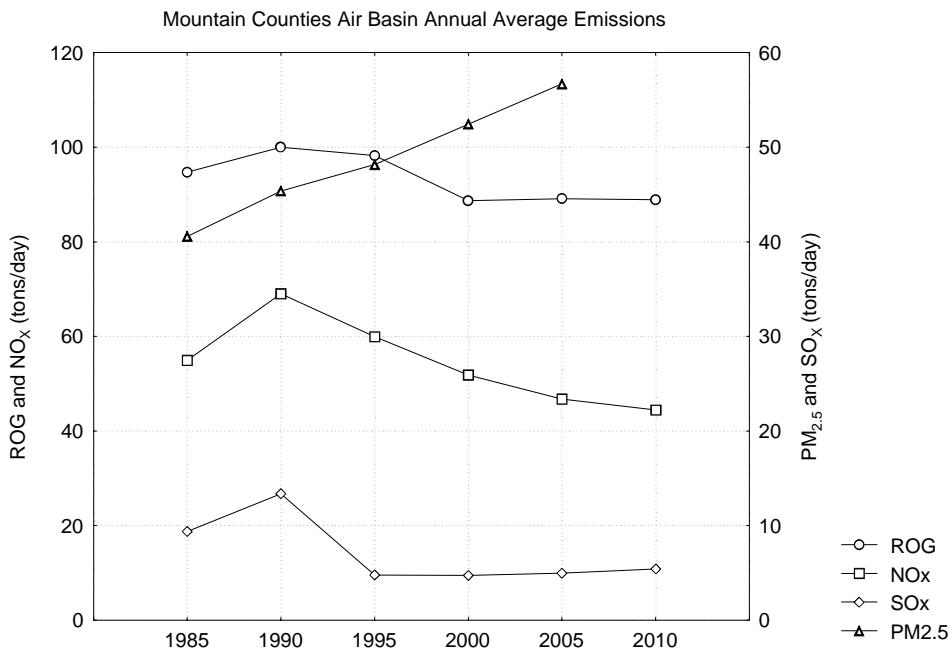


Figure 4-20 Estimated Annual Average Emissions in the Mountain Counties Air Basin from 1985 through 2010

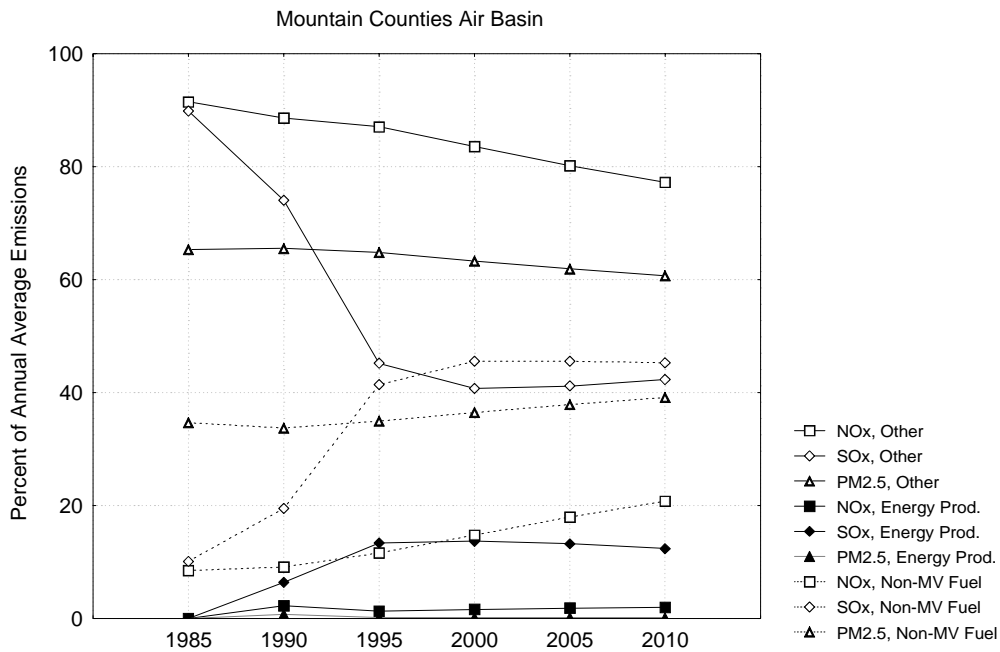


Figure 4-21 Contribution of Energy Production, Stationary Source Fuel Use and Other Sources to Annual Average Emissions in the Mountain Counties Air Basin from 1985 through 2010

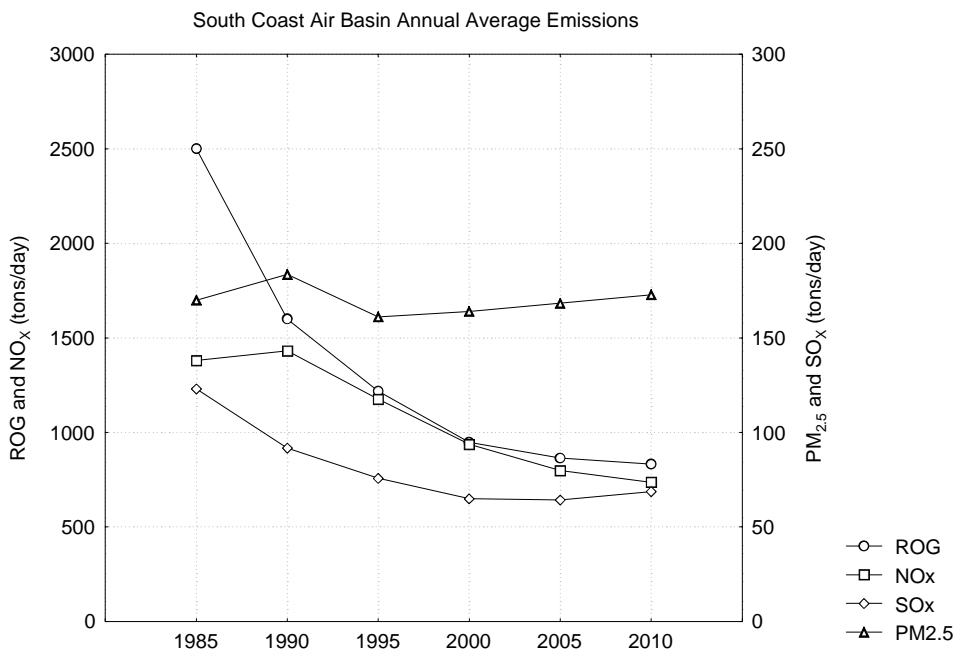


Figure 4-22 Estimated Annual Average Emissions in the South Coast Air Basin from 1985 through 2010

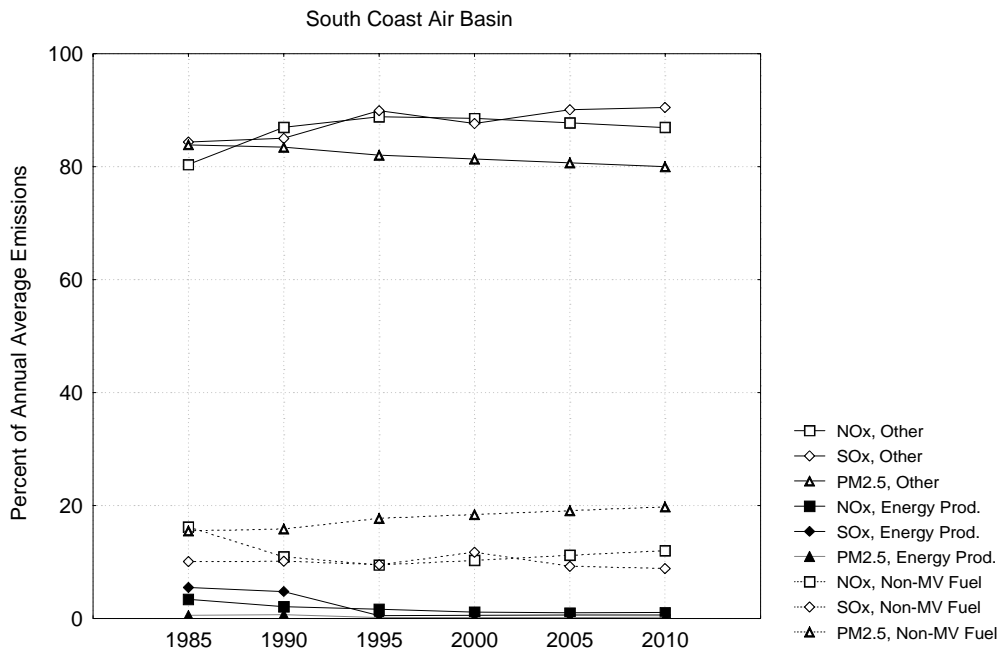


Figure 4-23 Contribution of Energy Production, Stationary Source Fuel Use and Other Sources to Annual Average Emissions in the South Coast Air Basin from 1985 through 2010

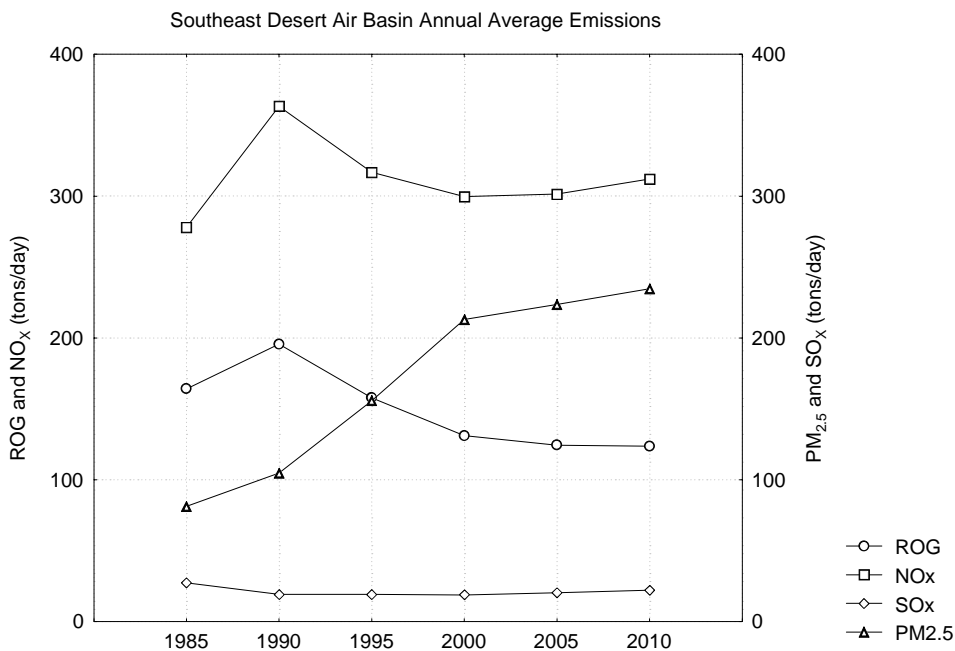


Figure 4-24 Estimated Annual Average Emissions in the Southeast Desert Air Basin from 1985 through 2010

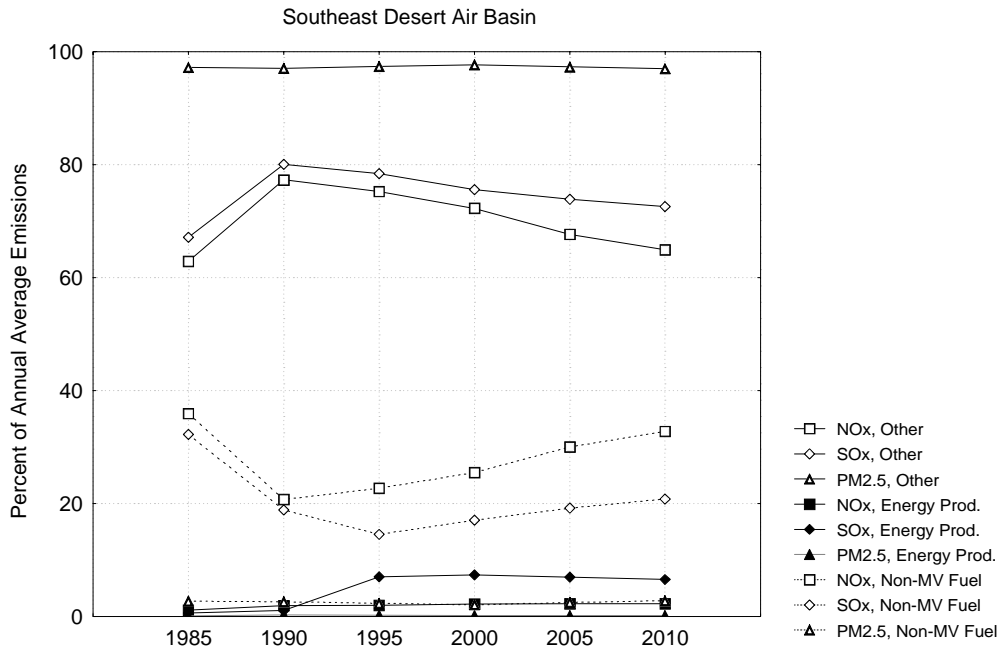


Figure 4-25 Contribution of Energy Production, Stationary Source Fuel Use and Other Sources to Annual Average Emissions in the Southeast Desert Air Basin from 1985 through 2010

5.0 MODELS FOR SOURCE-RECEPTOR RELATIONSHIPS

A variety of analytical techniques and models have been developed for use in assessing the contributions of emissions sources to visual air quality in visibility-protected areas and for estimating the visibility benefits to be derived from reducing emissions from those sources. In this section we identify and describe some of the available tools and review their capabilities and limitations.

5.1 Background

Two broad classes of analytical tools are used to assess the visibility impacts of sources – receptor models and source models. Receptor models use measured ambient air quality information at one or more locations, sometimes together with a characterization of emissions from representative sources or information on transport trajectories, to evaluate the contributions of various source categories or source regions to the ambient air quality. Source models calculate air quality at receptor locations from input information on source emissions and meteorology, using mathematical formulas that portray atmospheric transport, diffusion, deposition, and chemical processes. There are also hybrid techniques that incorporate features of both the source and receptor modeling approaches.

In general, assessment of the contributions of existing emission sources to air quality at receptor sites can be carried out using either source or receptor models. If ambient air quality data and emission source characterization data are available, the receptor techniques tend to be easier to apply. Source modeling has to be used, however, if the specific impact of one source in a field of many is sought. Furthermore, source modeling is the only method that can be used for determining the effects of proposed sources that do not yet exist,

Source modeling of visibility is typically carried out in two stages. First, the ambient concentration of visibility-impairing particulate matter is calculated, whether in a plume or over a region. Then, a radiative transfer model is used to convert the particulate matter information into visibility effects. These two stages of calculations may be done discretely, or they may be linked in a single modeling system. The particulate matter calculation is the more complex of the two, because it has to address many chemical species existing in particles of many sizes.

The approach is similar for receptor modeling. Because it is the diversity of particulate information that typically enables application of receptor modeling, that modeling necessarily addresses the particulate matter that causes the visibility impairment, rather than the visibility effect itself. The visibility impairment that corresponds to the measured particulate matter is again derived using some form of radiative transfer model, or through analysis of statistical relationships with concurrent measurements of visibility or other atmospheric optical properties.

For these reasons, the discussion below will first focus on modeling approaches that simulate the behavior of particulate matter, particularly $PM_{2.5}$, the fine fraction that accounts for most of the visibility impairment under most circumstances. Methods for calculating the visibility effects of these particles will receive mention when they are integral to a model, but those methods will then be addressed more generally in Section 5.4, after the discussion of the particulate matter modeling approaches.

5.2 Receptor Models for Particulate Matter

A recent report (Seigneur et al., 1997a) describes and evaluates 17 receptor modeling methods that are available for particulate matter source identification and apportionment. These methods include the EPA-approved chemical mass balance (CMB) approach for the apportionment of primary particles, several generic statistical analysis techniques (such as principal components analysis), and a variety of techniques that have been developed specifically for source apportionment and are available from their developers. About half the methods are able to apportion the secondary particles that are formed from gaseous emissions, as well as primary particles, although the apportionment is not always quantitative. The remaining methods, including CMB, are suitable solely for primary particles, and thus are not useful for most situations of visibility impairment in which secondary particles play an important role.

Table 5-1 summarizes key properties of 10 methods that have demonstrated an ability to apportion secondary aerosol. They are all described, with examples, in the Seigneur et al. review. Table 5-1 cites one publication that describes each method and its application; additional citations are in the Seigneur et al. report. The “Ease of use” evaluation in the table is based on a scale with a rating of “Easy” for the conventional CMB approach (which is absent from the table because it does not apportion secondary aerosol).

Half of the methods in Table 5-1 are able to provide quantitative apportionment of the secondary aerosol to sources, at least under appropriate circumstances. The others give qualitative information about the types and locations of sources. With one exception (Positive Matrix Factorization), these methods require more information than the single-site particulate matter composition data that are needed for inert species apportionment with CMB. Typically also needed is information about emissions from all sources that could affect air quality at the receptor, particulate matter composition data at more than one location, and/or transport trajectory information. Software is available from the developers of two of the methods (Positive Matrix Factorization and RMAPS), but these methods are difficult to apply. For the other quantitative methods, the calculations are less complex and the method is easier to use, but the software would have to be provided by the user.

We provide below brief descriptions of the five methods in Table 5-1 that are able to quantitatively apportion secondary aerosol (at least under some circumstances). Some of the methods are not limited to particulate matter. These descriptions include the principal assumptions underlying each method, the input data that are needed, and the output information that the method produces.

Table 5-1
Summary of Receptor Modeling Methods that Apportion Secondary Aerosol

(Adapted from Seigneur *et al.*, 1997a)

Method	Reference	Required Information				Quantitative Apportionment of Secondary Aerosol to Sources	Software Available	Ease of Use
		# of Ambient Samples	Source Profiles	Source Locations	Other			
Genetic Algorithm	Cartwright and Harris, 1993	≥1	No	No	None	No	Commercially available (MATLAB)	Difficult
Positive Matrix Factorization	Anttila <i>et al.</i> , 1995	≥30 -40	No	No	Total sample mass; uncertainty for every data point	Yes	Available from Pentti Paatero	Difficult
Empirical Orthogonal Function (EOF) Analysis	Malm <i>et al.</i> , 1990	Multiple sites; ≥30 samples per site	No	Yes	None	Sometimes	Most statistical packages	Easy
Receptor Model Applied to Patterns in Space (RMAPS)	Henry, 1997a	Multiple sites; ≥30 samples per site	No	No	Any spatial relationships or constraints	Yes	Available from Ronald Henry	Difficult
Residence Time Analysis	Poirot and Wishinski, 1986	≥40	No	Yes	Back trajectories	No; provides likely source areas	None	Easy
Area of Influence Analysis	Malm <i>et al.</i> , 1990	≥35	No	Yes	Back trajectories	No; provides likely source areas	None	Easy
Quantitative Transport Bias Analysis	Keeler and Samson, 1989	Better with multiple sites; ≥20 samples per site	No	Yes	Back trajectories; precipitation data along path of trajectory	No	None	Difficult
Potential Source Contribution Function (PSCF) Analysis	Ashbaugh <i>et al.</i> , 1985	≥35	No	Yes	Back trajectories	No; provides likely source areas	None	Easy

Table 5-1
Summary of Receptor Modeling Methods that Apportion Secondary Aerosol

(Adapted from Seigneur *et al.*, 1997a)

Method	Reference	Required Information				Quantitative Apportionment of Secondary Aerosol to Sources	Software Available	Ease of Use
		# of Ambient Samples	Source Profiles	Source Locations	Other			
PSCF with Apportionment	Cheng <i>et al.</i> , 1996	≥35	Yes	Yes; gridded emission inventory	Back trajectories	Yes; provides likely source areas	None	Easy
Residence Time Weighted Concentration	Stohl, 1996	≥35	No	Yes	Back trajectories	Possibly; provides likely source areas and estimates of their relative contributions	None	Easy

Positive Matrix Factorization. Positive matrix factorization is an enhanced factor analysis approach that provides a direct source apportionment analogous to that of a chemical mass balance (CMB) analysis. It is a new approach that appears promising but has received only limited use and testing.

The report by Seigneur *et al.* (1997a) provides a detailed description of an application of this method to IMPROVE measurements at seven locations in Alaska. Up to eight factor solutions were found to explain the measurements, with multiple regression r^2 of 0.74 to 0.95, depending on site. The principal factors were attributed to sea salt; forest fires and local wood burning; long range transport of sulfur, including possibly from oceanic sources; photochemical production of sulfate; incineration and/or nonferrous smelting; and motor vehicles.

This is the only one of the quantitative secondary aerosol methods whose implementation requires only particulate composition measurements. Qualitative information about sources is required to interpret the various factors in terms of the causal sources, though. The method can be applied to measurements taken over a period of time at one location or at many locations. Its application does require estimates of measurement uncertainty for every data point. As with all factor analysis methods (and perhaps all receptor modeling methods), experienced judgment is required to apply this approach, both for selecting the combination of factors that best describes the measurements and for assigning the factors to specific sources.

The other methods described below make the apportionment to sources easier and more definite by using additional spatial and temporal information about the ambient air quality or meteorological information that describes air parcel trajectories from source to receptor.

Empirical Orthogonal Function (EOF) Analysis. The EOF approach is mathematically equivalent to the principal component form of factor analysis, and software is available in most statistical packages. Factor analysis examines the variation of a number of measured species in multiple samples taken over time at a single site. EOF examines the spatial and temporal behavior of values of a single variable measured at multiple times at several sites. The site spacing must be smaller than the spatial scale of the air pollution variable. The result of the analysis is presented in terms of a set of spatial source patterns, the combination of which accounts for the measured behavior. The product of the analysis is typically portrayed as contour maps, one for each source pattern, that indicate the locations of sources or source regions.

The independent variable in the EOF analysis can be a secondary species, such as sulfate, or one can even use visibility. As in all factor analyses, the specific source and emitted pollutant must be identified through knowledge of the area and experienced insight, and so the process works best when there is a strong relationship between the emitted species and impact of interest.

As an example of its application, the EOF approach has been used to assess the contributions of sulfur sources to visibility on the Colorado Plateau (Malm et al., 1990).

SAFER (Henry, 1991) is a modified EOF approach that uses explicit external constraints to ease the challenge of finding the combination of eigenvectors that best describes the measurements. An updated version is named UNMIX.

Receptor Model Applied to Patterns in Space (RMAPS). RMAPS is combination of the EOF approach and the multivariate approach used in, for example, Chemical Mass Balance (CMB) receptor modeling. To produce a unique apportionment, the analyst imposes external constraints. Application of the method requires concurrent complete data sets taken over a period of time at multiple receptor sites, with no missing values, for the concentration of the species of interest. As with EOF, the spatial scale of the pollution must be large compared to the spacing between the sites. RMAPS also requires that there be sufficient observations so that at least one case of little or no effect of each of the sources, in turn, is reflected in the measurements.

The model apportions, for each receptor, the time-averaged concentration of the species of interest among several spatially distinct sources. The output is an assignment of average culpability to each source over the period of measurements. RMAPS can apportion secondary aerosol without assumptions concerning transformation or deposition rates. Expert judgment is required to apply the method, however; White (1997) shows how an application of RMAPS can attribute the measured concentrations to "phantom" sources.

Henry (1997b) and Henry (1997c) provide examples of applications of RMAPS to particulate sulfur apportionment in the Southwest and Pacific Northwest, respectively. In both cases the sulfur was apportioned to source regions that included power plants and area sources.

Potential Source Contribution Function (PSCF) Analysis with Apportionment. The basic PSCF method uses both chemical composition and meteorological data to construct concentration-weighted back trajectories that “point” at locations of source regions. The PSCF is, in effect, a transfer function that indicates the likelihood that the observed concentrations at the receptor site are related to emissions from each location in a grid of potential sources. The PSCFs can be for either primary or secondary species.

If a gridded emission inventory is available, then the emissions rates for each cell can be multiplied by the corresponding PSCF values to construct quantitative apportionments of receptor concentrations to specific source cells in the grid. Thus the principal limitation of the method is the requirement for availability of a source emissions inventory, for the species of interest and its precursors, on the same grid as that used to construct the PSCF.

A specific example of the method is its application by Cheng et al. (1996) to apportioning the contributions of NO_x emissions to NO_y concentrations measured at several locations in the South Coast Air Basin.

Residence Time Weighted Concentration. This is a new method of combining chemical concentration data with air parcel back trajectories. It also starts with development of a gridded concentration contribution field (similar to a PSCF) through calculation of trajectory-weighted mean concentrations for each cell. An iterative approach is then used to estimate the relative contributions of emissions in various source cells to the observed receptor concentrations.

The method is very new and, although promising, requires further testing and evaluation of the credibility of its attribution estimates.

5.3 Source Models for Particulate Matter

The source models available for particulate matter calculations for assessing visibility impacts range from simple screening models for regulatory permitting purposes to complex atmospheric dispersion, deposition and chemistry simulation systems. The models available include Lagrangian (plume) models for calculating the impacts of single sources or source regions and Eulerian (grid) models for the three-dimensional, regional treatment of emissions from multiple sources.

5.3.1 Regulatory Plume Models

In the regulatory arena, three models are prescribed for visibility assessments of single sources or source areas: VISCREEN, PLUVUE II, and CALPUFF. They are described below.

VISCREEN (U.S. EPA, 1992a) is a simple steady-state Gaussian plume model. It is intended for a first assessment of potential visibility impacts of single source plumes at receptors within 50 km.

VISCREEN only represents the effects of primary particles and NO₂ gas, and does not address the formation of secondary particles. It includes radiative transfer calculations for those viewing angles relative to the plume and the sun that produce the greatest visual effects

Because of its intended usage for screening, VISCREEN is designed to be highly conservative (i.e., to err on the side of overestimating impacts on visibility). In particular, the calculation of visibility effects is in conformity with this conservatism. Thus the model does not provide an accurate portrayal of the aerosol or its visibility effects.

PLUVUE II (U.S. EPA, 1992b) is a more sophisticated steady-state Gaussian plume model for emissions from a point or area source. It uses user-specified plume widths or will calculate them from the Pasquill-Gifford-Turner curves. It simulates dry deposition. PLUVUE II explicitly calculates the formation of sulfate and total nitrate using a 9-equation chemical mechanism with steady-state approximations. The model includes a radiative transfer calculation at multiple wavelengths that determines visibility effects along different sight paths through the plume against both sky and terrain backgrounds. The outputs of the model are plume concentrations and visual effects for specified lines of sight, at specified downwind distances

CALPUFF (U.S. EPA, 1995) is a multi-layer, multi-species, non steady-state, Gaussian puff dispersion model that can simulate the effects of time- and space-varying meteorological conditions on pollutant transport, transformation, and removal. Federal Land Managers have prescribed that CALPUFF is to be used for assessments of Class I and II area visibility impacts more than 50 km from a source, although it is also suited for shorter transport distances. It is used in association with a diagnostic meteorological model, CALMET, and an optical effects post-processor, CALPOST.

Using standard NWS aviation meteorological data or more detailed measurements as input, CALMET generates a gridded meteorological field that considers the effects of complex terrain. That meteorological field transports and disperses the CALPUFF puffs.

CALPUFF can handle point, line, area, and volume sources, with constant or variable emissions. It includes algorithms to represent the effects of such phenomena as plume downwash, wind shear, coastal effects, overwater transport, and dry and wet deposition.

The representations of the daytime chemical formation rates of sulfate and nitrate in CALPUFF consider solar radiation and the availability of ozone (a user-provided surrogate for the hydroxyl radical). The model simulates the effects of atmospheric moisture on particle formation through a relative humidity dependence, but this simplistic approach does not realistically represent in-cloud, aqueous chemical processes. Nighttime chemical formation rates are set at fixed values. The partitioning between gaseous nitric acid and particulate nitrate is addressed as a function of temperature, relative humidity, and background ammonia (the concentration of which must be input by the user). CALPUFF gives particle concentrations in surface-based grid cells.

The CALPOST processor contains a very simple algorithm that calculates, in each cell, the light extinction coefficient of the resulting haze, based on specified extinction efficiencies and relative humidity functions that represent the effects of particle growth. It does not calculate optical effects along specific lines of sight, as would be required for determining “plume blight” or the regional haze effects of the modeled sources. Interestingly, CALPOST calculates only the extinction effects of the secondary sulfate and nitrate, and not of primary particles or gases (even though CALPUFF calculates the concentrations of these primary species).

CALPUFF has been used in two recent studies of the contributions of coal fired power plants to visibility impairment – the Mt. Zirkel Visibility Study (Watson et al., 1996) in the Rocky Mountains and Project MOHAVE (Pitchford et al., 1999) near the Grand Canyon. In both cases the CALPOST visibility processor was not used, but rather CALPUFF was used to estimate sulfate impacts and then the extinction effects of that sulfate were calculated separately.

5.3.2 Advanced Plume Models

Each of the regulatory models described above has some shortcomings in representing the full visibility impact of a point source. VISCREEN is too simple and too conservative, and does not simulate secondary aerosol. PLUVUE II simulates the important chemical transformations and computes radiative transfer, but is limited by its steady-state Gaussian formulation to short travel distances over relatively simple terrain. CALPUFF overcomes the shortcomings of PLUVUE II, but its treatment of the chemical formation of secondary species is more primitive than that of PLUVUE. Furthermore, in its normal configuration, CALPUFF’s outputs do not include concentrations aloft for “plume blight” calculations.

A recently-developed plume model addresses these limitations, and others, of the regulatory models. The Reactive and Optics Model of Emissions (ROME; Seigneur et al., 1997b) is a “second-generation” model of chemical transformation in stack plumes and of the optical effects of those plumes. It includes formulations of plume rise and dispersion that can use second-order closure algorithms, of atmospheric chemistry with over 169 reactions in the gas phase and in droplets, and of aerosol dynamics using a sectional representation of the particle size distribution.

ROME is a Lagrangian model that simulates concentrations in a crosswind “slice” of the atmosphere (that includes the plume cross section) with a resolution of 10 columns of cells horizontally and 10 rows of cells vertically. The model treats chemical reactions pertaining to the emissions of SO₂, NO_x, reactive hydrocarbons, and particulate matter, in both the gaseous and aqueous (droplet) phases. It uses an aerosol thermodynamic equilibrium model, MARS, to simulate the inorganic particulate chemical composition. Condensation of organic chemicals is treated through an empirical formulation. The model treats both dry and wet deposition processes.

ROME treats atmospheric radiative transfer using a two-layer, plane-parallel atmosphere. It calculates the radiance of the sky with and without the presence of a plume along the selected sight path. A typical output of the visual effect calculation is the ratio of the background radiance with and without the plume at several wavelengths and several elevation angles. The predicted particulate matter and NO₂ concentrations at the receptor can also be used with species extinction efficiencies to calculate the regional haze effects of widely dispersed plumes.

ROME has undergone a formal performance evaluation (Gabruk et al., 1999) using plume concentration and optical measurements from studies at four power plants. The model predicted plume width and NO_x concentrations more accurately than the Pasquill-Gifford-Turner scheme that is typically used in Gaussian plume models. Its sulfur chemistry module has also been evaluated separately by Hudischewskyj and Seigneur (1989). The dispersion and chemistry capabilities of the model were further evaluated against aircraft measurements in the course of its application to assessing the visibility impacts of a coal-fired power plant plume near Dallas, Texas (Seigneur et al., 1999; Tombach et al., 1996a). The radiative transfer module of the model was not used in the Dallas study. Rather, the model was used to calculate sulfate concentrations and the optical effects of those sulfates were then calculated separately using the SCAPE thermodynamic equilibrium model and the ELSIE Mie theory radiative transfer model.

5.3.3 Advanced Regional Models

A variety of Eulerian grid models that simulate the regional transport, diffusion, deposition, and chemical transformation of fine particulate matter have been developed in recent years. Some of these models are adaptations of existing urban photochemistry models, with aerosol modules added on. Others are adaptations of regional acid deposition models. Yet others are new models or evolutionary enhancements of state of the art atmospheric models.

The review by Seigneur et al. (1997a) (summarized in Seigneur, 1997, and in updated form in Seigneur, 1998) identifies ten major air quality models that provide a three-dimensional treatment of chemical atmospheric fate and transport and some treatment of particulate matter. Seven of these models can be considered episodic, in that they are sufficiently demanding computationally that it is not practical to use them for simulating long periods (e.g., a year). The remaining three have simplifications that speed the computations and therefore make them practical for long term simulations. The main characteristics of these ten models are summarized in Table 5-2. We should note that Seigneur et al. (1997a) also describe several other models, but they consider the ones listed in Table 5-2 to represent the state of the art models most useful for urban and regional fine particulate matter and visibility analyses.

**Table 5-2
Summary of Urban and Regional Particulate Matter Models**

(Adapted from Seigneur, et al., 1997a and Seigneur 1997, 1998)

PM Model	Reference	Underlying AQ Model	Spatial Scale	Temporal Scale	Applications to Date	Applied with Meteorological Model
CIT	Meng <i>et al.</i> , 1998	--	Urban	Episodic	Los Angeles Basin	Diagnostic model
DAQM	Middleton, 1997	RADM	Mesoscale	Episodic	Denver	MM4
GATOR	Jacobson <i>et al.</i> , 1996; Jacobson, 1997a, 1997b	--	Mesoscale	Episodic	Los Angeles Basin	MMTD
Models 3/ CMAQ	U.S. EPA, 1998	--	Urban-to-Regional	Episodic	--	MM5
REMSAD	Guthrie <i>et al.</i> , 1995	UAM-V	Regional	Long term	Eastern U.S.	Diagnostic model or MM4
SAQM-AERO	Pai <i>et al.</i> , 1998	SAQM	Mesoscale	Episodic	Los Angeles Basin and San Joaquin Valley, CA	MM5
UAM-AERO	Kumar <i>et al.</i> , 1996; Lurmann <i>et al.</i> , 1997	UAM-IV	Urban	Episodic	Los Angeles Basin and San Joaquin Valley, CA	Various
UAM-AIM	Sun and Wexler, 1998	UAM-IV	Urban	Episodic	Los Angeles Basin	Various
UAM-LC	Lurmann and Kumar, 1996	UAM-LC	Urban	Long term	Los Angeles Basin	Diagnostic model
VISHWA	Venkatram <i>et al.</i> , 1997	ADOM	Regional	Long term	Southwestern U.S.	NGM and RAMS

Each of these models contains a gas-phase chemistry module -- a comprehensive one for the episodic models and a simplified one for the long-term models. As described below, aqueous phase chemistry is simulated by only some of the models. The thermodynamics of the inorganic aerosol are simulated by thermodynamic equilibrium models in the episodic models, and by simplified parameterizations in the long-term models. All models treat sulfate, nitrate, ammonium and water, and most treat many other inorganic species.

The formation of organic aerosol is not simulated in all models; those models that do simulate organic formation use various semi-empirical condensation and oxidation mechanisms.

Several of the models generate a particulate matter size distribution from first principles, while others either assume a particulate matter size distribution or require information on the ambient size distribution as input. All models simulate dry deposition and a few simulate wet deposition.

Brief descriptions of each of these models are provided in the following paragraphs. Except as noted, much of the following material is derived from the review by Seigneur et al. (1997a). The description of Models 3/CMAQ was obtained from the Models 3 User Manual (U.S. EPA, 1998) and from discussion with its developers.

CIT. The California Institute of Technology (CIT) model has been applied primarily to the simulation of photochemical smog in the Los Angeles Basin. It has been modified to include some treatment of the formation of particulate matter through gas-phase mechanisms. Its nitrate formation mechanism is more advanced than that of the other models considered here. It does not address aqueous processes or wet deposition.

The CIT model can use a variety of meteorological inputs. It simulates the atmosphere in 5 layers up to 1100 m, a vertical extent that is best suited for the urban scale.

The model is computationally intensive, requiring approximately 50 hours for a 24-hour simulation with an 80 x 30 x 5 grid on an IBM RS 6000/580 workstation.

The Georgia Institute of Technology has been using the CIT model as a foundation for developing a regional air quality and visibility model for the Southern Appalachian Mountains Initiative (SAMI).

DAQM. The Denver Air Quality Model (DAQM), developed by the State University of New York at Albany, is based on the Regional Acid Deposition Model (RADM) that was developed for the National Acid Precipitation Program (NAPAP). It has been applied to the Denver metropolitan area in a nested grid format, with the coarse grid including much of the state of Colorado and the fine grid encompassing the Northern Front Range region from Denver to Ft. Collins. The MM4 hydrostatic meteorological model was used to simulate the meteorology; the non-hydrostatic MM5 meteorological model is more appropriate for mountainous terrain, and is proposed for future applications.

DAQM includes both gas-phase and aqueous-phase particle formation mechanisms, although only the gas-phase mechanisms have been tested in the Denver simulations. For the Denver simulations described above, the formation of organic aerosol was prescribed to be an empirically-derived fraction for each species. The model now addresses the oxidation of VOC. The organic aerosol is assumed to be non-hygroscopic.

The visual effects of the aerosol are calculated with extinction coefficients that are derived through Mie scattering calculations using measured particle size distributions.

DAQM was evaluated against 7 to 17 hr average measurements for a few days of the 1987 Metro Denver Brown Cloud Study, with agreement of $\pm 50\%$ for most particulate matter species (Middleton et al., 1993). The light extinction tended to be underestimated by similar amounts.

DAQM requires about 7 hours of computation for a 24-hour Denver simulation, using an IBM RS 6000 workstation.

GATOR. In contrast to the two preceding models, GATOR was developed specifically to address atmospheric particulate matter. Also, unlike the other models considered here, the GATOR calculations of the radiative budget of the atmosphere provide feedback to the MMTD prognostic meteorological model. The MMTD model calculates not only the usual variables of wind and state, but also predicts the presence of clouds and fog.

The 20-layer GATOR modeling domain extends up to about 10 km, so the model provides a treatment of the atmospheric dynamics in both the planetary boundary layer and the free atmosphere above it. This means that GATOR can be used as a regional model.

GATOR provides a description of particulate matter, formed by both gaseous and aqueous processes, that is both chemically and size resolved. It generates a detailed representation of the size distribution of atmospheric particles, up to the size of cloud droplets. The treatment of organic particulate matter assumes that some organic species are water soluble.

GATOR has been applied to simulate a few days of measurements in the Los Angeles Basin during the South Coast Air Quality Study (SCAQS) of 1987. It tended to underestimate PM_{2.5} and PM₁₀ mass by about 30% and the predicted PM_{2.5} species concentrations tended to be within 50% of the measurements.

The model runs on a Cray computer at a rate of about 12 hours of computation per day of simulation.

Models 3/CMAQ. Models 3 is a newly released framework for urban to regional-scale modeling of photochemical oxidants, wet deposition, particulate matter, and visibility. The initial version of the framework contains the MM5 meteorological model and the Community Multiscale Air Quality (CMAQ) model. The framework includes options for user selection of modules, such as for atmospheric chemistry. CMAQ includes a plume-in-grid (PiG) simulation capability for more accurately calculating the near-field effects of point sources when a coarse grid is used.

Models 3 and CMAQ have been developed by the U.S. EPA and the system is currently being operationally tested. The first operational regional air quality simulations of the full model are just now beginning, in which the modeling system performance for ozone, particulate matter, and wet deposition will be evaluated against several databases in the East. Several model components have been used in previous studies. In particular, several of the components are improvements or enhancements of elements of RADM.

The particulate matter module in CMAQ is based on the Regional Particulate Model (RPM; Binkowski and Shankar, 1995), which was developed by the EPA as a particulate matter post processor for

RADM. It provides a size-resolved description of the particulate matter. Aqueous formation and removal processes are simulated. Although RPM treats only fine particulate matter, the version in CMAQ has been augmented to include coarse particles (PM10). RPM has been applied to eastern North America for three 30-day episodes .

Models 3 includes a Mie theory optical module that can calculate the light extinction in each grid cell.

The current version of Models 3 is configured for operation on a Sun UNIX workstation. An adaptation for a Silicon Graphics workstation is now being completed. The MM5 meteorological model runs on a remote Cray computer, via an Internet connection to the Sun workstation. A workstation version of MM5 is under development, which would eliminate the need for the remote Cray computation. Computation times for typical applications of Models 3 are just now being established.

REMSAD. The Regulatory Modeling System for Aerosols and Deposition (REMSAD) is an aerosol adaptation of the proprietary UAM-V photochemical model. Some aspects of UAM-V were simplified in order to provide for reasonable computation times for long term simulations with the added aerosol modules. For example, the PiG feature of UAM-V was removed and a reduced form chemical mechanism was substituted for the carbon bond (CBM-IV) mechanism in UAM-V.

The model does not treat the kinetics of formation of secondary organic particles. Rather, it approximates them as fixed fractions of the primary emissions of classes of VOC.

REMSAD was applied to the eastern half of the U.S. for several months in 1990. Sulfate predictions by the model, which at the time had a simplified, relative-humidity-dependent representation of cloud chemistry rates, tended to overstate measurements somewhat. It has since been applied to the entire United States for all of 1990 (Guthrie et al, 1998).

When run on a Silicon Graphics Power Challenge L workstation, the eastern U.S. simulation required 20 minutes of computation for each 24-hour period of simulation. Since then, the code has been speeded up by about a factor of three, so that the full U.S. simulation for a full year requires about a week of computing.

SAQM-AERO. SAQM-AERO is based on the SARMAP Air Quality Model (SAQM), to which an aerosol module has been added. It includes the ability to handle multiple levels of nested grids and includes a sub grid-scale treatment of plumes for large point sources. The MM5 prognostic meteorological model provides meteorological input.

An updated version of the SEQUILIB thermodynamic model is used for the treatment of inorganic particulate matter. SAQM-AERO simulates the formation of sulfate and nitrate in fog through an empirical representation of the oxidation kinetics. Secondary organic aerosol is treated according to

fractional yields of VOC and no water is associated with the organic fraction. An improved organic module is under development (Pai et al., 1998)

SAQM-AERO has been applied for particulate matter, without size distribution, for a few days in the summer of 1990 in the San Joaquin Valley. More recently, it was applied to a summer 1987 episode of SCAQS (Pai et al., 1998), in which it was found that it predicted sulfate concentrations quite well but underestimated organic particle concentrations.

UAM-AERO. UAM-AERO is based on the UAM-IV photochemical model, which has been augmented to treat particulate matter. The modeling domain height is limited in UAM-IV, so it is best used for urban scales and not regional scales, since transport in the free troposphere above the mixed layer is a consideration on the regional scale.

The model calculates the formation of organic particles through the oxidation of VOC; the resulting particles are assumed to be non-volatile and non-hygroscopic. Formation of inorganic particles in clouds is simulated with an empirical mechanism that reflects three reactions but fails to account for some of the nonlinearities of the process. The model has the ability to simulate the evolution of the particle size distribution.

UAM-AERO has been applied to the Los Angeles Basin and the San Joaquin Valley. In Los Angeles in summer, the model predicted 24-hr maximum PM_{2.5} mass concentration within 20% of measurements, but tended to underestimate the chemical species maxima. Model performance during three episodes in the San Joaquin Valley was judged to be too poor for application of the model to State Implementation Plan development (Lurmann et al., 1996). Emissions and meteorological data deficiencies are major sources of uncertainty for these simulations.

When used to calculate a size resolved particulate matter distribution over a 51 x 36 x 5 grid cell domain, UAM-AERO requires about 20 hours on a HP-C110 workstation for a 24-hour simulation. Without the PM size resolution, the same simulation takes about 5 hours.

UAM-AIM. This model is similar to UAM-AERO, with the exception that it has a different gas-particle conversion algorithm, an update of the Aerosol Inorganic Model (AIM). The model achieves computational efficiency by searching and interpolating pre-calculated values instead of carrying out full thermodynamic equilibrium calculations. The treatment of secondary organic, sulfate and nitric acid formation is identical to that of UAM-AERO.

UAM-AIM was applied to the same June 1987 episode as UAM-AERO. Although the species errors were different the overall performance of the two models, compared to measurements, was comparable.

On an IBM RS/6000 390 workstation, a three-day simulation with a 65 x 36 x 5 grid cells takes 24 hours of computer time.

UAM-LC. For long-term particulate matter calculations, the UAM-IV framework was modified by simplifying its chemical mechanism and adding a particulate matter module. The resulting model UAM-LC (for linear chemistry) contains parameterized representations of the atmospheric chemistry of interest for particulate matter analyses. Interestingly, the model no longer predicts ozone, which must be externally specified. It simulates aqueous phase oxidation of SO₂ with a formula that depends on relative humidity and season, which fails to represent the nonlinearities in the actual oxidation process.

UAM-LC has been applied to the Los Angeles Basin for simulating annual average PM₁₀ in 1995. It takes about 15 hours on a HP-C110 workstation to simulate one year over a gridded domain of 65 x 40 x 2 grid cells.

VISHWA. The Visibility and Haze in the Western Atmosphere (VISHWA) model was developed by adapting the episodic Acid Deposition and Oxidant Model (ADOM) for long term particulate matter predictions. The changes made included incorporation of a simplified chemical mechanism and addition of a post processor for particulate matter.

VISHWA simulates the aqueous formation of sulfate through oxidation with hydrogen peroxide. Organic particulate matter is estimated through fractional yields from VOC groups. The size distribution of particulate matter is not simulated.

The model has been used to simulate hourly speciated fine particulate matter concentrations for 1992 for the western U.S. A grid of 57 x 57 x 6 grid cells of 50 x 50 km cells was used. The wind field was defined initially by the Nested Grid Model (NGM) and later by RAMS. Its performance for this application is described by Tombach et al. (1996b).

For the above simulation, the model required about 3% of real time on an IBM RS6000/590 workstation, i.e., the one-year simulation required about 1 ½ weeks of actual computer time.

5.4 Calculating Visibility from the Particulate Matter Concentrations

The outputs of most of the models described above are particulate matter concentrations, typically by species, as functions of location and time. In some cases, a size distribution is also given. Very few of the models (namely VISCREEN, PLUVUE, CALPUFF, ROME, Models 3) calculate the optical effect of the particulate matter. Such calculations can always be done in a post-processing mode from the particulate matter field description, however, so it is possible to make any aerosol model into a visibility model.

For completeness, then, we mention here briefly the three principal ways in which the optical effects of aerosol can be calculated:

- Extinction Efficiency. The extinction coefficient resulting from the aerosol is calculated by multiplying the mass concentrations of the various species by extinction efficiencies. (See, for example, Equation 1 in Section 2.2 of this report). The extinction efficiencies are derived from the literature or are estimated using multiple linear regression of measurements of aerosol species and light extinction. Extinction efficiencies for hygroscopic species are multiplied by a relative humidity factor that reflects the enhancement of extinction by the growth of a particle as it takes up water. This is the approach used in CALPUFF.
- Mie Theory. The extinction due to the aerosol is computed from its chemical composition and size distribution using Mie theory. This is the approach used in Models 3/CMAQ.
- Radiative Transfer Modeling. In order to derive visual effects, such as changes in contrast or color of plumes, the model considers not only the extinction itself but also the effects of sun angle, sky illumination, and background. This is the approach used in the VISCREEN, PLUVUE-II and ROME plume models.

5.5 Assessment of Models

The above discussion shows that a variety of tools exist for modeling the particulate matter that causes visibility impairment. These models, of necessity, include significant simplifications or approximations, particularly in the simulation of the formation of particulate matter, that are dictated by the state of the science and the speed of computers. The predictive skills of the most recent models, which include fewer such limitations, are currently not well evaluated.

The reviews by Seigneur et al. (1997a) and Seigneur (1997, 1998) contain evaluations of modeling capabilities and needs for improvement. In addition, the availability, evaluation, use and limitations of air quality models for ozone and particulate matter are reviewed in a paper that was prepared for the consideration of the Federal Advisory Committee Act (FACA) Subcommittee on Ozone, PM, and Regional Haze (FACA, 1997).

The principal challenge in receptor modeling is how to determine quantitative source apportionments for secondary compounds that differ chemically and physically from the emitted materials. Studies suggest some ability of the available secondary particle receptor models to identify the likely locations of major sources of secondary particle precursors. Their ability to provide quantitative apportionment of the measured particulate matter mass depends on use of additional information, such as spatial or temporal variation, detailed source inventories, or transport trajectory information. The accuracy of such quantification of apportionment is not yet well established, however. Furthermore, the most advanced methods are not yet well enough developed for routine use.

Turning to the regional source models, the FACA review (FACA, 1997) asserts, "Models are available for use in designing ozone and PM SIPs, and for other regulatory modeling purposes." This is followed by the qualification, "However, quality of data bases and lack of rigorous performance evaluation should make one cautious in interpreting their output." In particular, "We need better emissions, meteorological and air quality data to apply the models with confidence." The experience of the Grand Canyon Visibility Transport Commission with the application of VISHWA (Tombach et al., 1996b) certainly supports this conclusion, particularly with regard to the need for high-quality detailed meteorological input data.

Input data quality and comprehensiveness are not the sole limits to the predictive ability of source models. The models themselves have shortcomings. For the purposes of visibility, two major shortcomings lie in the simulations of aqueous-phase particle formation and the formation of organic particles. Even though the chemical and physical mechanisms can be modeled, the in-cloud formation of particles is particularly challenging to simulate because one almost never has knowledge of the specific times when the emitted material is in clouds. As additional areas deserving of attention, Seigneur et al. (1997a) and Seigneur (1997, 1998) also recommend improvements in other aspects of the aerosol modules.

Thus, particulate matter and visibility models and input data have not yet reached the stage that their conclusions can be accepted uncritically. The initial testing of models for Project MOHAVE highlights this need for caution. There it was found that none of seven source and receptor models, applied with available meteorological data as needed, was able to reliably predict the measured ambient concentration of a tracer gas emitted from a 110-km distant power plant stack (Green and Tombach, 1999). Subsequent modeling, in which the tracer gas concentrations were used to improve dispersion estimates, enabled focus on aerosol mechanisms and appeared to produce reasonably reliable estimates of secondary sulfate concentrations.

The above presentation of the limitations of the models does not mean that the receptor and source modeling tools should not be used for the assessment of visibility impacts – only that their use requires critical oversight and experienced evaluation of the results. In the hands of an experienced and careful user, today's models can provide useful information for visibility and air quality management.

6.0 MEASUREMENT METHOD IMPROVEMENTS

The assessments of visibility spatial and temporal patterns as well as long-term trends that were presented in Sections 3.0 and 4.0 were limited by the spatial coverage within California. Although data were available from sites in most of California's air basins, direct measurements of optical characteristics were limited to measurements of the particle light scattering coefficient in the Sacramento Valley and Lake County Air Basins, measurements of the light extinction coefficient at three IMPROVE sites, and measurements of the particle light absorption coefficient at seven IMPROVE sites. Additionally, although $PM_{2.5}$ mass concentration data were available from sites throughout most of the state, extensive chemical composition data were available only from IMPROVE sites.

The ongoing implementation of the $PM_{2.5}$ measurement network in California as required by the U.S. EPA will greatly improve the spatial coverage for $PM_{2.5}$ mass and chemical composition data. The coverage for optical measurements will also improve as a result of planned expansions of the IMPROVE network. However, there is still likely to be a lack of optical data in urban areas in the state.

The assessment of visibility trends has also been limited by available measurement techniques for visual air quality and for related aerosol properties. Visual air quality can change rapidly, over periods of an hour or less. Thus, better temporal resolution of aerosol concentrations and chemical composition will be needed to fully understand the causes of reduced visibility and the variability of those causes. Also, accurate measurements of light extinction due to fine particles will be required to understand the changes in visibility that are likely to occur as a result of the new Federal $PM_{2.5}$ standards.

This section presents an overview of improvements that are currently in progress in the state of the science of visibility-related measurement techniques. The first section addresses visibility-related measurements, and the second addresses aerosol measurements.

6.1 Visibility Measurements

Measurement improvements are being tested for both components of light extinction, scattering and absorption. The particle light scattering coefficient data available from local-agency sites utilized enclosed nephelometers that can modify the sampled air by causing decreases in relative humidity. Most ambient light scattering measurements in recent years have been conducted using the OPTEC NGN-2 nephelometer, an open-air model that measures scattering from all particles without size segregation. The open-air design allows for minimal temperature modification of the aerosol. Development and testing are underway for a $PM_{2.5}$ version of the NGN nephelometer, maintaining temperature control but measuring scattering due only to fine particles. This fine particle version will allow better understanding of light extinction changes due to changes in the concentrations of $PM_{2.5}$ particles, which are the most efficient scatterers.

Light absorption is determined using an aethalometer, a device which measures light attenuation through a particulate sample collected on a filter strip. Existing aethalometers have measured absorption only for visible light. A new version, distributed by Andersen Instruments, measures light absorption in both the visible and ultraviolet (UV). Because aromatic compounds absorb in the UV, the combination of visible and UV absorption allows one to distinguish between compounds that contain aromatics (such as fresh diesel exhaust) and those that do not.

Measurements of relative humidity (RH) are critical in relating aerosol concentrations to light extinction. Light extinction efficiencies for individual chemical species (e.g., ammonium nitrate, organic carbon) can be applied to measured concentrations to calculate the extinction based on aerosol properties, termed the reconstructed extinction. These extinction efficiencies typically are expressed as a function of relative humidity, reflecting the tendency of particles to grow in size and to scatter light more effectively at higher humidities. These humidity functions are non-linear, becoming very steep at high humidities, and thus are very sensitive to uncertainties in humidity measurements at high RH. Uncertainties in the humidity functions themselves add to the overall uncertainty of the humidity/visibility relationship.

Improved humidity measurement devices, capable of reliable measurements at humidities exceeding 90%, have been developed and tested recently, with the ultimate goal of achieving accuracy and precision of $\pm 1\%$ RH at these high values. For example, the Vaisala HMP243 is especially designed for high-RH applications, and it was tested against other sensors this past winter by the California Air Resources Board (ARB) under high-RH conditions in Bakersfield. The results of this comparison are expected to be available this spring. With most humidity measurement devices, frequent calibrations increase the reliability of the measurements at high RH.

6.2 Aerosol Measurements

Reliable measurements of visual air quality with short time resolution (one hour or less) have been available for a decade or more. However, aerosol measurements with comparable time resolution have been possible only for gravimetric mass, using instruments such as the beta attenuation monitor (BAM) or the tapered element oscillating microbalance (TEOM). But mass measurements provide only a partial picture of the relationship of aerosols to visibility. Because different chemical components of the aerosol exhibit different light extinction efficiencies and because the chemical composition of the aerosol often changes over time, short time-resolved measurements of aerosol chemical composition are needed. The development and testing of such methods is the focus of much current research into aerosol measurement techniques.

Techniques are under development for continuous (i.e., approximately 1 hour or less) measurement of all of the principal components of the aerosol. For particulate nitrate, methods have been developed by Aerosol Dynamics, Inc. (ADI, directed by Susanne Hering) and by Atmospheric Research & Analysis, Inc. (ARA, directed by Eric Edgerton). Both systems were tested this past winter as part of

the ARB study in Bakersfield, and both use a commercially-available NO/NO_x monitor as the principal analytical device. The ADI method operates by collecting a small particulate sample and flashing it every few minutes, whereas the ARA method operates by denuder difference, utilizing several channels. Harvard University is also developing a continuous nitrate system, but it has not yet undergone extensive field tests.

The ADI system is expected to be commercially available within the next year or so through Rupprecht & Patashnick (R&P). In the meantime, it will undergo further field testing at the EPA supersite in Fresno, beginning this summer.

ADI is also developing a continuous method for particulate sulfate, also using the flashing technique but employing a commercial SO₂ monitor as the sensor. Harvard is also working toward a continuous sulfate method. The ADI system was tested in Bakersfield this past winter and may be employed at the EPA Fresno supersite. However, neither the ADI system nor the Harvard system is yet available commercially.

A continuous method for particulate carbon (the remaining principal component of the aerosol) is commercially available through R&P. Their instrument, however, quantifies only total carbon and does not distinguish between organic carbon (OC) and elemental carbon (EC). Currently, one typically uses an aethalometer in conjunction with the R&P instrument to estimate the OC/EC ratio.

Research is underway at Rutgers University (directed by Barbara Turpin) to develop a continuous instrument capable of distinguishing OC from EC. The method is based on the thermal optical reflectance (TOR) method of carbon analysis and, if successful, is expected to be made commercially available.

Research is also underway to develop effective methods for measuring precursors of secondary particles, especially ammonia and nitric acid. Commercial methods are available for ammonia, but their reliability at low concentrations (below about 30 ppb) is questionable. Research, principally by Eric Edgerton at ARA, is focusing on improving converter efficiency to achieve better ammonia measurements at low concentrations. The ARA denuder difference system, described above for nitrate measurements, is also being tested for measuring nitric acid.

The research described above is targeted toward improving the continuous measurement of the chemical components of the aerosol. Improvements in the continuous measurement of gravimetric mass are also underway. A disadvantage of the present TEOM is that it heats the sample as part of the measurement process, such that semi-volatile components of the particulate matter (e.g., organics, nitrate, and water) can be lost during sampling. A new version of the TEOM is under development by R&P that will maintain the sample near ambient temperature and humidity during sampling. This instrument was tested in Bakersfield this past winter and may be commercially available soon.

Another new continuous gravimetric mass instrument is under development at Harvard. Their Continuous Ambient Mass Monitor (CMM) measures the pressure drop across a filter as it loads with particulate matter. A calibration equation is used to relate the pressure drop to the mass concentration in real time. This instrument was also tested in Bakersfield this past winter.

All of the methods discussed above have the potential for commercial application and for routine use in field measurements. In addition, research is underway on advanced methods which, while not routinely applicable, could provide useful insights into aerosol properties.

Remote sensing instruments can provide reliable measurements of ammonia and nitric acid with temporal resolution of an hour or less. Tunable diode laser absorption spectroscopy (TDLAS) instruments are available commercially from Unisearch and TEI, and can be used to measure both ammonia and nitric acid. Ernie Tuazon at UC Riverside has used Fourier Transform Infrared (FTIR) technology to measure ammonia continuously with sub-ppb sensitivity. However, the FTIR method is especially labor-intensive and thus is limited to research applications, not routine measurements. In yet another technique, Fred Fehsenfeld at NCAR has used chemical ionization mass spectrometry to measure ambient ammonia accurately. However, this method is not suitable for routine field measurements.

Much current research is directed toward the development of techniques for chemical speciation of single particles. Prototype systems are being developed at UC Riverside (Kim Prather), the University of Delaware (Murray Johnston), NOAA-Boulder (Dan Murphy), Sandia Laboratories, and Aerodyne Corporation. The UC Riverside system, for example, employs a size-selective device followed by an aerosol time-of-flight mass spectrometer (ATOFMS) which fragments individual particles and determines their chemical composition. This technology allows precise temporal resolution because individual particles are analyzed in real time. Plus, it provides an understanding of the mixture of chemical components in each particle, thereby precluding the need for assumptions concerning internally versus externally mixed particles. Data processing is time consuming because data are recorded for each particle, resulting in a large volume of data. All of the currently available single particle methods are labor intensive and are in the research stages, so none are suitable for routine use.

7.0 CONCLUSIONS

The descriptions and analyses presented in previous sections lead to the following conclusions:

16. The highest fine particle concentrations in California are present in locations with surrounding topography that limits dispersion. These areas include the Central Valley, the South Coast Air Basin, the San Francisco Bay area and the Lake Tahoe Air Basin.
17. The highest concentrations at these locations generally occur during the fall or winter, when periods of low inversions and low wind speeds lead to the accumulation of emitted particulate matter.
18. Carbon-containing materials and ammonium nitrate are the major constituents of $PM_{2.5}$ at the locations with the highest $PM_{2.5}$ mass concentrations. Wood burning may be a major source of the carbon-containing materials, particularly at locations with cooler fall and winter temperatures, while the ammonium nitrate is formed from atmospheric reactions that involve nitrogen oxides and ammonia.
19. Concentrations at coastal locations, such as Redwood National Park and Point Reyes National Seashore, do not vary as much with season as concentrations at inland locations, although there is a tendency for higher concentrations to occur during fall and winter than during spring and summer.
20. Concentrations at Yosemite and Lassen Volcanic National Parks are highest during the summer, in contrast with the other locations, and sulfate is a larger contributor than ammonium nitrate. This behavior may be caused by summertime park visitors or by transport from the Central Valley.
21. Concentrations at San Geronio Wilderness Area are highest during spring and summer, when conditions are conducive to transport of material from the South Coast Air Basin.
22. Statistically significant decreases in concentrations occurred between 1989 and 1996 in several air basins. Most notable were decreases in the San Joaquin Valley during winter and at San Geronio Wilderness Area during spring, which are the times of year when concentrations are highest at these locations.
23. Estimated emissions of $PM_{2.5}$, nitrogen oxides and sulfur oxides decreased throughout the state between 1990 and 1995. These decreases are consistent with the observed decreases in concentrations. However, decreases in concentrations did not accompany decreases in emissions everywhere.

24. Emissions from energy production are small percentages of PM_{2.5}, nitrogen oxide and sulfur oxide emissions in California, so energy production likely does not contribute substantially to decreased visibility or increased PM_{2.5} concentrations.
25. Emissions from non-mobile source energy use are a larger percentage of total emissions than emissions from energy production. In particular, wood burning is a substantial contributor to PM_{2.5} emissions in cooler locations, such as the Lake Tahoe and Mountain Counties Air Basins. Therefore, emissions from non-mobile source energy use may be important contributors to reduced visibility and increased PM_{2.5} concentrations in some parts of the state.
26. Several atmospheric models exist that can be used to better understand relationships between emissions, atmospheric particulate matter, and visibility. However, their application generally requires extensive quantities of data and experience.
27. More extensive spatial coverage is needed to better understand the nature and causes of visibility and particulate matter concentrations in California. Implementation of the PM_{2.5} monitoring network in conjunction with expansion of the IMPROVE network will help provide this information in the future.
28. Recent and ongoing developments in measurement techniques for atmospheric optical parameters and particulate matter mass and constituents will also provide new information to better characterize visibility and particulate matter.

8.0 REFERENCES

- Anttila, P., P. Paatero, U. Tapper and O. Jarvinen (1995). Application of Positive Matrix Factorization to Source Apportionment: Results of a Study of Bulk Deposition Chemistry in Finland. *Atmos. Environ.* **29**: 1705-1709.
- Ashbaugh, L.L., W.C. Malm and W.Z. Sadeh (1985). A Residence Time Probability Analysis of Sulfur Concentrations at Grand Canyon National Park. *Atmos. Environ.* **19**: 1263-1270.
- Binkowski, F.S., and U. Shankar (1995). The Regional Particulate Matter Model. 1: Model Description and Preliminary Results. *J. Geophys. Res.* **100**: 26191-26209.
- California Air Resources Board (1997). California Ambient Air Quality Data. CD Number: TSD-97-008-CD.
- California Air Resources Board (1998). Data transmittal from Martin Johnson to Steven Heisler, ENSR, November 5, 1998.
- California Air Resources Board (1999). Data transmittal from Patrick Gaffney to Steven Heisler, ENSR, February 24, 1999.
- Cartwright, H.M., and S.P. Harris (1993). Analysis of the Distribution of Airborne Pollution Using Genetic Algorithms. *Atmos. Environ.* **27A**: 1783-1791.
- Cheng, M.D., N. Gao and P.K. Hopke (1996). Source Apportionment Study of Nitrogen Species Measured in Southern California in 1987. *J. Environ. Engineer.* **122**: 183-190.
- Federal Advisory Committee Act Subcommittee on Ozone, PM, and Regional Haze (1997). The Modeling process and Emissions inventories: Their Development, Availability, Evaluation, Use, and Limitations. Draft Paper, August 5.
- Gabruk, R.S., R.I. Sykes, C. Seigneur, P. Pai, P. Gillespie, R.W. Bergstrom and P. Saxena (1999). Evaluation of the Reactive and Optics Model of Emissions (ROME). *Atmos. Environ.*, in press.
- Green, M.C., and I. Tombach (1999). Use of Project MOHAVE Perfluorocarbon Tracer Data to Evaluate Source and Receptor Models. Submitted to *J. AWMA*.
- Guthrie, P.D., C.A. Emery, M.P. Ligocki, G.E. Mansell, A.K. Kuklin, and D. Gao (1995). Development and Preliminary Testing of the Regulatory Modeling System for Aerosols and Deposition

(REMSAD). Technical Memorandum SYSAPP-9611, Systems Applications International, San Rafael, CA.

Guthrie, P.D., D. Gao, and G.F. Mansell (1998). Evaluation of the Performance of the REMSAD Modeling System for Fine Particles and Deposition. Final Report SYSAPP-98/24, Systems Applications International, San Rafael, CA.

Henry, R.C. (1991). Multivariate Receptor Models, in **Receptor Modeling for Air Quality Management**, P.K. Hopke, ed., Elsevier Science Publishers, New York. pp. 117-148.

Henry, R.C. (1997a). Receptor Model Applied to Patterns in Space (RMAPS). Part 1 – Model Description. *J. AWMA* **47**: 216-219.

Henry, R.C. (1997b). Receptor Model Applied to Patterns in Space (RMAPS). Part 2 – Apportionment of Airborne Particulate Sulfur from Project MOHAVE. *J. AWMA* **47**: 220-225.

Henry, R.C. (1997c). Receptor Model Applied to Patterns in Space (RMAPS). Part 3 – Apportionment of Airborne Particulate Sulfur in Washington State. *J. AWMA* **47**: 226-230.

Hudischewkyj, A.B. and C. Seigneur (1989). Mathematical Modeling of the Chemistry and Physics of Aerosols in Plumes. *Environ. Sci. & Technol.* **23**: 423-421.

Jacobson, M.Z., R. Lu, R.P. Turco and O.B. Toon (1996). Development and Application of a New Air Pollution Modeling System, Part I: Gas Phase Simulations. *Atmos. Environ.* **30**: 1939-1963.

Jacobson, M.Z. (1997a). Development and Application of a New Air Pollution Modeling System, Part II: Aerosol Module Structure and Design. *Atmos. Environ.* **31**: 131-144.

Jacobson, M.Z. (1997b). Development and Application of a New Air Pollution Modeling System, Part III: Aerosol Phase Simulations. *Atmos. Environ.* **31**: 587-608.

Johnson, M.E. (1998) Personal Communication

Keeler, G.J., and P.J. Samson (1989). Spatial Representativeness of Trace Element Ratios. *Environ. Sci. Technol.* **23**: 1358-1384.

Kendall, M.G. (1970). **Rank Correlation Methods**, Griffin, London.

Kumar, N., F. Lurmann, A. Wexler, S. Pandis, and J. Seinfeld (1996). Development and Application of a Three-Dimensional Aerosol Model. **Proceedings of A&WMA Specialty Conference on**

Computing and Environmental Resource Management, Research Triangle Park, NC, Dec. 2-4. pp 69-86.

Lurmann, F.W., and N. Kumar (1996). Development of Chemical Transformation Algorithms for Annual PM10 Dispersion Models. Draft report STI-95410-1602-DFR for the South Coast Air Quality Management District, Diamond Bar, CA.

Lurmann, F.W., A.S. Wexler, S.N. Pandis, S. Musarra, N. Kumar and J.H. Seinfeld (1997). Modeling Urban and Regional Aerosols: II. Application to California's South Coast Air Basin. *Atmos. Environ.* **31**: 2695-2715.

Malm, W.C., K.A. Gebhart, and R.C. Henry (1990). An Investigation of the Dominant Source Regions of Fine Sulfur in the Western United States and Their Areas of Influence. *Atmos. Environ.* **24A**: 3047-3060.

Meng, Z., D. Dabdub and J.H. Seinfeld (1998). Size- and Chemically-Resolved Model of Atmospheric Aerosol Dynamics. *J. Geophys. Res.*, in press.

Middleton, P., K. Zhang, J. Chang, et al. (1993). Brown Cloud II: The Denver Air Quality Modeling Study. Atmospheric Sciences Research Center, State University of New York at Albany.

Middleton, P. (1997). DAQM – Simulated Spatial and Temporal Differences Among Visibility, PM, and Other Air Quality Concerns Under Realistic Emission Change Scenarios. *J. AWMA* **47**: 302-316.

Pai, P., K. Vijayaraghavan, C. Seigneur, J. Hegarty, M. Leidner, and J.-F. Louis (1998). Particulate Matter Modeling in the Los Angeles Basin using MM5 and SAQM-AERO – Preliminary Results. In **PM2.5: A Fine Particle Standard**, J. Chow and P. Koutrakis, Editors. VIP-81, Air and Waste Management Association, Pittsburgh. pp. 748-758

Pitchford, M., M. Green, H. Kuhns, I. Tombach, W. Malm, M. Scruggs, R. Farber and V. Mirabella (1999). Project MOHAVE Final Report.

Poirot, R.L., and P.R. Wishinski (1986). Visibility, Sulfate, and Air Mass History Associated with the Summertime Aerosol in Northern Vermont. *Atmos. Environ.* **20**: 1457-1469.

Seigneur, C. (1997). Review of Three-Dimensional Air Quality Models for Particulate Matter. In **Visual Air Quality, Aerosols, and Global Radiation Balance**. VIP-76, Air and Waste Management Association, Pittsburgh. pp. 5-15.

- Seigneur, C., P. Pai, J-F. Louis, P. Hopke, and D. Grosjean (1997a). Review of Air Quality Models for Particulate Matter. Report prepared for the American Petroleum Institute.
- Seigneur, C., X.A. Wu, E. Constantinou, P. Gillespie, R.W. Bergstrom, I. Sykes, A. Venkatram, and P. Karamchandani (1997b). Formulation of a Second-Generation Reactive Plume and Visibility Model. *J. AWMA* **47**: 176-184.
- Seigneur, C. (1998). PM-2.5 Modeling: Current Status and Research Needs. In **PM2.5: A Fine Particle Standard**, J. Chow and P. Koutrakis, Editors. VIP-81, Air and Waste Management Association, Pittsburgh. pp. 713-724.
- Seigneur, C., P. Pai, I. Tombach, C. McDade, P. Saxena, and P. Mueller (1999). Modeling of Potential Power Plant Plume Impacts on Dallas-Fort Worth Visibility. Accepted by *J. AWMA*.
- Sisler, J.F., W.C. Malm, and K. Gebhart (1996). SPATIAL AND SEASONAL PATTERNS AND LONG TERM VARIABILITY OF THE COMPOSITION OF THE HAZE IN THE UNITED STATES: An Analysis of Data from the IMPROVE Network. ISSN: 0737-5352-32, Center for Research in the Atmosphere, Colorado State University, Fort Collins, CO.
- Stohl, A. (1996). Trajectory Statistics – A New Method to Establish Source-Receptor Relationships of Air Pollutants and Its Application to the Transport of Particulate Sulfate in Europe. *Atmos. Environ.* **30**: 579-587.
- Sun, Q., and Wexler, A.S. (1998). Modeling Urban and Regional Aerosols near Acid Neutrality – Application to the June 24-25 SCAQS Episode. Submitted to *Atmos. Environ.*
- Tombach, I., C. Seigneur, C. McDade, and S. Heisler (1996a). Dallas-Fort Worth Winter Haze Project. Volume 3: Visibility Assessment. EPRI TR-106775-V3, Electric Power Research Institute, Palo Alto, CA.
- Tombach, I., P. Karamchandani, and P. Pai (1996b). Development, Evaluation, and Application of Transfer Coefficients for Predicting Colorado Plateau Air Quality. Paper 96-TP46.03, 89th Annual Meeting of the A&WMA, Nashville.
- U.S. Environmental Protection Agency (1992a). Workbook for Plume Visual Impact Screening and Analysis. EPA-450/4-88-015R.
- U.S. Environmental Protection Agency (1992b). Updated User's Guide for the Plume Visibility Model (PLUVUE II). Research Triangle Park, NC.

U.S. Environmental Protection Agency (1995). A User's Guide for the CALPUFF Dispersion Model. EPA-454/B-95-006.

U.S. Environmental Protection Agency (1998). EPA Third-Generation Air Quality Modeling System. Models-3. Volume 9B: User Manual. EPA-600/R-98/069(a).

Venkatram, A., P. Karamchandani, P. Pai, C. Sloane, P. Saxena and R. Goldstein (1997). The Development of a Model to Examine Source-Receptor Relationships for Visibility on the Colorado Plateau. *J. AWMA* **47**: 286-301.

Watson, J.G., D. Blumenthal, J. Chow, C. Cahill, L.W. Richards, D. Dietrich, R. Morris, J. Houck, R.J. Dickson and S. Andersen (1996). Mt. Zirkel Wilderness Area Reasonable Attribution Study of Visibility Impairment. Final Report by Desert Research Institute, Reno, NV.

White, W.H. (1996). Alternative Perspectives on a Trend in Eastern Fine-Particle Sulfur Concentrations. *Environmental Manager*, April.

White, W.H. (1997). Phantom Sources from Spatial Correlations: an Example. **In Visual Air Quality, Aerosols, and Global Radiation Balance**. VIP-76, Air and Waste Management Association. pp. 762-763.

APPENDIX A
SERIAL TIME PLOTS

CONTENTS

A.0 Introduction	A-1
A.1 Lake County Air Basin (Lakeport)	A-1
A.2 Lake Tahoe Air Basin (South Lake Tahoe)	A-4
A.3 Mountain Counties Air Basin (Yosemite National Park)	A-9
A.4 North Central Coast Air Basin (Pinnacles National Monument)	A-14
A.5 North Coast Air Basin (Redwood National Park)	A-19
A.6 Northeast Plateau Air Basin (Lassen Volcanic National Park)	A-24
A.7 Sacramento Valley Air Basin (Arbuckle, Chico, Colusa, Gridley, Pleasant Grove and Yuba City)	A-29
A.8 San Francisco Bay Air Basin (San Jose and Point Reyes National Seashore).....	A-42
A.9 San Joaquin Valley Air Basin (Bakersfield, Fresno, Madera, Modesto, Stockton and Visalia)...	A-49
A.10 Salton Sea Air Basin (El Centro).....	A-62
A.11 South Coast Air Basin (Azusa, Long Beach, Riverside and San Geronio Wilderness Area) .	A-65

LIST OF FIGURES

Figure A-1 Median Light Scattering Coefficient and Coefficient of Haze by Year During Spring at Lakeport A-2

Figure A-2 Median Light Scattering Coefficient and Coefficient of Haze by Year During Summer at Lakeport A-2

Figure A-3 Median Light Scattering Coefficient and Coefficient of Haze by Year During Fall at Lakeport A-3

Figure A-4 Median Light Scattering Coefficient and Coefficient of Haze by Year During Winter at Lakeport A-3

Figure A-5 Average Calculated and Measured Optical Data and PM_{2.5} Mass by Year During Spring at South Lake Tahoe A-5

Figure A-6 Average PM_{2.5} Mass, Sulfate and Nitrate by Year During Spring at South Lake Tahoe A-5

Figure A-7 Average Calculated and Measured Optical Data and PM_{2.5} Mass by Year During Summer at South Lake Tahoe A-6

Figure A-8 Average PM_{2.5} Mass, Sulfate and Nitrate by Year During Summer at South Lake Tahoe. A-6

Figure A-9 Average Calculated and Measured Optical Data and PM_{2.5} Mass by Year During Fall at South Lake Tahoe A-7

Figure A-10 Average PM_{2.5} Mass, Sulfate and Nitrate by Year During Fall at South Lake Tahoe..... A-7

Figure A-11 Average Calculated and Measured Optical Data and PM_{2.5} Mass by Year During Winter at South Lake Tahoe A-8

Figure A-12 Average PM_{2.5} Mass, Sulfate and Nitrate by Year During Winter at South Lake Tahoe.. A-8

Figure A-13 Average Calculated and Measured Optical Data and PM_{2.5} Mass by Year During Spring at Yosemite National Park A-10

Figure A-14 Average PM_{2.5} Mass, Sulfate and Nitrate by Year During Spring at Yosemite National Park A-10

Figure A-15 Average Calculated and Measured Optical Data and PM_{2.5} Mass by Year During Summer at Yosemite National Park A-11

Figure A-16 Average PM_{2.5} Mass, Sulfate and Nitrate by Year During Summer at Yosemite National Park A-11

Figure A-17 Average Calculated and Measured Optical Data and PM_{2.5} Mass by Year During Fall at Yosemite National Park A-12

Figure A-18 Average PM _{2.5} Mass, Sulfate and Nitrate by Year During Fall at Yosemite National Park	A-12
Figure A-19 Average Calculated and Measured Optical Data and PM _{2.5} Mass by Year During Winter at Yosemite National Park	A-13
Figure A-20 Average PM _{2.5} Mass, Sulfate and Nitrate by Year During Winter at Yosemite National Park	A-13
Figure A-21 Average Calculated and Measured Optical Data and PM _{2.5} Mass by Year During Spring at Pinnacles National Monument	A-15
Figure A-22 Average PM _{2.5} Mass, Sulfate and Nitrate by Year During Spring at Pinnacles National Monument	A-15
Figure A-23 Average Calculated and Measured Optical Data and PM _{2.5} Mass by Year During Summer at Pinnacles National Monument	A-16
Figure A-24 Average PM _{2.5} Mass, Sulfate and Nitrate by Year During Summer at Pinnacles National Monument	A-16
Figure A-25 Average Calculated and Measured Optical Data and PM _{2.5} Mass by Year During Fall at Pinnacles National Monument	A-17
Figure A-26 Average PM _{2.5} Mass, Sulfate and Nitrate by Year During Fall at Pinnacles National Monument	A-17
Figure A-27 Average Calculated and Measured Optical Data and PM _{2.5} Mass by Year During Winter at Pinnacles National Monument	A-18
Figure A-28 Average PM _{2.5} Mass, Sulfate and Nitrate by Year During Winter at Pinnacles National Monument	A-18
Figure A-29 Average Calculated and Measured Optical Data and PM _{2.5} Mass by Year During Spring at Redwood National Park.....	A-20
Figure A-30 Average PM _{2.5} Mass, Sulfate and Nitrate by Year During Spring at Redwood National Park	A-20
Figure A-31 Average Calculated and Measured Optical Data and PM _{2.5} Mass by Year During Summer at Redwood National Park.....	A-21
Figure A-32 Average PM _{2.5} Mass, Sulfate and Nitrate by Year During Summer at Redwood National Park	A-21
Figure A-33 Average Calculated and Measured Optical Data and PM _{2.5} Mass by Year During Fall at Redwood National Park.....	A-22
Figure A-34 Average PM _{2.5} Mass, Sulfate and Nitrate by Year During Fall at Redwood National Park.....	A-22

Figure A-35 Average Calculated and Measured Optical Data and PM _{2.5} Mass by Year During Winter at Redwood National Park.....	A-23
Figure A-36 Average PM _{2.5} Mass, Sulfate and Nitrate by Year During Winter at Redwood National Park	A-23
Figure A-37 Average Calculated and Measured Optical Data and PM _{2.5} Mass by Year During Spring at Lassen Volcanic National Park	A-25
Figure A-38 Average PM _{2.5} Mass, Sulfate and Nitrate by Year During Spring at Lassen Volcanic National Park.....	A-25
Figure A-39 Average Calculated and Measured Optical Data and PM _{2.5} Mass by Year During Summer at Lassen Volcanic National Park	A-26
Figure A-40 Average PM _{2.5} Mass, Sulfate and Nitrate by Year During Summer at Lassen Volcanic National Park.....	A-26
Figure A-41 Average Calculated and Measured Optical Data and PM _{2.5} Mass by Year During Fall at Lassen Volcanic National Park	A-27
Figure A-42 Average PM _{2.5} Mass, Sulfate and Nitrate by Year During Fall at Lassen Volcanic National Park	A-27
Figure A-43 Average Calculated and Measured Optical Data and PM _{2.5} Mass by Year During Winter at Lassen Volcanic National Park	A-28
Figure A-44 Average PM _{2.5} Mass, Sulfate and Nitrate by Year During Winter at Lassen Volcanic National Park.....	A-28
Figure A-45 Median Light Scattering Coefficient and Coefficient of Haze by Year During Spring at Arbuckle	A-30
Figure A-46 Median Light Scattering Coefficient and Coefficient of Haze by Year During Spring at Chico	A-30
Figure A-47 Median Light Scattering Coefficient and Coefficient of Haze by Year During Spring at Colusa	A-31
Figure A-48 Median Light Scattering Coefficient and Coefficient of Haze by Year During Spring at Gridley	A-31
Figure A-49 Median Light Scattering Coefficient and Coefficient of Haze by Year During Spring at Pleasant Grove	A-32
Figure A-50 Median Light Scattering Coefficient and Coefficient of Haze by Year During Spring at Yuba City.....	A-32
Figure A-51 Median Light Scattering Coefficient and Coefficient of Haze by Year During Summer at Arbuckle	A-33

Figure A-52 Median Light Scattering Coefficient and Coefficient of Haze by Year During Summer at Chico	A-33
Figure A-53 Median Light Scattering Coefficient and Coefficient of Haze by Year During Summer at Colusa	A-34
Figure A-54 Median Light Scattering Coefficient and Coefficient of Haze by Year During Summer at Gridley	A-34
Figure A-55 Median Light Scattering Coefficient and Coefficient of Haze by Year During Summer at Pleasant Grove	A-35
Figure A-56 Median Light Scattering Coefficient and Coefficient of Haze by Year During Summer at Yuba City	A-35
Figure A-57 Median Light Scattering Coefficient and Coefficient of Haze by Year During Fall at Arbuckle	A-36
Figure A-58 Median Light Scattering Coefficient and Coefficient of Haze by Year During Fall at Chico	A-36
Figure A-59 Median Light Scattering Coefficient and Coefficient of Haze by Year During Fall at Colusa	A-37
Figure A-60 Median Light Scattering Coefficient and Coefficient of Haze by Year During Fall at Gridley	A-37
Figure A-61 Median Light Scattering Coefficient and Coefficient of Haze by Year During Fall at Pleasant Grove	A-38
Figure A-62 Median Light Scattering Coefficient and Coefficient of Haze by Year During Fall at Yuba City.....	A-38
Figure A-63 Median Light Scattering Coefficient and Coefficient of Haze by Year During Winter at Arbuckle	A-39
Figure A-64 Median Light Scattering Coefficient and Coefficient of Haze by Year During Winter at Chico	A-39
Figure A-65 Median Light Scattering Coefficient and Coefficient of Haze by Year During Winter at Colusa	A-40
Figure A-66 Median Light Scattering Coefficient and Coefficient of Haze by Year During Winter at Gridley	A-40
Figure A-67 Median Light Scattering Coefficient and Coefficient of Haze by Year During Winter at Pleasant Grove	A-41
Figure A-68 Median Light Scattering Coefficient and Coefficient of Haze by Year During Winter at Yuba City.....	A-41

Figure A-69 Median PM_{2.5} Mass and PM₁₀ Nitrate and Sulfate by Year During Spring at San Jose A-43

Figure A-70 Average Calculated and Measured Optical Data and PM_{2.5} Mass by Year During Spring at Point Reyes National Seashore A-43

Figure A-71 Average PM_{2.5} Mass, Sulfate and Nitrate by Year During Spring at Point Reyes National Seashore A-44

Figure A-72 Median PM_{2.5} Mass and PM₁₀ Nitrate and Sulfate by Year During Summer at San Jose A-44

Figure A-73 Average Calculated and Measured Optical Data and PM_{2.5} Mass by Year During Summer at Point Reyes National Seashore A-45

Figure A-74 Average PM_{2.5} Mass, Sulfate and Nitrate by Year During Summer at Point Reyes National Seashore A-45

Figure A-75 Median PM_{2.5} Mass and PM₁₀ Nitrate and Sulfate by Year During Fall at San Jose A-46

Figure A-76 Average Calculated and Measured Optical Data and PM_{2.5} Mass by Year During Fall at Point Reyes National Seashore A-46

Figure A-77 Average PM_{2.5} Mass, Sulfate and Nitrate by Year During Fall at Point Reyes National Seashore A-47

Figure A-78 Median PM_{2.5} Mass and PM₁₀ Nitrate and Sulfate by Year During Winter at San Jose A-47

Figure A-79 Average Calculated and Measured Optical Data and PM_{2.5} Mass by Year During Winter at Point Reyes National Seashore A-48

Figure A-80 Average PM_{2.5} Mass, Sulfate and Nitrate by Year During Winter at Point Reyes National Seashore A-48

Figure A-81 Median PM_{2.5} Mass and PM₁₀ Nitrate and Sulfate by Year During Spring at Bakersfield A-50

Figure A-82 Median PM_{2.5} Mass and PM₁₀ Nitrate and Sulfate by Year During Spring at Fresno A-50

Figure A-83 Median PM_{2.5} Mass and PM₁₀ Nitrate and Sulfate by Year During Spring at Madera A-51

Figure A-84 Median PM_{2.5} Mass and PM₁₀ Nitrate and Sulfate by Year During Spring at Modesto .. A-51

Figure A-85 Median Light Scattering Coefficient, Coefficient of Haze, PM_{2.5} Mass and PM₁₀ Nitrate and Sulfate by Year During Spring at Stockton A-52

Figure A-86 Median PM_{2.5} Mass and PM₁₀ Nitrate and Sulfate by Year During Spring at Visalia A-52

Figure A-87 Median PM_{2.5} Mass and PM₁₀ Nitrate and Sulfate by Year During Summer at Bakersfield A-53

Figure A-88 Median PM _{2.5} Mass and PM ₁₀ Nitrate and Sulfate by Year During Summer at Fresno ..	A-53
Figure A-89 Median PM _{2.5} Mass and PM ₁₀ Nitrate and Sulfate by Year During Summer at Madera	A-54
Figure A-90 Median PM _{2.5} Mass and PM ₁₀ Nitrate and Sulfate by Year During Summer at Modesto.....	A-54
.....	A-54
Figure A-91 Median Light Scattering Coefficient, Coefficient of Haze, PM _{2.5} Mass and PM ₁₀ Nitrate and Sulfate by Year During Summer at Stockton.....	A-55
.....	A-55
Figure A-92 Median PM _{2.5} Mass and PM ₁₀ Nitrate and Sulfate by Year During Summer at Visalia ..	A-55
Figure A-93 Median PM _{2.5} Mass and PM ₁₀ Nitrate and Sulfate by Year During Fall at Bakersfield...	A-56
Figure A-94 Median PM _{2.5} Mass and PM ₁₀ Nitrate and Sulfate by Year During Fall at Fresno.....	A-56
Figure A-95 Median PM _{2.5} Mass and PM ₁₀ Nitrate and Sulfate by Year During Fall at Madera.....	A-57
Figure A-96 Median PM _{2.5} Mass and PM ₁₀ Nitrate and Sulfate by Year During Fall at Modesto.....	A-57
Figure A-97 Median Light Scattering Coefficient, Coefficient of Haze, PM _{2.5} Mass and PM ₁₀ Nitrate and Sulfate by Year During Fall at Stockton.....	A-58
.....	A-58
Figure A-98 Median PM _{2.5} Mass and PM ₁₀ Nitrate and Sulfate by Year During Fall at Visalia	A-58
Figure A-99 Median PM _{2.5} Mass and PM ₁₀ Nitrate and Sulfate by Year During Winter at Bakersfield	A-59
.....	A-59
Figure A-100 Median PM _{2.5} Mass and PM ₁₀ Nitrate and Sulfate by Year During Winter at Fresno...	A-59
Figure A-101 Median PM _{2.5} Mass and PM ₁₀ Nitrate and Sulfate by Year During Winter at Madera..	A-60
Figure A-102 Median PM _{2.5} Mass and PM ₁₀ Nitrate and Sulfate by Year During Winter at Modesto	A-60
.....	A-60
Figure A-103 Median Light Scattering Coefficient, Coefficient of Haze, PM _{2.5} Mass and PM ₁₀ Nitrate and Sulfate by Year During Winter at Stockton.....	A-61
.....	A-61
Figure A-104 Median PM _{2.5} Mass and PM ₁₀ Nitrate and Sulfate by Year During Winter at Visalia ...	A-61
Figure A-105 Median PM _{2.5} Mass and PM ₁₀ Nitrate and Sulfate by Year During Spring at El Centro.....	A-63
.....	A-63
Figure A-106 Median PM _{2.5} Mass and PM ₁₀ Nitrate and Sulfate by Year During Summer at El Centro ...	A-63
.....	A-63
Figure A-107 Median PM _{2.5} Mass and PM ₁₀ Nitrate and Sulfate by Year During Fall at El Centro....	A-64
Figure A-108 Median PM _{2.5} Mass and PM ₁₀ Nitrate and Sulfate by Year During Winter at El Centro.....	A-64
.....	A-64
Figure A-109 Median PM _{2.5} Mass and PM ₁₀ Nitrate and Sulfate by Year During Spring at Azusa	A-66

Figure A-110 Median PM _{2.5} Mass and PM ₁₀ Nitrate and Sulfate by Year During Spring at Long Beach	A-66
Figure A-111 Median PM _{2.5} Mass and PM ₁₀ Nitrate and Sulfate by Year During Spring at Riverside	A-67
Figure A-112 Average Calculated and Measured Optical Data and PM _{2.5} Mass by Year During Spring at San Geronio Wilderness Area	A-67
Figure A-113 Average PM _{2.5} Mass, Sulfate and Nitrate by Year During Spring at San Geronio Wilderness Area.....	A-68
Figure A-114 Median PM _{2.5} Mass and PM ₁₀ Nitrate and Sulfate by Year During Summer at Azusa. A-68	
Figure A-115 Median PM _{2.5} Mass and PM ₁₀ Nitrate and Sulfate by Year During Summer at Long Beach	A-69
Figure A-116 Median PM _{2.5} Mass and PM ₁₀ Nitrate and Sulfate by Year During Summer at Riverside	A-69
Figure A-117 Average Calculated and Measured Optical Data and PM _{2.5} Mass by Year During Summer at San Geronio Wilderness Area	A-70
Figure A-118 Average PM _{2.5} Mass, Sulfate and Nitrate by Year During Summer at San Geronio Wilderness Area.....	A-70
Figure A-119 Median PM _{2.5} Mass and PM ₁₀ Nitrate and Sulfate by Year During Fall at Azusa.....	A-71
Figure A-120 Median PM _{2.5} Mass and PM ₁₀ Nitrate and Sulfate by Year During Fall at Long Beach	A-71
Figure A-121 Median PM _{2.5} Mass and PM ₁₀ Nitrate and Sulfate by Year During Fall at Riverside....	A-72
Figure A-122 Average Calculated and Measured Optical Data and PM _{2.5} Mass by Year During Fall at San Geronio Wilderness Area.....	A-72
Figure A-123 Average PM _{2.5} Mass, Sulfate and Nitrate by Year During Fall at San Geronio Wilderness Area.....	A-73
Figure A-124 Median PM _{2.5} Mass and PM ₁₀ Nitrate and Sulfate by Year During Winter at Azusa	A-73
Figure A-125 Median PM _{2.5} Mass and PM ₁₀ Nitrate and Sulfate by Year During Winter at Long Beach	A-74
Figure A-126 Median PM _{2.5} Mass and PM ₁₀ Nitrate and Sulfate by Year During Winter at Riverside	A-74
Figure A-127 Average Calculated and Measured Optical Data and PM _{2.5} Mass by Year During Winter at San Geronio Wilderness Area	A-75

Figure A-128 Average PM_{2.5} Mass, Sulfate and Nitrate by Year During Winter at San Geronio
Wilderness Area..... A-75

A.0 Introduction

This appendix contains serial time plots of median values (local-agency sites) and average values (IMPROVE sites) of the available optical and particulate matter data. The plots are grouped by air basin. One plot is presented for each local-agency site during each season showing all of the median values measured during each year. Two plots are presented for each IMPROVE site during each season. The first plot shows measured seasonal average light extinction and absorption coefficients and $PM_{2.5}$ mass concentration, and calculated seasonal average light scattering and absorption coefficients. The second plot shows seasonal average $PM_{2.5}$, nitrate and sulfate concentrations. The sulfate concentrations were calculated by multiplying the measured sulfur concentration by three.

A.1 Lake County Air Basin (Lakeport)

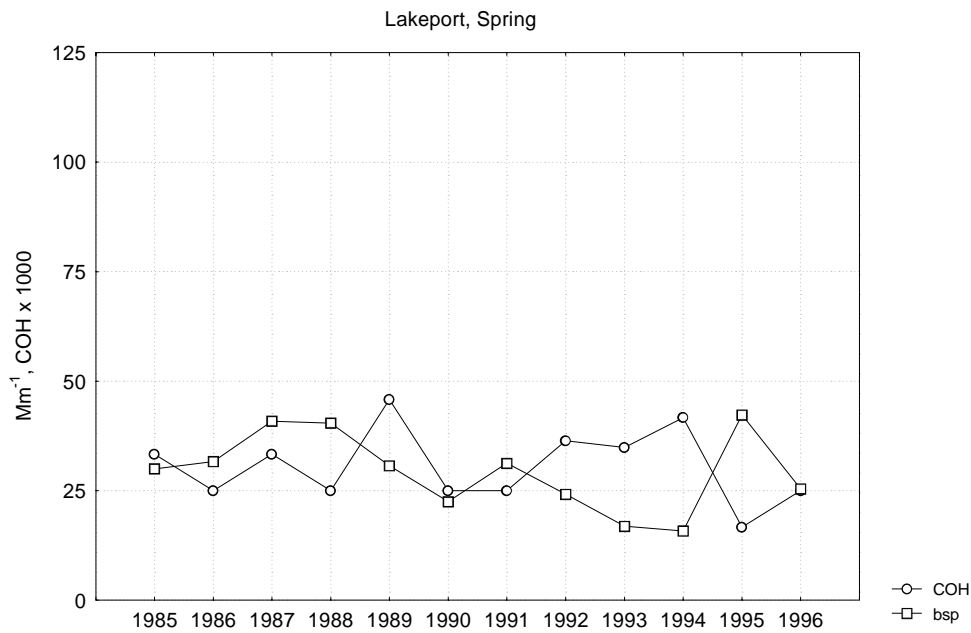


Figure A-1 Median Light Scattering Coefficient and Coefficient of Haze by Year During Spring at Lakeport

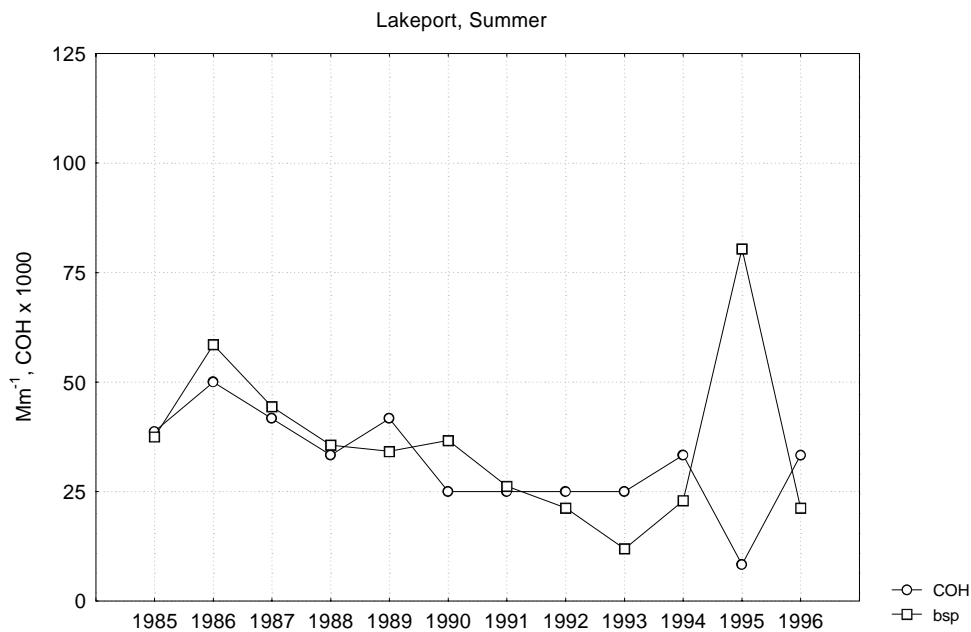


Figure A-2 Median Light Scattering Coefficient and Coefficient of Haze by Year During Summer at Lakeport

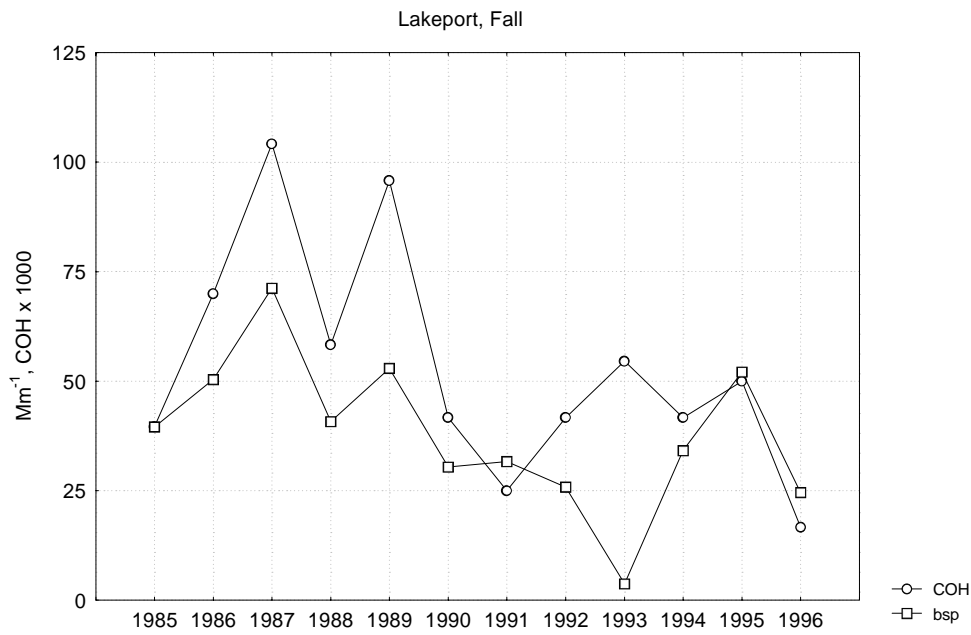


Figure A-3 Median Light Scattering Coefficient and Coefficient of Haze by Year During Fall at Lakeport

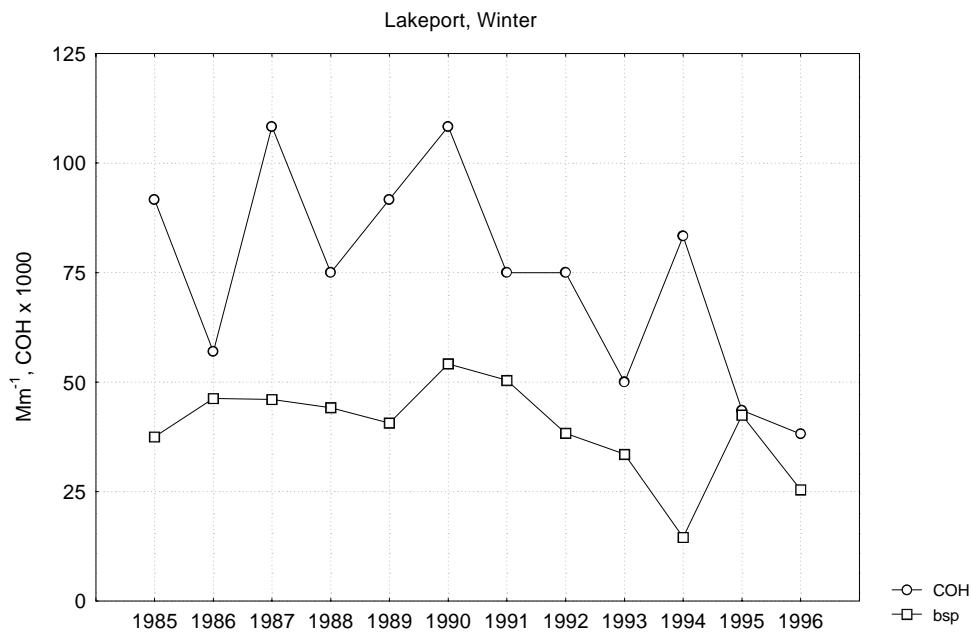


Figure A-4 Median Light Scattering Coefficient and Coefficient of Haze by Year During Winter at Lakeport

A.2 Lake Tahoe Air Basin (South Lake Tahoe)

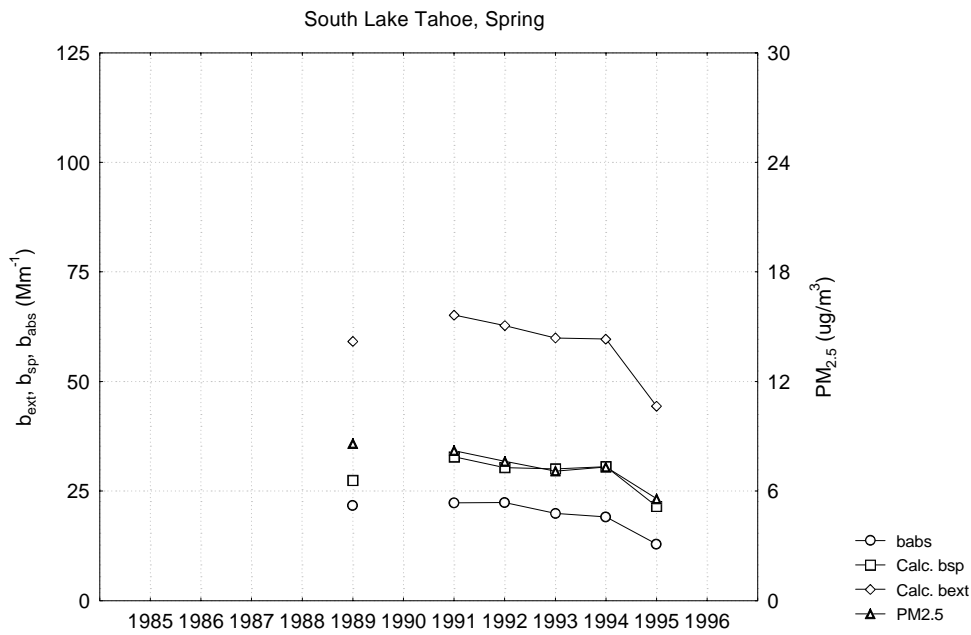


Figure A-5 Average Calculated and Measured Optical Data and PM_{2.5} Mass by Year During Spring at South Lake Tahoe

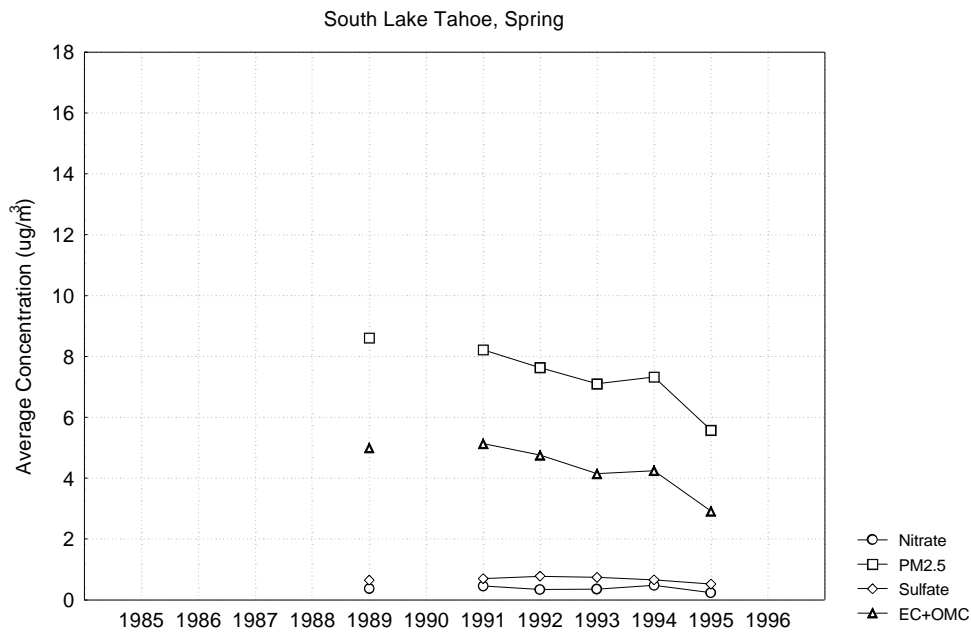


Figure A-6 Average PM_{2.5} Mass, Sulfate and Nitrate by Year During Spring at South Lake Tahoe

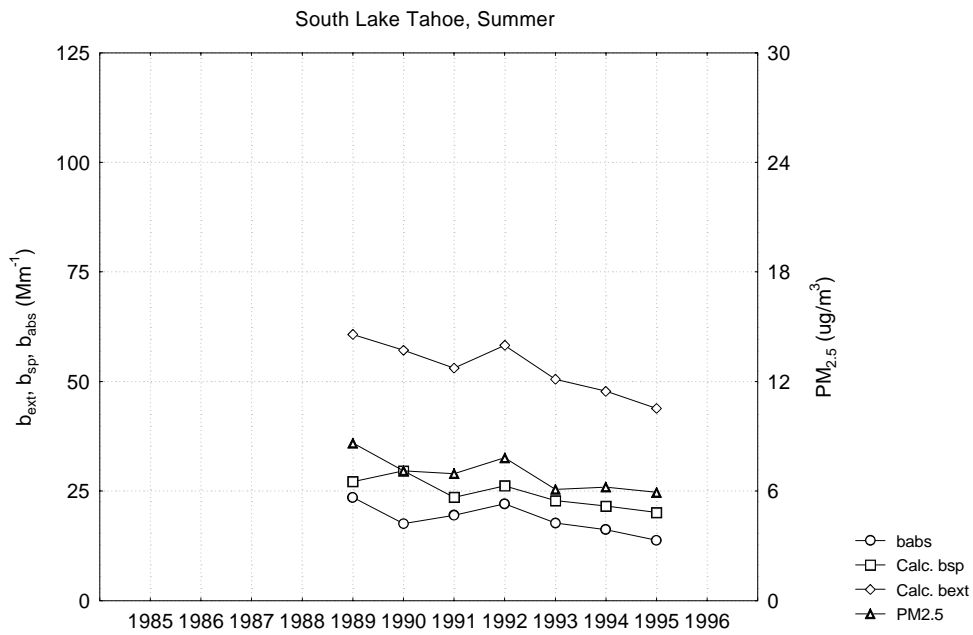


Figure A-7 Average Calculated and Measured Optical Data and PM_{2.5} Mass by Year During Summer at South Lake Tahoe

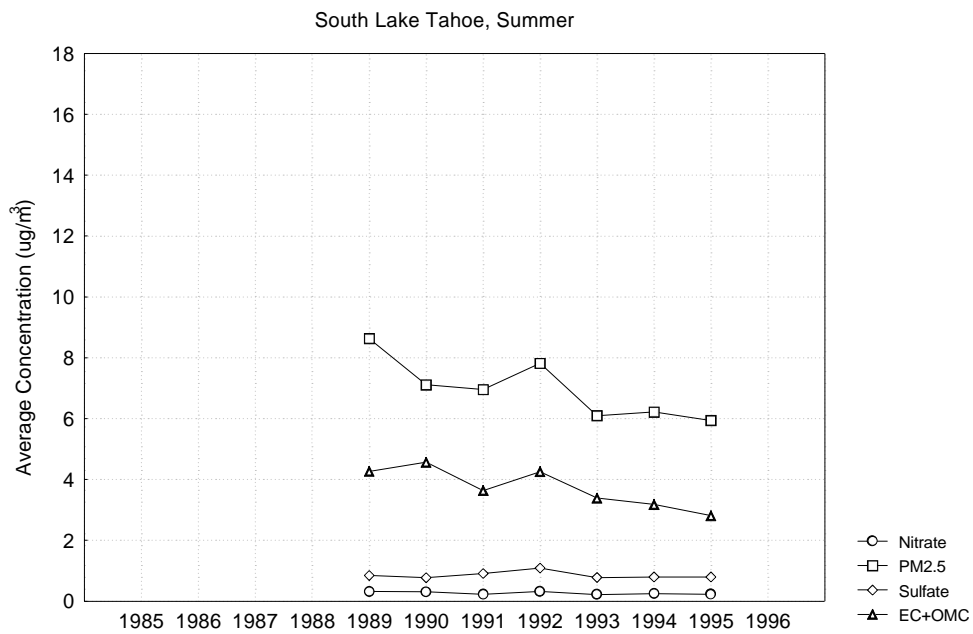


Figure A-8 Average PM_{2.5} Mass, Sulfate and Nitrate by Year During Summer at South Lake Tahoe

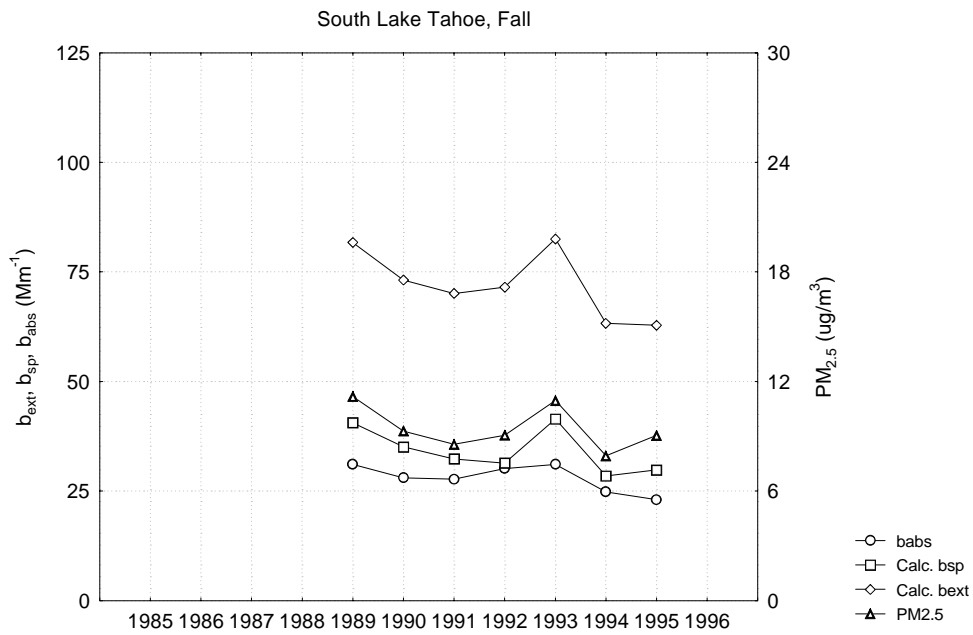


Figure A-9 Average Calculated and Measured Optical Data and PM_{2.5} Mass by Year During Fall at South Lake Tahoe

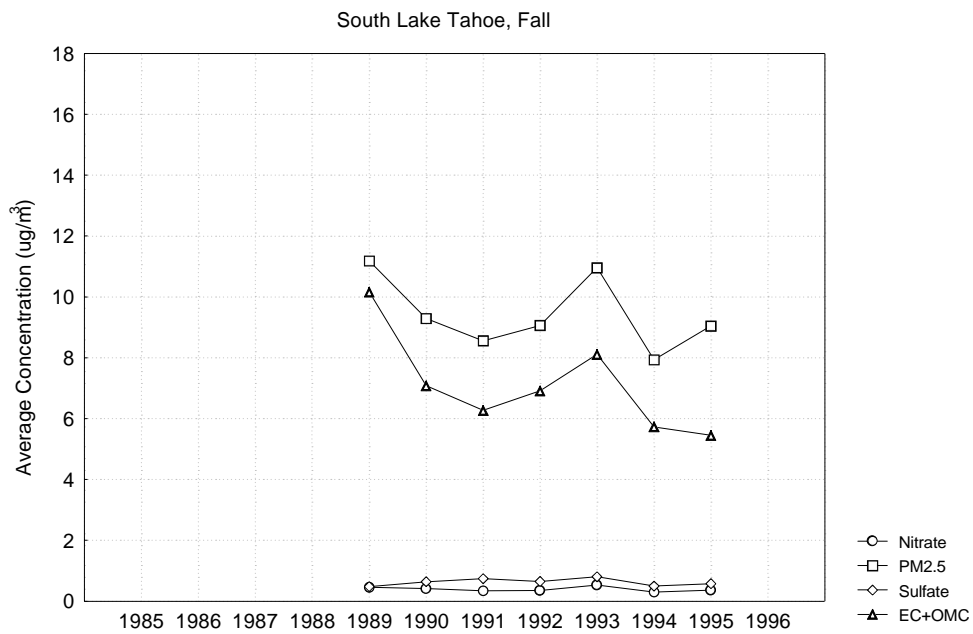


Figure A-10 Average PM_{2.5} Mass, Sulfate and Nitrate by Year During Fall at South Lake Tahoe

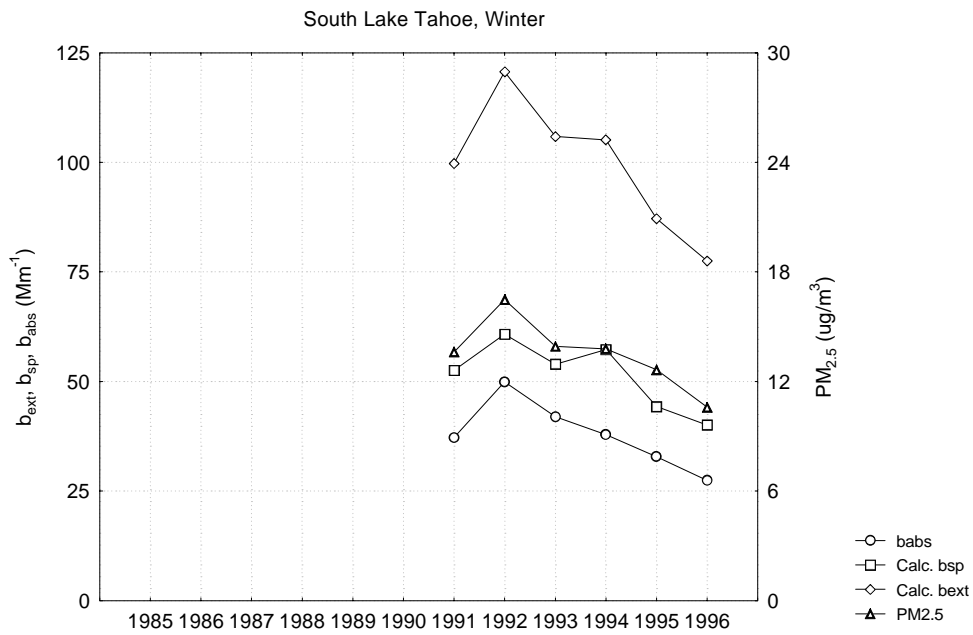


Figure A-11 Average Calculated and Measured Optical Data and PM_{2.5} Mass by Year During Winter at South Lake Tahoe

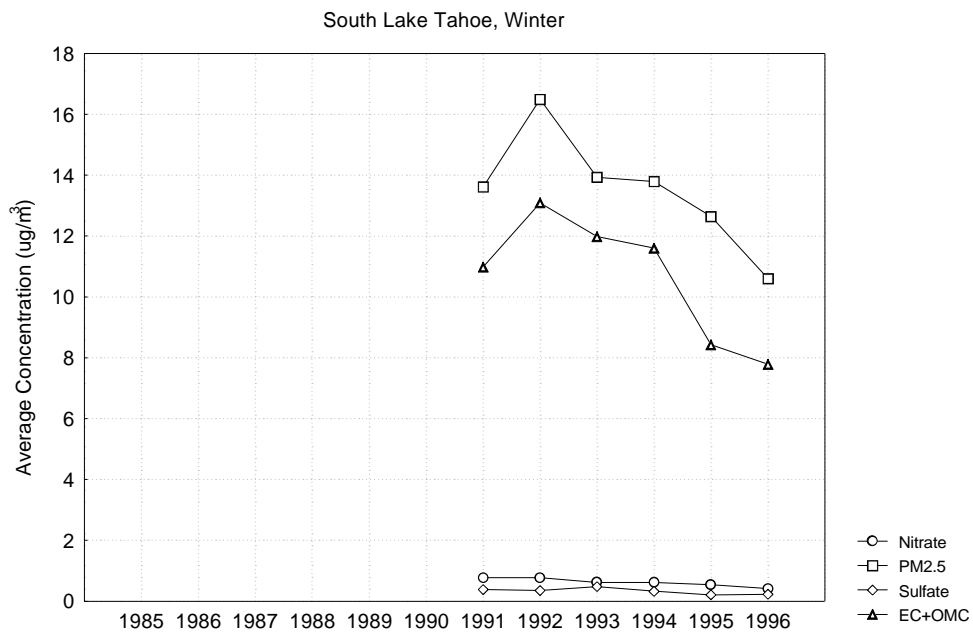


Figure A-12 Average PM_{2.5} Mass, Sulfate and Nitrate by Year During Winter at South Lake Tahoe

A.3 Mountain Counties Air Basin (Yosemite National Park)

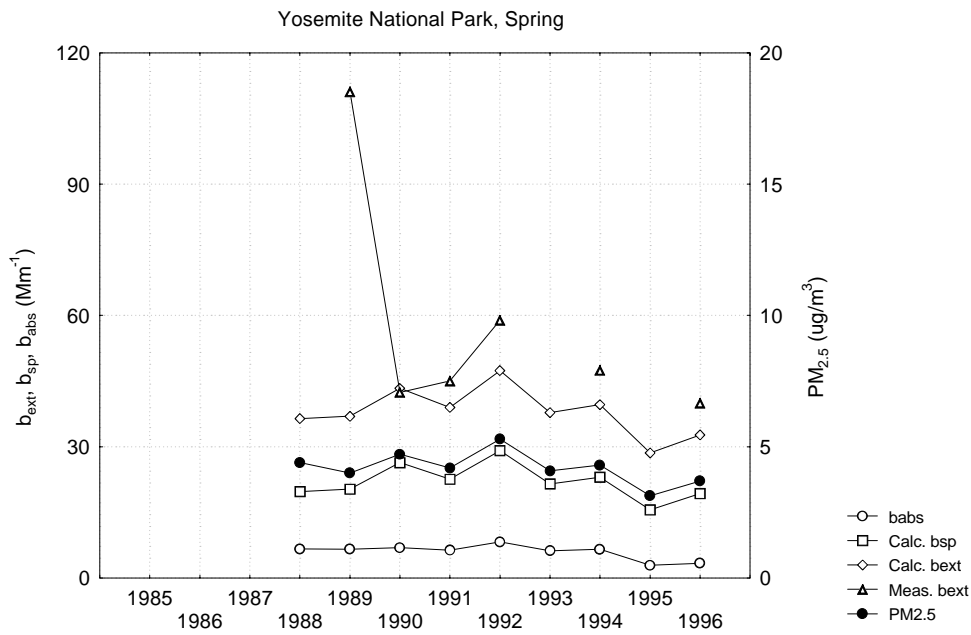


Figure A-13 Average Calculated and Measured Optical Data and PM_{2.5} Mass by Year During Spring at Yosemite National Park

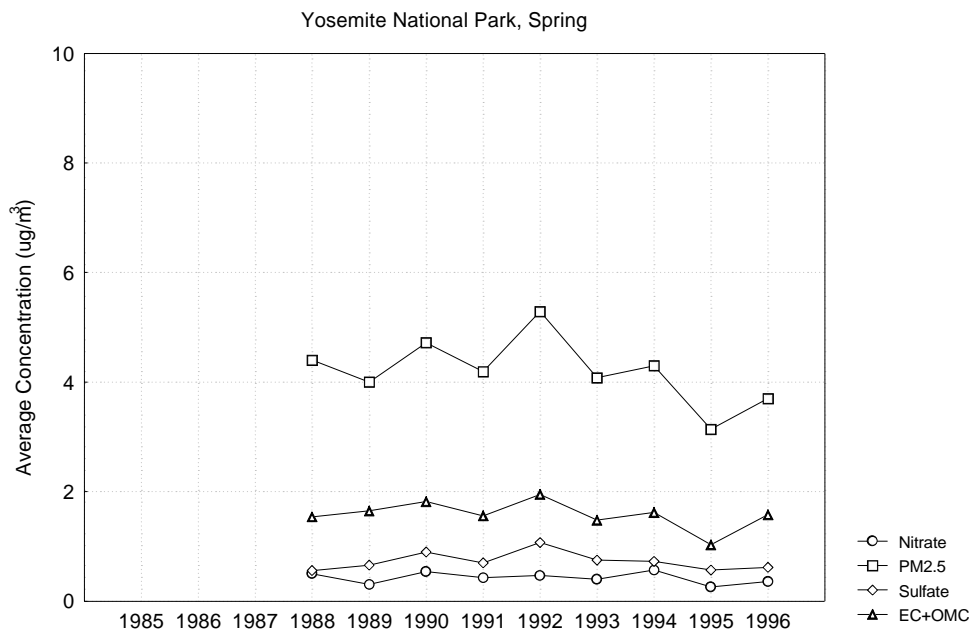


Figure A-14 Average PM_{2.5} Mass, Sulfate and Nitrate by Year During Spring at Yosemite National Park

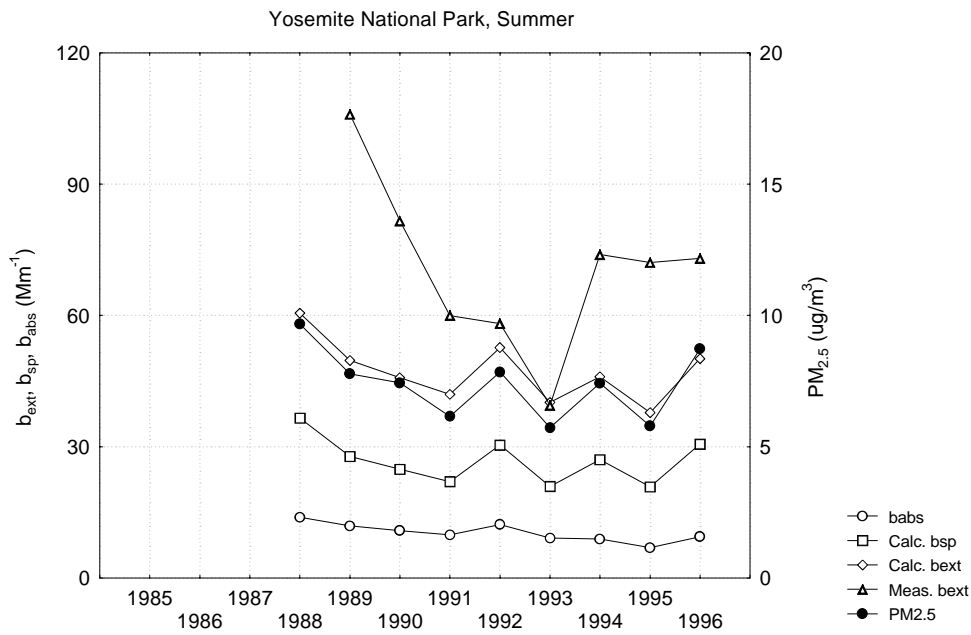


Figure A-15 Average Calculated and Measured Optical Data and PM_{2.5} Mass by Year During Summer at Yosemite National Park

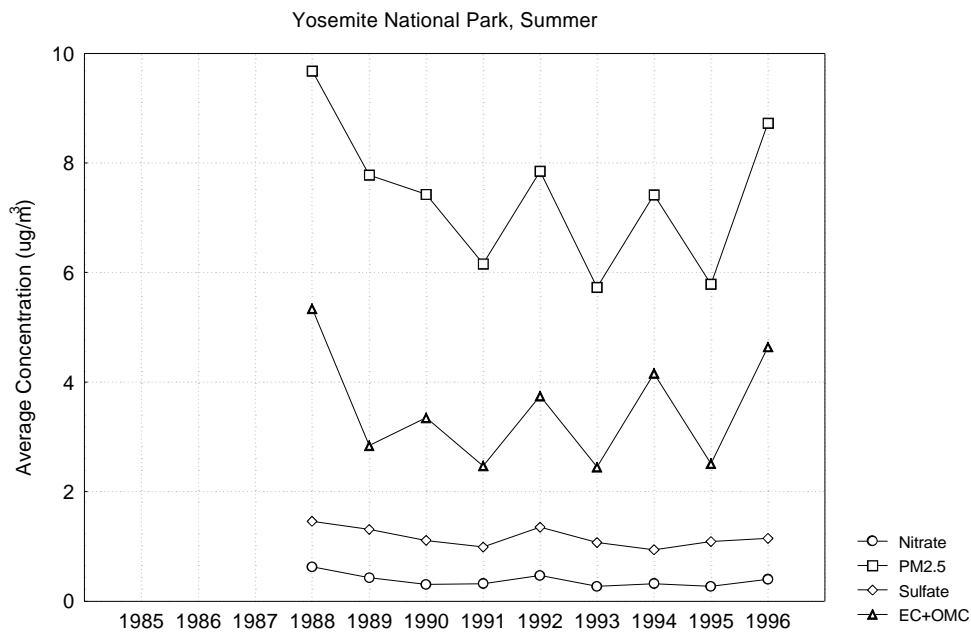


Figure A-16 Average PM_{2.5} Mass, Sulfate and Nitrate by Year During Summer at Yosemite National Park

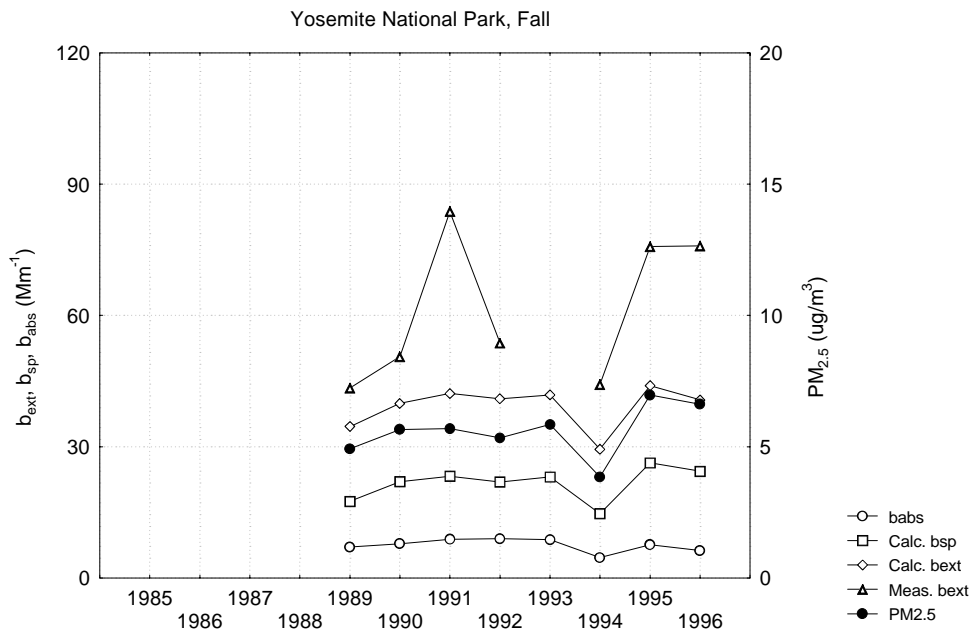


Figure A-17 Average Calculated and Measured Optical Data and PM_{2.5} Mass by Year During Fall at Yosemite National Park

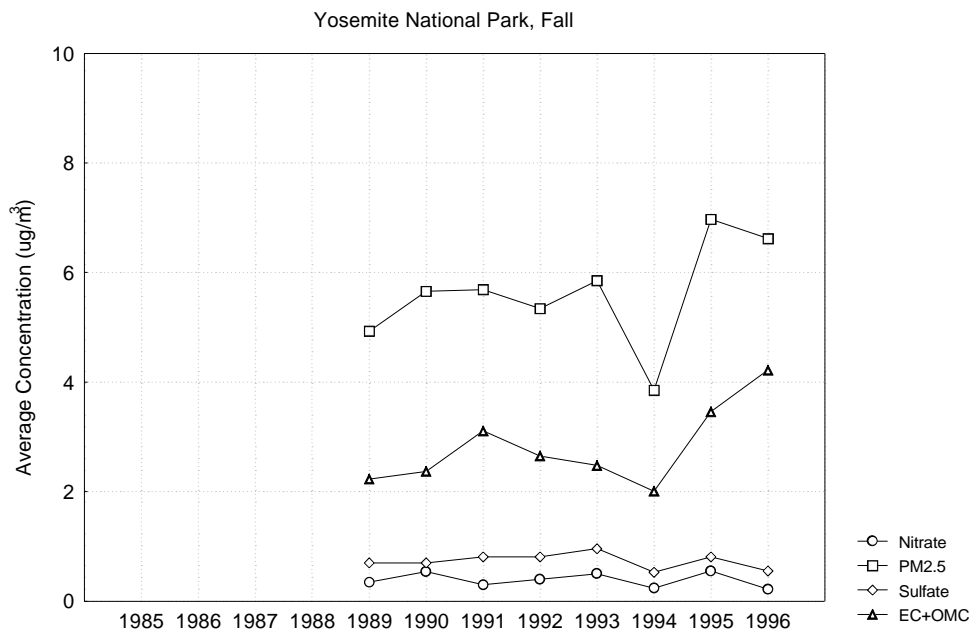


Figure A-18 Average PM_{2.5} Mass, Sulfate and Nitrate by Year During Fall at Yosemite National Park

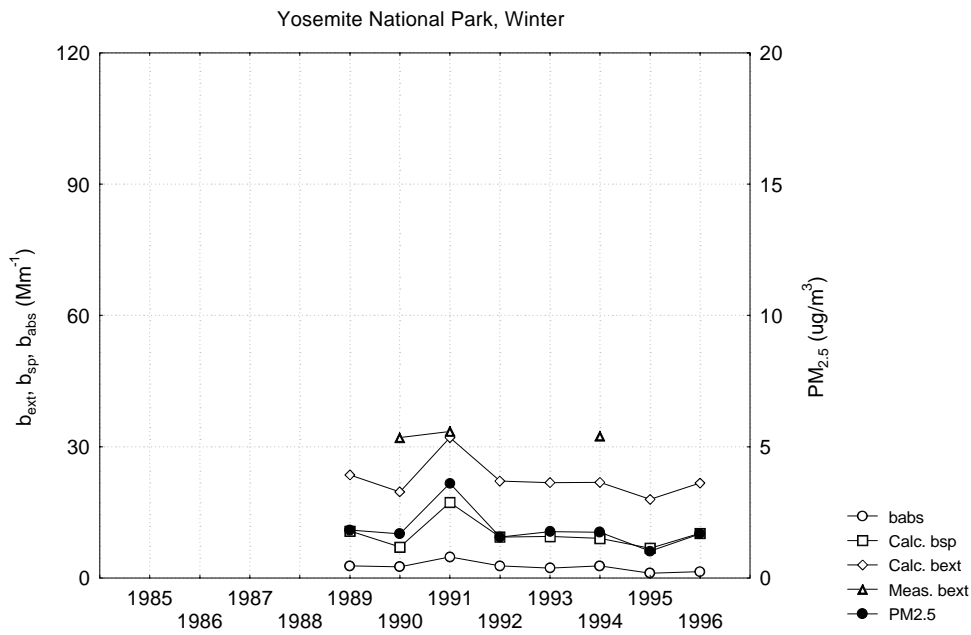


Figure A-19 Average Calculated and Measured Optical Data and PM_{2.5} Mass by Year During Winter at Yosemite National Park

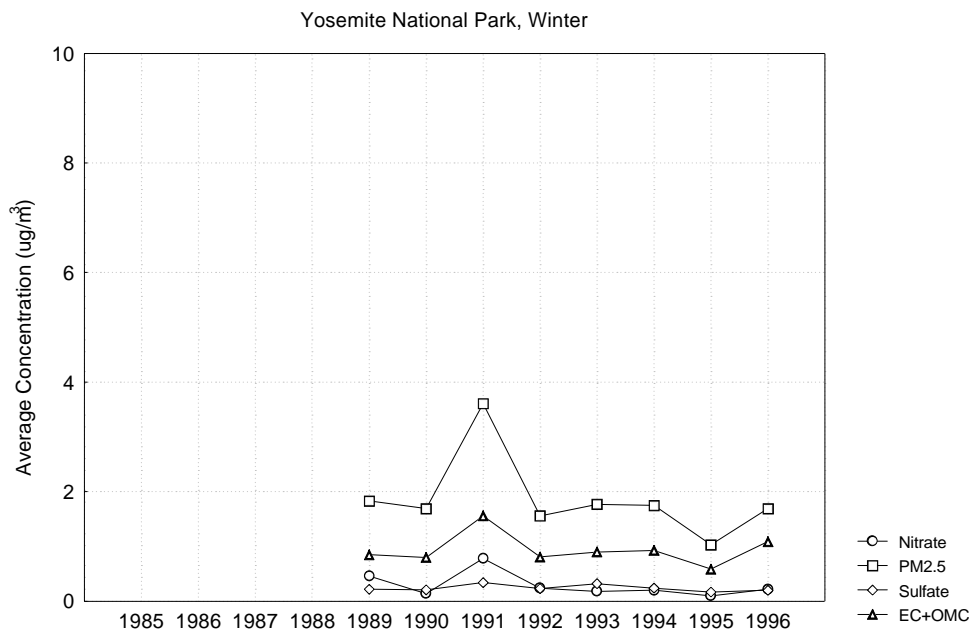


Figure A-20 Average PM_{2.5} Mass, Sulfate and Nitrate by Year During Winter at Yosemite National Park

A.4 North Central Coast Air Basin (Pinnacles National Monument)

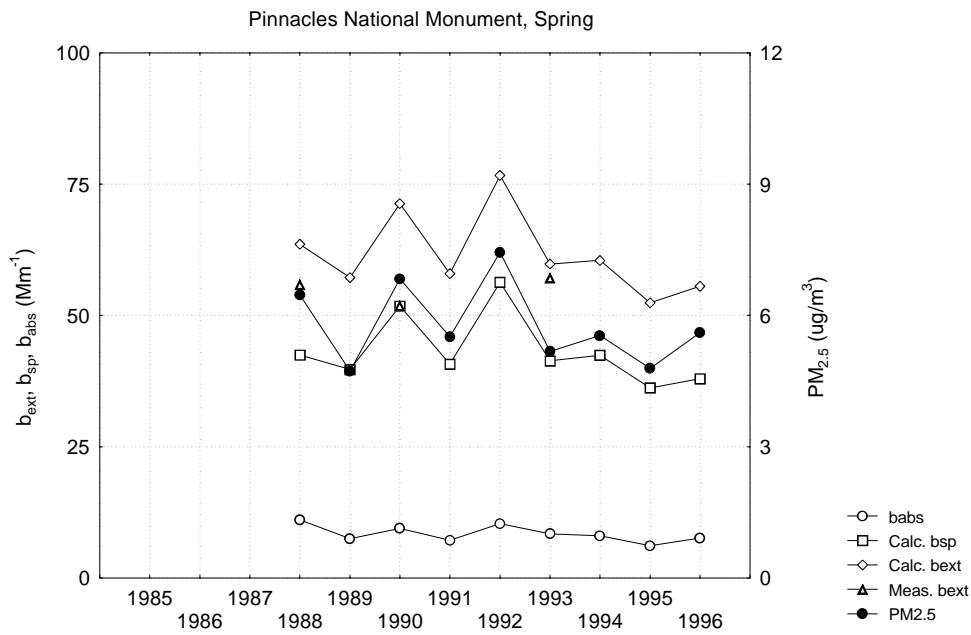


Figure A-21 Average Calculated and Measured Optical Data and PM_{2.5} Mass by Year During Spring at Pinnacles National Monument

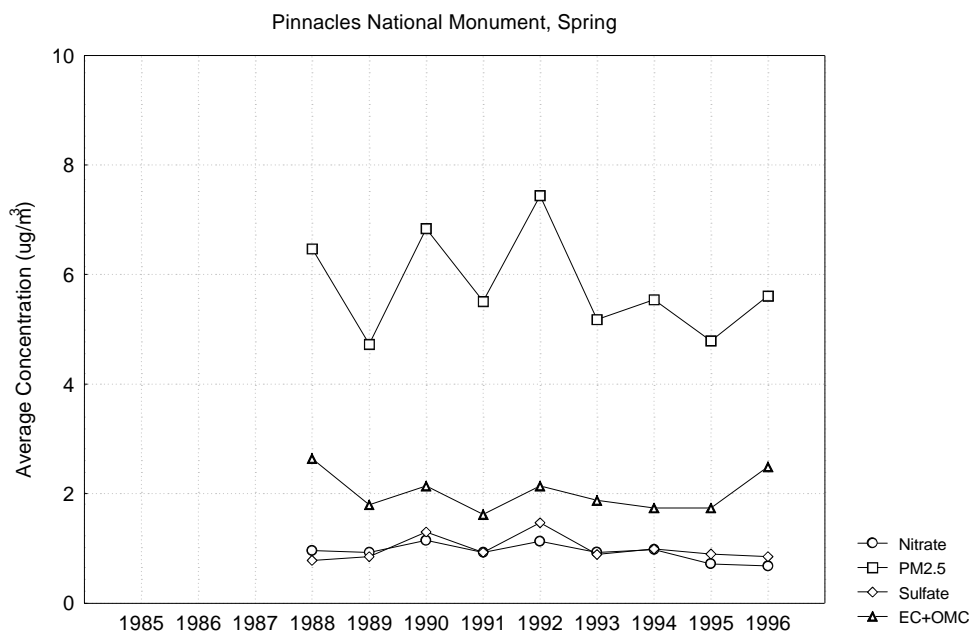


Figure A-22 Average PM_{2.5} Mass, Sulfate and Nitrate by Year During Spring at Pinnacles National Monument

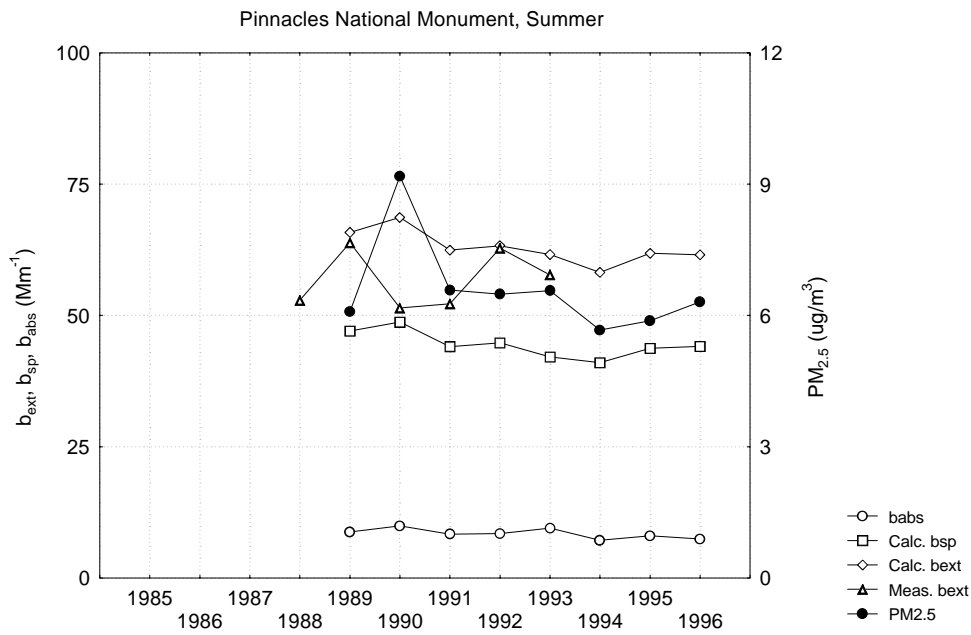


Figure A-23 Average Calculated and Measured Optical Data and PM_{2.5} Mass by Year During Summer at Pinnacles National Monument

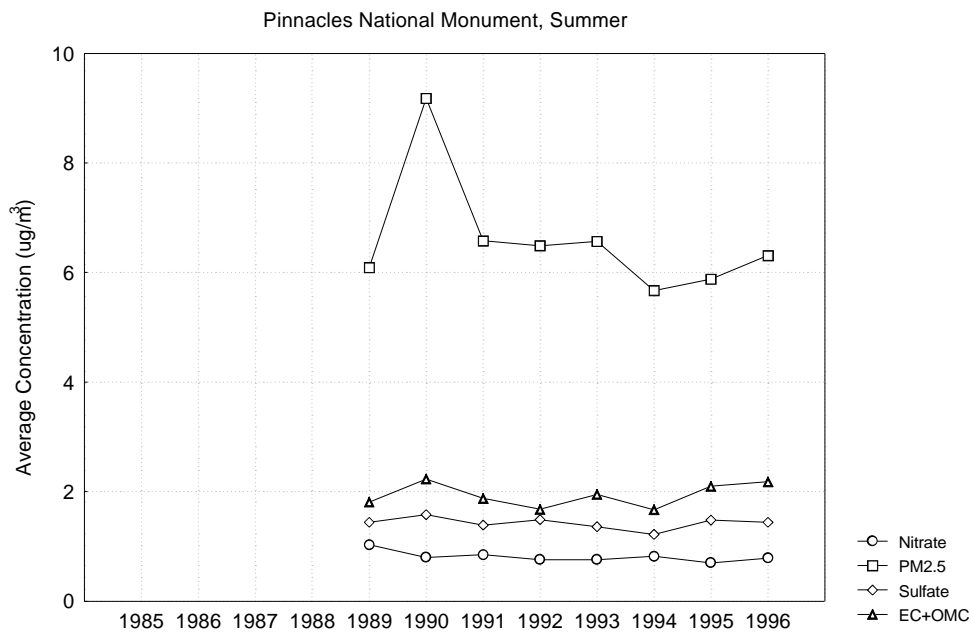


Figure A-24 Average PM_{2.5} Mass, Sulfate and Nitrate by Year During Summer at Pinnacles National Monument

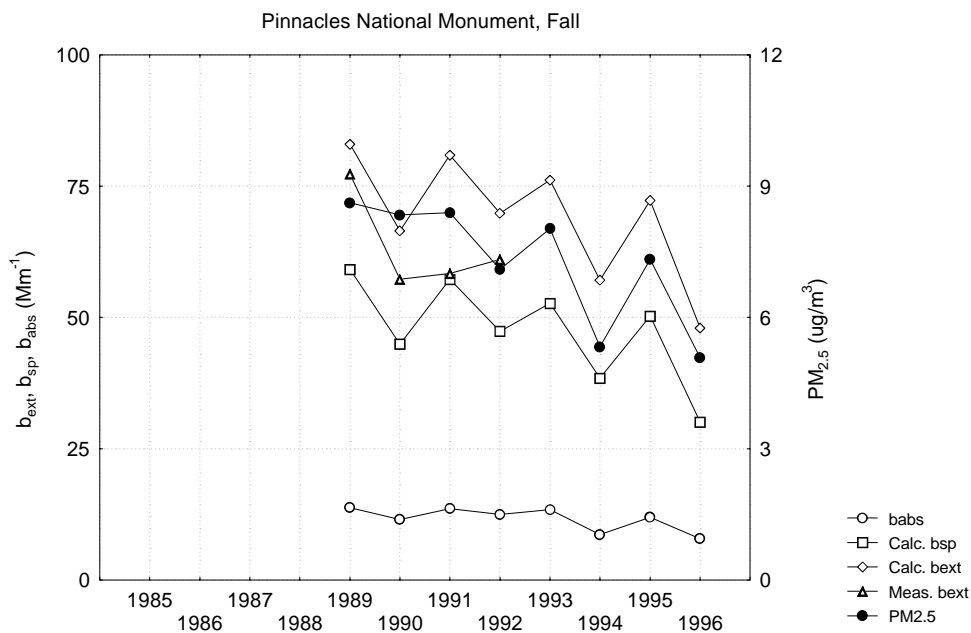


Figure A-25 Average Calculated and Measured Optical Data and PM_{2.5} Mass by Year During Fall at Pinnacles National Monument

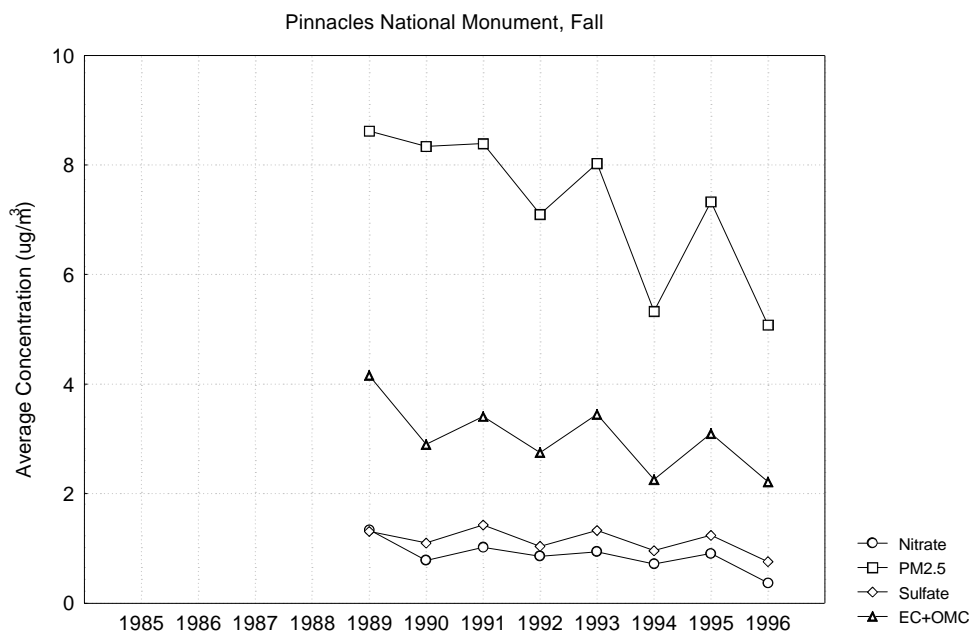


Figure A-26 Average PM_{2.5} Mass, Sulfate and Nitrate by Year During Fall at Pinnacles National Monument

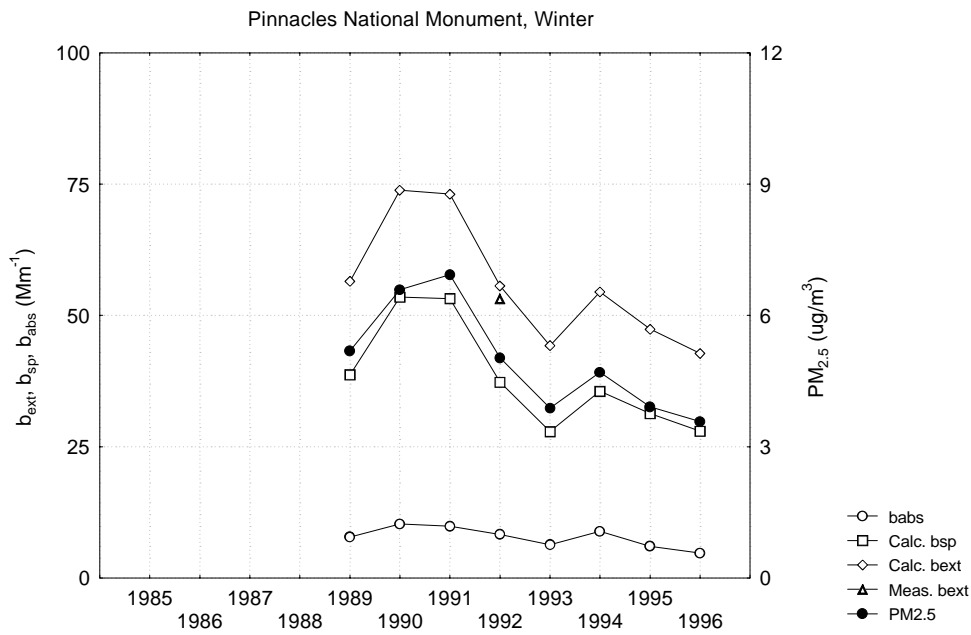


Figure A-27 Average Calculated and Measured Optical Data and PM_{2.5} Mass by Year During Winter at Pinnacles National Monument

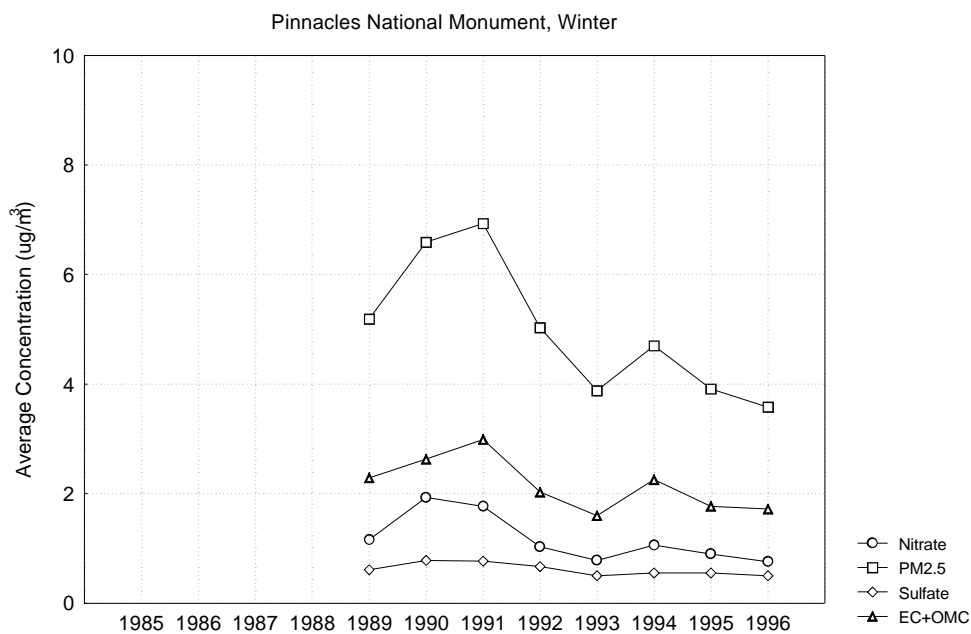


Figure A-28 Average PM_{2.5} Mass, Sulfate and Nitrate by Year During Winter at Pinnacles National Monument

A.5 North Coast Air Basin (Redwood National Park)

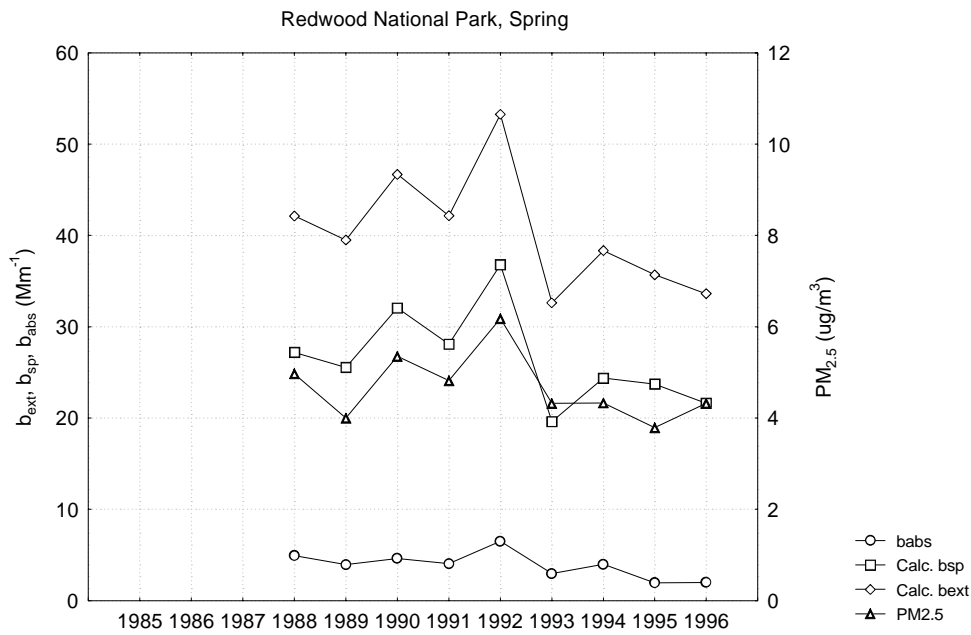


Figure A-29 Average Calculated and Measured Optical Data and PM_{2.5} Mass by Year During Spring at Redwood National Park

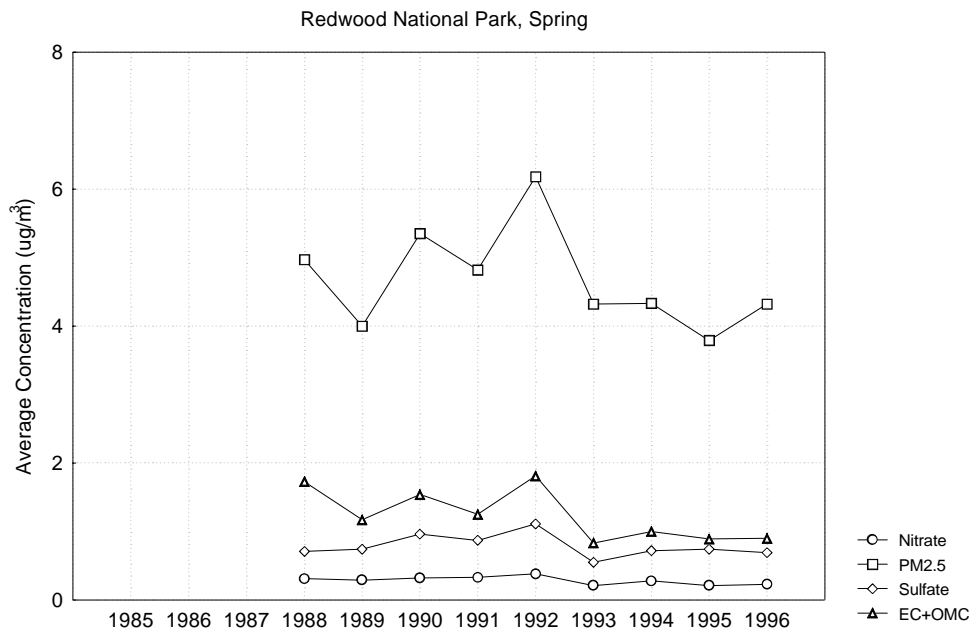


Figure A-30 Average PM_{2.5} Mass, Sulfate and Nitrate by Year During Spring at Redwood National Park

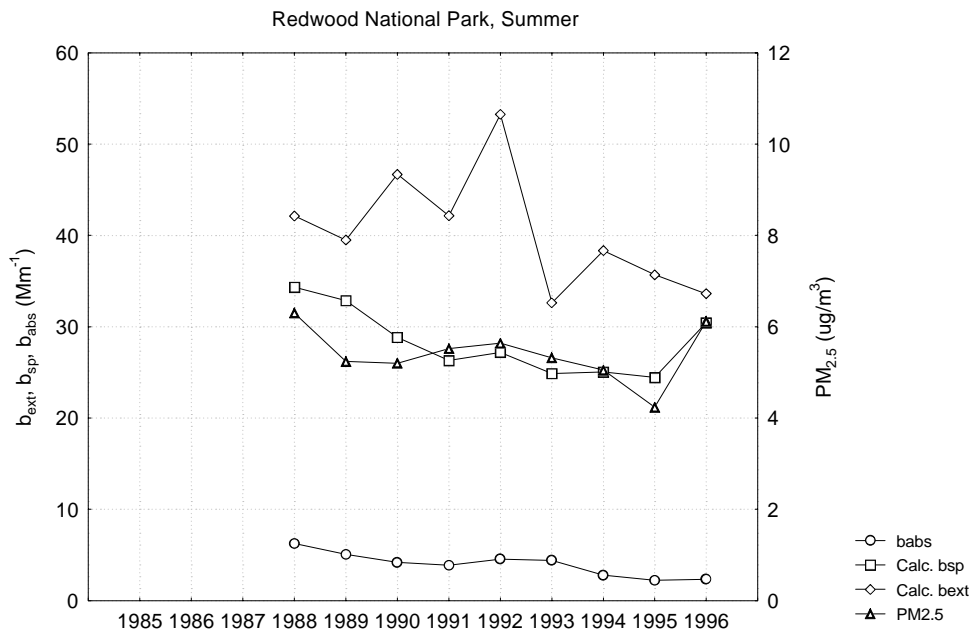


Figure A-31 Average Calculated and Measured Optical Data and PM_{2.5} Mass by Year During Summer at Redwood National Park

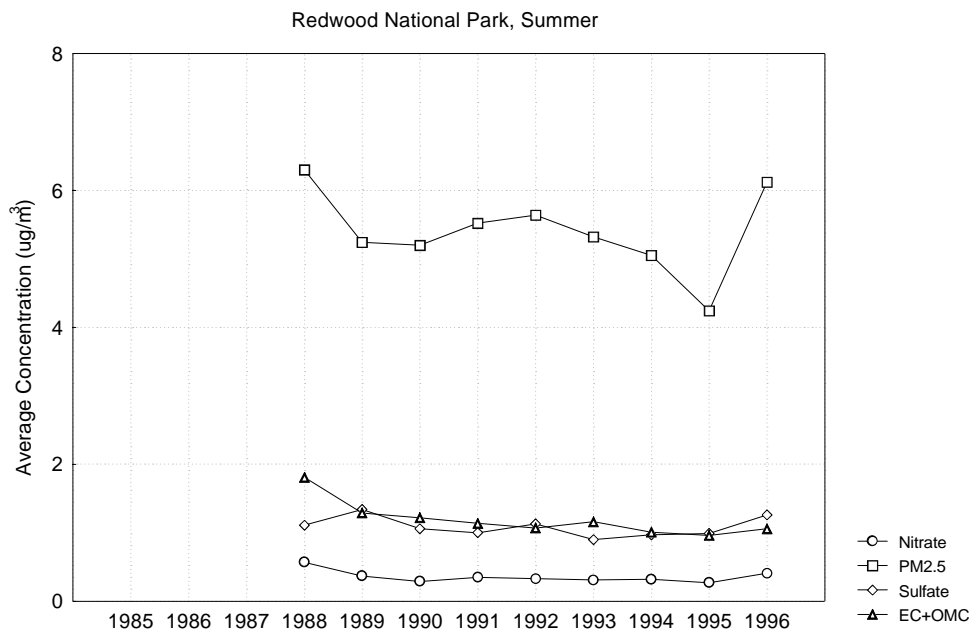


Figure A-32 Average PM_{2.5} Mass, Sulfate and Nitrate by Year During Summer at Redwood National Park

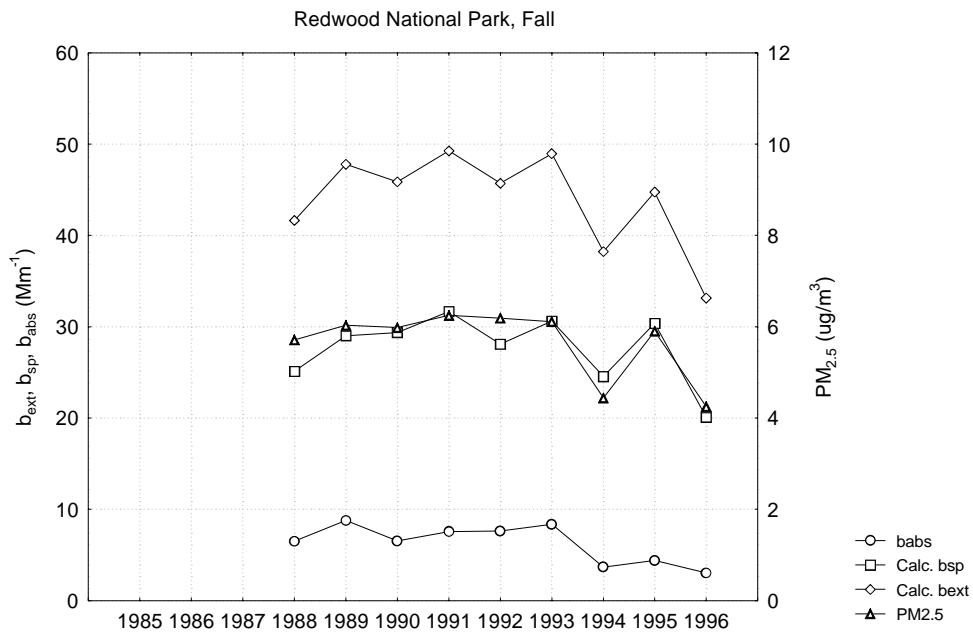


Figure A-33 Average Calculated and Measured Optical Data and PM_{2.5} Mass by Year During Fall at Redwood National Park

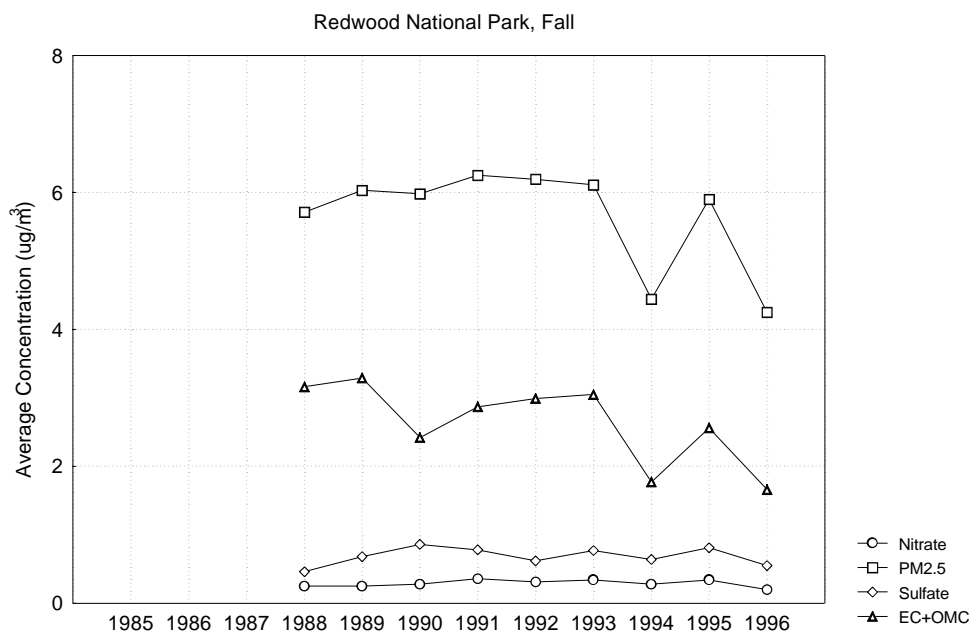


Figure A-34 Average PM_{2.5} Mass, Sulfate and Nitrate by Year During Fall at Redwood National Park

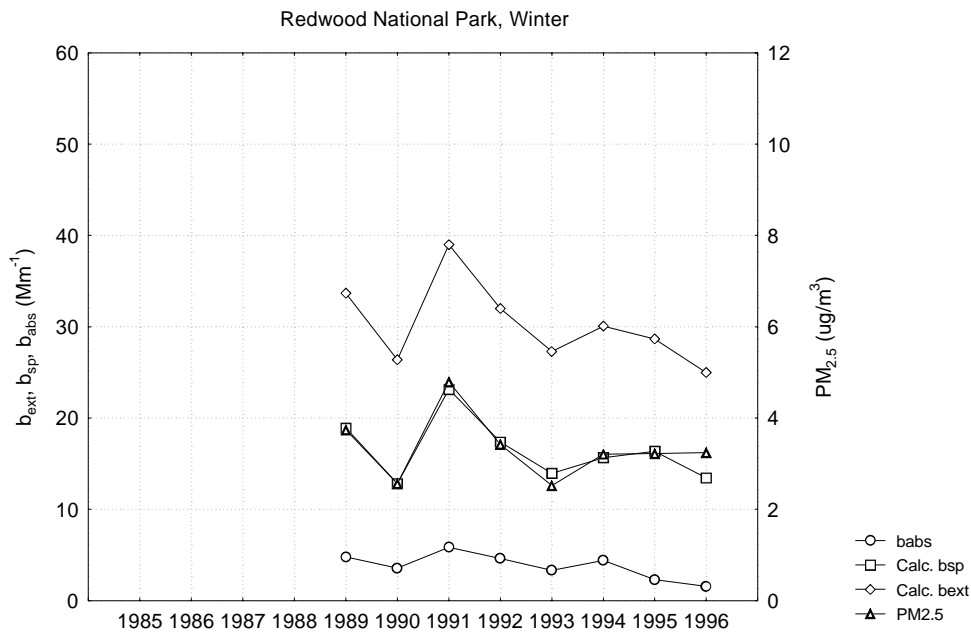


Figure A-35 Average Calculated and Measured Optical Data and PM_{2.5} Mass by Year During Winter at Redwood National Park

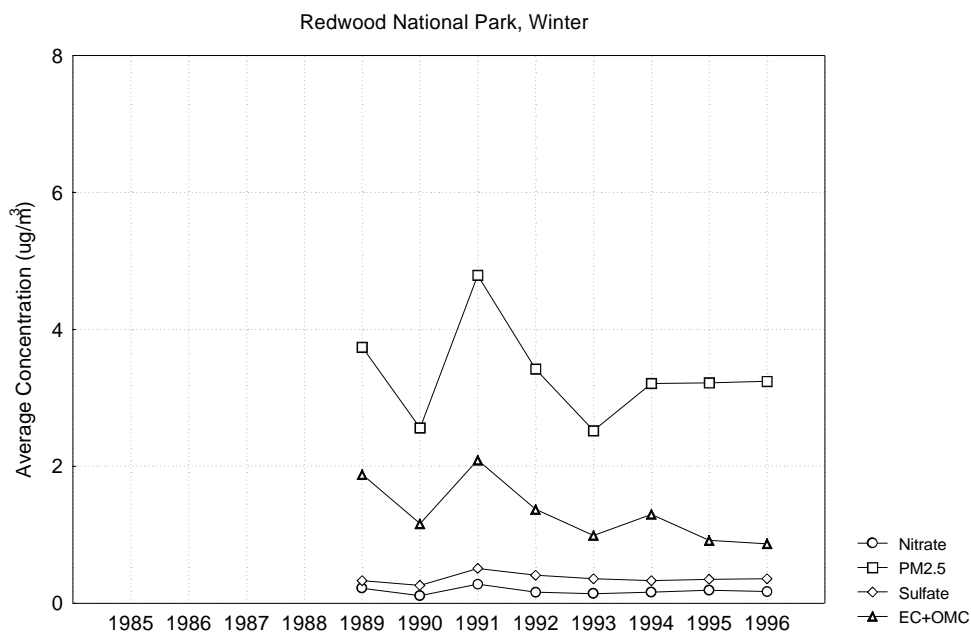


Figure A-36 Average PM_{2.5} Mass, Sulfate and Nitrate by Year During Winter at Redwood National Park

A.6 Northeast Plateau Air Basin (Lassen Volcanic National Park)

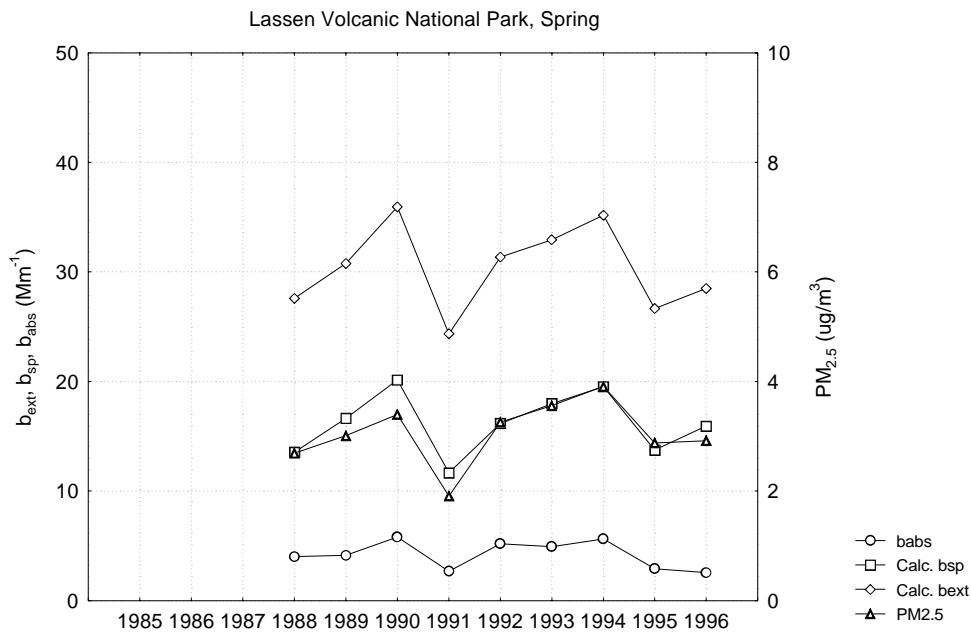


Figure A-37 Average Calculated and Measured Optical Data and PM_{2.5} Mass by Year During Spring at Lassen Volcanic National Park

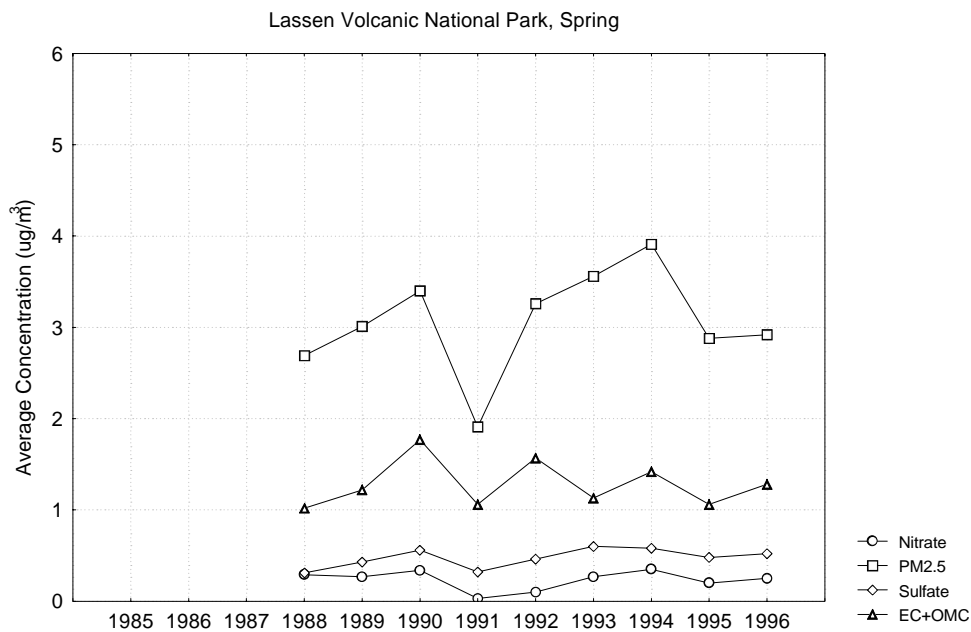


Figure A-38 Average PM_{2.5} Mass, Sulfate and Nitrate by Year During Spring at Lassen Volcanic National Park

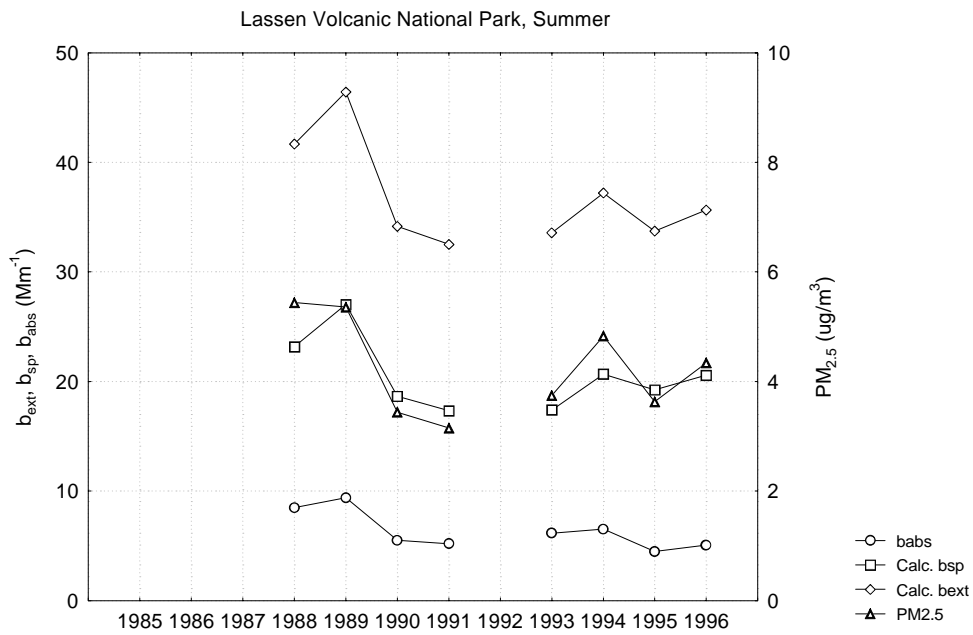


Figure A-39 Average Calculated and Measured Optical Data and PM_{2.5} Mass by Year During Summer at Lassen Volcanic National Park

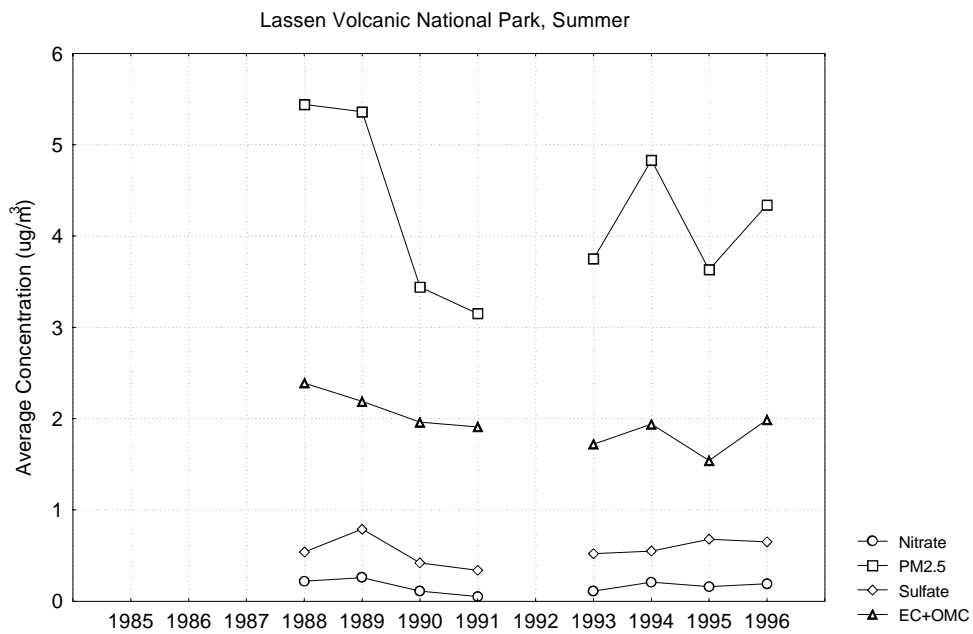


Figure A-40 Average PM_{2.5} Mass, Sulfate and Nitrate by Year During Summer at Lassen Volcanic National Park

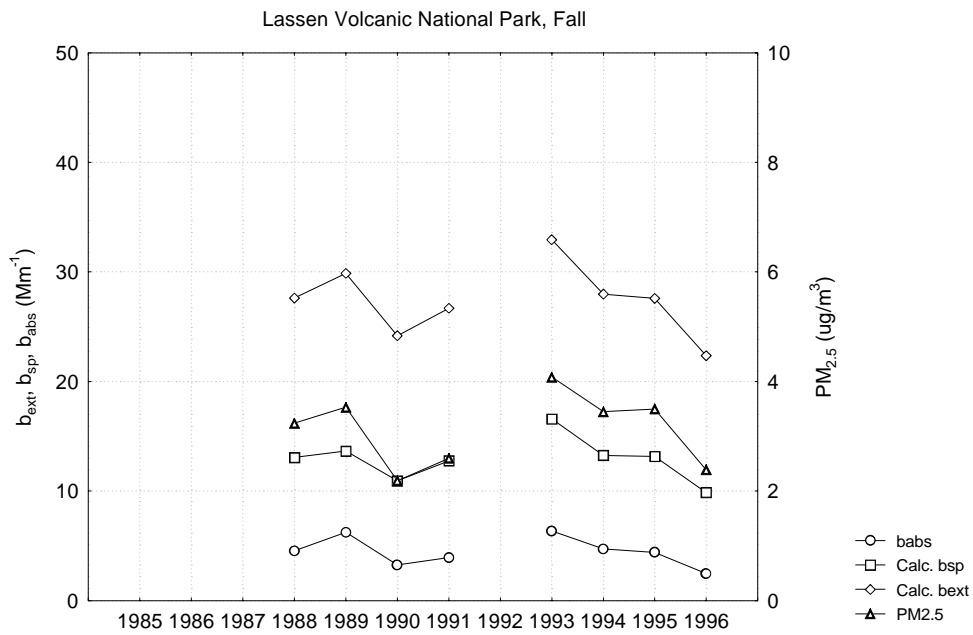


Figure A-41 Average Calculated and Measured Optical Data and PM_{2.5} Mass by Year During Fall at Lassen Volcanic National Park

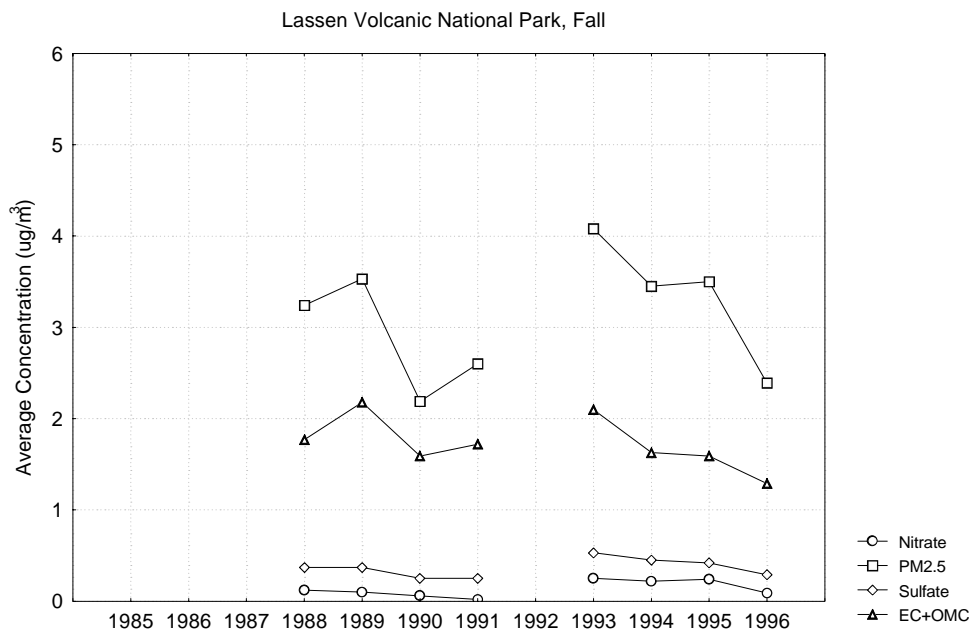


Figure A-42 Average PM_{2.5} Mass, Sulfate and Nitrate by Year During Fall at Lassen Volcanic National Park

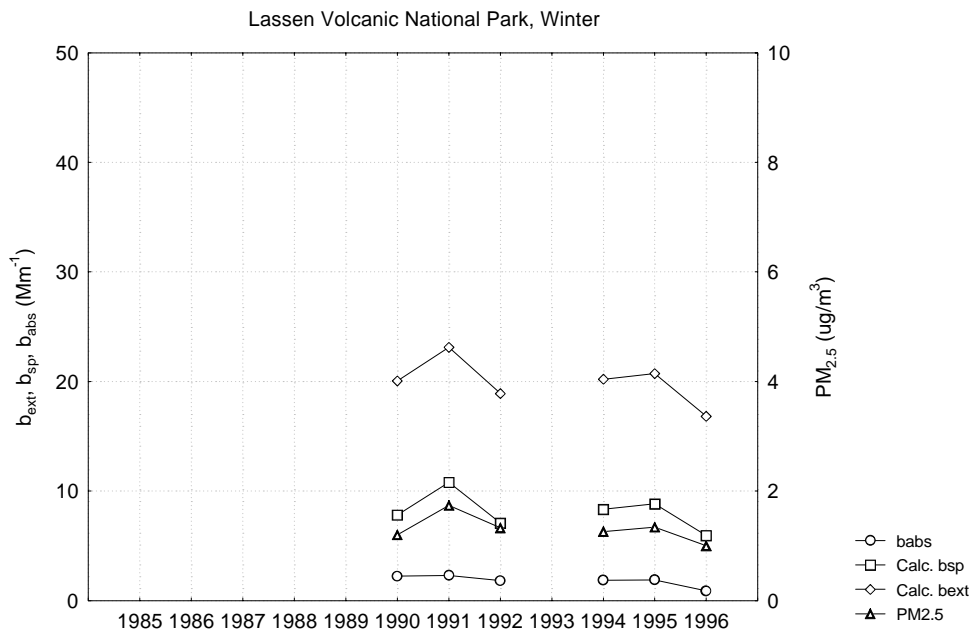


Figure A-43 Average Calculated and Measured Optical Data and PM_{2.5} Mass by Year During Winter at Lassen Volcanic National Park

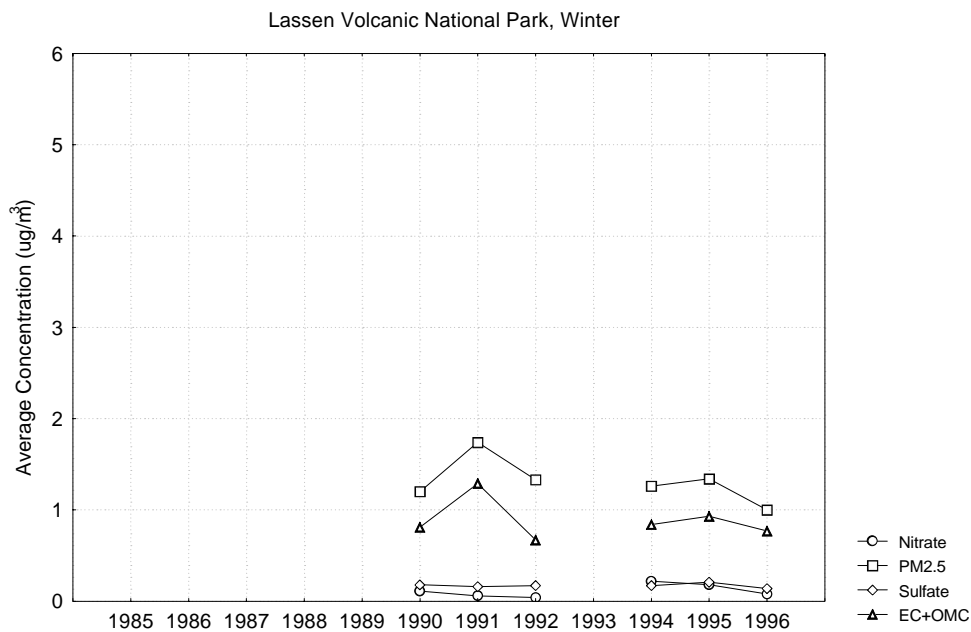


Figure A-44 Average PM_{2.5} Mass, Sulfate and Nitrate by Year During Winter at Lassen Volcanic National Park

A.7 Sacramento Valley Air Basin (Arbuckle, Chico, Colusa, Gridley, Pleasant Grove and Yuba City)

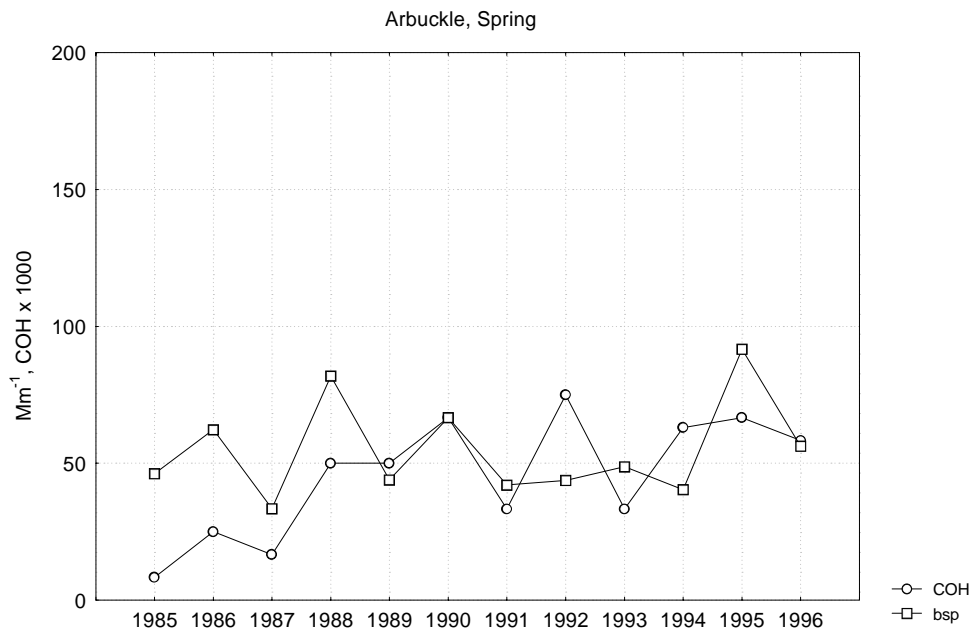


Figure A-45 Median Light Scattering Coefficient and Coefficient of Haze by Year During Spring at Arbuckle

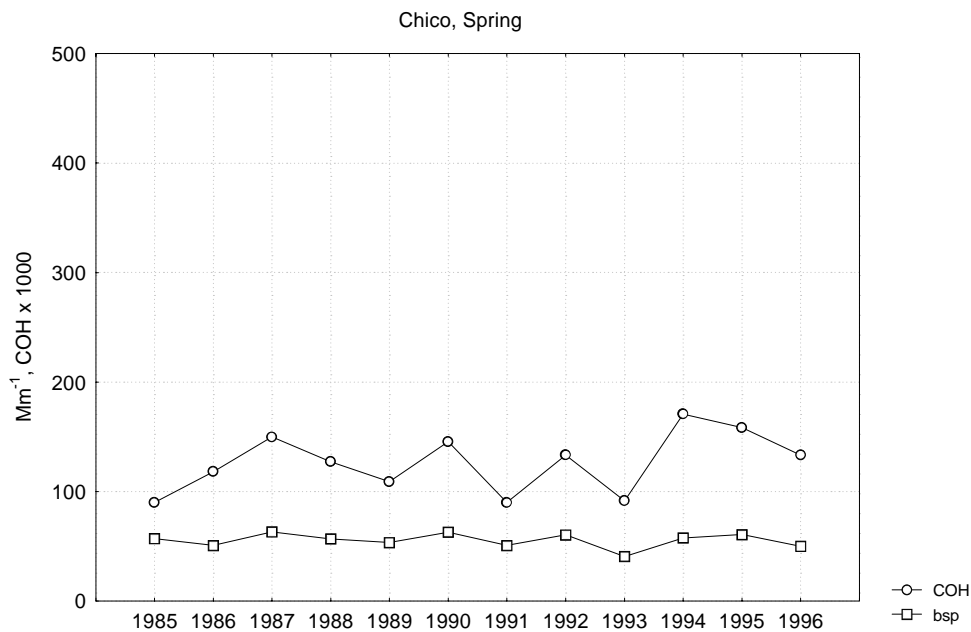


Figure A-46 Median Light Scattering Coefficient and Coefficient of Haze by Year During Spring at Chico

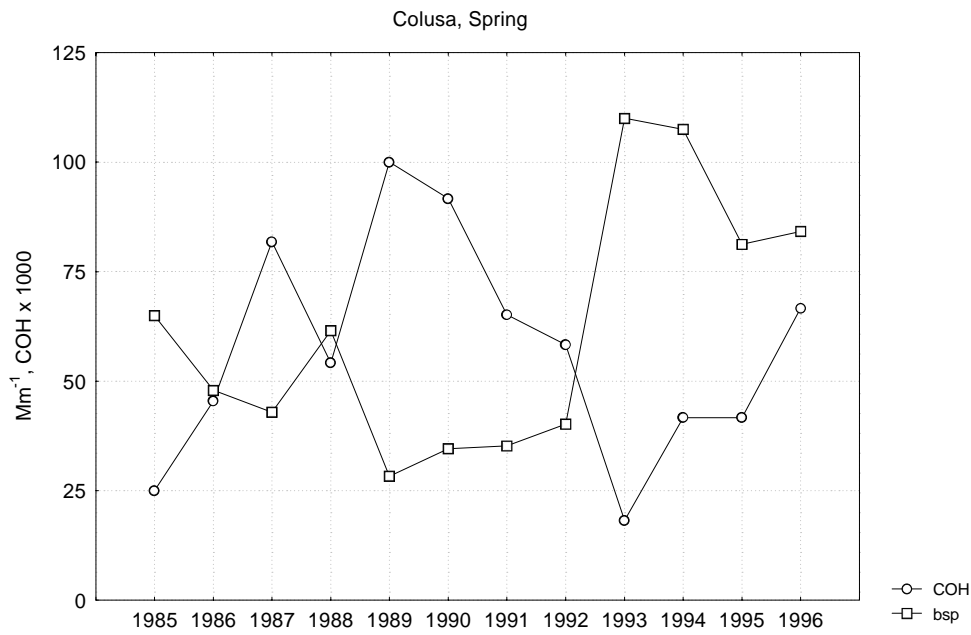


Figure A-47 Median Light Scattering Coefficient and Coefficient of Haze by Year During Spring at Colusa

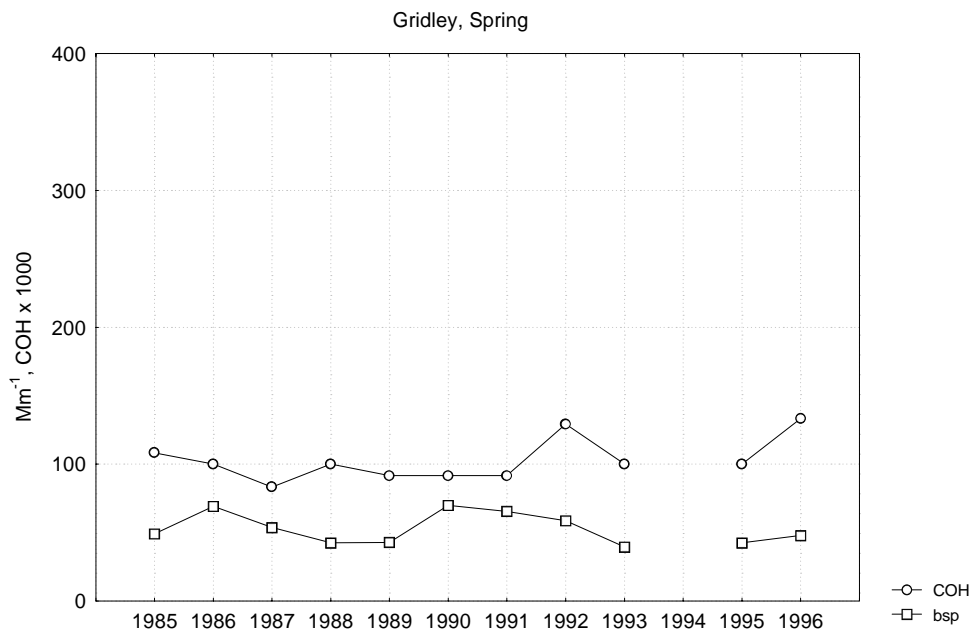


Figure A-48 Median Light Scattering Coefficient and Coefficient of Haze by Year During Spring at Gridley

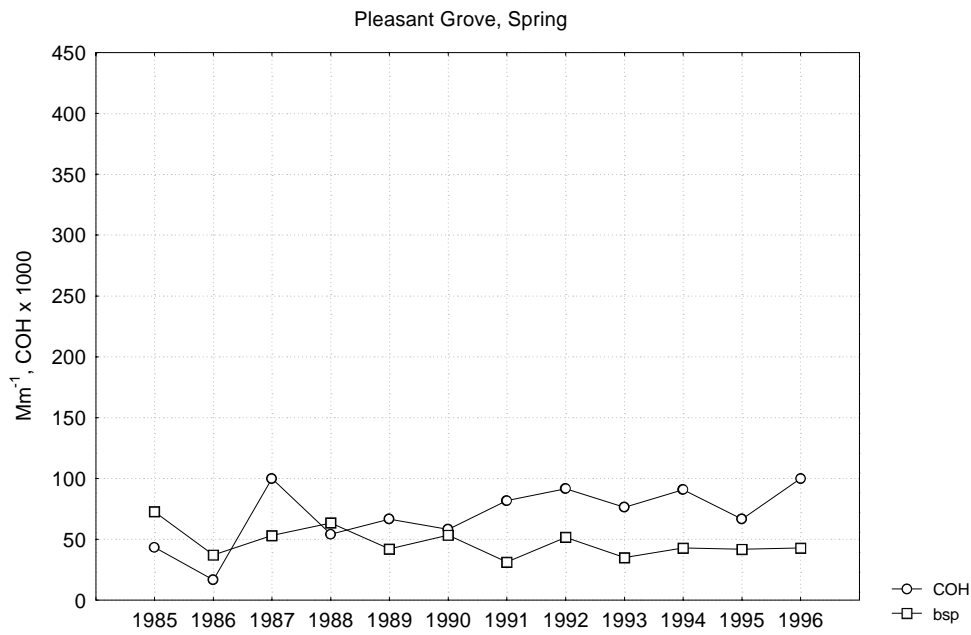


Figure A-49 Median Light Scattering Coefficient and Coefficient of Haze by Year During Spring at Pleasant Grove

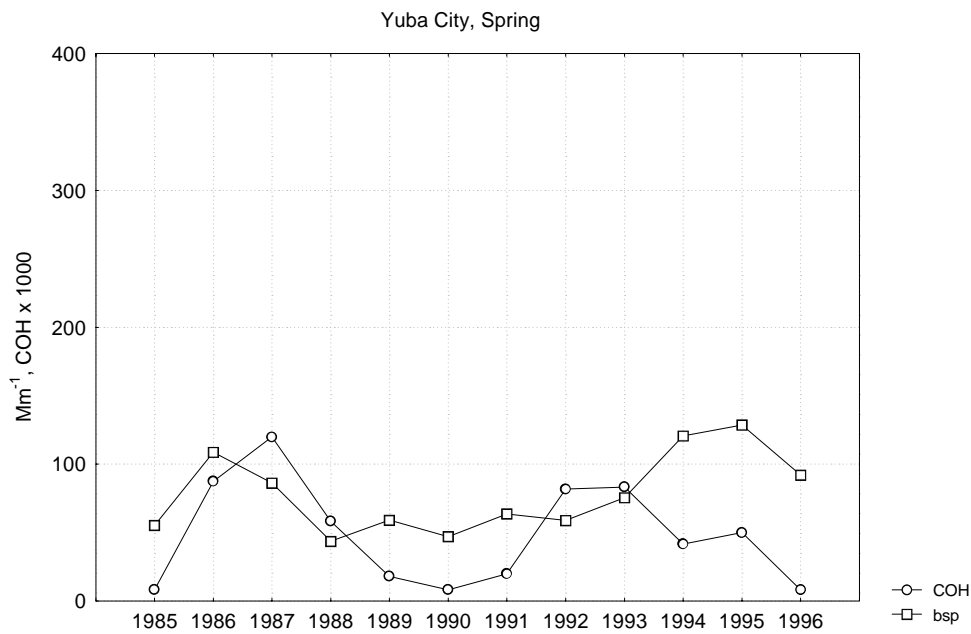


Figure A-50 Median Light Scattering Coefficient and Coefficient of Haze by Year During Spring at Yuba City

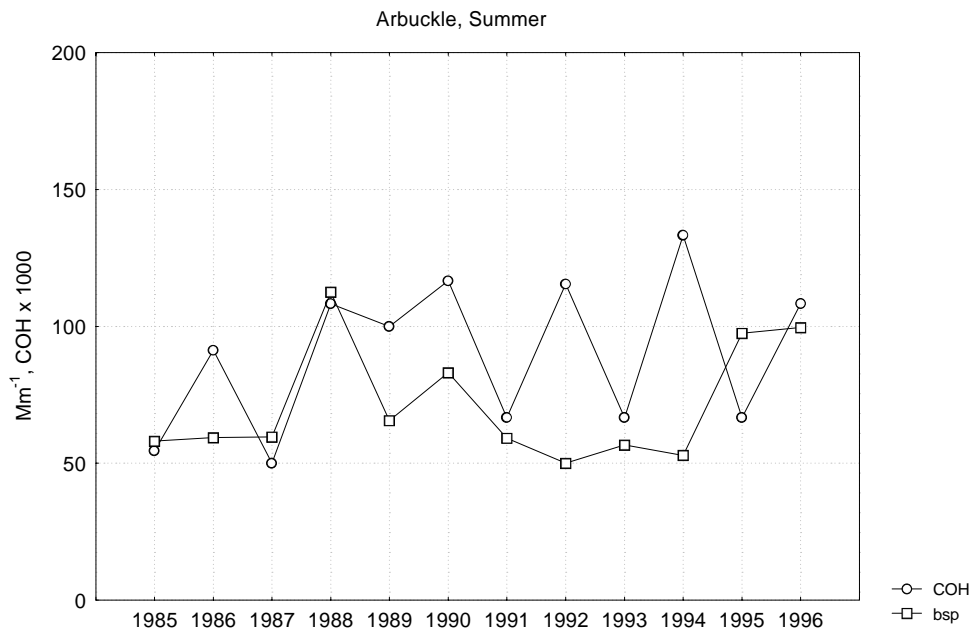


Figure A-51 Median Light Scattering Coefficient and Coefficient of Haze by Year During Summer at Arbuckle

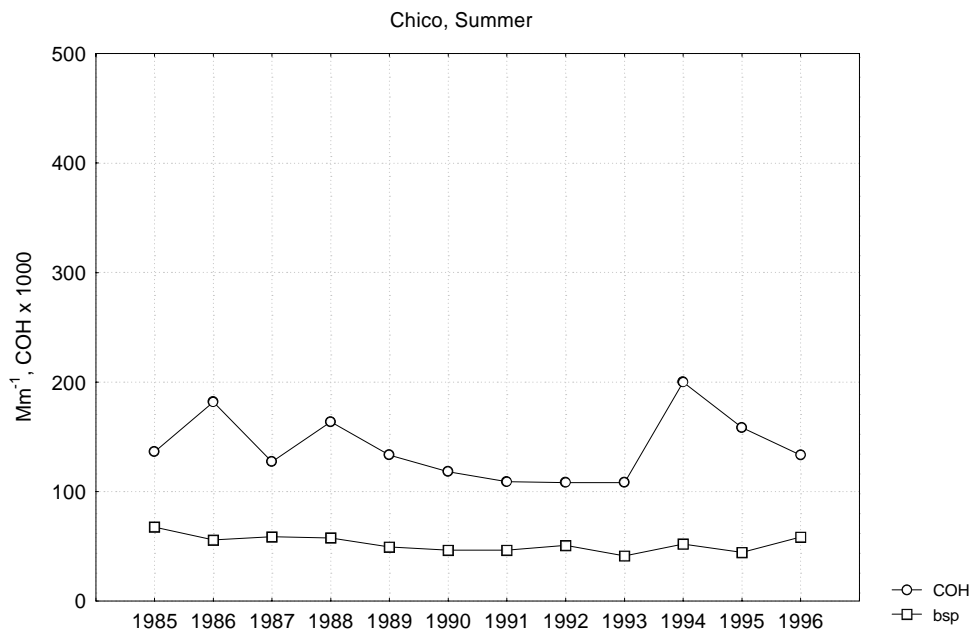


Figure A-52 Median Light Scattering Coefficient and Coefficient of Haze by Year During Summer at Chico

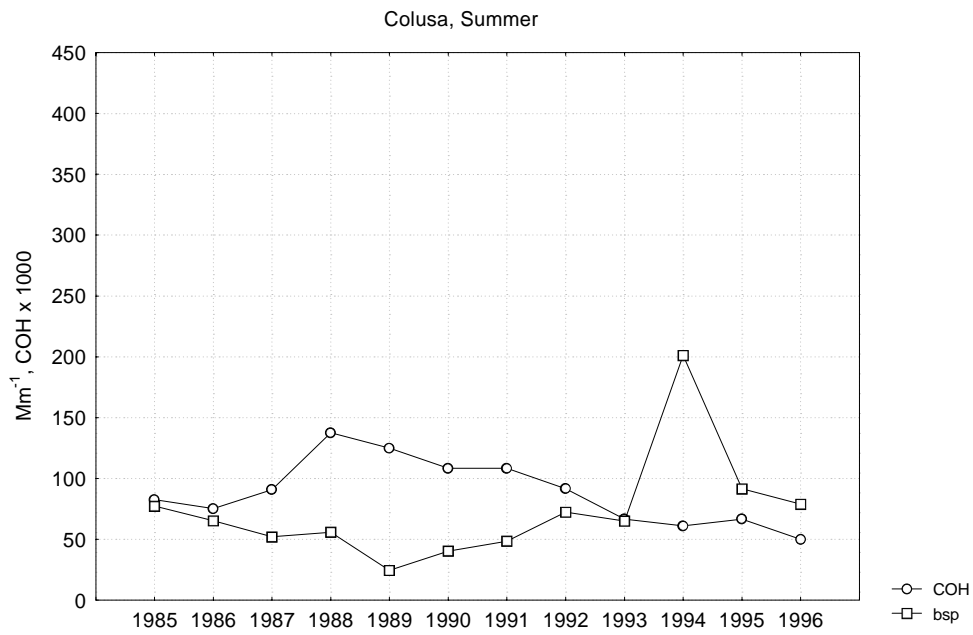


Figure A-53 Median Light Scattering Coefficient and Coefficient of Haze by Year During Summer at Colusa

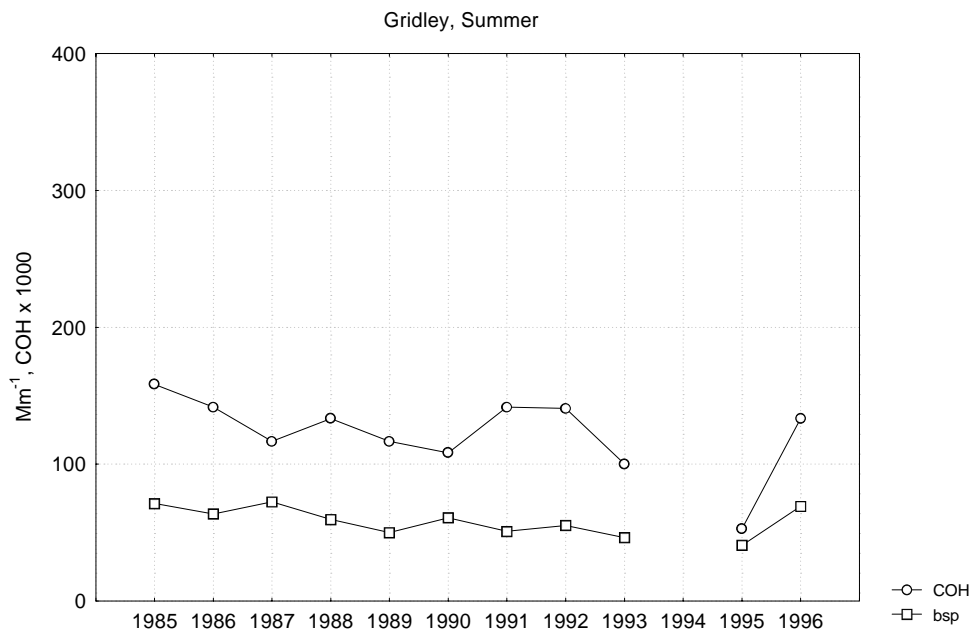


Figure A-54 Median Light Scattering Coefficient and Coefficient of Haze by Year During Summer at Gridley

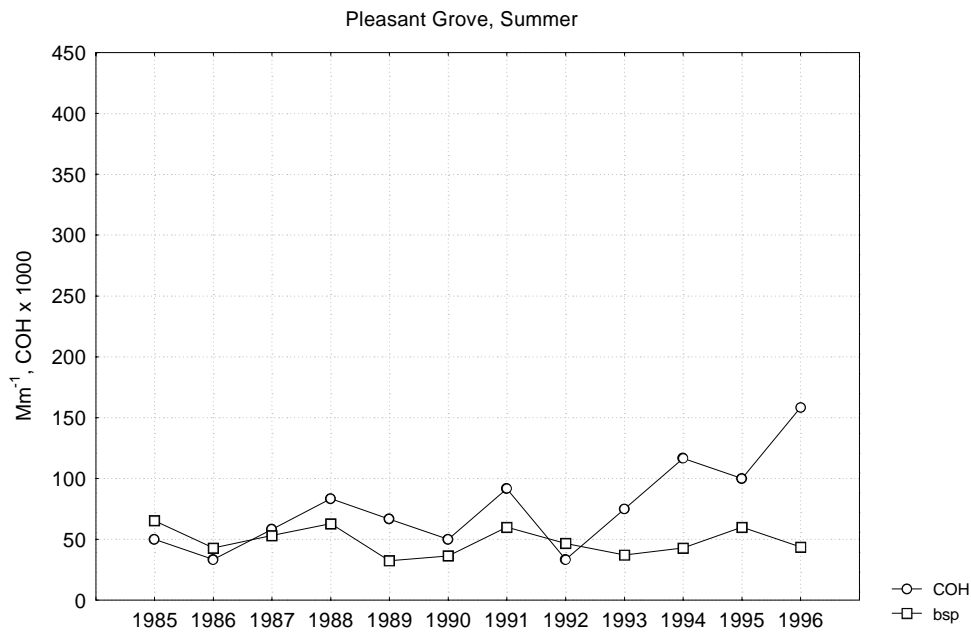


Figure A-55 Median Light Scattering Coefficient and Coefficient of Haze by Year During Summer at Pleasant Grove

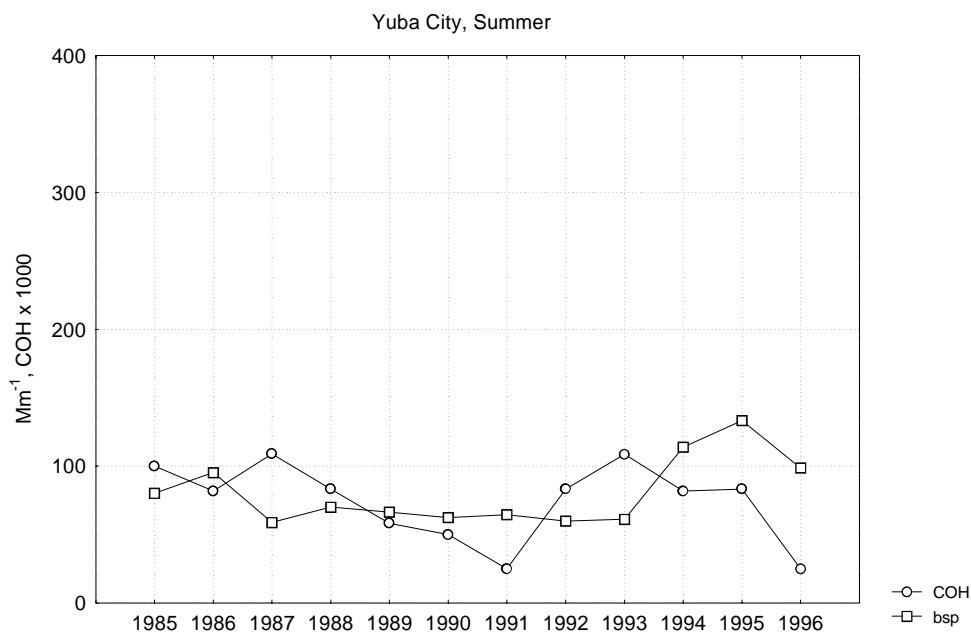


Figure A-56 Median Light Scattering Coefficient and Coefficient of Haze by Year During Summer at Yuba City

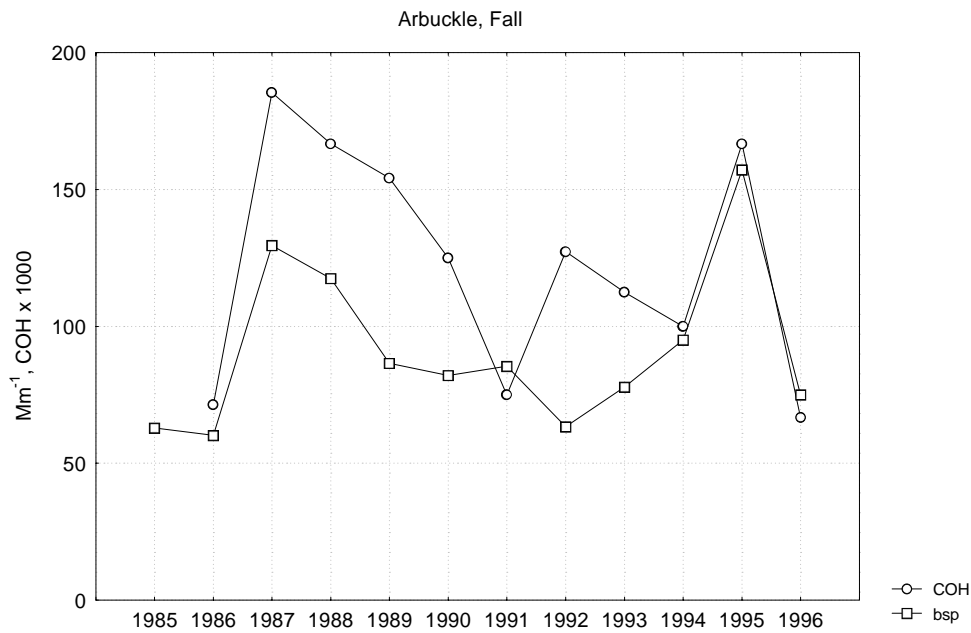


Figure A-57 Median Light Scattering Coefficient and Coefficient of Haze by Year During Fall at Arbuckle

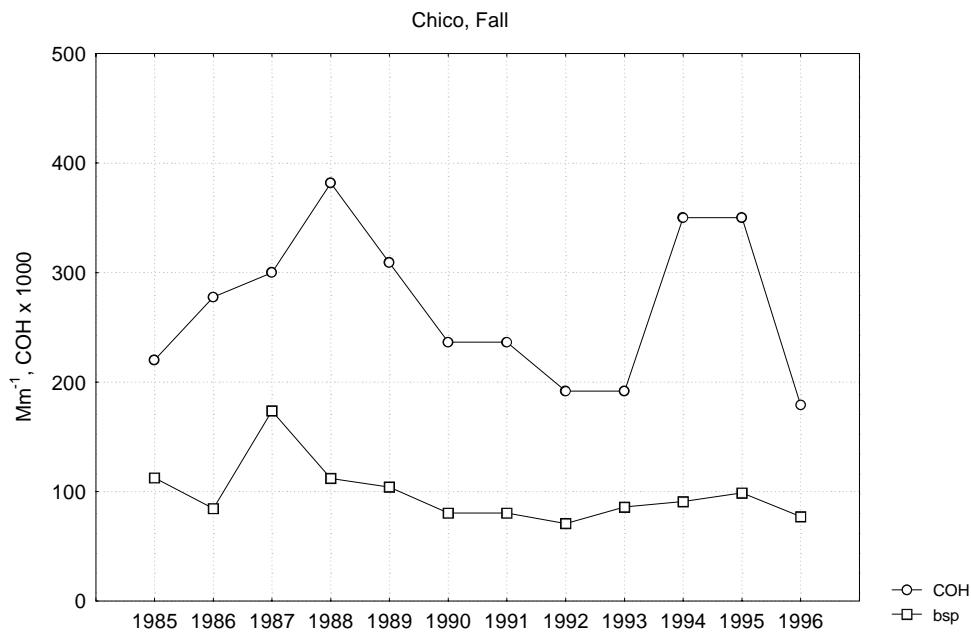


Figure A-58 Median Light Scattering Coefficient and Coefficient of Haze by Year During Fall at Chico

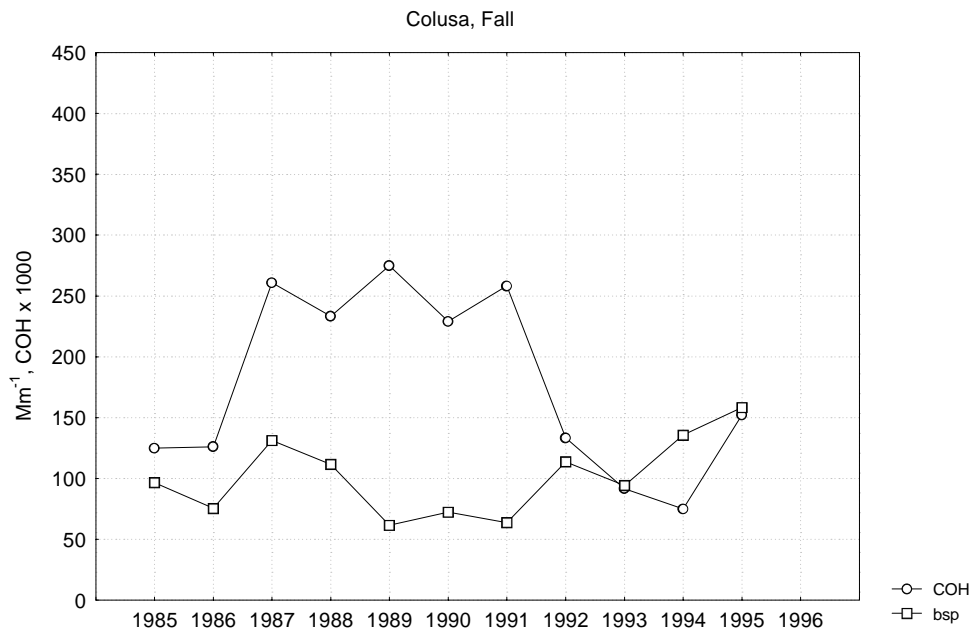


Figure A-59 Median Light Scattering Coefficient and Coefficient of Haze by Year During Fall at Colusa

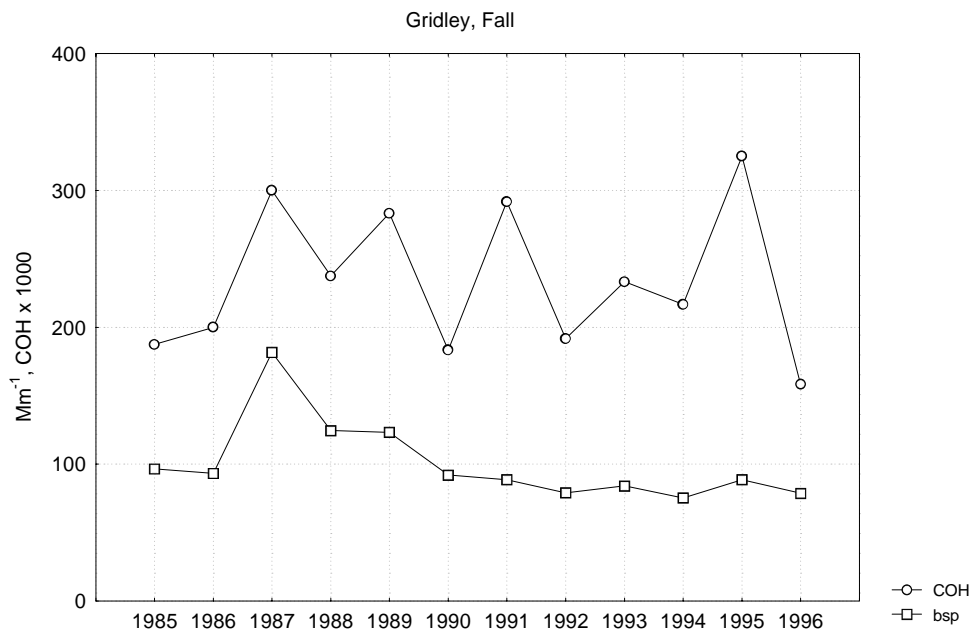


Figure A-60 Median Light Scattering Coefficient and Coefficient of Haze by Year During Fall at Gridley

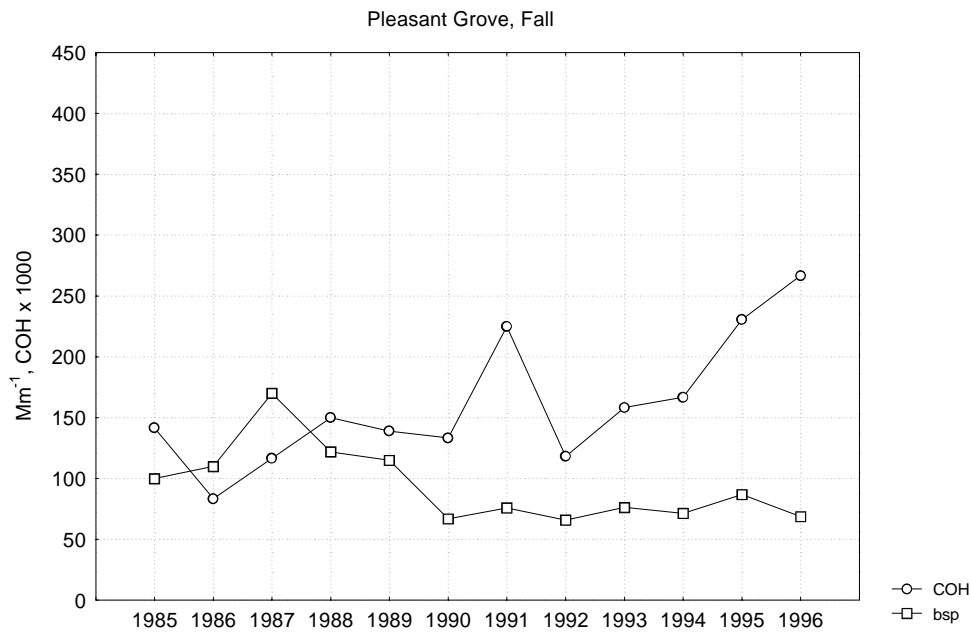


Figure A-61 Median Light Scattering Coefficient and Coefficient of Haze by Year During Fall at Pleasant Grove

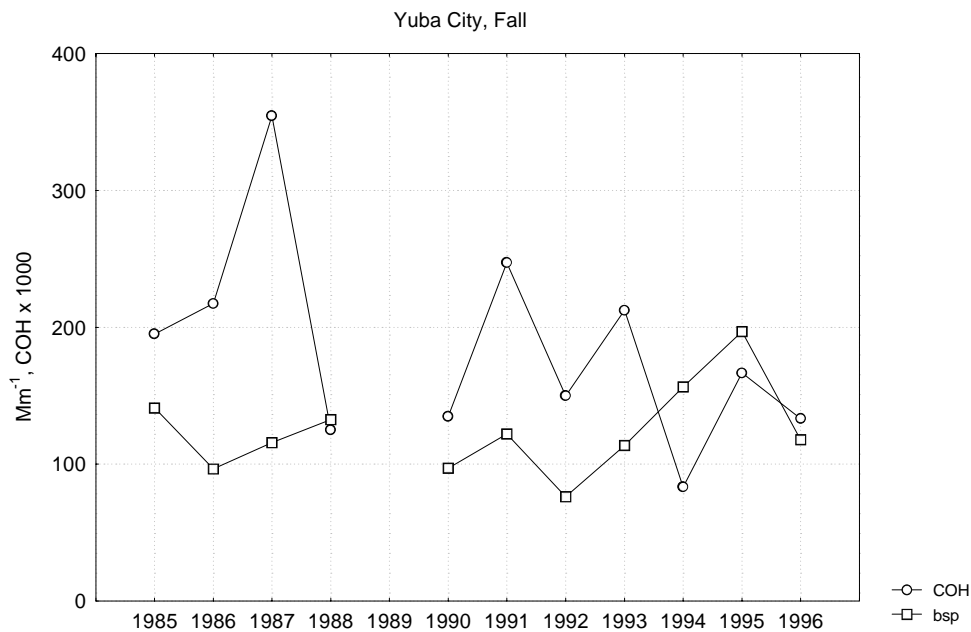


Figure A-62 Median Light Scattering Coefficient and Coefficient of Haze by Year During Fall at Yuba City

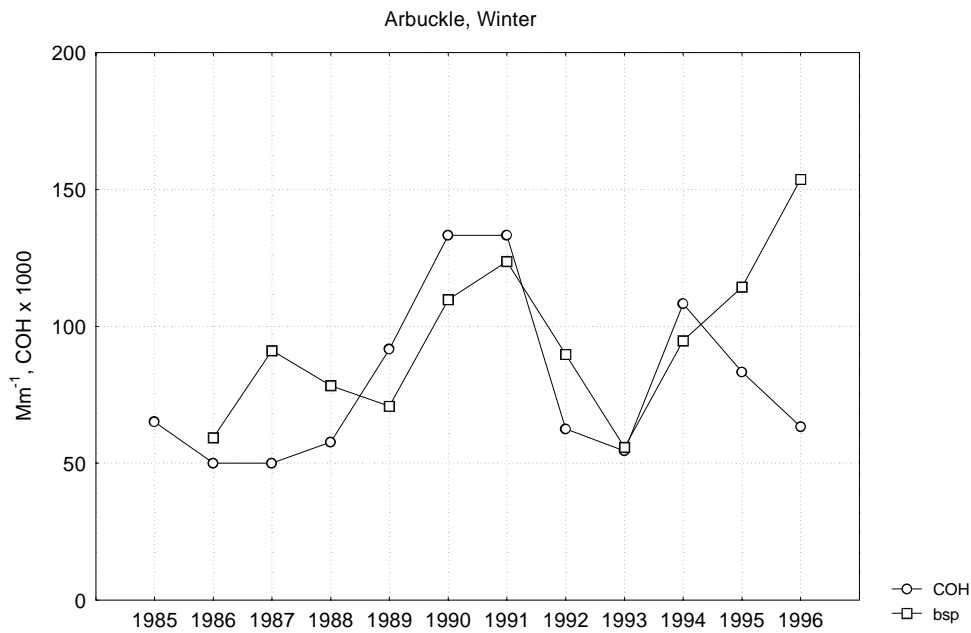


Figure A-63 Median Light Scattering Coefficient and Coefficient of Haze by Year During Winter at Arbuckle

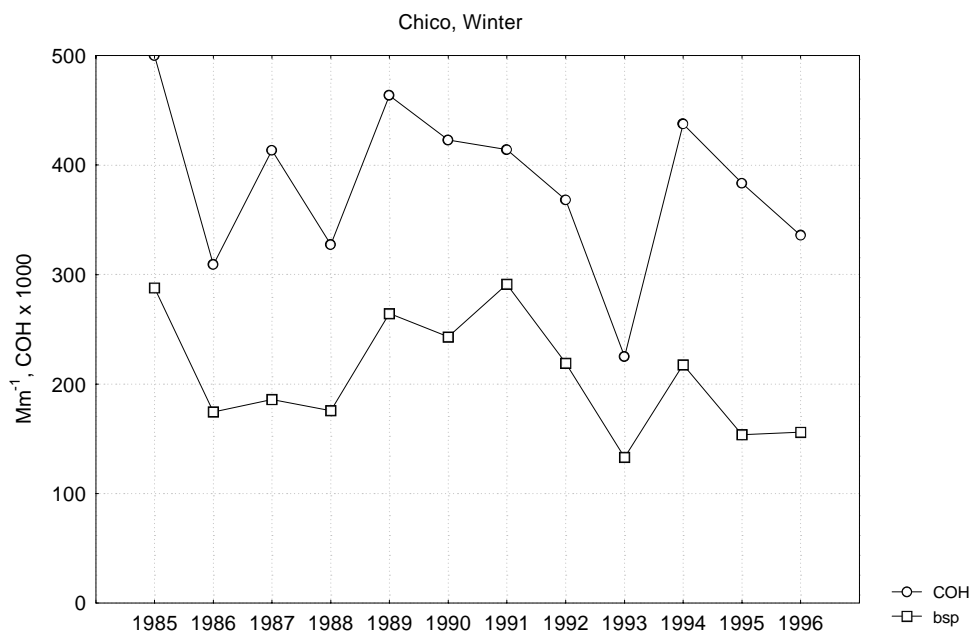


Figure A-64 Median Light Scattering Coefficient and Coefficient of Haze by Year During Winter at Chico

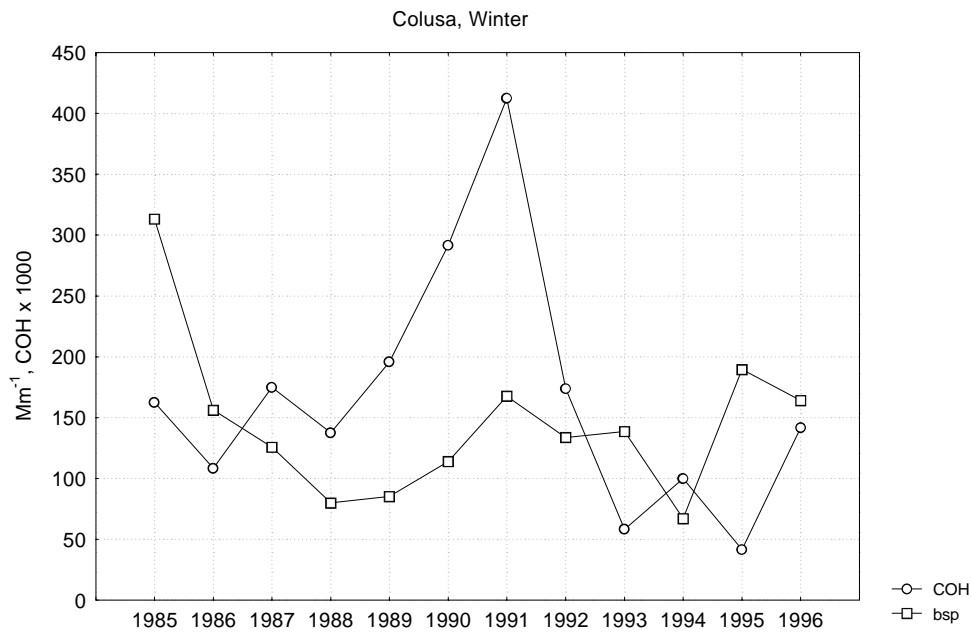


Figure A-65 Median Light Scattering Coefficient and Coefficient of Haze by Year During Winter at Colusa

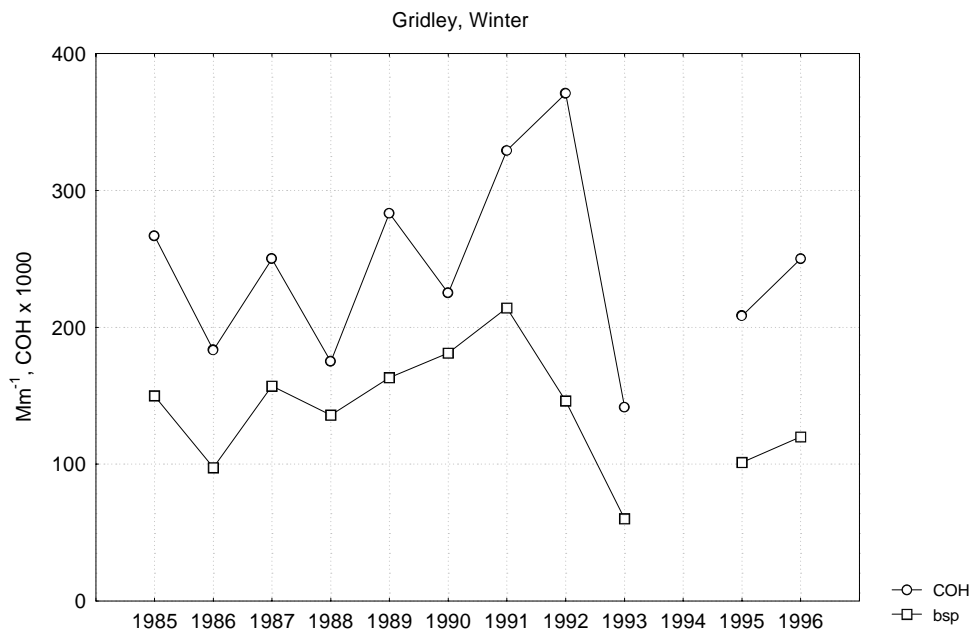


Figure A-66 Median Light Scattering Coefficient and Coefficient of Haze by Year During Winter at Gridley

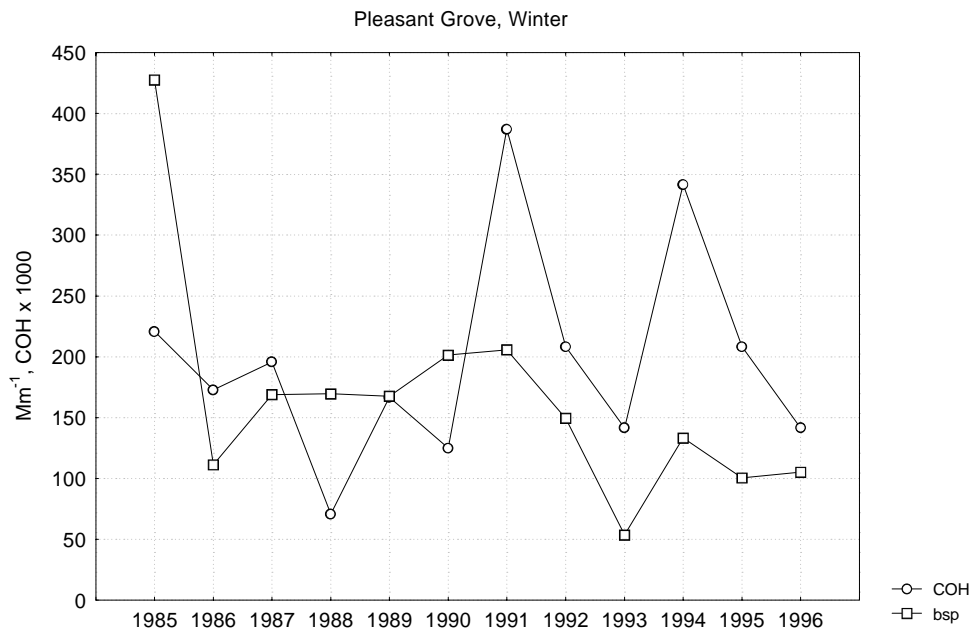


Figure A-67 Median Light Scattering Coefficient and Coefficient of Haze by Year During Winter at Pleasant Grove

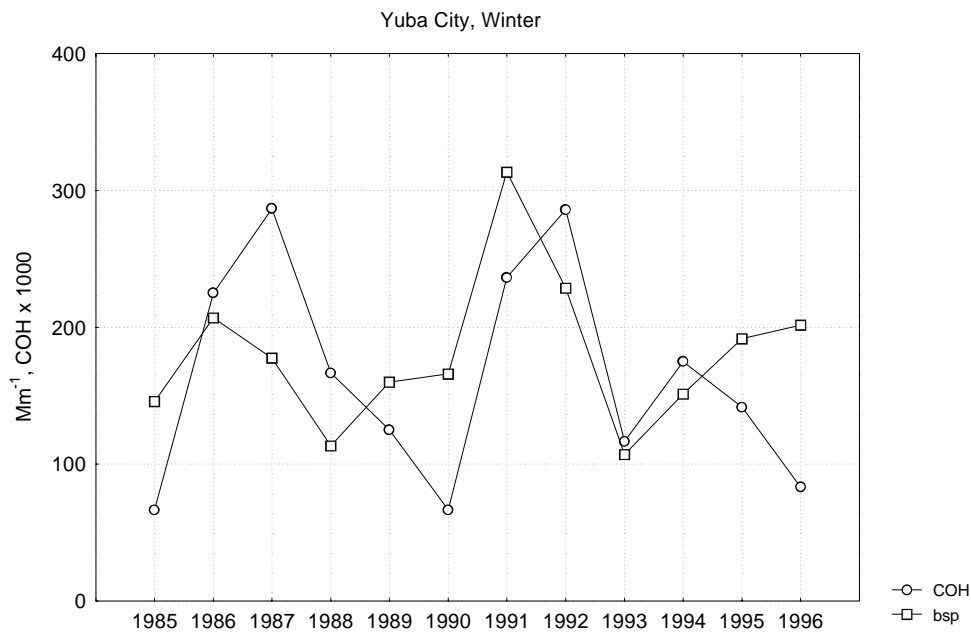


Figure A-68 Median Light Scattering Coefficient and Coefficient of Haze by Year During Winter at Yuba City

A.8 San Francisco Bay Air Basin (San Jose and Point Reyes National Seashore)

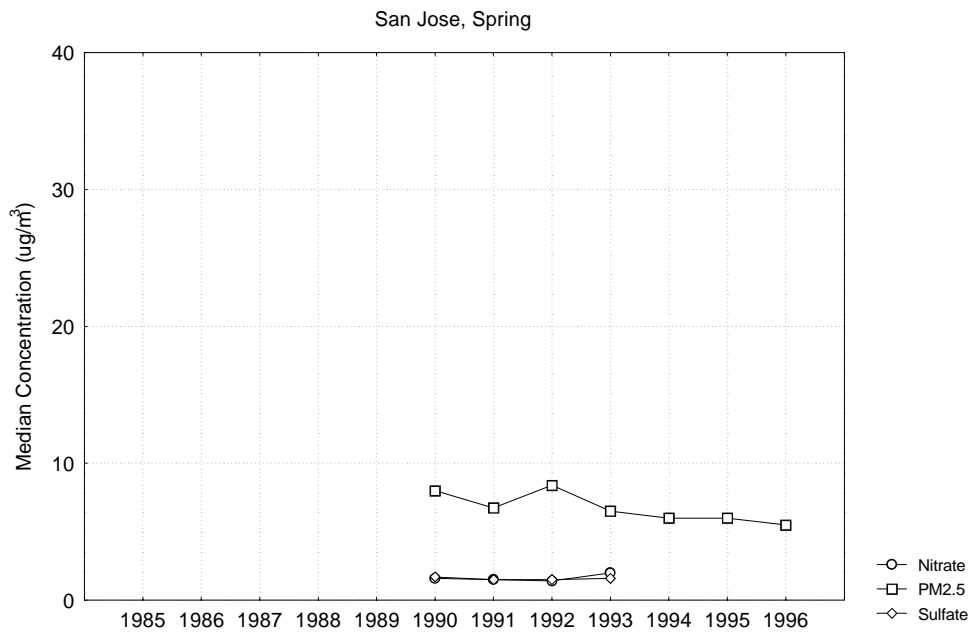


Figure A-69 Median PM_{2.5} Mass and PM₁₀ Nitrate and Sulfate by Year During Spring at San Jose

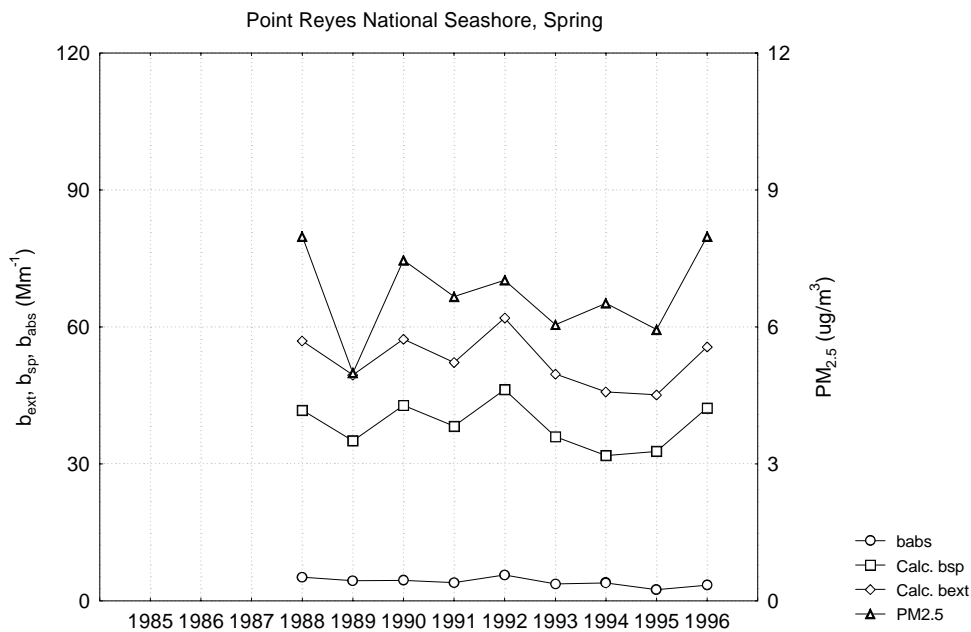


Figure A-70 Average Calculated and Measured Optical Data and PM_{2.5} Mass by Year During Spring at Point Reyes National Seashore

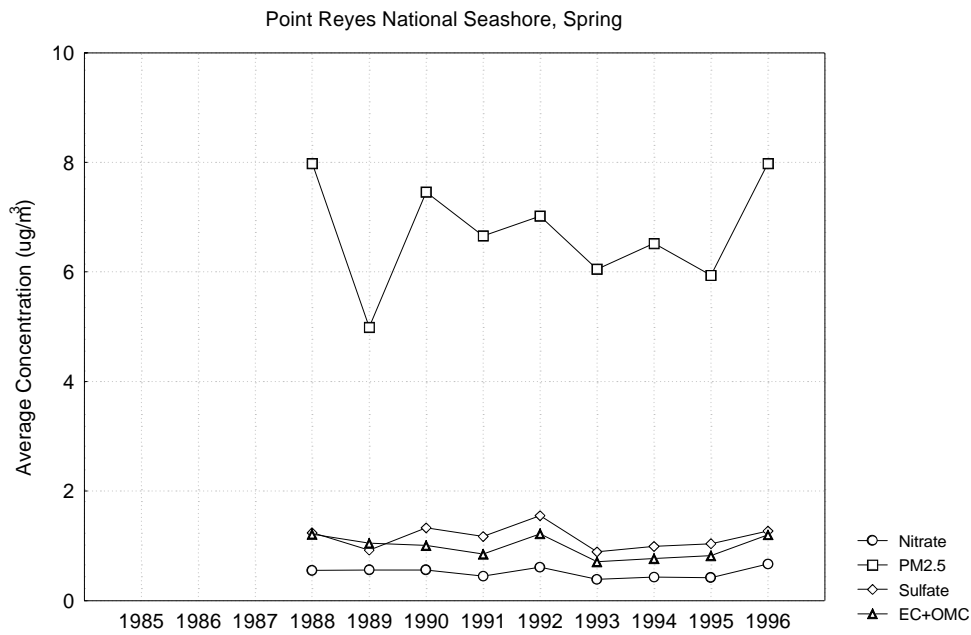


Figure A-71 Average PM_{2.5} Mass, Sulfate and Nitrate by Year During Spring at Point Reyes National Seashore

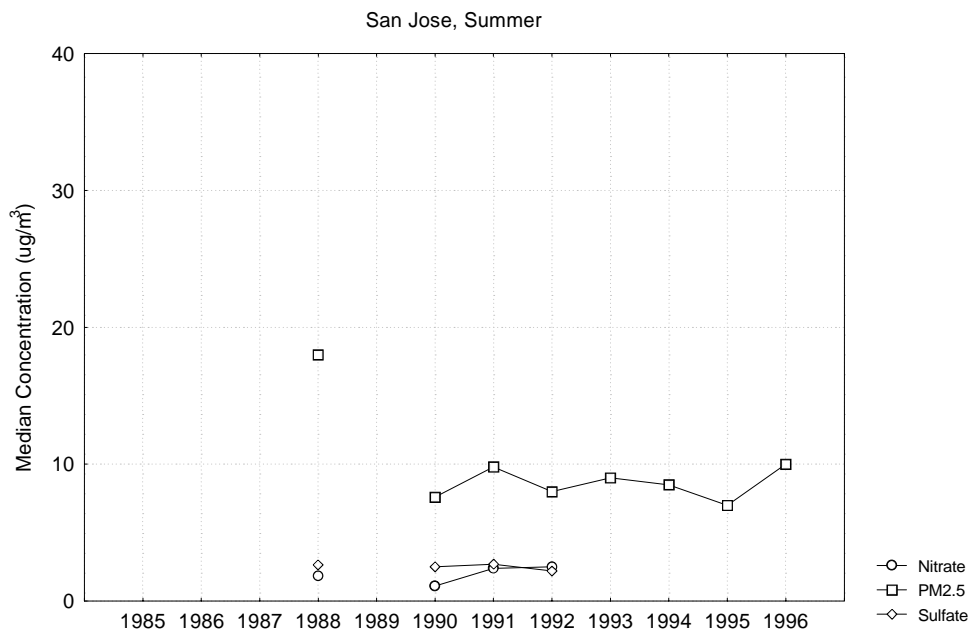


Figure A-72 Median PM_{2.5} Mass and PM₁₀ Nitrate and Sulfate by Year During Summer at San Jose

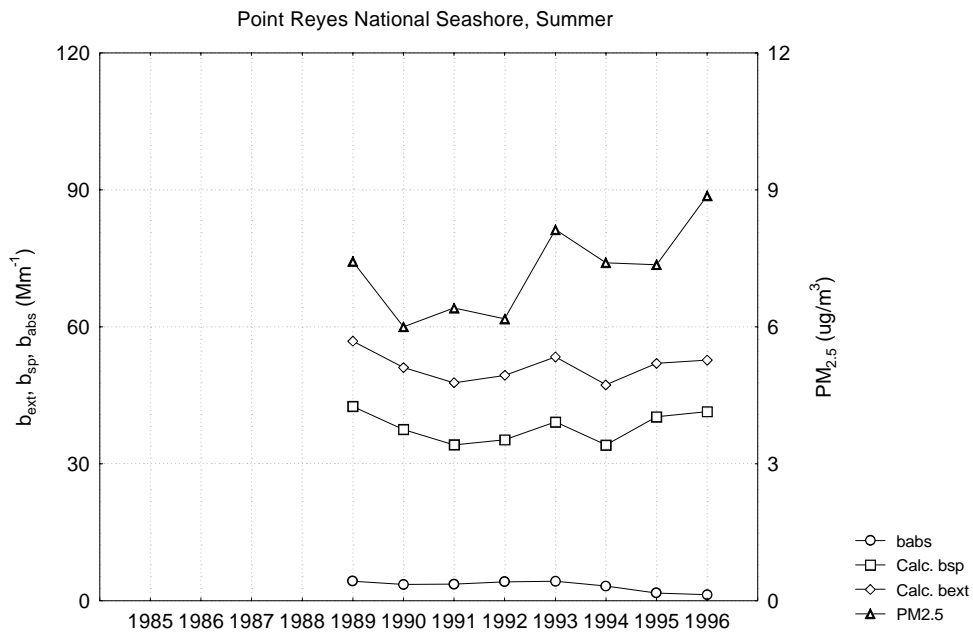


Figure A-73 Average Calculated and Measured Optical Data and PM_{2.5} Mass by Year During Summer at Point Reyes National Seashore

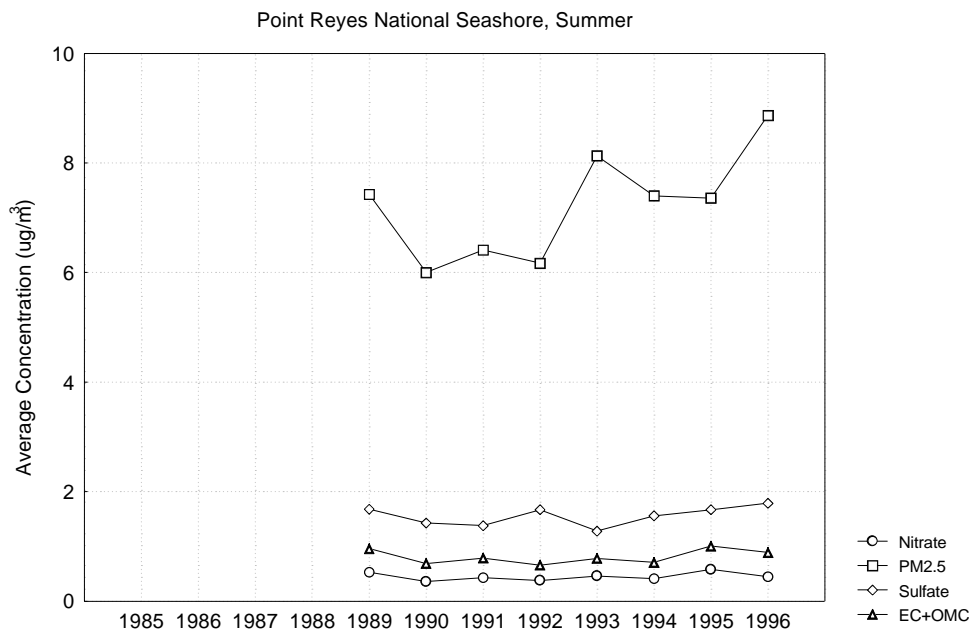


Figure A-74 Average PM_{2.5} Mass, Sulfate and Nitrate by Year During Summer at Point Reyes National Seashore

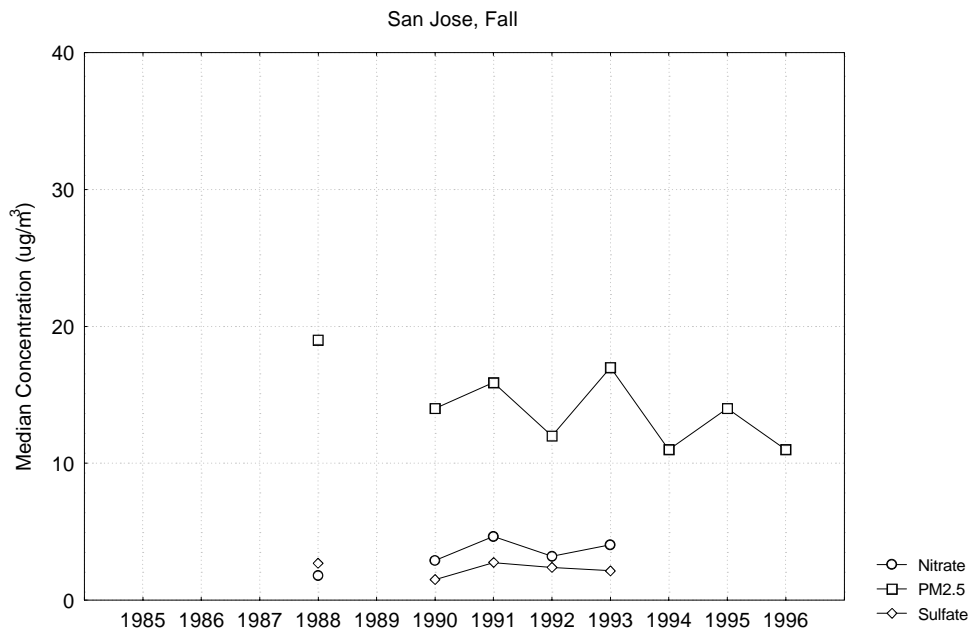


Figure A-75 Median PM_{2.5} Mass and PM₁₀ Nitrate and Sulfate by Year During Fall at San Jose

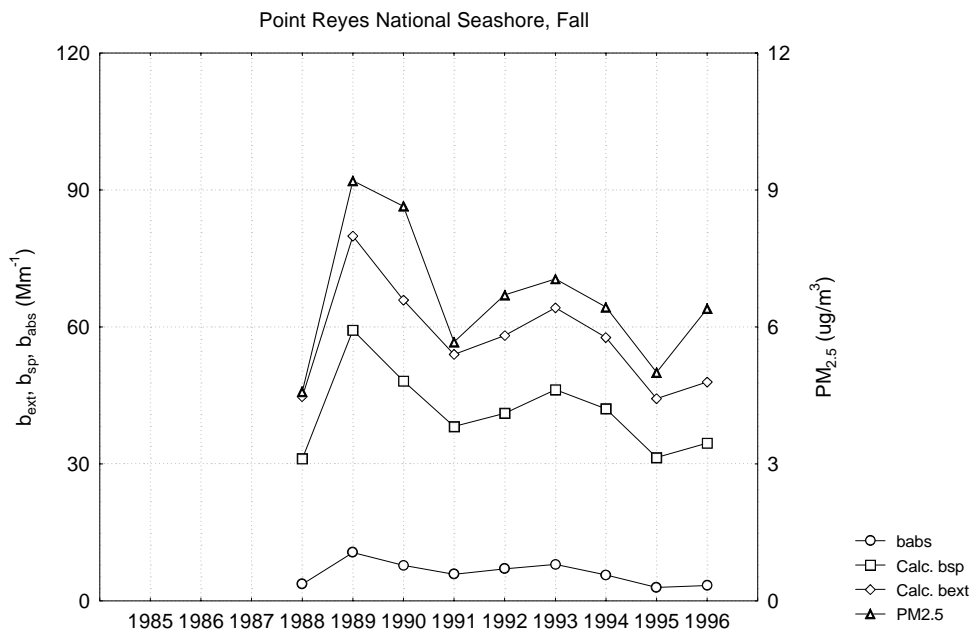


Figure A-76 Average Calculated and Measured Optical Data and PM_{2.5} Mass by Year During Fall at Point Reyes National Seashore

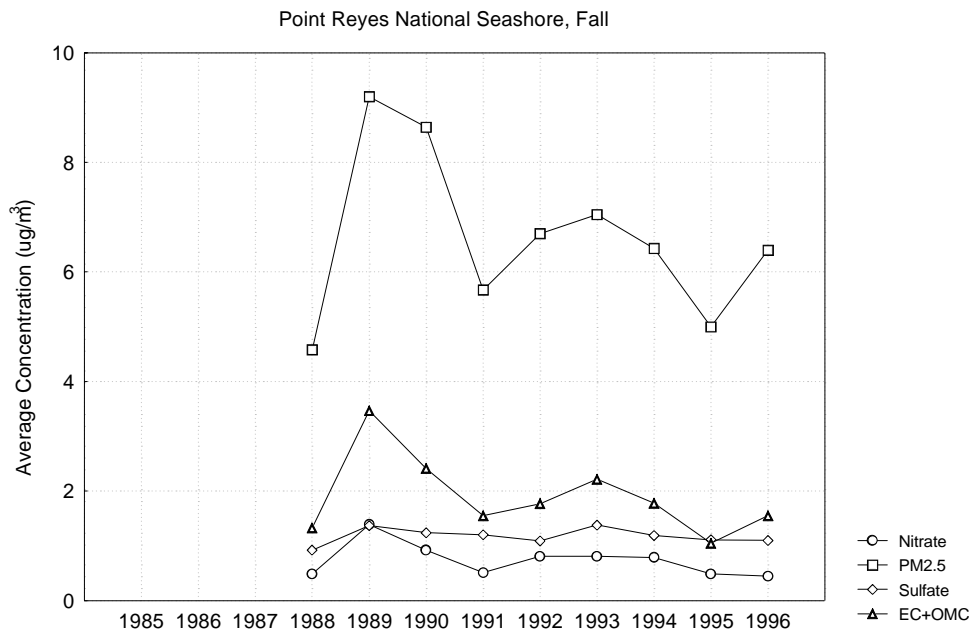


Figure A-77 Average $\text{PM}_{2.5}$ Mass, Sulfate and Nitrate by Year During Fall at Point Reyes National Seashore

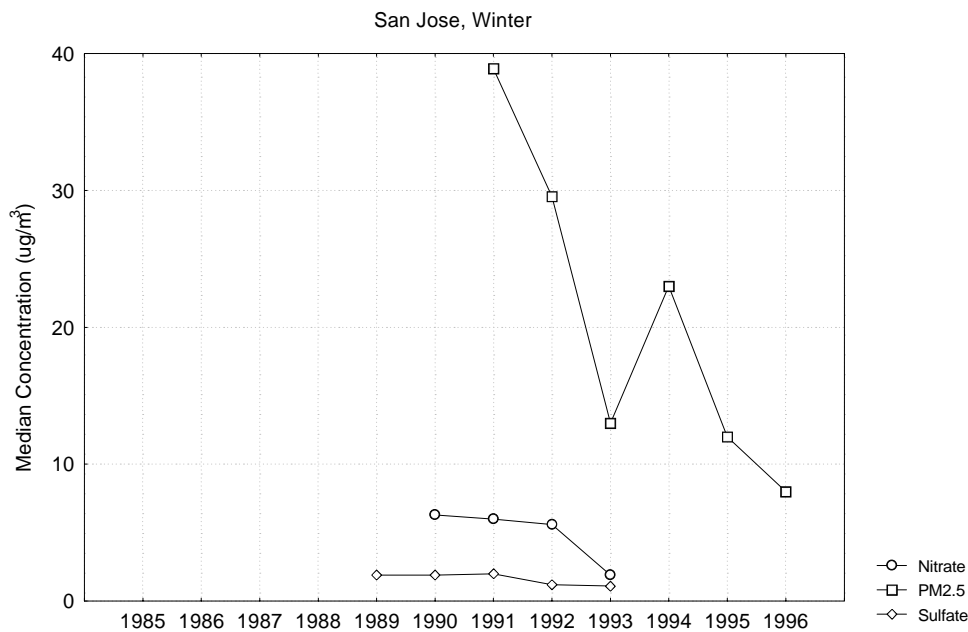


Figure A-78 Median $\text{PM}_{2.5}$ Mass and PM_{10} Nitrate and Sulfate by Year During Winter at San Jose

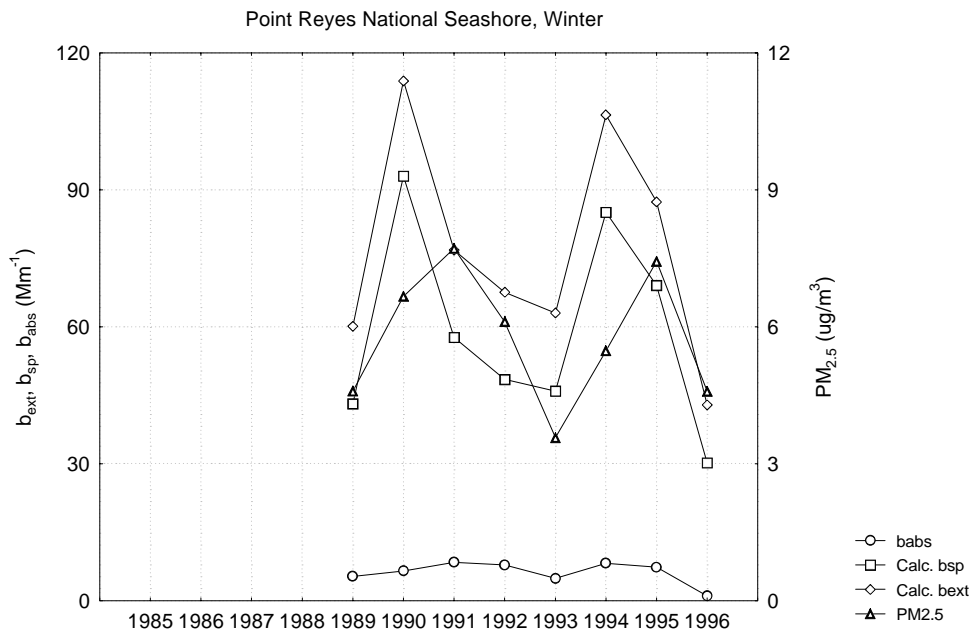


Figure A-79 Average Calculated and Measured Optical Data and PM_{2.5} Mass by Year During Winter at Point Reyes National Seashore

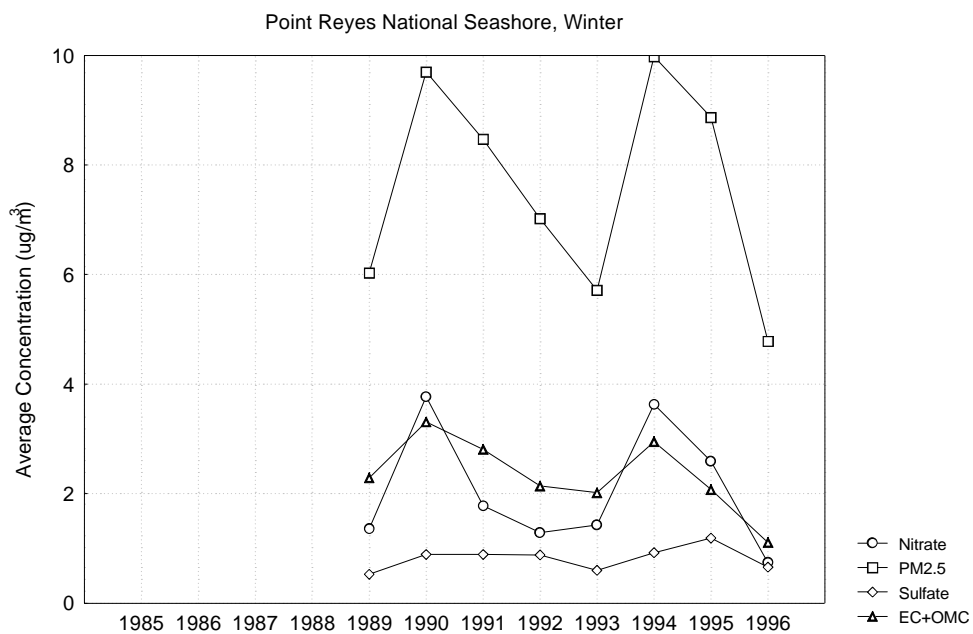


Figure A-80 Average PM_{2.5} Mass, Sulfate and Nitrate by Year During Winter at Point Reyes National Seashore

A.9 San Joaquin Valley Air Basin (Bakersfield, Fresno, Madera, Modesto, Stockton and Visalia)

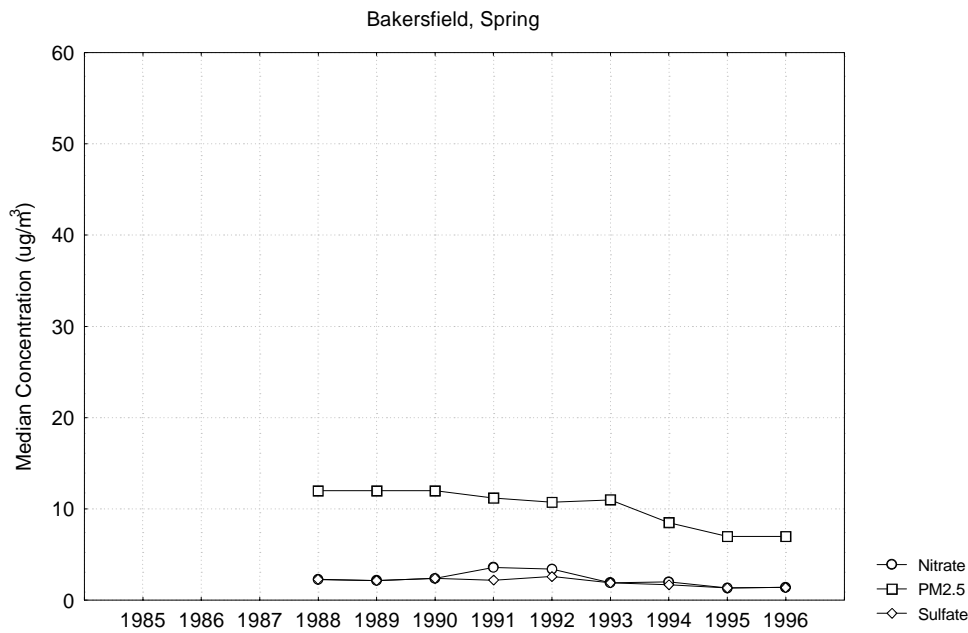


Figure A-81 Median PM_{2.5} Mass and PM₁₀ Nitrate and Sulfate by Year During Spring at Bakersfield

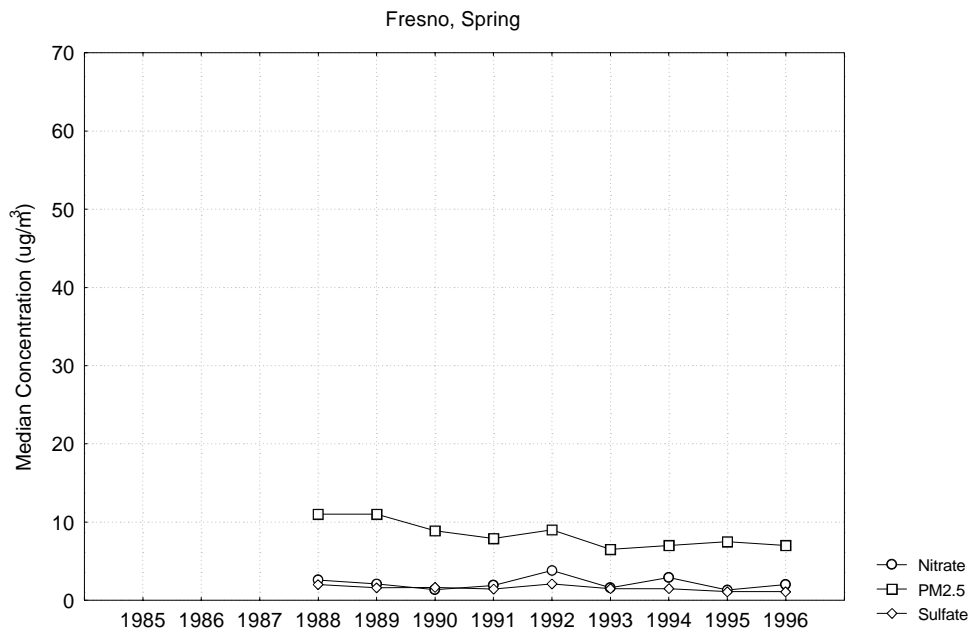


Figure A-82 Median PM_{2.5} Mass and PM₁₀ Nitrate and Sulfate by Year During Spring at Fresno

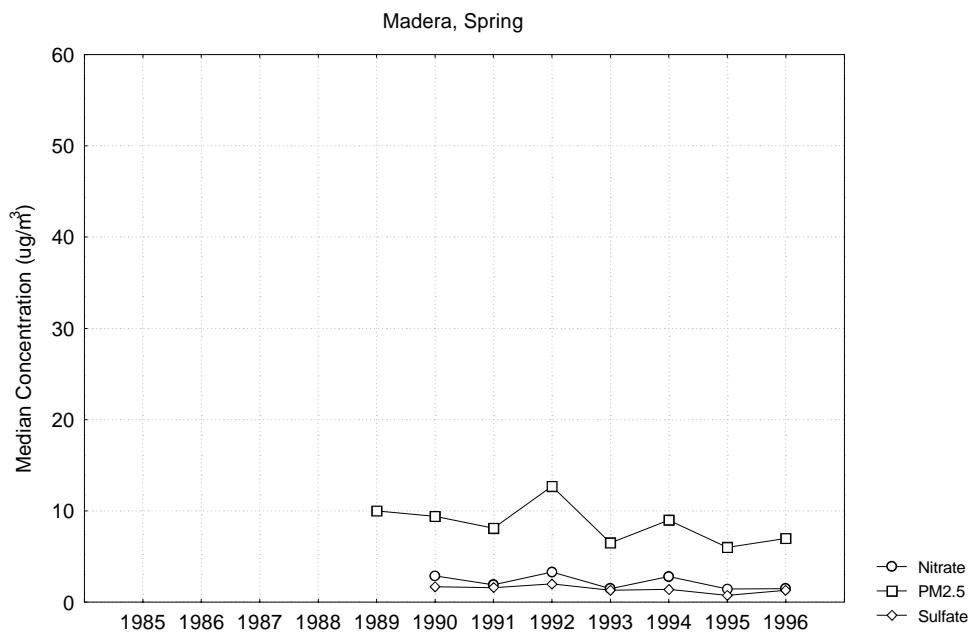


Figure A-83 Median PM_{2.5} Mass and PM₁₀ Nitrate and Sulfate by Year During Spring at Madera

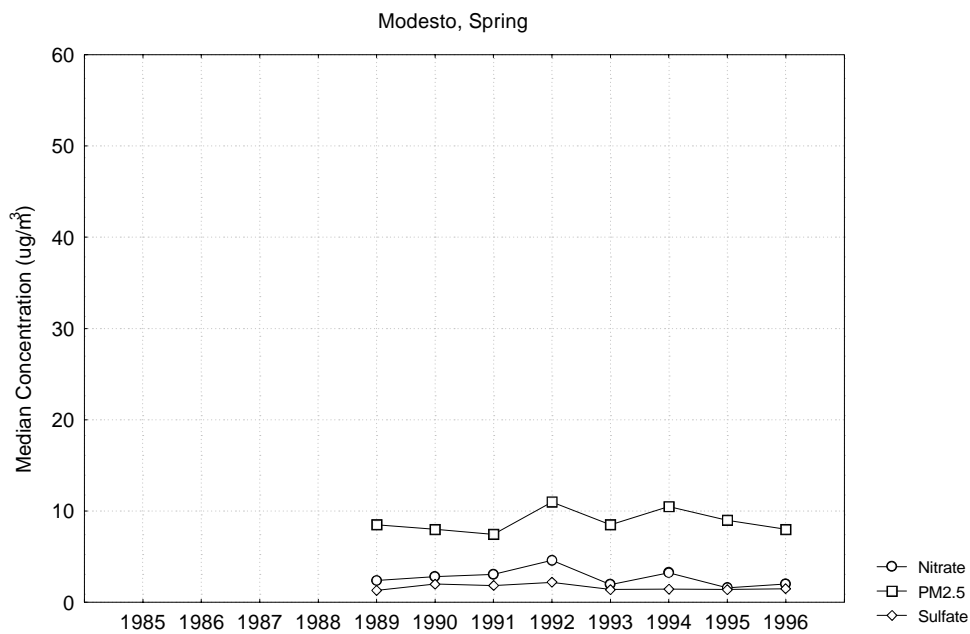


Figure A-84 Median PM_{2.5} Mass and PM₁₀ Nitrate and Sulfate by Year During Spring at Modesto

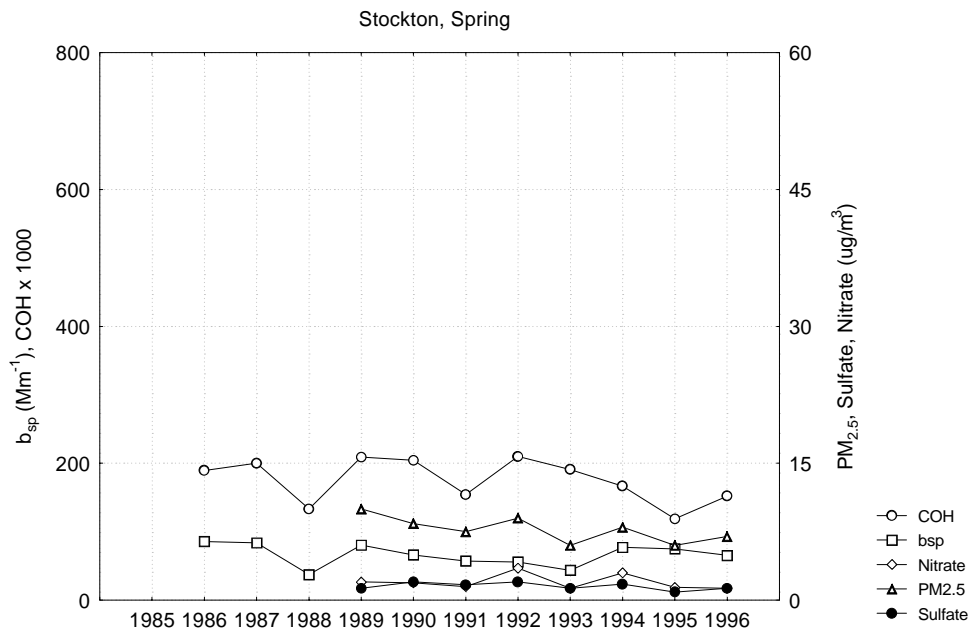


Figure A-85 Median Light Scattering Coefficient, Coefficient of Haze, PM_{2.5} Mass and PM₁₀ Nitrate and Sulfate by Year During Spring at Stockton

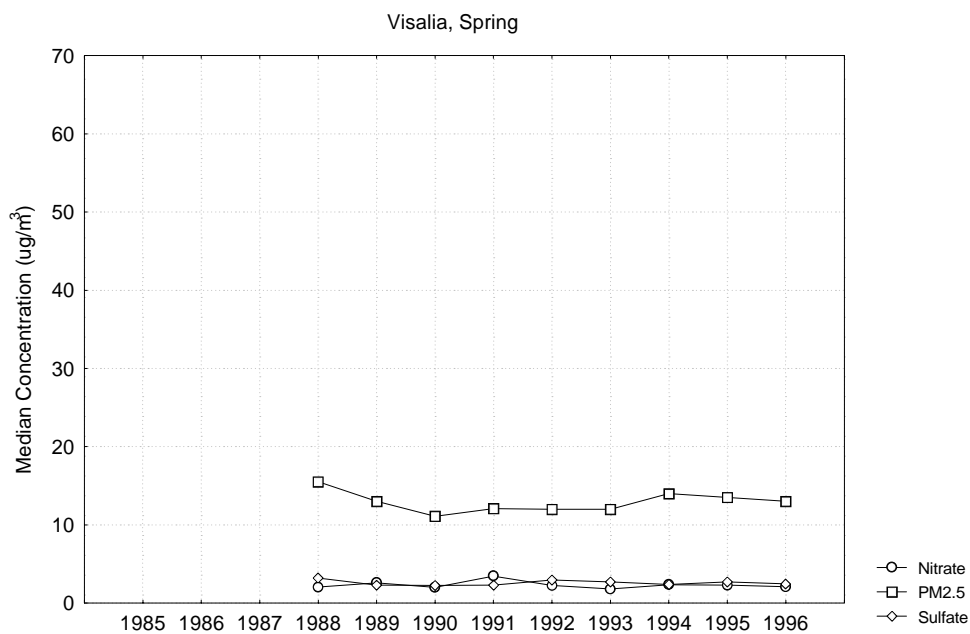


Figure A-86 Median PM_{2.5} Mass and PM₁₀ Nitrate and Sulfate by Year During Spring at Visalia

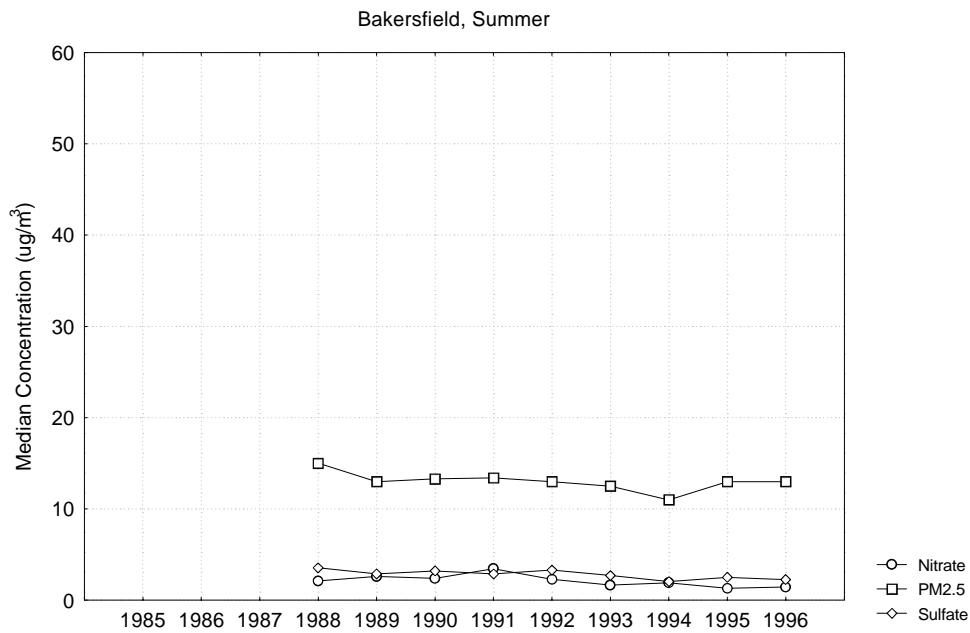


Figure A-87 Median PM_{2.5} Mass and PM₁₀ Nitrate and Sulfate by Year During Summer at Bakersfield

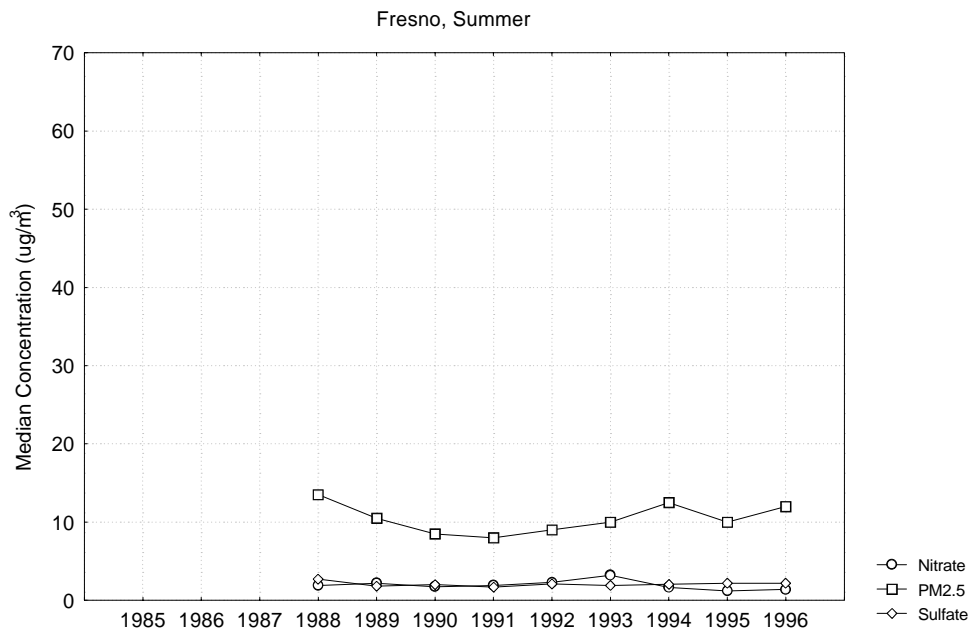


Figure A-88 Median PM_{2.5} Mass and PM₁₀ Nitrate and Sulfate by Year During Summer at Fresno

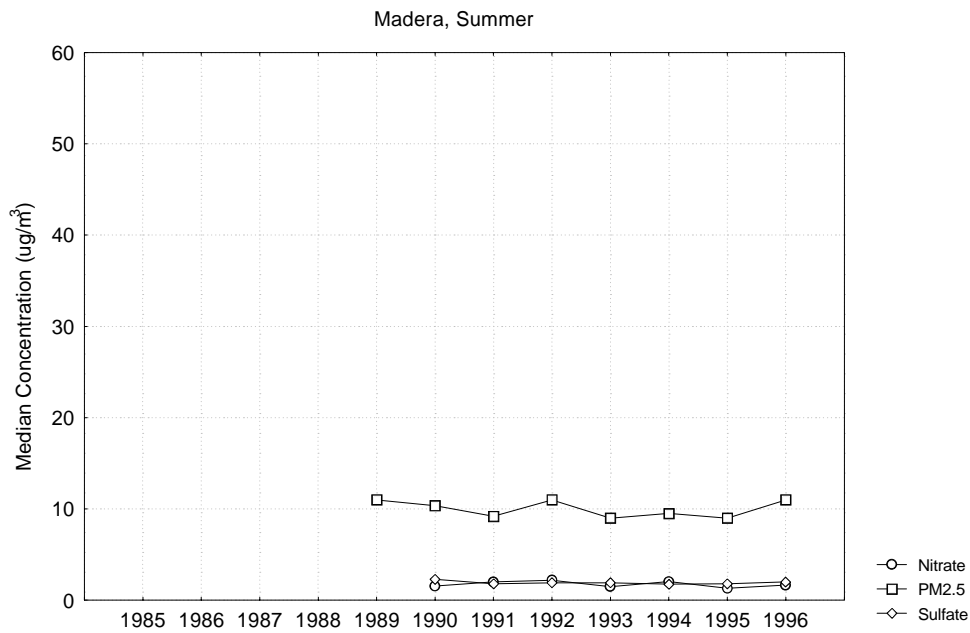


Figure A-89 Median PM_{2.5} Mass and PM₁₀ Nitrate and Sulfate by Year During Summer at Madera

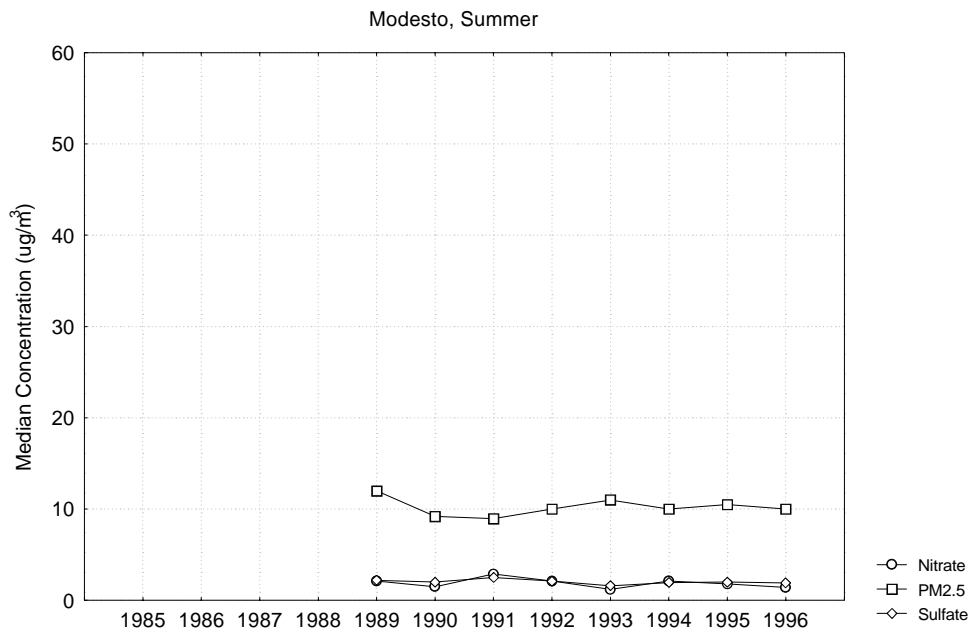


Figure A-90 Median PM_{2.5} Mass and PM₁₀ Nitrate and Sulfate by Year During Summer at Modesto

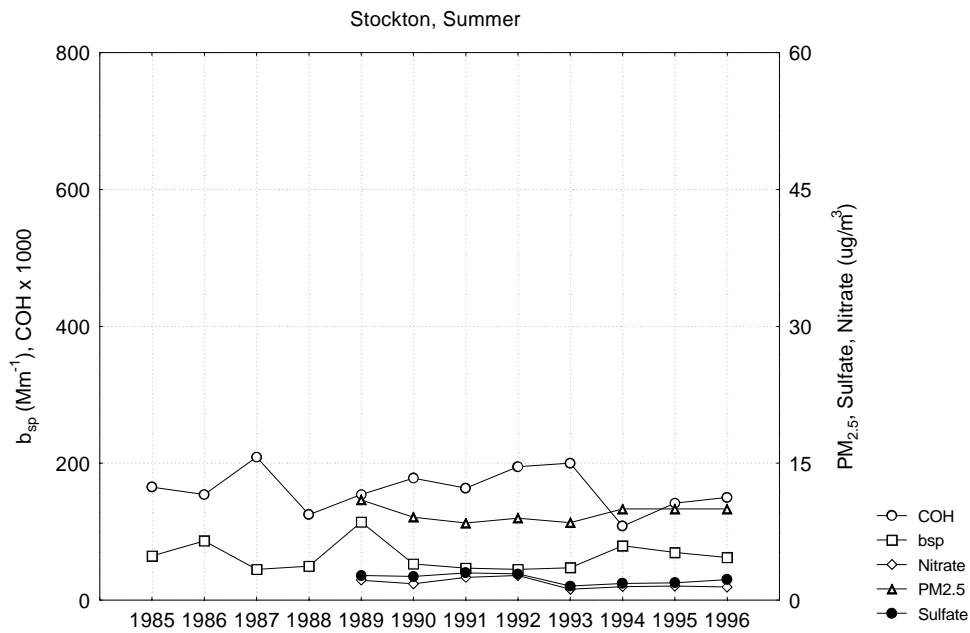


Figure A-91 Median Light Scattering Coefficient, Coefficient of Haze, PM_{2.5} Mass and PM₁₀ Nitrate and Sulfate by Year During Summer at Stockton

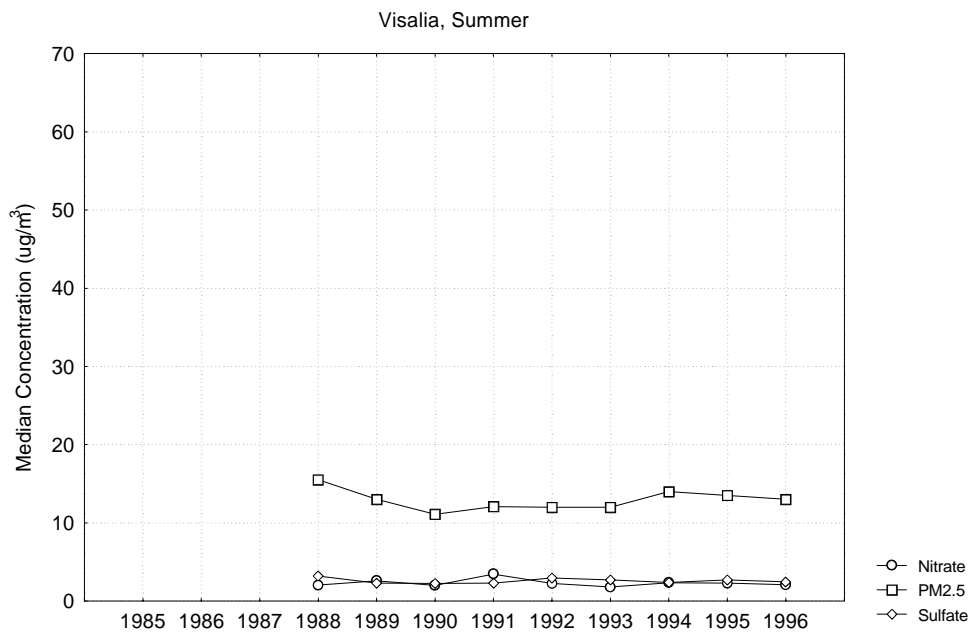


Figure A-92 Median PM_{2.5} Mass and PM₁₀ Nitrate and Sulfate by Year During Summer at Visalia

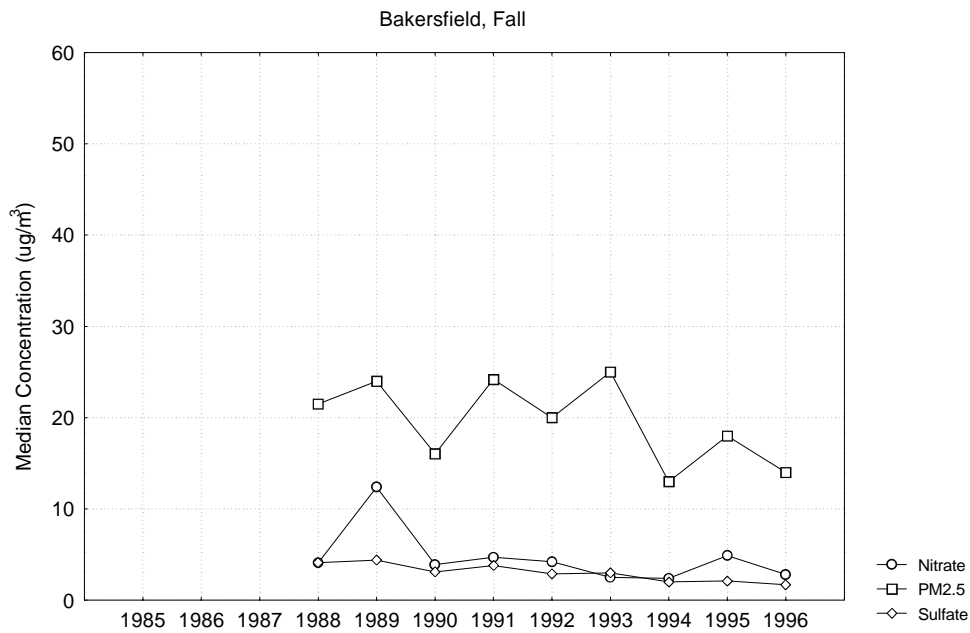


Figure A-93 Median PM_{2.5} Mass and PM₁₀ Nitrate and Sulfate by Year During Fall at Bakersfield

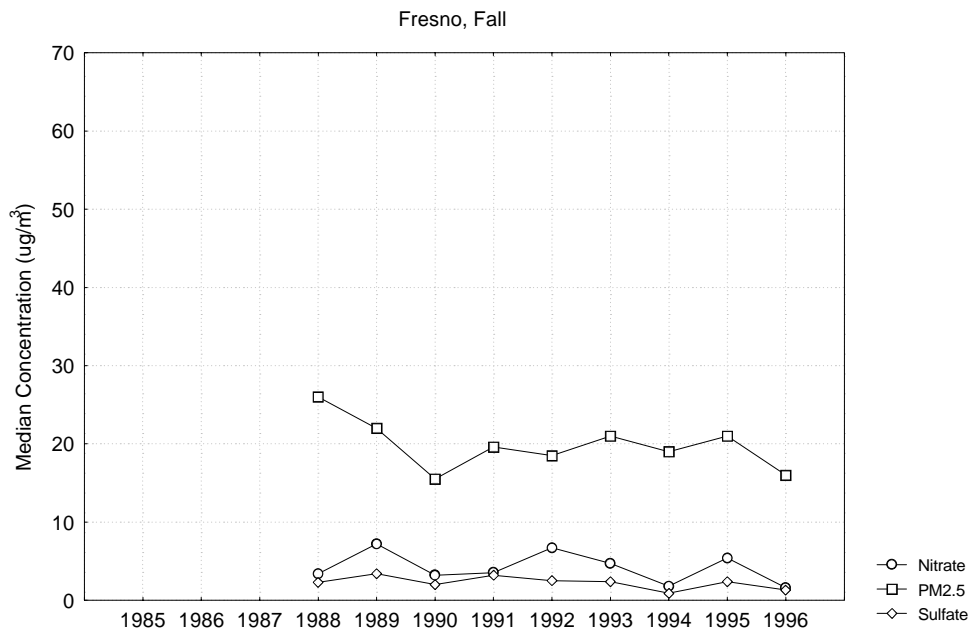


Figure A-94 Median PM_{2.5} Mass and PM₁₀ Nitrate and Sulfate by Year During Fall at Fresno

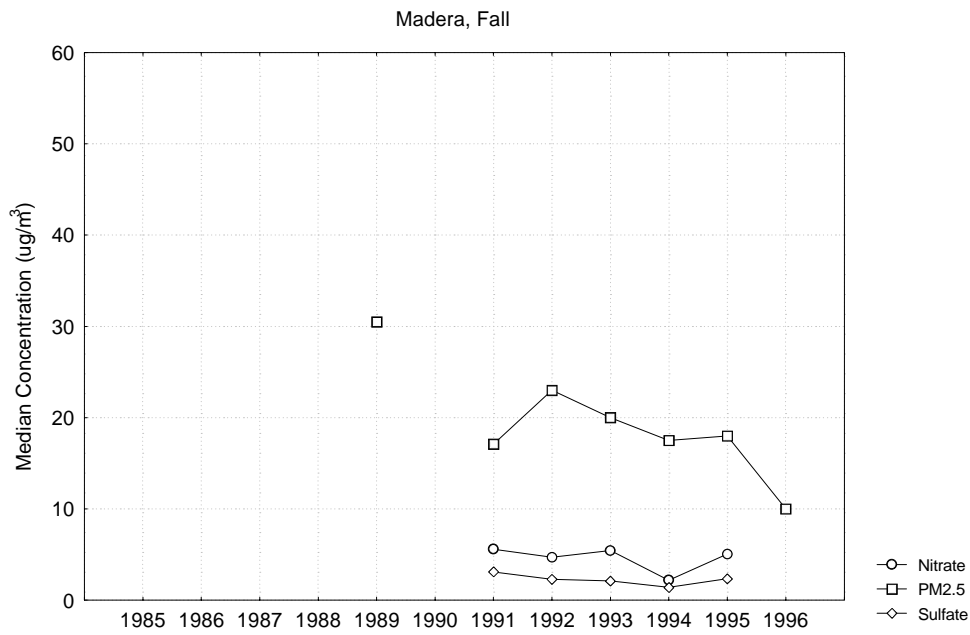


Figure A-95 Median PM_{2.5} Mass and PM₁₀ Nitrate and Sulfate by Year During Fall at Madera

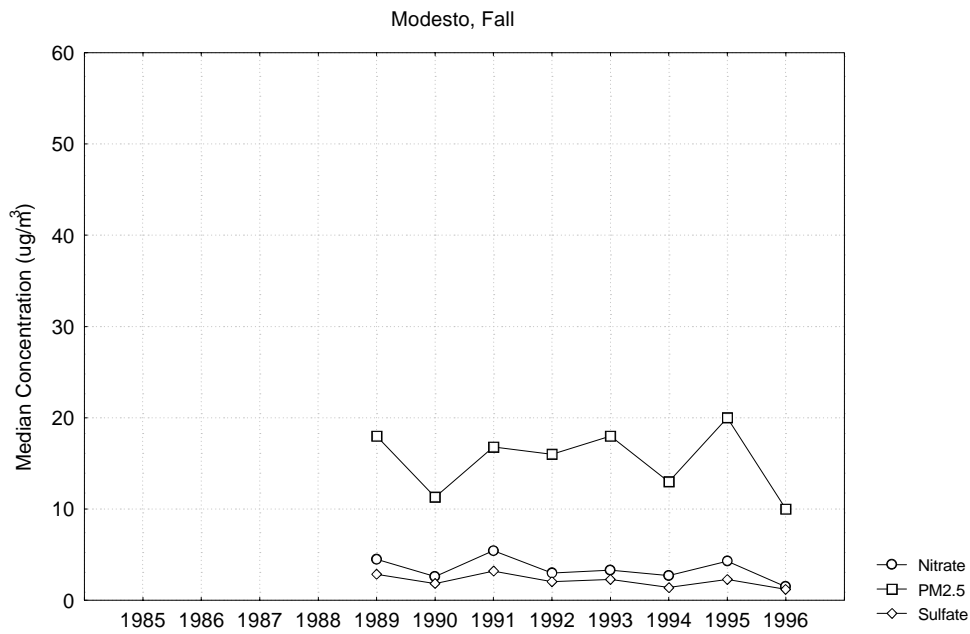


Figure A-96 Median PM_{2.5} Mass and PM₁₀ Nitrate and Sulfate by Year During Fall at Modesto

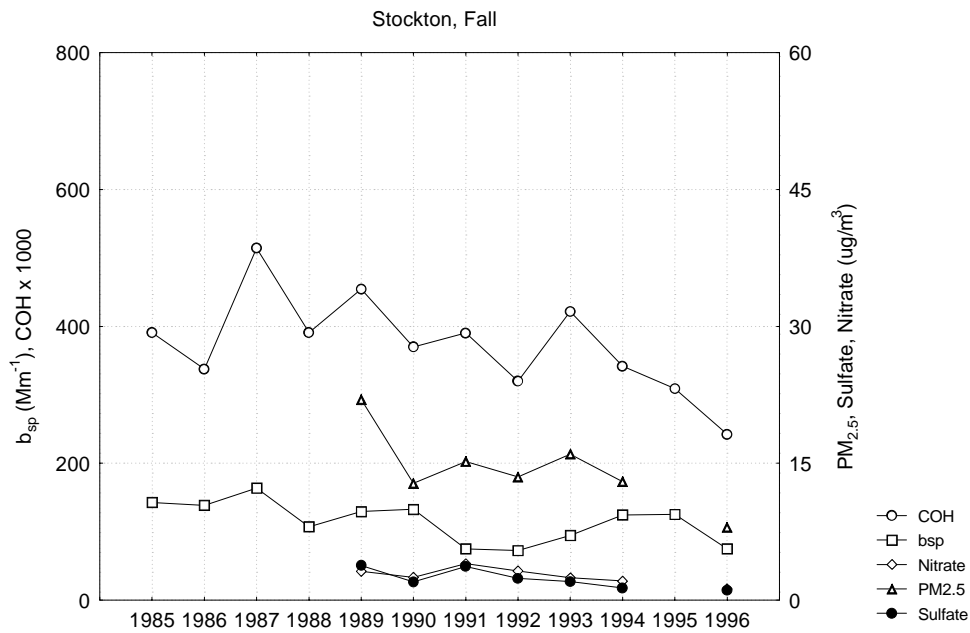


Figure A-97 Median Light Scattering Coefficient, Coefficient of Haze, PM_{2.5} Mass and PM₁₀ Nitrate and Sulfate by Year During Fall at Stockton

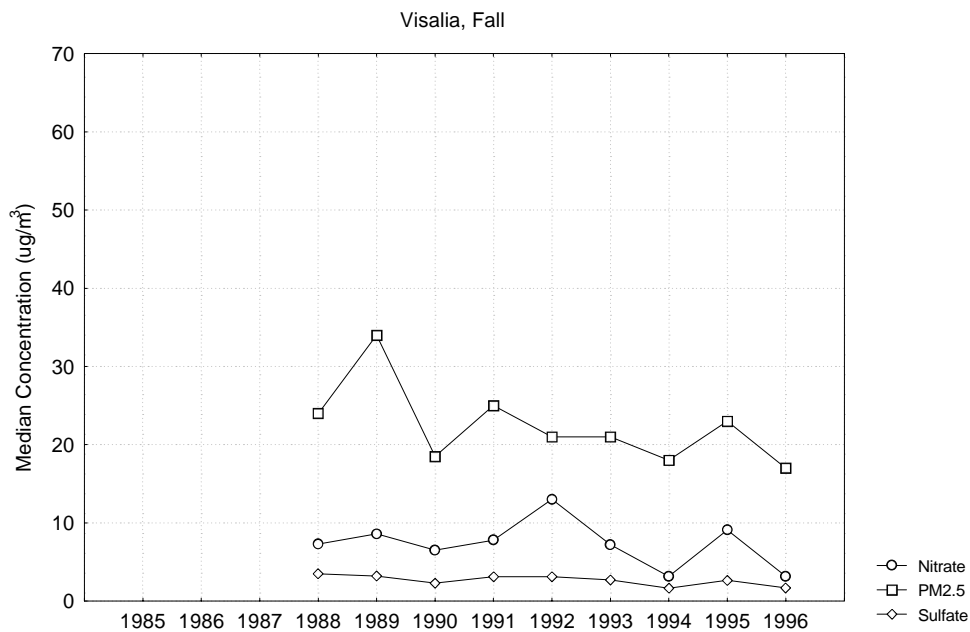


Figure A-98 Median PM_{2.5} Mass and PM₁₀ Nitrate and Sulfate by Year During Fall at Visalia

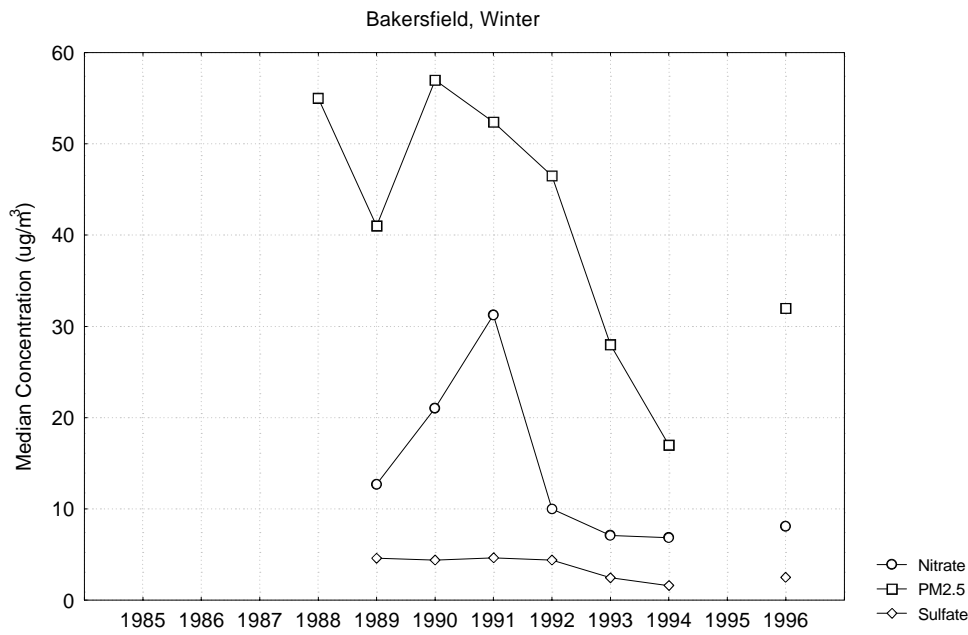


Figure A-99 Median PM_{2.5} Mass and PM₁₀ Nitrate and Sulfate by Year During Winter at Bakersfield

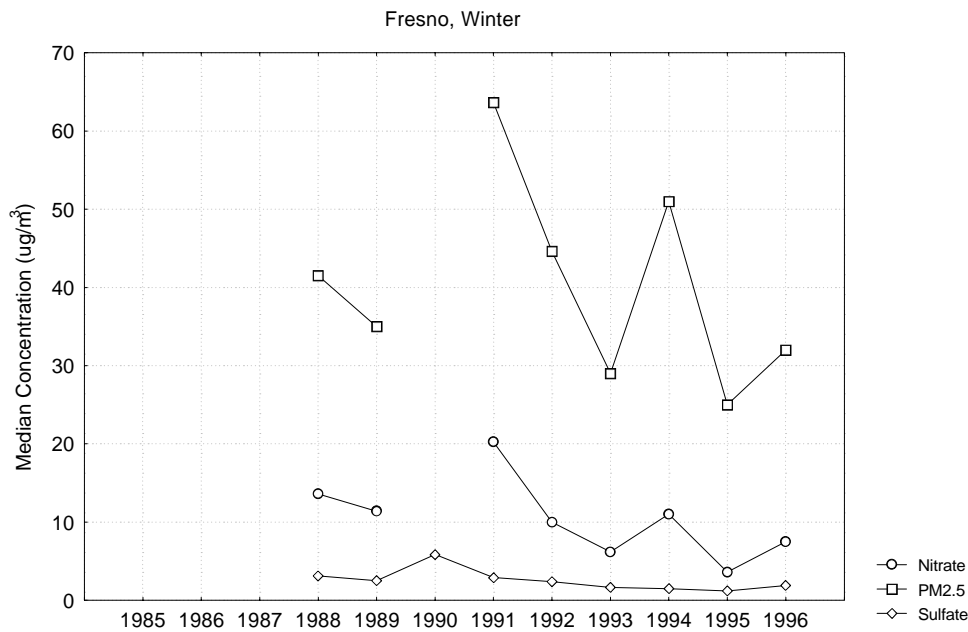


Figure A-100 Median PM_{2.5} Mass and PM₁₀ Nitrate and Sulfate by Year During Winter at Fresno

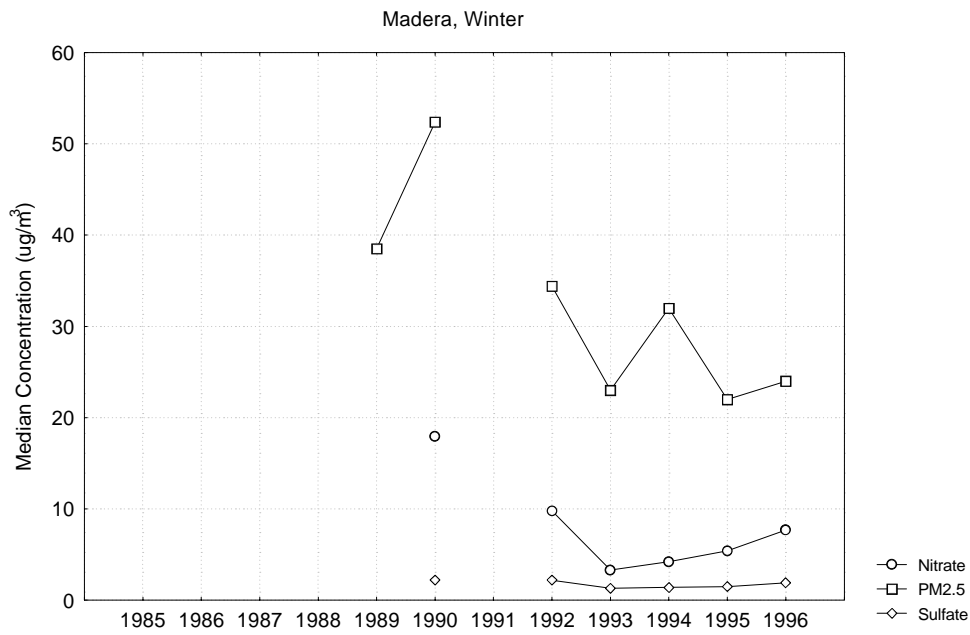


Figure A-101 Median PM_{2.5} Mass and PM₁₀ Nitrate and Sulfate by Year During Winter at Madera

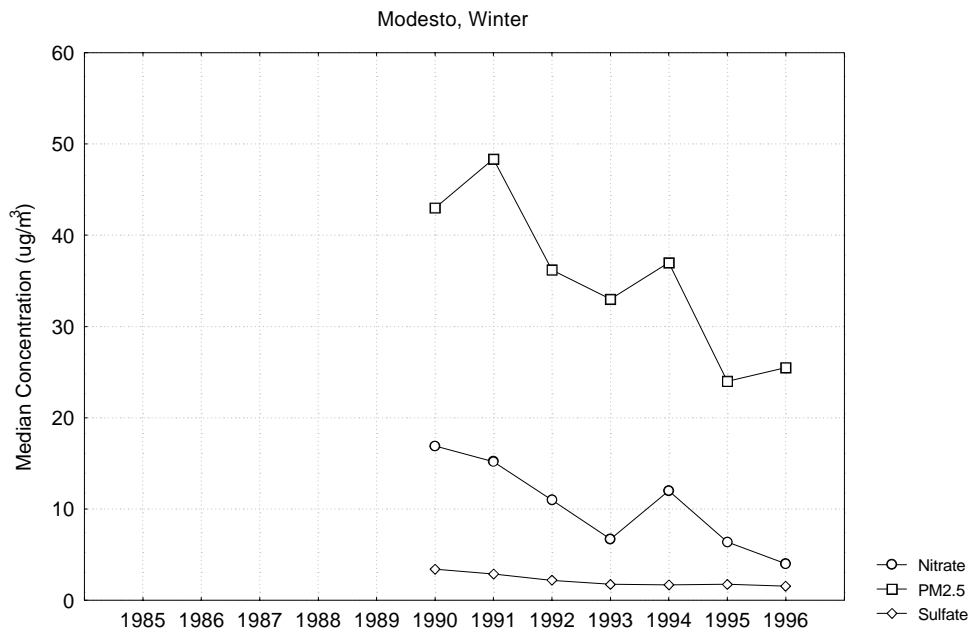


Figure A-102 Median PM_{2.5} Mass and PM₁₀ Nitrate and Sulfate by Year During Winter at Modesto

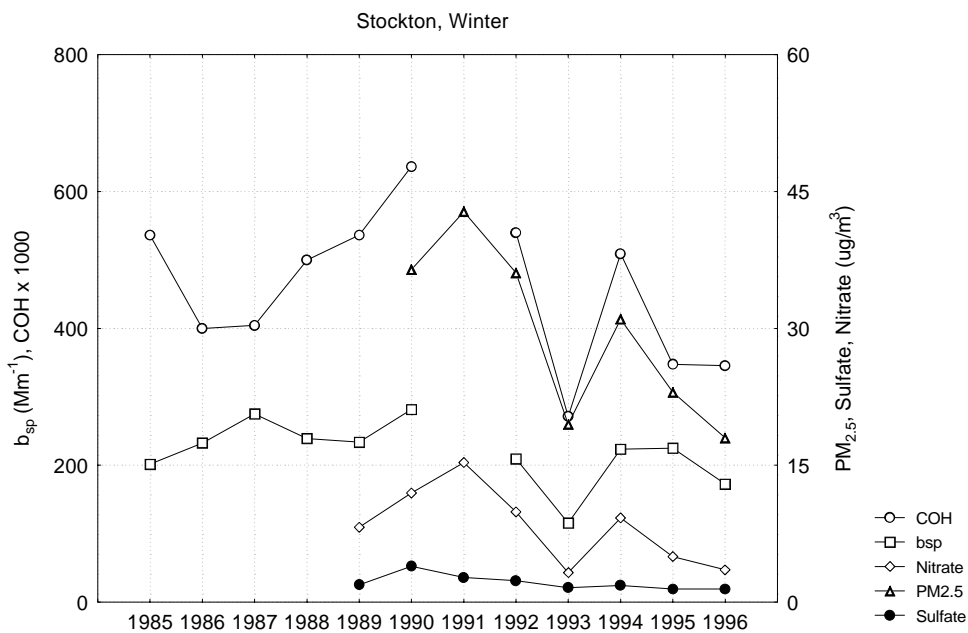


Figure A-103 Median Light Scattering Coefficient, Coefficient of Haze, PM_{2.5} Mass and PM₁₀ Nitrate and Sulfate by Year During Winter at Stockton

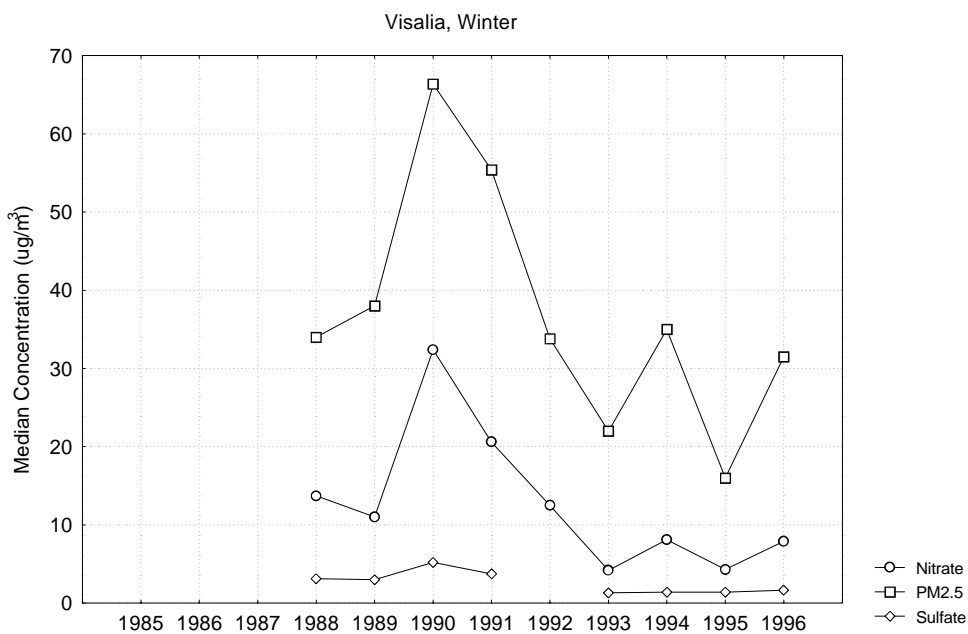


Figure A-104 Median PM_{2.5} Mass and PM₁₀ Nitrate and Sulfate by Year During Winter at Visalia

A.10 Salton Sea Air Basin (El Centro)

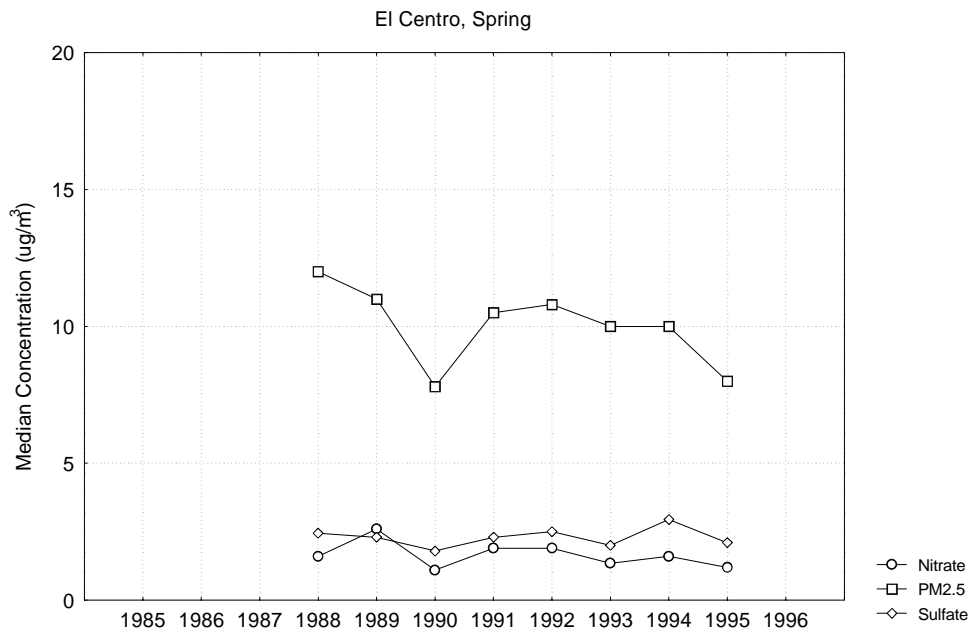


Figure A-105 Median PM_{2.5} Mass and PM₁₀ Nitrate and Sulfate by Year During Spring at El Centro

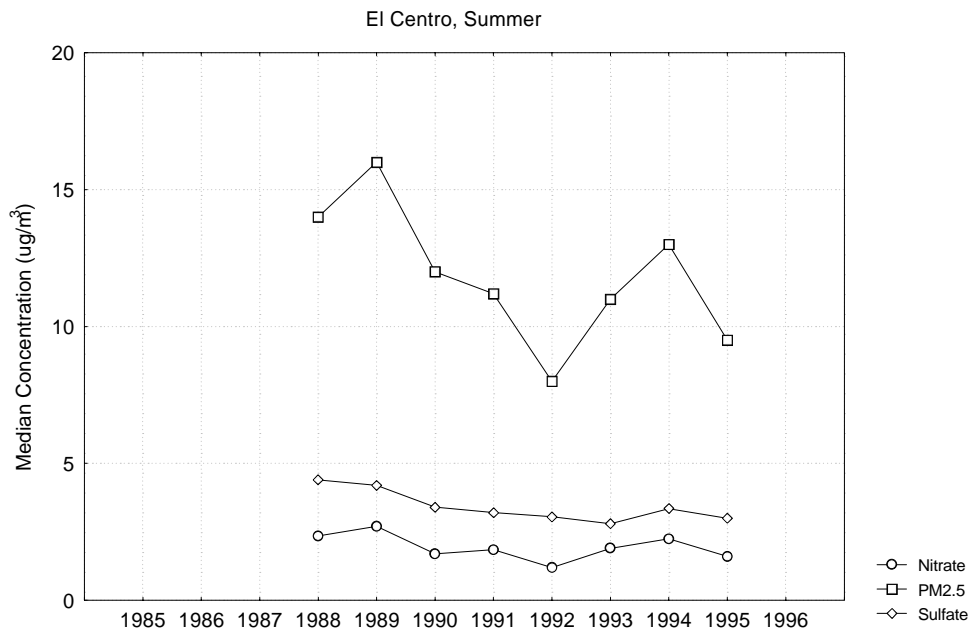


Figure A-106 Median PM_{2.5} Mass and PM₁₀ Nitrate and Sulfate by Year During Summer at El Centro

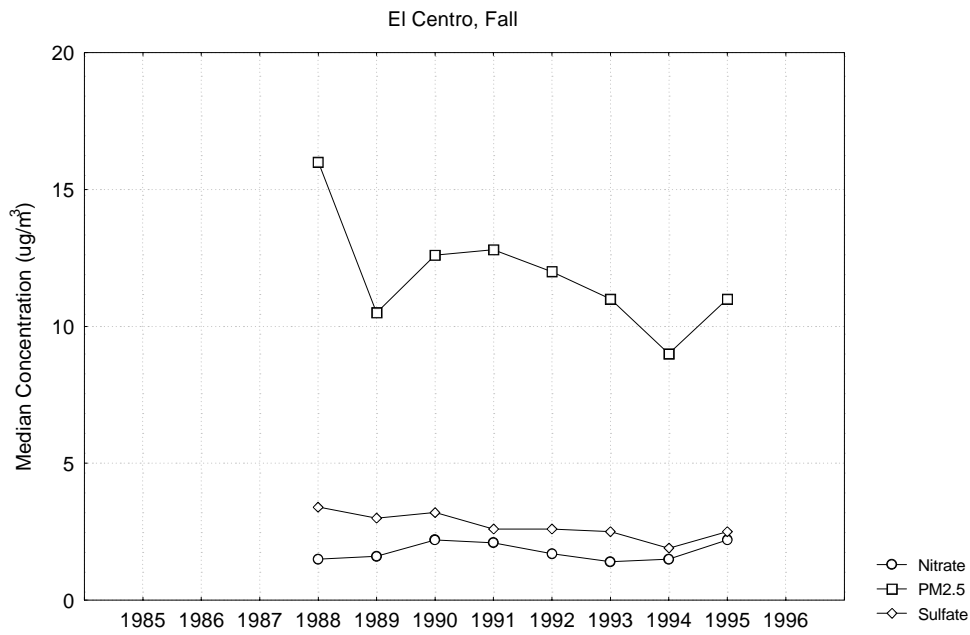


Figure A-107 Median PM_{2.5} Mass and PM₁₀ Nitrate and Sulfate by Year During Fall at El Centro

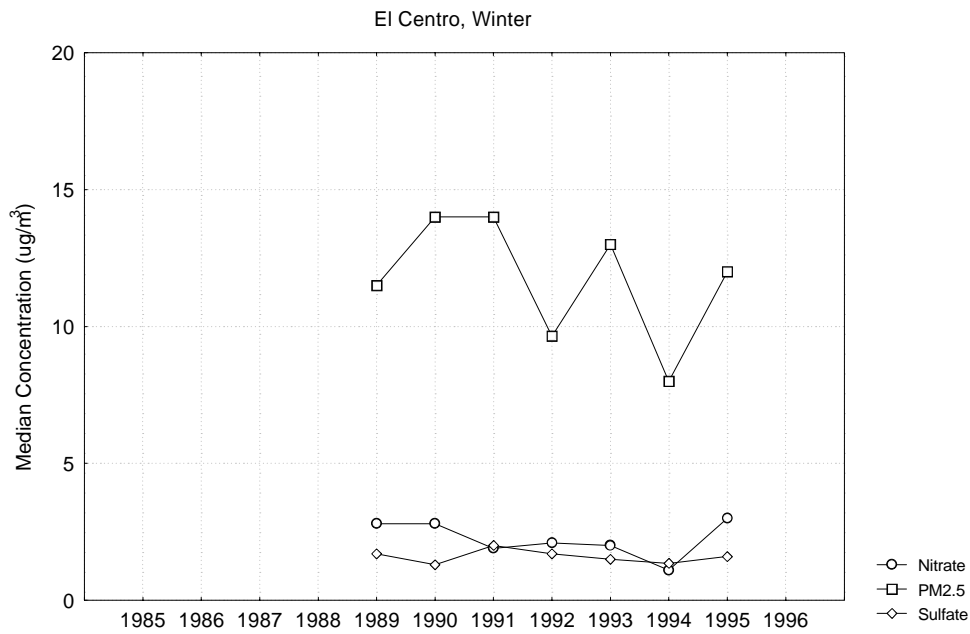


Figure A-108 Median PM_{2.5} Mass and PM₁₀ Nitrate and Sulfate by Year During Winter at El Centro

A.11 South Coast Air Basin (Azusa, Long Beach, Riverside and San Geronio Wilderness Area)

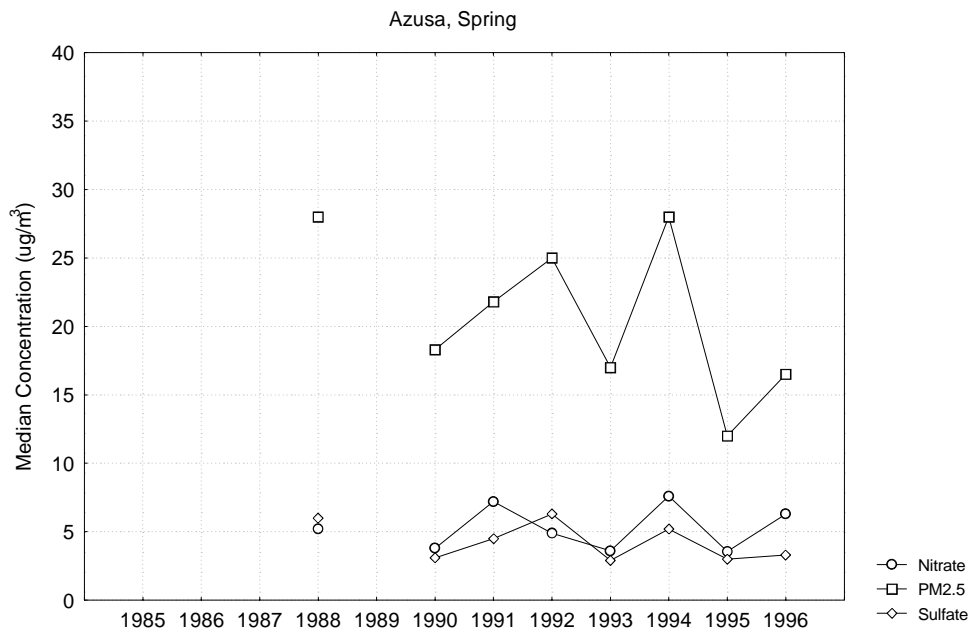


Figure A-109 Median PM_{2.5} Mass and PM₁₀ Nitrate and Sulfate by Year During Spring at Azusa

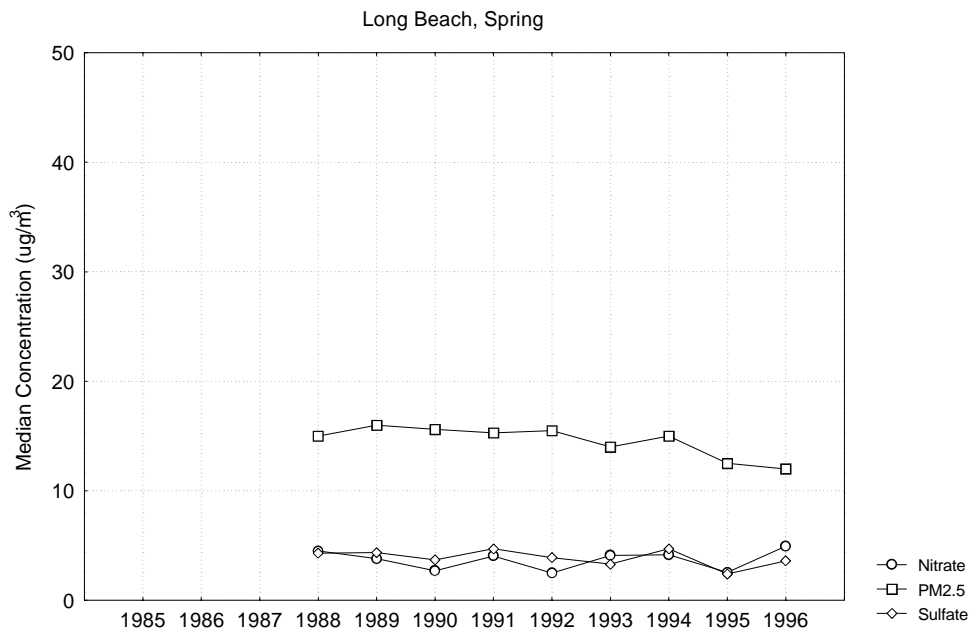


Figure A-110 Median PM_{2.5} Mass and PM₁₀ Nitrate and Sulfate by Year During Spring at Long Beach

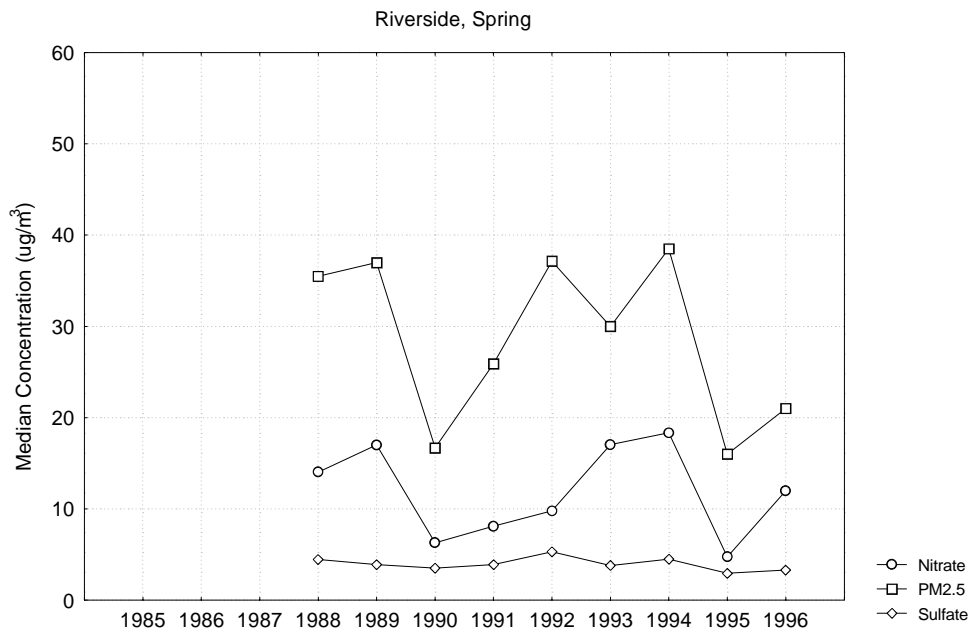


Figure A-111 Median PM_{2.5} Mass and PM₁₀ Nitrate and Sulfate by Year During Spring at Riverside

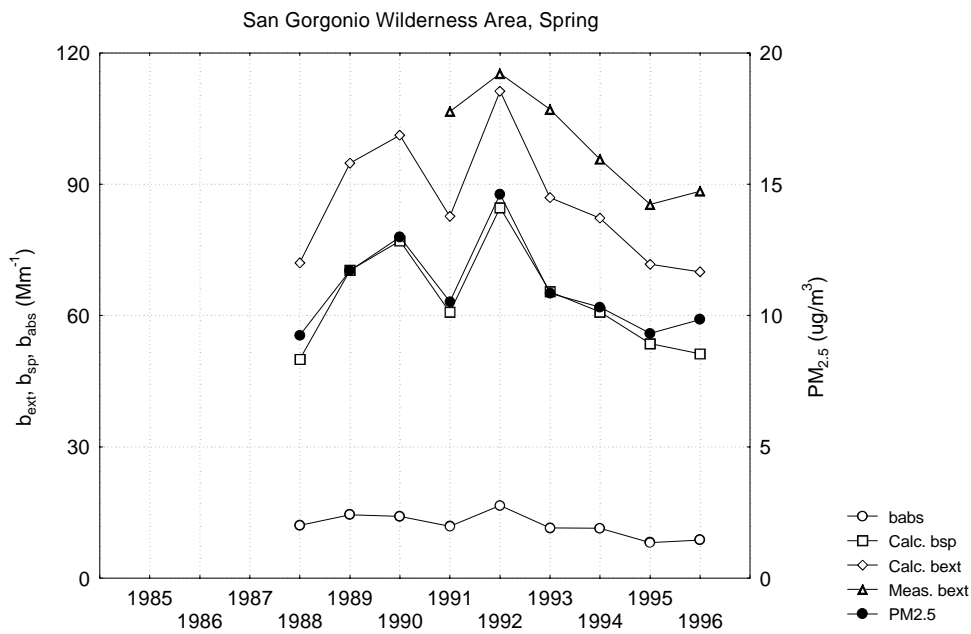


Figure A-112 Average Calculated and Measured Optical Data and PM_{2.5} Mass by Year During Spring at San Geronio Wilderness Area

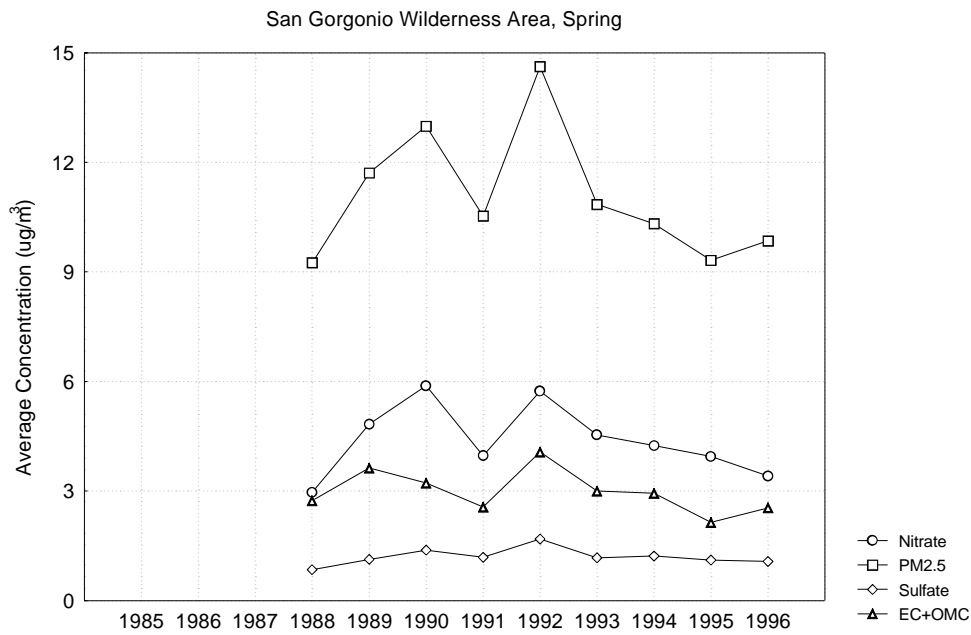


Figure A-113 Average PM_{2.5} Mass, Sulfate and Nitrate by Year During Spring at San Gorgonio Wilderness Area

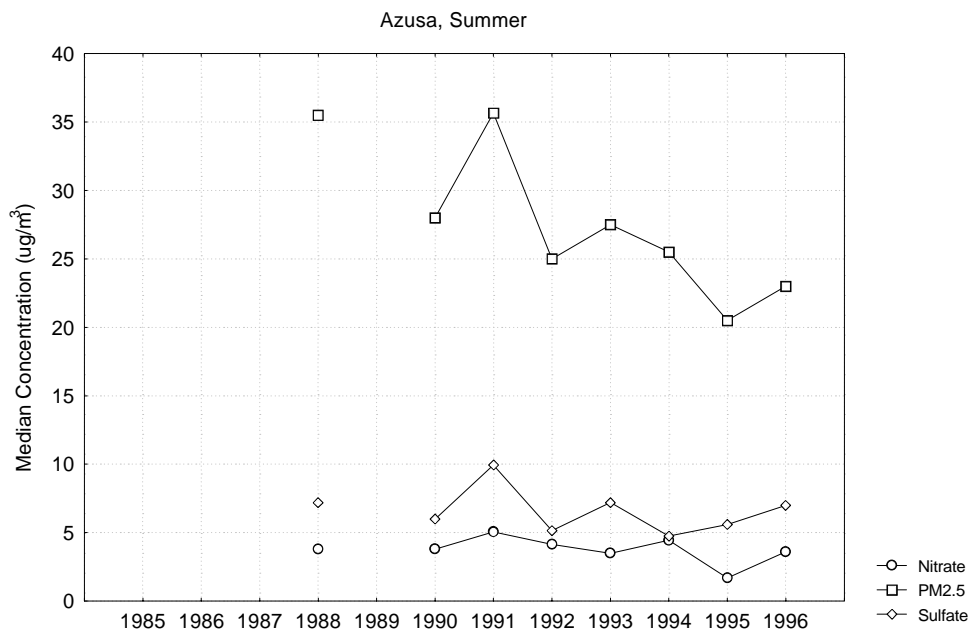


Figure A-114 Median PM_{2.5} Mass and PM₁₀ Nitrate and Sulfate by Year During Summer at Azusa

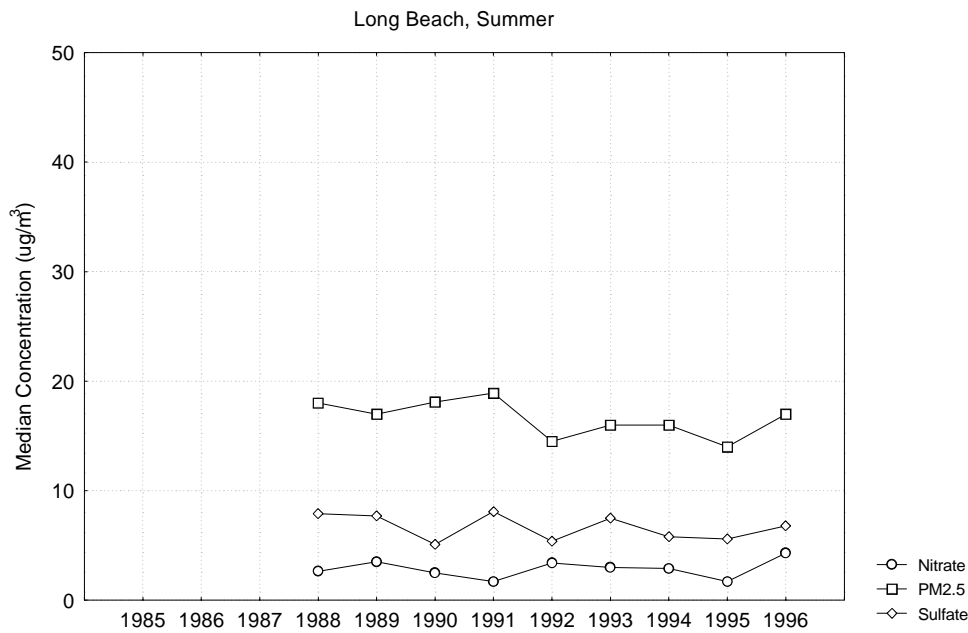


Figure A-115 Median PM_{2.5} Mass and PM₁₀ Nitrate and Sulfate by Year During Summer at Long Beach

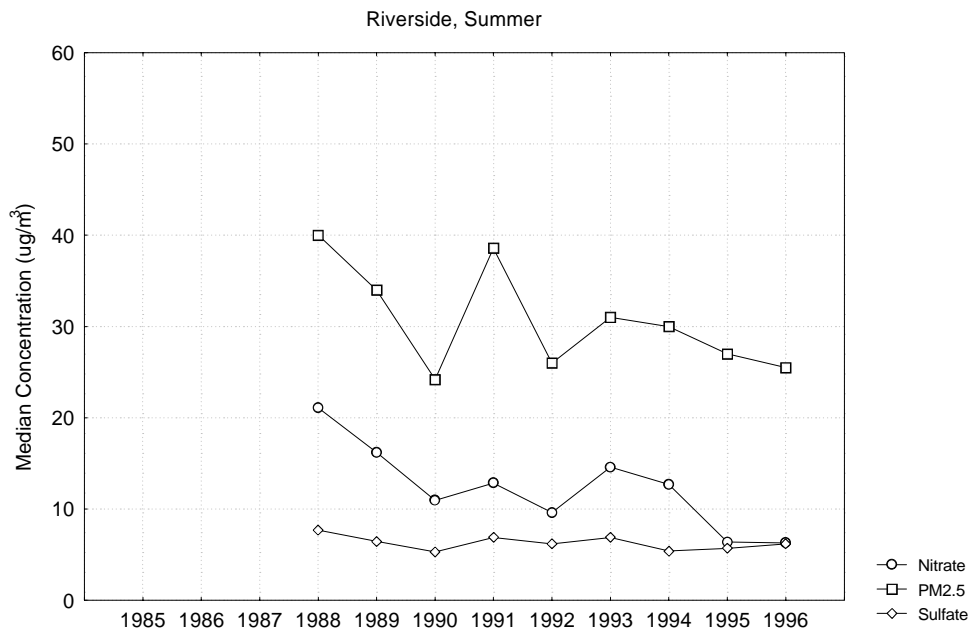


Figure A-116 Median PM_{2.5} Mass and PM₁₀ Nitrate and Sulfate by Year During Summer at Riverside

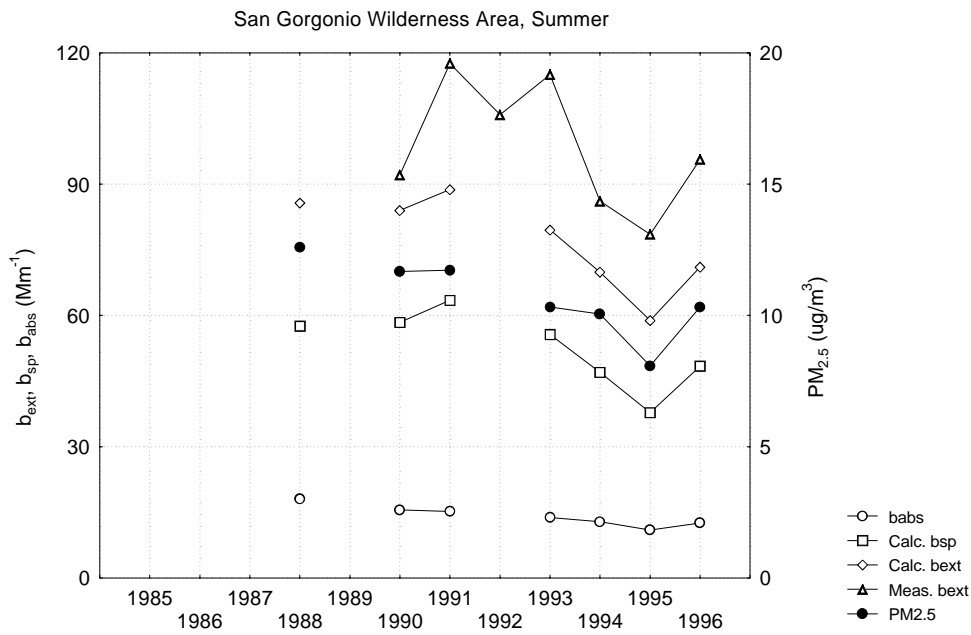


Figure A-117 Average Calculated and Measured Optical Data and PM_{2.5} Mass by Year During Summer at San Gorgonio Wilderness Area

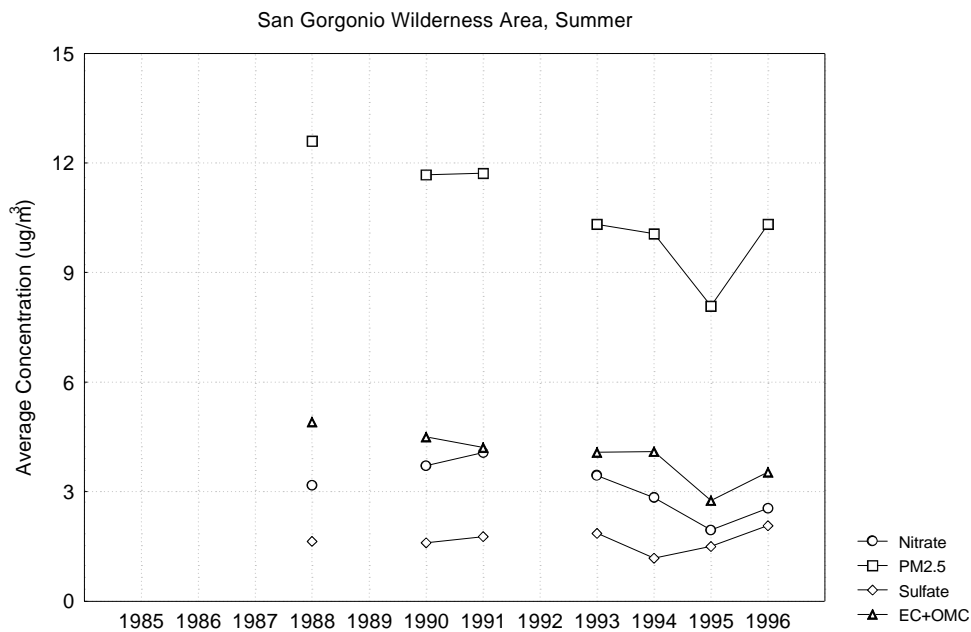


Figure A-118 Average PM_{2.5} Mass, Sulfate and Nitrate by Year During Summer at San Gorgonio Wilderness Area

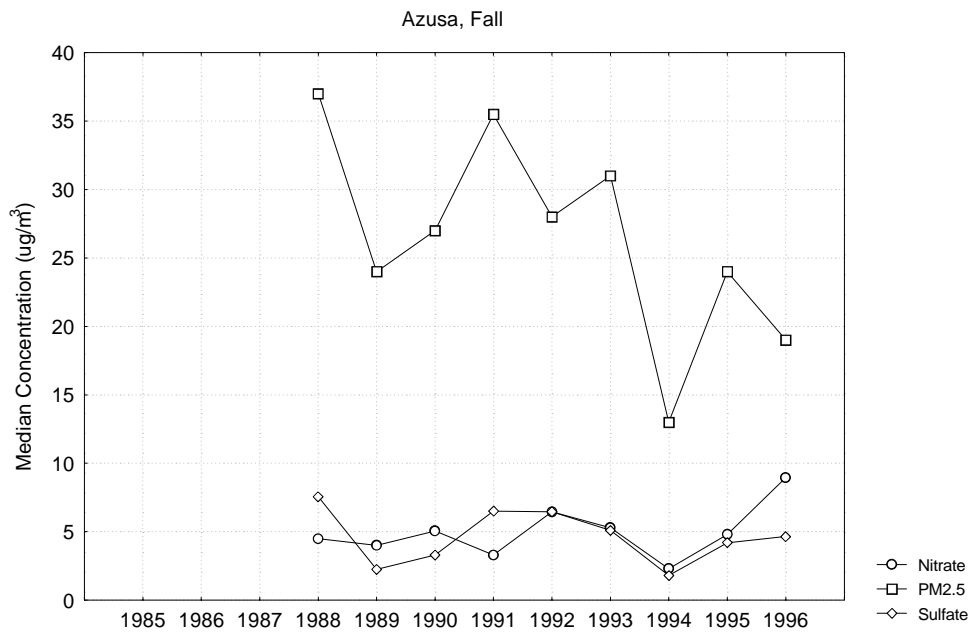


Figure A-119 Median PM_{2.5} Mass and PM₁₀ Nitrate and Sulfate by Year During Fall at Azusa

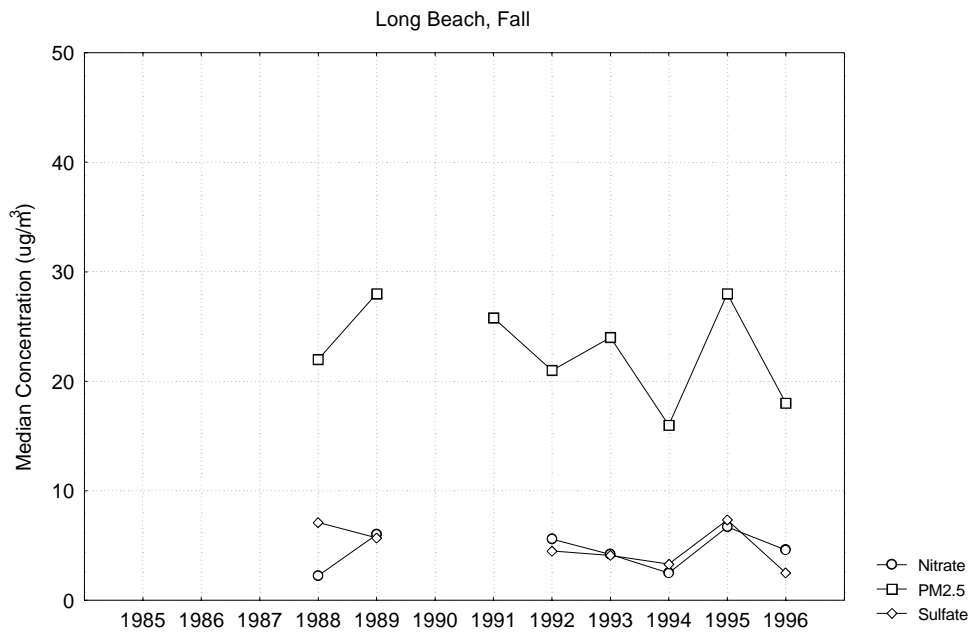


Figure A-120 Median PM_{2.5} Mass and PM₁₀ Nitrate and Sulfate by Year During Fall at Long Beach

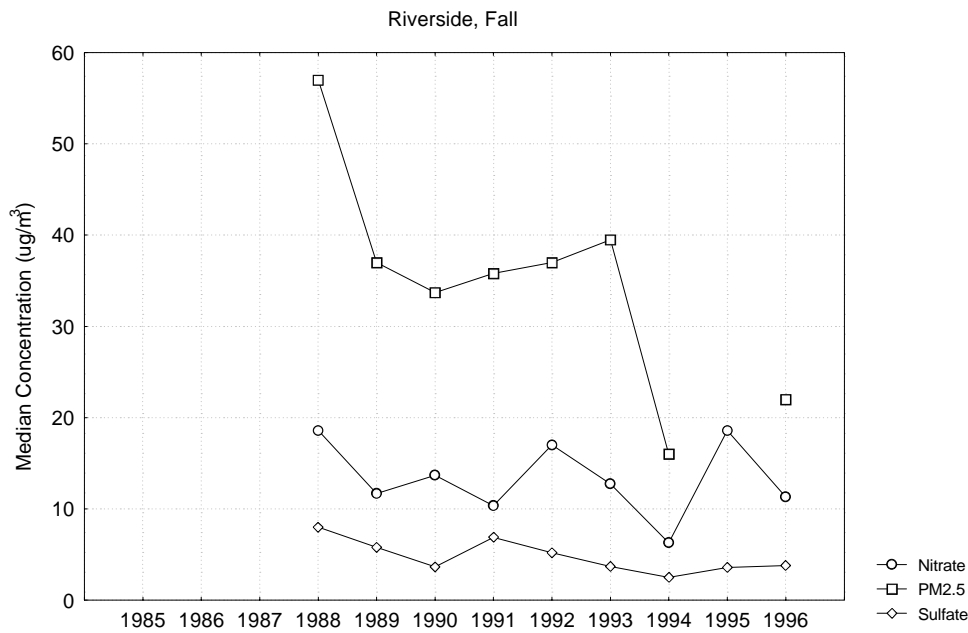


Figure A-121 Median PM_{2.5} Mass and PM₁₀ Nitrate and Sulfate by Year During Fall at Riverside

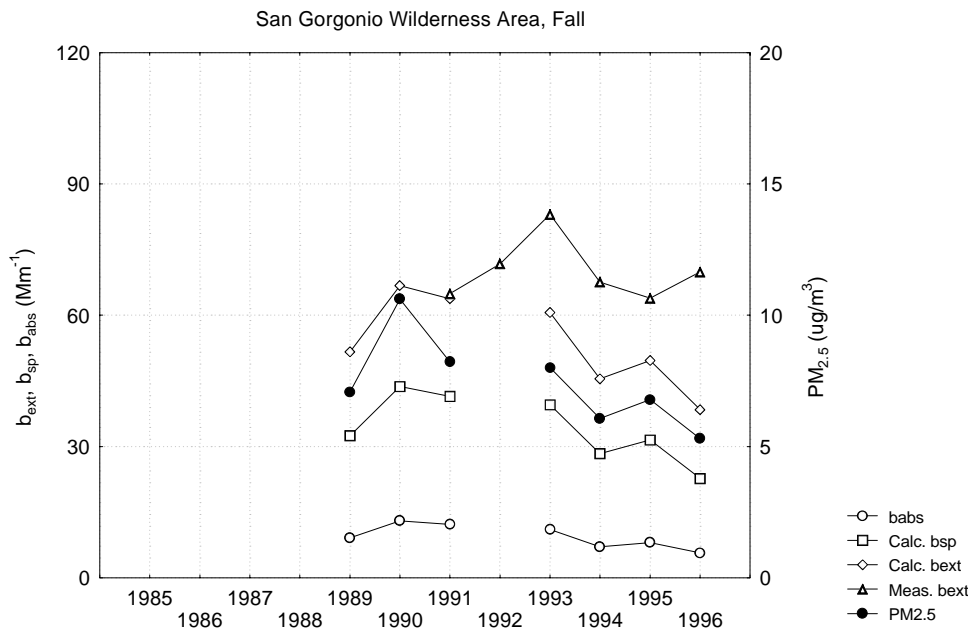


Figure A-122 Average Calculated and Measured Optical Data and PM_{2.5} Mass by Year During Fall at San Gorgonio Wilderness Area

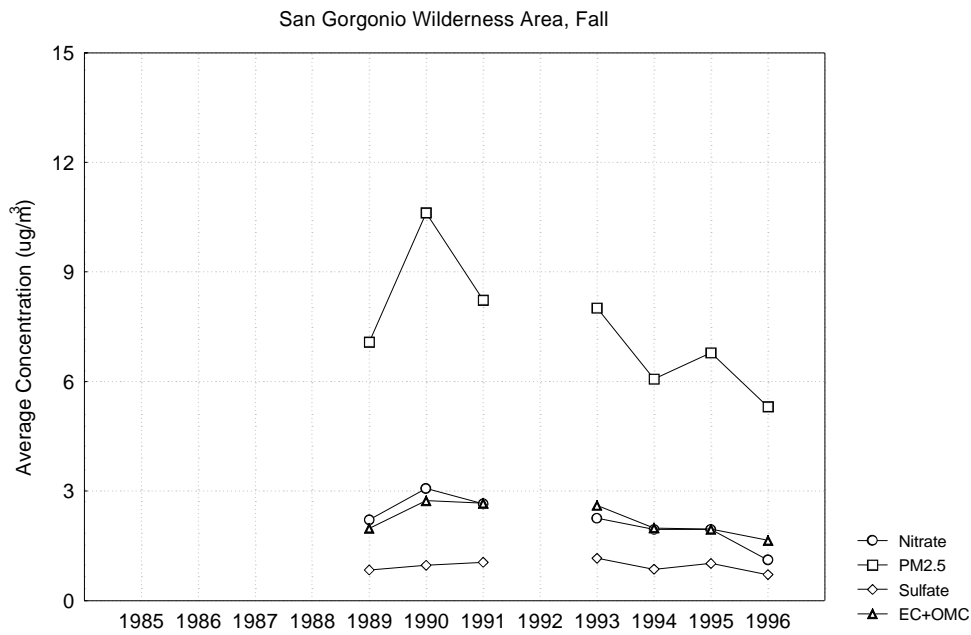


Figure A-123 Average PM_{2.5} Mass, Sulfate and Nitrate by Year During Fall at San Gorgonio Wilderness Area

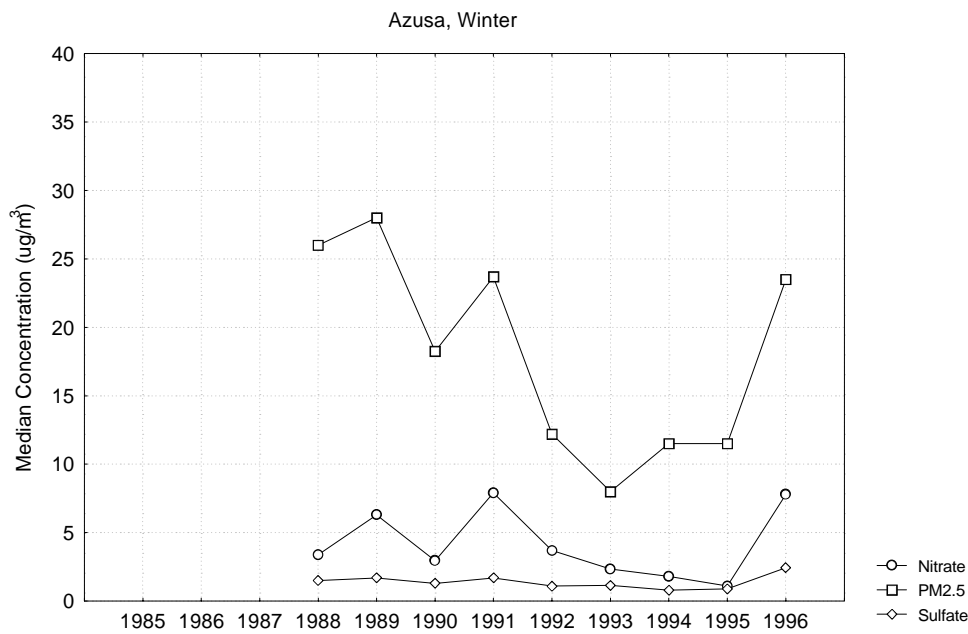


Figure A-124 Median PM_{2.5} Mass and PM₁₀ Nitrate and Sulfate by Year During Winter at Azusa

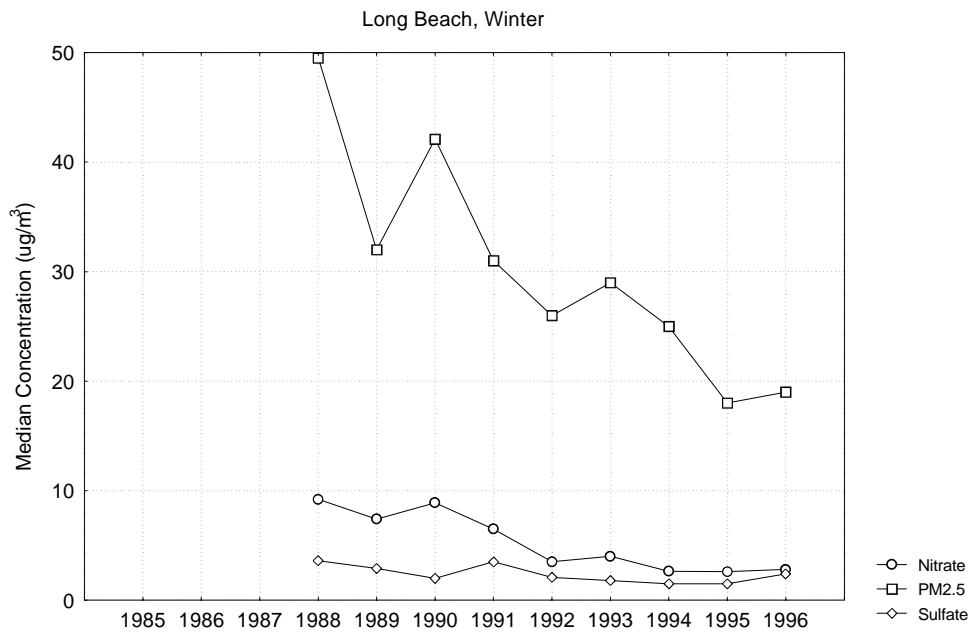


Figure A-125 Median PM_{2.5} Mass and PM₁₀ Nitrate and Sulfate by Year During Winter at Long Beach

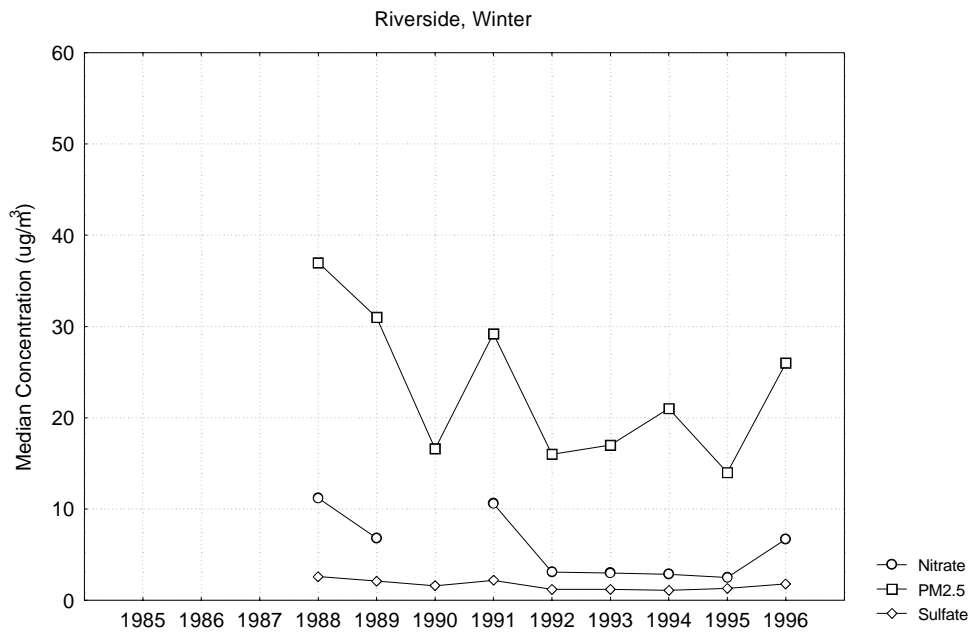


Figure A-126 Median PM_{2.5} Mass and PM₁₀ Nitrate and Sulfate by Year During Winter at Riverside

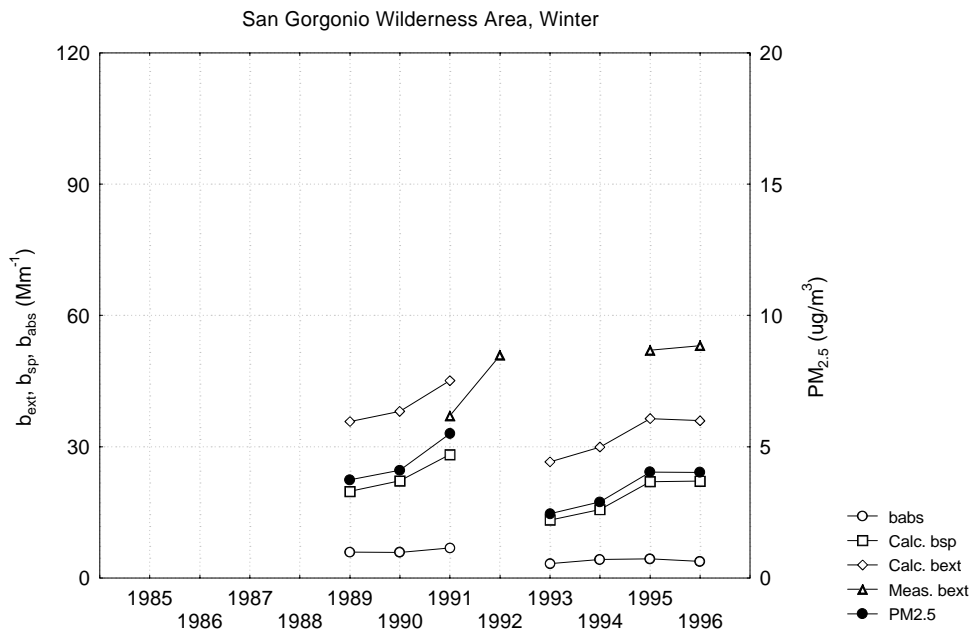


Figure A-127 Average Calculated and Measured Optical Data and PM_{2.5} Mass by Year During Winter at San Gorgonio Wilderness Area

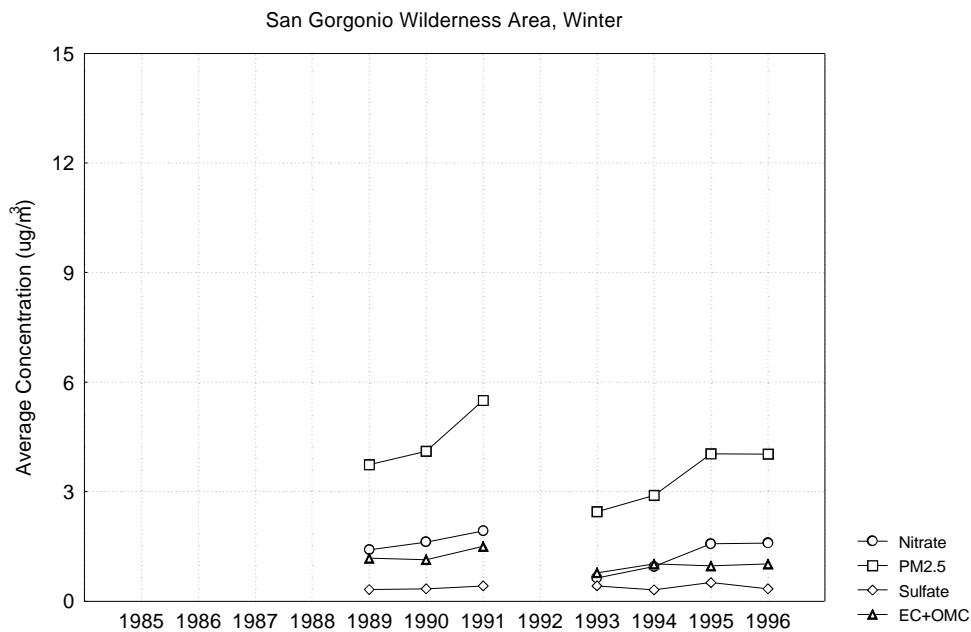


Figure A-128 Average PM_{2.5} Mass, Sulfate and Nitrate by Year During Winter at San Gorgonio Wilderness Area

APPENDIX B

SPEARMAN RANK ORDER CORRELATIONS

The following table presents the results of the calculations of Spearman rank order correlation coefficients between year and seasonal median (local-agency sites) and average (IMPROVE sites) optical and particulate matter data. Data from 1989 through 1996 were included in the calculations. The column labeled "Number Valid" is the number of years with at least half the possible values available during the season. The column labeled "Spearman-R" is the value of the correlation coefficient, and the column labeled "p-Level" is the probability that the a value as large as the observed absolute value of the correlation coefficient could have occurred by chance.

Air Basin	Season	Site	Quantity	Number Valid	Spearman R	p-Level
Lake County	Spring	Lakeport	bsp	8	-0.024	0.955
Lake County	Spring	Lakeport	COH	8	-0.415	0.307
Lake County	Summer	Lakeport	bsp	8	-0.287	0.490
Lake County	Summer	Lakeport	COH	8	-0.179	0.672
Lake County	Fall	Lakeport	bsp	8	-0.310	0.456
Lake County	Fall	Lakeport	COH	8	-0.366	0.373
Lake County	Winter	Lakeport	bsp	8	-0.595	0.120
Lake County	Winter	Lakeport	COH	8	-0.826	0.011
Lake Tahoe	Summer	South Lake Tahoe	babs	7	-0.750	0.052
Lake Tahoe	Summer	South Lake Tahoe	Calc. bext	7	-0.893	0.007
Lake Tahoe	Summer	South Lake Tahoe	Calc. bsp	7	-0.929	0.003
Lake Tahoe	Summer	South Lake Tahoe	PM2.5	7	-0.857	0.014
Lake Tahoe	Summer	South Lake Tahoe	Nitrate	7	-0.564	0.187
Lake Tahoe	Summer	South Lake Tahoe	Sulfate	7	-0.126	0.788
Lake Tahoe	Summer	South Lake Tahoe	EC+OMC	7	-0.929	0.003
Lake Tahoe	Fall	South Lake Tahoe	babs	7	-0.679	0.094
Lake Tahoe	Fall	South Lake Tahoe	Calc. bext	7	-0.607	0.148
Lake Tahoe	Fall	South Lake Tahoe	Calc. bsp	7	-0.607	0.148
Lake Tahoe	Fall	South Lake Tahoe	PM2.5	7	-0.571	0.180
Lake Tahoe	Fall	South Lake Tahoe	Nitrate	7	-0.321	0.482
Lake Tahoe	Fall	South Lake Tahoe	Sulfate	7	0.107	0.819
Lake Tahoe	Fall	South Lake Tahoe	EC+OMC	7	-0.750	0.052
Mountain Counties	Spring	Yosemite NP	babs	8	-0.714	0.047
Mountain Counties	Spring	Yosemite NP	Calc. bext	8	-0.452	0.260

Air Basin	Season	Site	Quantity	Number Valid	Spearman R	p-Level
Mountain Counties	Spring	Yosemite NP	Calc. bsp	8	-0.452	0.260
Mountain Counties	Spring	Yosemite NP	PM2.5	8	-0.452	0.260
Mountain Counties	Spring	Yosemite NP	Nitrate	8	-0.190	0.651
Mountain Counties	Spring	Yosemite NP	Sulfate	8	-0.429	0.289
Mountain Counties	Spring	Yosemite NP	EC+OMC	8	-0.524	0.183
Mountain Counties	Summer	Yosemite NP	bext	8	-0.333	0.420
Mountain Counties	Summer	Yosemite NP	babs	8	-0.714	0.047
Mountain Counties	Summer	Yosemite NP	Calc. bext	8	-0.095	0.823
Mountain Counties	Summer	Yosemite NP	Calc. bsp	8	0.000	1.000
Mountain Counties	Summer	Yosemite NP	PM2.5	8	-0.048	0.911
Mountain Counties	Summer	Yosemite NP	Nitrate	8	-0.253	0.545
Mountain Counties	Summer	Yosemite NP	Sulfate	8	-0.238	0.570
Mountain Counties	Summer	Yosemite NP	EC+OMC	8	0.333	0.420
Mountain Counties	Fall	Yosemite NP	bext	7	0.500	0.253
Mountain Counties	Fall	Yosemite NP	babs	8	-0.381	0.352
Mountain Counties	Fall	Yosemite NP	Calc. bext	8	0.262	0.531
Mountain Counties	Fall	Yosemite NP	Calc. bsp	8	0.500	0.207
Mountain Counties	Fall	Yosemite NP	PM2.5	8	0.548	0.160
Mountain Counties	Fall	Yosemite NP	Nitrate	8	-0.214	0.610
Mountain Counties	Fall	Yosemite NP	Sulfate	8	-0.135	0.750
Mountain Counties	Fall	Yosemite NP	EC+OMC	8	0.548	0.160
Mountain Counties	Winter	Yosemite NP	babs	8	-0.690	0.058
Mountain Counties	Winter	Yosemite NP	Calc. bext	8	-0.524	0.183
Mountain Counties	Winter	Yosemite NP	Calc. bsp	8	-0.310	0.456
Mountain Counties	Winter	Yosemite NP	PM2.5	8	-0.503	0.204
Mountain Counties	Winter	Yosemite NP	Nitrate	8	-0.405	0.320
Mountain Counties	Winter	Yosemite NP	Sulfate	8	-0.333	0.420
Mountain Counties	Winter	Yosemite NP	EC+OMC	8	0.143	0.736
North Central Coast	Spring	Pinnacles NM	babs	8	-0.190	0.651
North Central Coast	Spring	Pinnacles NM	Calc. bext	8	-0.405	0.320
North Central Coast	Spring	Pinnacles NM	Calc. bsp	8	-0.405	0.320
North Central Coast	Spring	Pinnacles NM	PM2.5	8	0.095	0.823
North Central Coast	Spring	Pinnacles NM	Nitrate	8	-0.586	0.127
North Central Coast	Spring	Pinnacles NM	Sulfate	8	-0.204	0.629
North Central Coast	Spring	Pinnacles NM	EC+OMC	8	0.133	0.754
North Central Coast	Summer	Pinnacles NM	babs	8	-0.714	0.047
North Central Coast	Summer	Pinnacles NM	Calc. bext	8	-0.833	0.010
North Central Coast	Summer	Pinnacles NM	Calc. bsp	8	-0.619	0.102

Air Basin	Season	Site	Quantity	Number Valid	Spearman R	p-Level
North Central Coast	Summer	Pinnacles NM	PM2.5	8	-0.476	0.233
North Central Coast	Summer	Pinnacles NM	Nitrate	8	-0.611	0.108
North Central Coast	Summer	Pinnacles NM	Sulfate	8	-0.252	0.548
North Central Coast	Summer	Pinnacles NM	EC+OMC	8	0.143	0.736
North Central Coast	Fall	Pinnacles NM	babs	8	-0.690	0.058
North Central Coast	Fall	Pinnacles NM	Calc. bext	8	-0.619	0.102
North Central Coast	Fall	Pinnacles NM	Calc. bsp	8	-0.619	0.102
North Central Coast	Fall	Pinnacles NM	PM2.5	8	-0.857	0.007
North Central Coast	Fall	Pinnacles NM	Nitrate	8	-0.619	0.102
North Central Coast	Fall	Pinnacles NM	Sulfate	8	-0.524	0.183
North Central Coast	Fall	Pinnacles NM	EC+OMC	8	-0.619	0.102
North Central Coast	Winter	Pinnacles NM	babs	8	-0.667	0.071
North Central Coast	Winter	Pinnacles NM	Calc. bext	8	-0.857	0.007
North Central Coast	Winter	Pinnacles NM	Calc. bsp	8	-0.786	0.021
North Central Coast	Winter	Pinnacles NM	PM2.5	8	-0.833	0.010
North Central Coast	Winter	Pinnacles NM	Nitrate	8	-0.810	0.015
North Central Coast	Winter	Pinnacles NM	Sulfate	8	-0.747	0.033
North Central Coast	Winter	Pinnacles NM	EC+OMC	8	-0.714	0.047
North Coast	Spring	Redwood NP	babs	8	-0.619	0.102
North Coast	Spring	Redwood NP	Calc. bext	8	-0.643	0.086
North Coast	Spring	Redwood NP	Calc. bsp	8	-0.643	0.086
North Coast	Spring	Redwood NP	PM2.5	8	-0.323	0.435
North Coast	Spring	Redwood NP	Nitrate	8	-0.623	0.099
North Coast	Spring	Redwood NP	Sulfate	8	-0.551	0.157
North Coast	Spring	Redwood NP	EC+OMC	8	-0.619	0.102
North Coast	Summer	Redwood NP	babs	8	-0.786	0.021
North Coast	Summer	Redwood NP	Calc. bext	8	-0.619	0.102
North Coast	Summer	Redwood NP	Calc. bsp	8	-0.452	0.260
North Coast	Summer	Redwood NP	PM2.5	8	0.048	0.911
North Coast	Summer	Redwood NP	Nitrate	8	-0.071	0.867
North Coast	Summer	Redwood NP	Sulfate	8	-0.333	0.420
North Coast	Summer	Redwood NP	EC+OMC	8	-0.857	0.007
North Coast	Fall	Redwood NP	babs	8	-0.738	0.037
North Coast	Fall	Redwood NP	Calc. bext	8	-0.714	0.047
North Coast	Fall	Redwood NP	Calc. bsp	8	-0.357	0.385
North Coast	Fall	Redwood NP	PM2.5	8	-0.619	0.102
North Coast	Fall	Redwood NP	Nitrate	8	-0.048	0.910
North Coast	Fall	Redwood NP	Sulfate	8	-0.381	0.352

Air Basin	Season	Site	Quantity	Number Valid	Spearman R	p-Level
North Coast	Fall	Redwood NP	EC+OMC	8	-0.619	0.102
North Coast	Winter	Redwood NP	babs	8	-0.762	0.028
North Coast	Winter	Redwood NP	Calc. bext	8	-0.524	0.183
North Coast	Winter	Redwood NP	Calc. bsp	8	-0.357	0.385
North Coast	Winter	Redwood NP	PM2.5	8	-0.286	0.493
North Coast	Winter	Redwood NP	Nitrate	8	-0.048	0.910
North Coast	Winter	Redwood NP	Sulfate	8	0.217	0.606
North Coast	Winter	Redwood NP	EC+OMC	8	-0.762	0.028
Northeast Plateau	Spring	Lassen Volcanic NP	babs	8	-0.381	0.352
Northeast Plateau	Spring	Lassen Volcanic NP	Calc. bext	8	-0.214	0.610
Northeast Plateau	Spring	Lassen Volcanic NP	Calc. bsp	8	-0.286	0.493
Northeast Plateau	Spring	Lassen Volcanic NP	PM2.5	8	-0.048	0.911
Northeast Plateau	Spring	Lassen Volcanic NP	Nitrate	8	-0.072	0.866
Northeast Plateau	Spring	Lassen Volcanic NP	Sulfate	8	0.405	0.320
Northeast Plateau	Spring	Lassen Volcanic NP	EC+OMC	8	-0.192	0.649
Northeast Plateau	Summer	Lassen Volcanic NP	babs	7	-0.643	0.119
Northeast Plateau	Summer	Lassen Volcanic NP	Calc. bext	7	-0.107	0.819
Northeast Plateau	Summer	Lassen Volcanic NP	Calc. bsp	7	0.036	0.939
Northeast Plateau	Summer	Lassen Volcanic NP	PM2.5	7	0.036	0.939
Northeast Plateau	Summer	Lassen Volcanic NP	Nitrate	7	0.072	0.878
Northeast Plateau	Summer	Lassen Volcanic NP	Sulfate	7	0.179	0.702
Northeast Plateau	Summer	Lassen Volcanic NP	EC+OMC	7	-0.357	0.432
Northeast Plateau	Fall	Lassen Volcanic NP	babs	7	-0.321	0.482
Northeast Plateau	Fall	Lassen Volcanic NP	Calc. bext	7	-0.321	0.482
Northeast Plateau	Fall	Lassen Volcanic NP	Calc. bsp	7	-0.321	0.482
Northeast Plateau	Fall	Lassen Volcanic NP	PM2.5	7	-0.107	0.819
Northeast Plateau	Fall	Lassen Volcanic NP	Nitrate	7	0.321	0.482
Northeast Plateau	Fall	Lassen Volcanic NP	Sulfate	7	0.306	0.504
Northeast Plateau	Fall	Lassen Volcanic NP	EC+OMC	7	-0.685	0.090
Sacramento Valley	Spring	Arbuckle	bsp	8	0.214	0.610
Sacramento Valley	Spring	Arbuckle	COH	8	0.133	0.754
Sacramento Valley	Summer	Arbuckle	bsp	8	0.262	0.531
Sacramento Valley	Summer	Arbuckle	COH	8	-0.049	0.909
Sacramento Valley	Fall	Arbuckle	bsp	8	0.000	1.000
Sacramento Valley	Fall	Arbuckle	COH	8	-0.310	0.456
Sacramento Valley	Winter	Arbuckle	bsp	8	0.429	0.289
Sacramento Valley	Winter	Arbuckle	COH	8	-0.443	0.272
Sacramento Valley	Spring	Chico	bsp	8	-0.214	0.610

Air Basin	Season	Site	Quantity	Number Valid	Spearman R	p-Level
Sacramento Valley	Spring	Chico	COH	8	0.407	0.317
Sacramento Valley	Summer	Chico	bsp	8	0.228	0.588
Sacramento Valley	Summer	Chico	COH	8	0.361	0.379
Sacramento Valley	Fall	Chico	bsp	8	-0.143	0.736
Sacramento Valley	Fall	Chico	COH	8	-0.133	0.753
Sacramento Valley	Winter	Chico	bsp	8	-0.762	0.028
Sacramento Valley	Winter	Chico	COH	8	-0.571	0.139
Sacramento Valley	Spring	Colusa	bsp	8	0.786	0.021
Sacramento Valley	Spring	Colusa	COH	8	-0.563	0.146
Sacramento Valley	Summer	Colusa	bsp	8	0.881	0.004
Sacramento Valley	Summer	Colusa	COH	8	-0.952	0.000
Sacramento Valley	Fall	Colusa	bsp	7	0.929	0.003
Sacramento Valley	Fall	Colusa	COH	7	-0.750	0.052
Sacramento Valley	Winter	Colusa	bsp	8	0.429	0.289
Sacramento Valley	Winter	Colusa	COH	8	-0.738	0.037
Sacramento Valley	Spring	Gridley	bsp	7	-0.429	0.337
Sacramento Valley	Spring	Gridley	COH	7	0.842	0.017
Sacramento Valley	Summer	Gridley	bsp	7	0.000	1.000
Sacramento Valley	Summer	Gridley	COH	7	-0.214	0.645
Sacramento Valley	Fall	Gridley	bsp	8	-0.743	0.035
Sacramento Valley	Fall	Gridley	COH	8	-0.143	0.736
Sacramento Valley	Winter	Gridley	bsp	7	-0.714	0.071
Sacramento Valley	Winter	Gridley	COH	7	-0.357	0.432
Sacramento Valley	Spring	Pleasant Grove	bsp	8	-0.072	0.866
Sacramento Valley	Spring	Pleasant Grove	COH	8	0.551	0.157
Sacramento Valley	Summer	Pleasant Grove	bsp	8	0.503	0.204
Sacramento Valley	Summer	Pleasant Grove	COH	8	0.762	0.028
Sacramento Valley	Fall	Pleasant Grove	bsp	8	-0.095	0.823
Sacramento Valley	Fall	Pleasant Grove	COH	8	0.714	0.047
Sacramento Valley	Winter	Pleasant Grove	bsp	8	-0.738	0.037
Sacramento Valley	Winter	Pleasant Grove	COH	8	0.072	0.865
Sacramento Valley	Spring	Yuba City	bsp	8	0.810	0.015
Sacramento Valley	Spring	Yuba City	COH	8	0.192	0.649
Sacramento Valley	Summer	Yuba City	bsp	8	0.500	0.207
Sacramento Valley	Summer	Yuba City	COH	8	0.145	0.733
Sacramento Valley	Fall	Yuba City	bsp	7	0.536	0.215
Sacramento Valley	Fall	Yuba City	COH	7	-0.357	0.432
Sacramento Valley	Winter	Yuba City	bsp	8	0.024	0.955

Air Basin	Season	Site	Quantity	Number Valid	Spearman R	p-Level
Sacramento Valley	Winter	Yuba City	COH	8	-0.024	0.955
Salton Sea	Spring	El Centro	PM2.5	7	-0.414	0.355
Salton Sea	Spring	El Centro	Nitrate	7	-0.414	0.355
Salton Sea	Spring	El Centro	Sulfate	7	0.180	0.699
Salton Sea	Summer	El Centro	PM2.5	7	-0.500	0.253
Salton Sea	Summer	El Centro	Nitrate	7	-0.286	0.535
Salton Sea	Summer	El Centro	Sulfate	7	-0.714	0.071
Salton Sea	Fall	El Centro	PM2.5	7	-0.324	0.478
Salton Sea	Fall	El Centro	Nitrate	7	-0.090	0.848
Salton Sea	Fall	El Centro	Sulfate	7	-0.891	0.007
Salton Sea	Winter	El Centro	PM2.5	7	-0.342	0.452
Salton Sea	Winter	El Centro	Nitrate	7	-0.126	0.788
Salton Sea	Winter	El Centro	Sulfate	7	-0.234	0.613
San Francisco	Spring	Point Reyes NS	babs	8	-0.786	0.021
San Francisco	Spring	Point Reyes NS	Calc. bext	8	-0.262	0.531
San Francisco	Spring	Point Reyes NS	Calc. bsp	8	-0.238	0.570
San Francisco	Spring	Point Reyes NS	PM2.5	8	0.214	0.610
San Francisco	Spring	Point Reyes NS	Nitrate	8	-0.108	0.799
San Francisco	Spring	Point Reyes NS	Sulfate	8	0.000	1.000
San Francisco	Spring	Point Reyes NS	EC+OMC	8	-0.190	0.651
San Francisco	Summer	Point Reyes NS	babs	8	-0.762	0.028
San Francisco	Summer	Point Reyes NS	Calc. bext	8	-0.095	0.823
San Francisco	Summer	Point Reyes NS	Calc. bsp	8	0.024	0.955
San Francisco	Summer	Point Reyes NS	PM2.5	8	0.476	0.233
San Francisco	Summer	Point Reyes NS	Nitrate	8	0.262	0.531
San Francisco	Summer	Point Reyes NS	Sulfate	8	0.252	0.548
San Francisco	Summer	Point Reyes NS	EC+OMC	8	0.238	0.570
San Francisco	Fall	Point Reyes NS	babs	8	-0.810	0.015
San Francisco	Fall	Point Reyes NS	Calc. bext	8	-0.810	0.015
San Francisco	Fall	Point Reyes NS	Calc. bsp	8	-0.762	0.028
San Francisco	Fall	Point Reyes NS	PM2.5	8	-0.690	0.058
San Francisco	Fall	Point Reyes NS	Nitrate	8	-0.850	0.007
San Francisco	Fall	Point Reyes NS	Sulfate	8	-0.548	0.160
San Francisco	Fall	Point Reyes NS	EC+OMC	8	-0.707	0.050
San Francisco	Winter	Point Reyes NS	babs	8	-0.214	0.610
San Francisco	Winter	Point Reyes NS	Calc. bext	8	-0.143	0.736
San Francisco	Winter	Point Reyes NS	Calc. bsp	8	-0.143	0.736
San Francisco	Winter	Point Reyes NS	PM2.5	8	-0.143	0.736

Air Basin	Season	Site	Quantity	Number Valid	Spearman R	p-Level
San Francisco	Winter	Point Reyes NS	Nitrate	8	-0.190	0.651
San Francisco	Winter	Point Reyes NS	Sulfate	8	0.347	0.399
San Francisco	Winter	Point Reyes NS	EC+OMC	8	-0.619	0.102
San Francisco	Spring	San Jose	PM2.5	7	-0.883	0.008
San Francisco	Summer	San Jose	PM2.5	7	0.214	0.645
San Francisco	Fall	San Jose	PM2.5	7	-0.491	0.263
San Joaquin Valley	Spring	Bakersfield	PM2.5	8	-0.964	0.000
San Joaquin Valley	Spring	Bakersfield	Nitrate	8	-0.738	0.037
San Joaquin Valley	Spring	Bakersfield	Sulfate	8	-0.762	0.028
San Joaquin Valley	Summer	Bakersfield	PM2.5	8	-0.457	0.255
San Joaquin Valley	Summer	Bakersfield	Nitrate	8	-0.881	0.004
San Joaquin Valley	Summer	Bakersfield	Sulfate	8	-0.743	0.035
San Joaquin Valley	Fall	Bakersfield	PM2.5	8	-0.452	0.260
San Joaquin Valley	Fall	Bakersfield	Nitrate	8	-0.452	0.260
San Joaquin Valley	Fall	Bakersfield	Sulfate	8	-0.929	0.001
San Joaquin Valley	Winter	Bakersfield	PM2.5	7	-0.679	0.094
San Joaquin Valley	Winter	Bakersfield	Nitrate	7	-0.750	0.052
San Joaquin Valley	Winter	Bakersfield	Sulfate	7	-0.757	0.049
San Joaquin Valley	Spring	Fresno	PM2.5	8	-0.743	0.035
San Joaquin Valley	Spring	Fresno	Nitrate	8	-0.095	0.823
San Joaquin Valley	Spring	Fresno	Sulfate	8	-0.699	0.054
San Joaquin Valley	Summer	Fresno	PM2.5	8	0.503	0.204
San Joaquin Valley	Summer	Fresno	Nitrate	8	-0.571	0.139
San Joaquin Valley	Summer	Fresno	Sulfate	8	0.778	0.023
San Joaquin Valley	Fall	Fresno	PM2.5	8	-0.168	0.691
San Joaquin Valley	Fall	Fresno	Nitrate	8	-0.500	0.207
San Joaquin Valley	Fall	Fresno	Sulfate	8	-0.647	0.083
San Joaquin Valley	Winter	Fresno	PM2.5	7	-0.500	0.253
San Joaquin Valley	Winter	Fresno	Nitrate	7	-0.714	0.071
San Joaquin Valley	Winter	Fresno	Sulfate	8	-0.786	0.021
San Joaquin Valley	Spring	Madera	PM2.5	8	-0.667	0.071
San Joaquin Valley	Spring	Madera	Nitrate	7	-0.667	0.102
San Joaquin Valley	Spring	Madera	Sulfate	7	-0.775	0.041
San Joaquin Valley	Summer	Madera	PM2.5	8	-0.246	0.558
San Joaquin Valley	Summer	Madera	Nitrate	7	-0.214	0.645
San Joaquin Valley	Summer	Madera	Sulfate	7	-0.236	0.610
San Joaquin Valley	Fall	Madera	PM2.5	7	-0.607	0.148
San Joaquin Valley	Winter	Madera	PM2.5	7	-0.786	0.036

Air Basin	Season	Site	Quantity	Number Valid	Spearman R	p-Level
San Joaquin Valley	Spring	Modesto	PM2.5	8	0.217	0.606
San Joaquin Valley	Spring	Modesto	Nitrate	8	-0.357	0.385
San Joaquin Valley	Spring	Modesto	Sulfate	8	-0.072	0.866
San Joaquin Valley	Summer	Modesto	PM2.5	8	0.049	0.909
San Joaquin Valley	Summer	Modesto	Nitrate	8	-0.415	0.307
San Joaquin Valley	Summer	Modesto	Sulfate	8	-0.659	0.076
San Joaquin Valley	Fall	Modesto	PM2.5	8	-0.144	0.734
San Joaquin Valley	Fall	Modesto	Nitrate	8	-0.429	0.289
San Joaquin Valley	Fall	Modesto	Sulfate	8	-0.551	0.157
San Joaquin Valley	Winter	Modesto	PM2.5	7	-0.821	0.023
San Joaquin Valley	Winter	Modesto	Nitrate	7	-0.893	0.007
San Joaquin Valley	Winter	Modesto	Sulfate	7	-0.937	0.002
San Joaquin Valley	Spring	Stockton	bsp	8	-0.143	0.736
San Joaquin Valley	Spring	Stockton	COH	8	-0.714	0.047
San Joaquin Valley	Spring	Stockton	PM2.5	8	-0.719	0.045
San Joaquin Valley	Spring	Stockton	Nitrate	8	-0.467	0.243
San Joaquin Valley	Spring	Stockton	Sulfate	8	-0.417	0.304
San Joaquin Valley	Summer	Stockton	bsp	8	0.071	0.867
San Joaquin Valley	Summer	Stockton	COH	8	-0.452	0.260
San Joaquin Valley	Summer	Stockton	PM2.5	8	0.122	0.774
San Joaquin Valley	Summer	Stockton	Nitrate	8	-0.619	0.102
San Joaquin Valley	Summer	Stockton	Sulfate	8	-0.571	0.139
San Joaquin Valley	Fall	Stockton	bsp	8	-0.371	0.365
San Joaquin Valley	Fall	Stockton	COH	8	-0.786	0.021
San Joaquin Valley	Fall	Stockton	PM2.5	7	-0.536	0.215
San Joaquin Valley	Fall	Stockton	Nitrate	7	-0.714	0.071
San Joaquin Valley	Fall	Stockton	Sulfate	7	-0.786	0.036
San Joaquin Valley	Winter	Stockton	bsp	7	-0.536	0.215
San Joaquin Valley	Winter	Stockton	COH	7	-0.679	0.094
San Joaquin Valley	Winter	Stockton	PM2.5	7	-0.857	0.014
San Joaquin Valley	Winter	Stockton	Nitrate	8	-0.571	0.139
San Joaquin Valley	Winter	Stockton	Sulfate	8	-0.826	0.011
San Joaquin Valley	Spring	Visalia	PM2.5	8	-0.898	0.002
San Joaquin Valley	Spring	Visalia	Nitrate	8	-0.361	0.379
San Joaquin Valley	Spring	Visalia	Sulfate	8	-0.914	0.001
San Joaquin Valley	Summer	Visalia	PM2.5	8	0.506	0.201
San Joaquin Valley	Summer	Visalia	Nitrate	8	-0.262	0.531
San Joaquin Valley	Summer	Visalia	Sulfate	8	0.578	0.133

Air Basin	Season	Site	Quantity	Number Valid	Spearman R	p-Level
San Joaquin Valley	Fall	Visalia	PM2.5	8	-0.587	0.126
San Joaquin Valley	Fall	Visalia	Nitrate	8	-0.311	0.453
San Joaquin Valley	Fall	Visalia	Sulfate	8	-0.659	0.076
San Joaquin Valley	Winter	Visalia	PM2.5	8	-0.762	0.028
San Joaquin Valley	Winter	Visalia	Nitrate	8	-0.690	0.058
San Joaquin Valley	Winter	Visalia	Sulfate	7	-0.559	0.192
South Coast	Spring	Azusa	PM2.5	7	-0.464	0.294
South Coast	Spring	Azusa	Nitrate	7	-0.036	0.939
South Coast	Spring	Azusa	Sulfate	7	-0.143	0.760
South Coast	Summer	Azusa	PM2.5	7	-0.821	0.023
South Coast	Summer	Azusa	Nitrate	7	-0.500	0.253
South Coast	Summer	Azusa	Sulfate	7	-0.214	0.645
South Coast	Fall	Azusa	PM2.5	8	-0.455	0.257
South Coast	Fall	Azusa	Nitrate	8	0.310	0.456
South Coast	Fall	Azusa	Sulfate	8	0.048	0.911
South Coast	Winter	Azusa	PM2.5	8	-0.515	0.192
South Coast	Winter	Azusa	Nitrate	8	-0.333	0.420
South Coast	Winter	Azusa	Sulfate	8	-0.240	0.568
South Coast	Spring	Long Beach	PM2.5	8	-0.952	0.000
South Coast	Spring	Long Beach	Nitrate	8	0.405	0.320
South Coast	Spring	Long Beach	Sulfate	8	-0.467	0.243
South Coast	Summer	Long Beach	PM2.5	8	-0.506	0.201
South Coast	Summer	Long Beach	Nitrate	8	0.072	0.866
South Coast	Summer	Long Beach	Sulfate	8	-0.143	0.736
South Coast	Fall	Long Beach	PM2.5	7	-0.450	0.310
South Coast	Winter	Long Beach	PM2.5	8	-0.929	0.001
South Coast	Winter	Long Beach	Nitrate	8	-0.881	0.004
South Coast	Winter	Long Beach	Sulfate	8	-0.491	0.217
South Coast	Spring	Riverside	PM2.5	8	-0.190	0.651
South Coast	Spring	Riverside	Nitrate	8	0.071	0.867
South Coast	Spring	Riverside	Sulfate	8	-0.407	0.317
South Coast	Summer	Riverside	PM2.5	8	-0.310	0.456
South Coast	Summer	Riverside	Nitrate	8	-0.690	0.058
South Coast	Summer	Riverside	Sulfate	8	-0.169	0.690
South Coast	Fall	Riverside	PM2.5	7	-0.414	0.355
South Coast	Fall	Riverside	Nitrate	8	-0.024	0.955
South Coast	Fall	Riverside	Sulfate	8	-0.500	0.207
South Coast	Winter	Riverside	PM2.5	8	-0.333	0.420

Air Basin	Season	Site	Quantity	Number Valid	Spearman R	p-Level
South Coast	Winter	Riverside	Nitrate	7	-0.607	0.148
South Coast	Winter	Riverside	Sulfate	8	-0.395	0.333
South Coast	Spring	San Gorgonio WA	babs	8	-0.833	0.010
South Coast	Spring	San Gorgonio WA	Calc. bext	8	-0.786	0.021
South Coast	Spring	San Gorgonio WA	Calc. bsp	8	-0.714	0.047
South Coast	Spring	San Gorgonio WA	PM2.5	8	-0.762	0.028
South Coast	Spring	San Gorgonio WA	Nitrate	8	-0.762	0.028
South Coast	Spring	San Gorgonio WA	Sulfate	8	-0.476	0.233
South Coast	Spring	San Gorgonio WA	EC+OMC	8	-0.714	0.047
South Coast	Summer	San Gorgonio WA	bext	7	-0.429	0.337
South Coast	Fall	San Gorgonio WA	babs	7	-0.750	0.052
South Coast	Fall	San Gorgonio WA	Calc. bext	7	-0.750	0.052
South Coast	Fall	San Gorgonio WA	Calc. bsp	7	-0.750	0.052
South Coast	Fall	San Gorgonio WA	PM2.5	7	-0.750	0.052
South Coast	Fall	San Gorgonio WA	Nitrate	7	-0.775	0.041
South Coast	Fall	San Gorgonio WA	Sulfate	7	-0.143	0.760
South Coast	Fall	San Gorgonio WA	EC+OMC	7	-0.643	0.119
South Coast	Winter	San Gorgonio WA	babs	7	-0.643	0.119
South Coast	Winter	San Gorgonio WA	Calc. bext	7	-0.143	0.760
South Coast	Winter	San Gorgonio WA	Calc. bsp	7	-0.107	0.819
South Coast	Winter	San Gorgonio WA	PM2.5	7	-0.143	0.760
South Coast	Winter	San Gorgonio WA	Nitrate	7	-0.107	0.819
South Coast	Winter	San Gorgonio WA	Sulfate	7	0.255	0.582
South Coast	Winter	San Gorgonio WA	EC+OMC	7	-0.613	0.144

